

Proceedings of the Second Noncontact Temperature Measurement Workshop

January 17-19, 1989
Pasadena, CA

Robert R. Hale
Editor

(NASA-CP-161287) PROCEEDINGS OF THE SECOND
NONCONTACT TEMPERATURE MEASUREMENT WORKSHOP
(JPL) 359 D CSCL 13P

N90-17594
--THRU--
N90-17926
Unclass
0260600

63/31

June 1, 1989



National Aeronautics and
Space Administration

Jet Propulsion Laboratory
California Institute of Technology
Pasadena, California

Proceedings of the Second Noncontact Temperature Measurement Workshop

January 17–19, 1989
Pasadena, CA

Robert R. Hale
Editor

June 1, 1989

NASA

National Aeronautics and
Space Administration

Jet Propulsion Laboratory
California Institute of Technology
Pasadena, California

This publication was prepared by the Jet Propulsion Laboratory, California Institute of Technology, under a contract with the National Aeronautics and Space Administration.

ABSTRACT

A Workshop was held January 17 through 19, 1989 in Pasadena, California to review the state of the art in noncontact temperature measurement (NCTM) technology and to identify the NCTM requirements of the National Aeronautics and Space Administration (NASA) microgravity materials processing community. The workshop scope included technical presentations and discussions which ranged from research on advanced concepts for temperature measurement to laboratory research and development regarding measurement principles and state-of-the-art engineering practices for NCTM methodology in commercial and industrial applications.

Technical presentations were made concerning (1) NCTM needs as perceived by several NASA centers, (2) recent ground-based NCTM research and development of industry, NASA, academia and selected national laboratories, (3) work-in-progress communication and, (4) technical issues of the implementation of temperature measurement in the space environment to facilitate future U.S. materials science investigations.

The workshop was attended by approximately eighty scientists and engineers from diverse organizations including academia, industry, NASA and selected national laboratories. These proceedings contain the manuscripts and abstracts which were submitted by the authors of the invited papers, together with the summaries of findings and recommendations of the session chairs. The recommendations address identified needs to establish and extend thermophysical and thermoradiative materials properties data in support of fundamental temperature measurement, to identify and develop a series of objective temperature measurement instrument evaluation criteria and standards (particularly for thermal-imaging instruments), to continue vigorous research concerning applicability and limits of error for various radiation thermometry methodologies, and to continue the development of new NCTM technologies which will facilitate future quantitative materials science investigations.

FOREWORD

The space environment permits scientists from around the world access to a completely new laboratory unfettered by the constraints of our earthbound habitat. Unique to this new laboratory environment is microgravity, where very low accelerations can be achieved and maintained for significant durations; this permits detailed study of the behavior of materials in a variety of temperature regimes. One facility under development for this new laboratory is a containerless processing facility. Here, samples can be positioned in free space without the externally applied reaction forces which would be required to counteract the gravitational acceleration that would be encountered on earth.

The potential for science investigations in both microgravity and containerless science are exciting and broad because of the variety of materials and temperature ranges which can be explored. However, the conduct of scientific investigations in this new laboratory requires advanced capabilities and instruments that allow noncontact sample and process characterization. A very important area for this characterization is noncontact temperature measurement (NCTM), for which this workshop was convened in January 1989 in Pasadena, California.

The need for noncontact temperature measurement was identified at the April-May 1987 National Aeronautics and Space Administration (NASA) workshop held in Washington, D.C., and chaired by Dr. Mark C. Lee. The proceedings are documented as NASA Conference Publication 2503, dated 1988, and available from NASA's Scientific and Technical Information Division. An excerpt from the foreword of that document identifies NCTM and several other areas of advanced technology development:

"Noncontact Temperature Measurement instrument has been identified as one of the eight advanced technology development (ATD) areas to support the Microgravity Science and Applications Division's effort in developing the six space Station Flight Experiment Facilities. The other seven ATDs are high resolution/high rate video technology, microgravity fluid diagnostics, laser light scattering instrument, vibration isolation technology, high temperature furnace technology, high temperature material [sic] technology, and interface measurement. Those ATD areas are defined as generic areas of technology advancement that will enhance the scientific integrity and quality of flight experiments. These technologies shall not be in the critical path of ongoing programs or near term facility development programs."

Further clarification of particular scientific needs is required to effectively manage the advanced technology that is oriented toward the enhancement and enablement of space-science experiments. The scope of the reported work includes approaches to instrumentation for the measurement of temperature over rather broad ranges and a general consideration of materials and processes that require temperature measurement. The materials include both condensed and uncondensed matter; much of the scientifically interesting phenomenology involves changes of state and nonequilibrium processes, including solidification and the processes of crystallization.

Significant progress has been made in investigating capabilities of advanced techniques for temperature measurement. However, further work is needed to establish the requirements for NCTM in support of future, and undesignated, science experiments. As this requirements definition proceeds, the adequacy of developing NCTM capabilities can be evaluated, and further technical advancements which are needed can be identified. Because of the ongoing nature of this work, it is anticipated that a follow-up workshop will be held near January 1991 to extend our understanding of the fundamental technological barriers of NCTM for advanced science experiments, and to revisit the technological capabilities in NCTM that are under continuing development.

ACKNOWLEDGMENTS

I am pleased to recognize the support and participation of several organizations and individuals in both conducting the workshop and preparing these proceedings. The first of these is the National Aeronautics and Space Administration (NASA) Headquarters' Microgravity Science and Applications Division (MSAD), Code EN, whose financial sponsorship is gratefully acknowledged. J. Kreer and L. Spencer developed and defined the programmatic work statements relating to this broad area of technology development; M.C. Lee's enthusiasm and untiring energy championed the development of Noncontact Temperature Measurement (NCTM) as an essential tool for advanced materials science experiments.

I am especially grateful for the effective and timely help of A. Fripp and M. Buoncristiani of Langley Research Center (LaRC), G. Santoro and P. Greenberg of Lewis Research Center (LeRC), and Dinah Higgins of Marshall Space Flight Center (MSFC). Also, I appreciate the thoughtful discussions on initial technical planning during fiscal year 1988 held with LaRC's C. Byvik (presently affiliated with W.J. Shaefer Associates, Incorporated) and J. Heyman; LeRC's J. Salzman and T. Glasgow; and MSFC's A. Lehosky, R. Yoel, and C. Daugherty.

I congratulate, commend, and thank the splinter work-session chairs and cochairs for their expert assistance in preparing for, leading, and documenting the technical deliberations in several topical areas; these individuals are A. Cezairliyan, D.P. DeWitt, C.Y. Ho, H. Kaplan, R.L. Shepard, and R.E. Spjut. The presenters, authors, and workshop participants are also acknowledged.

From JPL, I am grateful for the support of and helpful discussions with the MCPF Project Office, particularly F. Schutz, D.W. Lewis, A.D. Morrison, and E.H. Trinh. The professionalism of P. McLane, JPL Conference Coordinator, and her staff in arranging and managing the meeting logistics was important to the effectiveness and success of this conference. Important to this publication was the competent editorial services support of P. South of JPL's Documentation Section.

Robert R. Hale

SUMMARY OF PROCEEDINGS CONTENTS

Robert R. Hale

This document is organized into sections that closely parallel the framework of the technical workshop itself.

Section 1, NASA NCTM Needs by Center, contains the manuscripts prepared by each Center that describe the perceived needs for noncontact temperature measurement (NCTM) in support of science thrusts and microgravity science laboratory facilities at the various centers. The contributing National Aeronautics and Space Administration (NASA) Centers are the Jet Propulsion Laboratory (JPL), NASA Langley Research Center (LaRC), NASA Lewis Research Center (LeRC), and NASA Marshall Space Flight Center (MSFC). The breadth of the temperature measurement needs is well described in the presentations by G. Santoro of Lewis and E. Trinh of JPL.

Session 1 emphasized the state of the hardware for commercial and industrial thermal measurement and imaging systems. Of these papers, that by Chairman H. Kaplan provides a definitive organization and description of various types of thermal measurement instruments, their use in industrial and commercial materials and process measurement, and a list of manufacturers and suppliers.

The other papers dealing with thermal imagers described both in-process and planned development work in infrared imaging systems for use in space experimentation.

Section 2 contains technical discussions regarding capabilities in NCTM ranging from advanced concepts and innovative approaches to developmental temperature-measurement instruments. In the former area, important physical principles involving photoacoustic and thermal-wave phenomena and magnetic-resonance imaging are introduced. These topics are in keeping with the initial intent of the advanced technology development, which is to explore the characterization and measurement that enable advanced, and as yet undesignated, microgravity materials science. In addition to this long-term potential, instruments under development provide a nearer-term capability that, with adequate further development, may lead to successful flight instrumentation in a few years. Also, there are presently available industrial and commercial thermal imagers that have the potential for at least relative thermal measurements in ground-based and flight experiments. These instruments provide large amounts of imaging information of high value for defense and industrial uses. The successful adaptation of such thermal imagers to quantitative scientific temperature measurement will require a significant technical effort.

Other papers in this section describe the calculation of true temperatures from radiance measurements made at a number of different wavelengths (Kahn), the use of ellipsometry to determine optical constants and temperature (Krishnan), an instrument using multiwavelength imaging pyrometry to measure small moving samples (Frish), and innovative uses of thermal imaging anomalies for the control of crystal growth (Wargo).

The original plan for Section 2 was to investigate, in depth, the technical issues in the dynamic response of thermal measurement and its relationship to thermal control. This was considered important for two reasons. The first is the rapidity with which some microgravity experiments occur. An example is recalescence in which a spontaneous and very rapid temperature increase is seen subsequent to subcooling a liquid. The second is the detailed knowledge required of the dynamic interaction of the measured signal with the time response of the control element. This knowledge will be needed for the expected future use of the temperature measurement signal as an element for control within the experiment itself. Because much temperature measurement work involves temperatures that are unchanging or changing slowly, special emphasis on this topic with regard to microgravity science is indicated. Considering that much of the actual technical work involving dynamic response is inextricably linked to thermal and thermal radiative properties of materials, it was felt necessary to combine the technical expertise and experience of the Session 3 chairs with those of Session 2.

Section 3 is an update regarding the thermal requirements for materials science investigations. These requirements will be used to help define more specifically the thermal measurement barriers that limit the characterization of fundamental behavior in advanced materials science.

In this section is previously undocumented research in materials science, including polymeric materials investigations (Coulter) and overview comments on thermal issues relating to high T_c materials – an emerging materials and process technology (Bishop).

Section 3 also discusses significant differences in the time regimes, temperature ranges, temperature change rates, and spatial temperature gradients, which are of importance in understanding and controlling an experiment or process.

Because of the interrelationship and time rates of change of radiant intensity as a function of wavelength, dynamic response also is associated with multicolor pyrometry. Therefore, Session 4 was also combined with 2 and 3, making one large concurrent splinter session. (The paper by C. Y. Ho describing the numerical database (CINDAS) at Purdue University was presented in plenary session prior to segregation into the splinter work groups.) Section 4 contains the technical papers presented within the splinter work sessions.

Section 5 presents the summary findings of each of the session chairs. Many were unable to present consensus findings because of time limitations and the combination of the three topical sessions into one large splinter group.

Section 6 contains Appendixes. Appendix A is a list of attendees to the workshop; Appendix B is a list of NCTM Requirements as extracted from NASA Conference Publication 2503 in 1988 (Mark C. Lee, Editor); Appendix C consists of letters of invitation and welcome, the final program, and selected abstracts from the workshop.

CONTENTS

Executive Summary.....	ES-1
------------------------	------

SECTION 1

NASA NCTM NEEDS BY CENTER

Materials and Thermal Science Overview, R. R. Hale.....	3
Noncontact Temperature Measurement Requirements of Ground-Based Research and Flight Programs at JPL, E. H. Trinh.....	5
Temperature Profiles in High Gradient Furnaces, A. L. Fripp et al.	11
Microgravity Noncontact Temperature Requirements at NASA Lewis Research Center, G. Santoro.....	19
Marshall Space Flight Center Noncontact Temperature Measurement Requirements, D. B. Higgins and W. K. Witherow (Proceedings only - this paper was not presented at the workshop).....	33

SECTION 2

NCTM CAPABILITIES TECHNICAL PAPERS

Introduction and Noncontact Science and Technology, R. R. Hale	41
Optical Johnson Noise Thermometry, R. L. Shepard, et al.....	42
Noncontact Temperature Measurements in Support of Microgravity Combustion Experiments, P. S. Greenberg.....	50
Solid State Lasers for Use in Noncontact Temperature Measurements, A. M. Buoncristiani.....	60
Signal Processing Applied to Photothermal Techniques for Materials Characterization, J. A. Rooney (Abstract only).....	70
Radiation Thermometry at NIST: An Update of Services and Research Activities, G. B. Hillard.....	71
Infrared Thermal Imaging Figures of Merit, H. Kaplan.....	80

A Multicolor Imaging Pyrometer, M. B. Frish, and J. H. Frank.....	90
Noncontact True Temperature Measurements in the Microgravity Environment, M. A. Khan.....	98
Spectral Emissivities and Optical Constants of Electro- magnetically Levitated Liquid Metals as Functions of Temperature and Wavelength, S. Krishnan et al.....	110
A Potential Nuclear Magnetic Resonance Imaging Approach for Noncontact Temperature Measurement, S. L. Manatt.....	141
IR Optical Fiber-based Noncontact Pyrometer for Drop Tube Instrumentation, R. G. May, et al.....	150
Use of Anomalous Thermal Imaging Effects for Multimode Systems Control During Crystal Growth, M. J. Wargo.....	158

SECTION 3

MICROGRAVITY MATERIALS SCIENCE THERMAL REQUIREMENTS

Comments on Containerless Bulk Crystal Growth and Epitaxy in Space and on Their Implications Regarding Noncontact Temperature Measurements, K. J. Bachmann.....	171
Noncontact Temperature Measurement of a Falling Drop, W. Hofmeister and R. J. Bayuzick.....	183
Polymeric Materials Science in the Microgravity Environment, D. R. Coulter.....	203
Temperature Control and Calibration Issues in the Growth, Processing, and Characterization of Electronic Materials, B. A. Wilson.....	210
Flux Lattice Melting in the High T _c Superconductors, D. J. Bishop et al.....	217
Combustion Process Science and Technology, R. R. Hale.....	220
On the Temperature of Surfaces, J. A. Mann, Jr.....	221
Noncontact Temperature Requirements (NCTM) for Drop and Bubble Physics, A. B. Hmelo and T. G. Wang.....	230
Materials Properties Numerical Database System Established and Operational at CINDAS/Purdue University, C. Y. Ho.....	236

SECTION 4

SPLINTER SESSION TECHNICAL PAPERS

An Update of Commercial Infrared Sensing and Imaging
Instruments, H. Kaplan..... 253

A Space-Qualified Thermal Imaging System Using a Pt Si
Detector Array, R. W. Astheimer..... 271

Development of an Infrared Imaging System for the Surface
Tension Driven Convection Experiment Aboard the
USML-1 Spacelab Mission, A. D. Pline..... 284

SECTION 5

WORKSHOP SUMMARIES

Session 1, IR Thermal Measurement Instruments, H. Kaplan..... 297

Session 2, Dynamic Response for Thermal Control and
Measurement and Fast Radiation Thermometry,
R. L. Shepard and A. Cezairliyan..... 299

Session 3, Materials Thermal and Thermoradiative Properties/
Characterization Technology, D. DeWitt and C. Y. Ho..... 303

Session 4, Multicolor Pyrometry, R. E. Spjut..... 317

APPENDIXES

APPENDIX A - List of Attendees..... A-1

APPENDIX B - NCTM Requirements List (Extracted from
NASA Conference Publication No. 2503,
1988, Mark C. Lee, Editor)..... B-1

APPENDIX C - Invitation Letter, Workshop Final Program
and Selected Abstracts..... C-1

EXECUTIVE SUMMARY

A National Aeronautics and Space Administration (NASA) technical workshop was convened by the Jet Propulsion Laboratory (JPL) January 17-19, 1989 in Pasadena, California. The purpose was to exchange information and review issues concerning advanced non-contact temperature measurement (NCTM) instrument methods and techniques applicable to future space investigations. The focus was on technology needs for the microgravity and containerless processing field of materials science. The sponsor of the meeting was NASA Headquarters, Code EN, Microgravity Science and Applications Division. Robert R. Hale, of JPL, was General Chairman for the national meeting.

Technical NCTM highlights included accounts of the science measurement needs of several NASA Centers, reviews of selected materials science experiment needs, concept papers on advanced methods of temperature measurement, descriptions of work-in-process research and development, and working splinter sessions to discuss current issues and findings. A general consensus emerged that several NCTM instruments are likely to be needed, that the effective use of each will be application-specific, and that the workshop itself is an effective forum to facilitate communication between the experimental users and the instrument developers. Several areas were identified in which further technical work is needed. These included: (1) Development of objective NCTM performance verification technology for scientific purposes, (2) Education of prospective users in available and developing NCTM capabilities, (3) Extension of the use of advanced optical and IR detector focal plane array technology to NCTM, (4) Adaptation and improvement of image processing software to facilitate time-resolved multi-spectral radiometry, (5) Development of related instruments and techniques for ancillary and concurrent non-contact science characterization, (6) Research on the behavior of spectral emissivity together with surface optical scattering characteristics for NCTM, (7) Application of "data physics" to synthesize materials properties estimates from existing knowledge, (8) Development of appropriate models to allow mathematical extraction of higher quality inferences from multispectral radiation thermometry measurements, (9) Continuation of NCTM research in fundamental and applied science as well as in novel and enabling experimental methods and techniques.

Imminent problems such as the engineering implementation of NCTM techniques for immediate space missions were not treated in depth at this workshop, since the emphasis was on Advanced Technology Development (ATD). The near-term measurement problem posed by a (moving) specular molten metallic sphere, which is not radiating to free space, was considered by many to be a major challenge for radiation thermometry NCTM. Careful consideration of the sample's radiative transfer with the experimental apparatus is required for a case such as this. One other area which was not adequately addressed was that of identifying thresholds of acceptability to ensure that the science being investigated is not perturbed by the diagnostic method. This is critically important for laser-based measurements in reflectometry or polarimetry, for example. As specific science experiment objectives evolve and are selected, more detailed definitions and priorities will be established. Because of the new and ongoing nature of the NCTM ATD work, a follow-up workshop is contemplated about January 1991.

SECTION 1

NASA NCTM NEEDS BY CENTER

MATERIALS AND THERMAL SCIENCE OVERVIEW

Robert R. Hale
Jet Propulsion Laboratory
California Institute of Technology

On behalf of NASA Microgravity Science and Applications Division (MSAD), Code EN, the Jet Propulsion Laboratory (JPL) convened a workshop from January 17 to 19, 1989 at Pasadena, California. The purpose of the workshop was to address the technical issues which will facilitate noncontact temperature measurement (NCTM) of experimental materials in microgravity and containerless science investigations. The stated objective of the task was to "identify and remove the technological barriers to the accurate noncontact determination of temperatures to enable research, development, and understanding of the properties and behavior of both 'conventional' and 'unusual' materials in various states and ensembles over a range of environmental conditions, including those which vary spatially, temporally and in gravitational field intensity."

The classes of engineering materials and processes which were thought to have scientific interest for fundamental and applied investigations included metals and alloys, biological protein crystals, ceramics, glasses, carbon allotropes, "electronic materials," polymeric materials, fluids, and combustion processes.

The states of matter of interest for such experimentation include both condensed matter (including solids, particulates, and liquids), and uncondensed matter represented by vapors and plasmas (which include ions, electrons, and fundamental particles). Many processes are of interest which involve changes of state such as solidification and evaporation, or changes of structural order such as crystallization. In some cases the materials science of interest involves nonequilibrium thermodynamics and thermochemistry. The general topic, therefore, of materials whose temperature is to be measured, is broad and comprehensive. Because of the interest in providing a flexible and adaptable advanced technology capability for scientific investigation, there have not been selected, focused priorities for the measurements to support specific experiments.

The following six ranges of temperatures to be measured were established for purposes of this workshop. Only the last three were given primary attention. The identified ranges are: (1) less than 1 Kelvin, (2) 0.3 to 30K, (3) 5 to 300K, (4) 300 to 1,300K, (5) 1,000 to 3,500K and, (6) above 3,000K.

Although relative radiance maps ("thermograms"), may have some scientific utility, the principal objective is to establish fundamental, quantitative temperature measurement for science applications in advanced experimentation in the microgravity environment and in containerless processes. A number of parameters relating to temperature measurement were identified as an aid to communication during technical discussions on temperature measurement. This is critically important in helping to identify and establish the specific needs of the scientist for temperature measurement, as distinguished from those of the process engineer, for example. In the latter case, it can often be found that repeatability and relative changes of temperature are actually more important than absolute accuracy or precision. The mapping of areal fields of temperature as well as spatial fields associated with volumetric distribution can lead to technical challenges in the measurement and presentation of temperature distribution data. Furthermore, the relatively mature field of radiation thermometry rests upon numerous technical assumptions which may have insufficient validity to permit useful scientific temperature measurements. Because of the known limitations of some of these fundamental assumptions related to radiation thermometry, selected other areas of noncontact temperature measurement were conceptualized and explored regarding their initial feasibility for certain postulated experiments and experimental objectives.

To introduce the topic of NCTM to persons who were not already familiar with it, each Center was asked to present the technical perception it has of the noncontact temperature measurement needs of its ground-based and flight program activities. This served to provide an overview of the similarities and differences among the centers, and the materials science being conducted and planned for in the foreseeable future. The intent was to continue the intercenter cooperative and collaborative technical work, and to provide synergism and effectiveness in the technical coupling of instrumental solutions to temperature measurement problems.

For the present work, the emphasis on the advanced technology development (ATD) task was on levitated samples, fluids science, and drop tubes or drop towers.

NON-CONTACT TEMPERATURE MEASUREMENT REQUIREMENTS OF GROUND-BASED RESEARCH AND FLIGHT PROGRAMS AT JPL

E.H. TRINH
JET PROPULSION LABORATORY
CALIFORNIA INSTITUTE OF TECHNOLOGY

INTRODUCTION

The Modular Containerless Processing Facility project at the Jet Propulsion Laboratory is responsible for the development of flight equipment and of the accompanying scientific and technological research necessary to carry out containerless investigations in the low gravity of Earth orbit. The requirement for sample temperature measurement is just one of the many physical properties determination needs that must be satisfied before the useful exploitation of low gravity and containerless experimentation techniques can be achieved. The specific implementation of temperature measurement for the ground-based research program is different from that of the flight hardware development project. The needs of the latter must also be differentiated according to the chronological order of the relevant space flight missions. Immediate demands of Spacelab instruments must be addressed by the adaptation of existing reliable technology to the special and restrictive on-orbit environment, while more advanced and yet unperfected techniques will be assigned to enterprises further in the future. The wide range of application of the containerless methods to the study of phenomena involving different states of matter and environmental conditions requires the satisfaction of a variety of boundary conditions through different approaches. An important issue to be resolved will be whether an integrated program dedicated to solve the problems of all the Microgravity experimental effort will allow the solution of specific demands of existing as well as future flight equipment.

1. CONTAINERLESS PROCESSING TECHNIQUES AND INVESTIGATIONS

The access to near-Earth orbit and the opportunity of performing investigations sensitive to, or enabled by the drastic reduction the gravitational level has justified the development of containerless positioning and manipulation technology for interdisciplinary scientific and technological studies in microgravity. Existing techniques under consideration for space

applications have been adapted from existing Earth-based methods, or have been specifically developed for the low gravity environment. Electromagnetic, acoustic or ultrasonic, and electrostatic or electrophoretic approaches are the current areas of concentration in the Microgravity Science and Applications program. The European effort also involves the development of a version of high temperature aerodynamic positioning. Very preliminary work is being initiated at the Jet Propulsion Laboratory on microwave applications to containerless sample positioning and heating.

Electromagnetic levitation has been in use for many years in the investigation of the high temperature behavior of liquid metals and alloys. The environment around the specimen under investigation may be a gas or a high vacuum. Progress has been made in terms of the control of sample stability (rotational and vibrational), and in the decoupling of the heating and positioning functions for operation in low gravity, but the sample manipulation capabilities remain fairly limited. Only fairly conductive solids or melts are appropriate, and all the ground-based applications have been at higher temperatures (at least 1000 °C). Space Shuttle flight equipment exists, and improved versions are also under development. Potential flight opportunities exist in the near future.

Acoustic or ultrasonic levitation techniques have also been first developed for use in Earth-based laboratories, and have been adopted for applications in microgravity. Sample manipulation and control capabilities are extensive, and all types of materials are appropriate. The working environment must be a fluid to support the propagation of the sound waves. Flight equipment exists and improved devices are also under development. Previous devices have already flown in space, and future flights are scheduled beginning in 1992.

Electrodynamic levitation of micron-size samples has been extensively used in ground-based laboratories for various experimental investigations. Electrostatic levitation techniques have been mainly developed for space applications using larger samples (on the order of a centimeter), but have also been used on Earth for room temperature experiments. Permanent electric charges are required in order to provide a significant force on the sample in the case of electrostatic positioning, but the electrophoretic technique can rely on induced charges if the force magnitude can be reduced. The working environment can be high vacuum or a fluid at ambient or higher temperature. Limited sample manipulation capabilities exist, but are under current development. No flight equipment exists, and no space flight is yet scheduled for the future.

In summary, the general characteristics of these containerless positioning techniques are multi-disciplinary applications using a wide range of materials properties and environments. Some of the methods can be productively used on Earth, but all are

still experimental and yet untested for space operation, and all also require the development of accompanying diagnostic techniques for the non-contact and non-perturbing measurement of the specimen physical properties. One of the more fundamental of these properties is the true thermodynamic temperature.

2. EXPERIMENT REQUIREMENTS

Specific requirements for identified experiments using containerless processing techniques may be obtained by examining past or ongoing projects. More generic requirements will be listed in this paper in order to gain an overall view of the magnitude of the problem. In general, the requirements for any given experiment will not include all the conditions listed below at the same time, but the basic requirement for observing the sample in an optically inhomogeneous medium is invariably present.

An arbitrary division of the potential investigations requiring containerless positioning and manipulation can be made to distinguish experiments carried out at moderate and ambient temperatures from those performed at high and ultra-high temperatures.

A. GENERIC MODERATE TEMPERATURE EXPERIMENT REQUIREMENTS

- Low or moderate temperature radiative background
- Slower time variations of the temperature (0.1 to 10°C/sec)
- Larger samples (0.1 to 2.5 cm)
- Temperature range: 30 to 500°C
- Absolute accuracy for temperature measurement: +/-0.1 to 1°C
- Spatial temperature distribution or gradient (1 to 50°C/cm)
- Spatial resolution to 0.1 cm
- Single-phase or multi-phase samples
- Single-or multi-component samples
- Environment temperature distribution measurement required
- Temperature control to 0.01°C
- Temperature generally not the crucial element of the experiment
- Temperature data acquisition rate < 10/sec

- Liquid and solid samples: organic, inorganic, metallic, polymeric.
- Optical properties: Mainly transparent and semi-transparent materials, some opaque materials (specular and diffuse surfaces)
- Internal temperature distribution also desired for samples
- Sample completely stationary, slowly rotating or oscillating
- Sample spot heated from broadband or monochromatic radiant sources
- Fluid environment gas or liquid
- Optical light paths include windows and thermally non-uniform (refractive) environments
- Sample emissive properties generally known or measureable. In situ emittance measurement desired
- Single or small number of samples

B. GENERIC HIGH TEMPERATURE EXPERIMENT REQUIREMENTS

- High, moderate, or low temperature radiative background
- Faster time variation of the temperature (10^{-1} to 10^6 C/sec)
- Smaller sample (0.05 to 1 cm)
- Temperature range 500 to 2000°C
- Absolute accuracy +/-1 to 10°C
- Sample temperature distribution / gradient (1 to 100°C/cm)
- Spatial resolution to 0.05 cm
- Single-and multi-phase samples
- Single-and multi-component samples
- Environmental temperature distribution
- Temperature control to 1°C
- Temperature is generally a crucial element of the experiment
- Temperature acquisition data rate between 10 to 10^6 /sec

- Liquid and solid samples: Pure metals and alloys, glasses, ceramics, refractories, polymers, minerals
- Optical properties: transparent, semi-transparent, opaque (specular, diffuse, or both)
- Internal temperature distribution
- Sample stationary, oscillating, rotating, or both
- Temperature measurement of spot heated samples from broadband and monochromatic radiant sources
- Sample environment: vacuum, gas, or high temperature slag or glass
- Optical paths highly inhomogeneous
- Sample emissive properties generally unknown, and in-situ measurement required
- Sample generally outgassing
- High temperature reaction kinetics measurement required
- Significant free charge present. High electric, magnetic and sonic fields present
- Single, small and large number of samples

The above list is a compilation of general projected requirements which could be included in future specific experiments. They are based on a variety of existing ground-based as well as flight investigations.

3. JPL GROUND-BASED RESEARCH: ADVANCED TECHNOLOGY AND SCIENCE

Earth-based experimental facilities used for containerless experiments include electromagnetic, electrostatic, ultrasonic, and aerodynamic levitation devices. Other techniques make use of drop tubes as well as drop towers together with some vertical wind tunnels. The non-contact temperature measurement characteristics used are mostly based on radiometric methods, and are typically commercially available or are experimental and one-of-a-kind devices specially developed by the experimenter. These apparatuses could be elaborate and bulky, and are capable of accommodating high data acquisition rate and storage. They could be operated with complicated procedures, and a high failure rate is probably acceptable. Advanced concepts and development

programs are also generally acceptable for use in Earth-based laboratories.

The present research program at JPL involves high temperature acoustic and ultrasonic levitation in isothermal or quasi-isothermal furnaces (30 -1500°C), or with the use of radiant beam heaters. Electrostatic levitation in isothermal furnaces or in vacuum chambers with the use of radiant beam heaters is also under current investigation. Preliminary research is also carried out in acoustic levitation in combination with microwave heating.

Research topics in both materials science and fluid dynamics involve the dynamics of acoustically levitated melts in 1 g and in low gravity, the undercooling and nucleation studies of levitated melts as well as solidification phenomena, the measurement of the thermophysical properties of levitated materials, crystal growth from electrostatically and acoustically levitated solutions, and finally the dynamics of levitated charged liquid samples.

4. FLIGHT HARDWARE PROGRAM AT JPL

Containerless experiments will be carried out during the USML-1 Spacelab flight in 1992 using the Drop Physics Module, an experimental facility precursor to Space Station hardware. JPL is responsible for the design and fabrication of the apparatus which will fit within a Spacelab double rack. Ambient as well as moderately high temperature experiments will be carried out in this instrument, and a non-contact temperature measurement capability is required. The current approach to satisfying this requirement will be to use available thermal imaging technology adapted to the low gravity and Spacelab environments.

The characteristics associated with flight equipment are quite different from those acceptable for ground-based experimentation: High reliability, automation, and low power consumption are prominent requirements. Constraints on available time for flights scheduled in the near future limit the candidate devices to current technology and perhaps even to commercially available units. Advanced technology development aiming to develop the NCTM capability for flight facilities to be scheduled in the future space station will probably be required to provide prototype units for precursor flights in this coming decade.

TEMPERATURE PROFILES IN HIGH GRADIENT FURNACES

by

A. L. Fripp, W. J. Debnam, G. A. Woodell and R. Berry
NASA Langley Research Center
Hampton, Virginia 23665

R. K. Crouch
NASA Headquarters
Washington, D.C. 20546

and

S. K. Sorokach
Planning Research Corporation
Hampton, Virginia 23666

INTRODUCTION

Accurate temperature measurement of the furnace environment is very important in both the science and technology of crystal growth as well as many other materials processing operations. A high degree of both accuracy and precision is acutely needed in the directional solidification of compound semiconductors in which the temperature profiles control the freezing isotherm which, in turn, affects the composition of the growth with a concomitant feedback perturbation on the temperature profile.

Directional solidification, by its very nature, requires a furnace configuration that will transport heat through the sample being grown. A common growth procedure is the Bridgman Stockbarger technique which basically consists of a hot zone and a cold zone separated by an insulator. In a normal growth procedure the material, contained in an ampoule, is melted in the hot zone and is then moved relative to the furnace toward the cold zone and solidification occurs in the insulated region. Since the primary path of heat between the hot and cold zones is through the sample, both axial and radial temperature gradients exist in the region of the growth interface.

The interaction of temperature profile and interface shape was first shown in the seminal paper by Chang and Wilcox¹ and then expanded by others²⁻⁴. The effect of the interface shape on composition and convection in the liquid has also been shown in the literature⁵⁻⁸. The temperature and thermophysical properties of the sample also interact with those of the furnace wall and result in a growth rate that does not equal the relative furnace-ampoule translation rate⁹⁻¹¹. From this discussion, there is clearly a need to know the temperature profile of the growth furnace with the crystal that is to be grown as the thermal load. However it is usually not feasible to insert thermocouples inside an ampoule and thermocouples attached to the outside wall

of the ampoule have both a thermal and a mechanical contact problem as well as a view angle problem.

The objective of this paper is to present a technique of calibrating a furnace with a thermal load that closely matches the sample to be grown and to describe procedures that circumvent both the thermal and mechanical contact problems.

PROCEDURE

The procedure is actually in three parts. First to be discussed is the selection of a suitable material that will properly emulate the crystal to be grown. Next the thermocouples have to be fixed to this test sample to overcome the mechanical, thermal and view factor problems. The third step is to perform an in-situ measurement of the thermocouple positions at the growth temperature. Each of these steps will be discussed in turn.

Since the primary heat flow between the hot and cold furnace zones is through the sample (and ampoule walls) it is necessary to match the thermophysical properties of the sample to those of the crystal to be grown. A complete match would include matching the thermal conductivity, thermal diffusivity and emissivity of the two. Since these factors are functions of temperature, with a discontinuity at the interface, a full match is virtually impossible especially if the latent heat of fusion is considered. The most important single factor and easiest to match is thermal conductivity. The thermal diffusivity becomes important in transient portions of the testing and can also be important when using high growth rates or in samples of high values of diffusivity. The match of emissivity can be accomplished by choosing the same ampoule for the test sample as will be used for the crystal. This ampoule choice is necessary if its thermal conductivity is on the same order or higher than that of the sample. However if the ampoule is transparent over a significant range of the thermal emission of the furnace (note Wein's law) then the sample/ crystal emissivity match still has to be considered.

Once the sample material has been chosen, it has to be instrumented for temperature measurement. Although various temperature sensitive resistors might be used for measurement the most common procedure is to use bimetallic thermocouples and this will be the only technique discussed in this paper.

The thermocouples have to be attached to the ampoule to obtain a sound mechanical and thermal contact. If pressed only to the surface of the sample the thermocouple is only in partial contact and will measure an average temperature between the sample and the ambient. The lack of a sound contact will also result in a relative motion between the sample and the thermocouple due to the mismatch of thermal coefficients of expansion. If the thermocouples are inside an ampoule then the emissivity factor can be ignored to the extent that the ampoule is opaque to the incident radiation.

Concomitant to the problem of a sound thermal contact is the need to minimize the heat flow in the thermocouple wires.¹¹ This is especially important for low thermal conductivity samples in which a significant portion of the total heat flux could be in the metal thermocouple leads.

The final test for mechanical integrity of the contact is to x-ray the instrumented sample at both room temperature and at the maximum operating temperature to observe the movement of the thermocouple wires. Since most operational furnaces are not amenable to x-ray penetration, a special furnace can was built for this test. The precise temperature distribution was not important for this test.

An additional variable that has to be considered in furnace calibration is the pull rate or simulated growth rate of the sample. Heat is transferred from the hot zone to the cold zone by both thermal conductivity and, when the sample is physically moving, by heat capacity and the temperature difference between zones. This effect, often characterized by the Peclet number, is not easily quantifiable without numerical analysis or physical measurement.

RESULTS

The material chosen for the test sample was fused silica (SiO_2). This material was chosen because of its inert nature, the ease of thermocouple insertion and, primarily, because of its thermal conductivity match to the crystalline material of interest, PbSnTe .

The relative movement of the thermocouples with respect to the sample is shown in figure 1. The thermocouples are attached to a fused silica rod by various techniques and inserted into a furnace. The cross hairs are wires placed on the exterior of the furnace and are not affected by the heating of the furnace; hence they represent a fixed reference point. Figure 1a shows the setup at room temperature and figure 1b shows the same setup at 1000°C . The relative movement of thermocouples with respect to the lab frame is as much as 2.5mm.

This extent of movement is clearly unacceptable when trying to characterize a high temperature, high gradient furnace in which it is required to measure a 1°C difference between the sample center and surface while the axial gradient may be in excess of $150^\circ\text{C}/\text{cm}$. Also note that the attachment schemes shown in figure 1 do not compensate for axial heat flow nor do they form a sound contact to the sample.

Figure 2 is a drawing that shows an improved technique in which a similar silica rod is used but the thermocouples are attached in a superior fashion. In this technique of thermocouple attachment small holes are drilled into the fused silica with an ultrasonic impact grinder. The holes are sized to accommodate the sheathed thermocouple.

The effect of translation speed on the thermal profile is shown in figure 3. In this experiment a thermocouple is attached to a fused quartz rod and translated through the furnace first at one centimeter per hour then at one centimeter per minute. The slow pull rate is a quasi static measurement and it can be seen that the higher pull rate can displace the liquid solid interface by as much as 2.5cm. This amount of displacement can move the interface from the hot zone to the cold zone which means that the interface could potentially change from convex to concave by just changing the pull rate. This type of profile shift with respect to ampoule pull rate has also been shown by Clyne¹¹ in liquid metals.

SUMMARY

The thermal profile within the crystal growth ampoule must be accurately known to check thermal modeling and to predict interface shape and extent of fluid convection. An instrumented, inert, sample can be constructed to measure axial gradients in the typical Bridgman Stockbarger directional solidification furnace. Specific care has to be taken to avoid undesired thermocouple movement.

REFERENCES

1. C. E. Chang and W. R. Wilcox, "Control of Interface Shape in the Vertical Bridgman-Stockbarger Technique", *J. Crystal Growth*, 21, 135-140 (1974).
2. L. Y. Chin and F. M. Carlson, "Finite Element Analysis of the Control of Interface Shape in Bridgman Crystal Growth", *J. Crystal Growth*, 62, 561-567 (1983).
3. T. W. Fu and W. R. Wilcox, "Influence of Insulation on Stability of Interface Shape and Position in the Vertical Bridgman-Stockbarger Technique", *J. Crystal Growth*, 48, 416-424 (1980).
4. C. E. Huang, D. Elwell, and R. S. Feigelson, "Influence of Thermal Conductivity on Interface Shape During Bridgman Growth", *J. Crystal Growth*, 64, 441-447 (1983).
5. F. M. Carlson, A. L. Fripp, and R. C. Crouch, "Thermal Convection During Bridgman Crystal Growth", *J. Crystal Growth*, 68, 747-756 (1984).
6. F. M. Carlson, L. Y. Chin, A. L. Fripp, and R. C. Crouch, "Finite Element Analysis of the Effect of a Non-Planar Solid-Liquid Interface of the Lateral Solute Segregation During Unidirectional Solidification", *Materials Processing in the Reduced Gravity Environment of Space*, G.E. Rindone, ed., Elsevier Science Publishing Company, Inc., New York, 1982.
7. S. R. Coriell and R. F. Sekerka, "Lateral Solute Segregation During Unidirectional Solidification of a Binary Alloy with a Curved Solid-Liquid Interface", *J. Crystal Growth*, 46, 479-482 (1979).
8. P. M. Adornato and R. A. Brown, "Convection and Segregation in Directional Solidification of Dilute and Non-Dilute Binary Alloys: Effects of Furnace Design", *J. Crystal Growth*, 80, 155-190 (1987).
9. T. I. Ejim, W. A. Jesser, and A. L. Fripp, "Solidification Behavior of Low and High Thermal Conductivity Materials in a Bridgman-Stockbarger Furnace", *J. Crystal Growth*, 69, 509-514 (1984).
10. P. C. Sukanek, "Deviation of Freezing Rate from Translation Rate in the Bridgman-Stockbarger Technique", *J. Crystal Growth*, 58, 208-218 (1982).
11. T. W. Clyne, "Heat Flow in Controlled Directional Solidification of Metals", *J. Crystal Growth*, 50, 684-690 (1980).

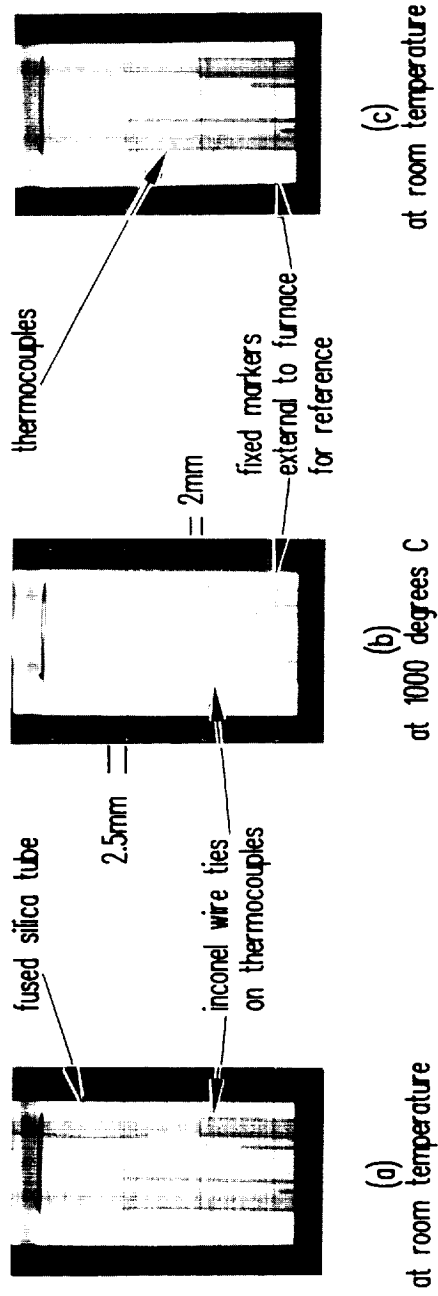


FIGURE 1. X-ray image of thermocouple movement due to temperature change. Six thermocouples were placed circumferentially in grooves on a fused silica tube. All thermocouples were tied to the tube with inonel wire. Three were additionally bonded with ceramic cement. Figure 1a is an X-ray image taken before heating. Figure 1b is an image taken at 1000 degrees C. Figure 1c is an image taken after the furnace had returned to room temperature.

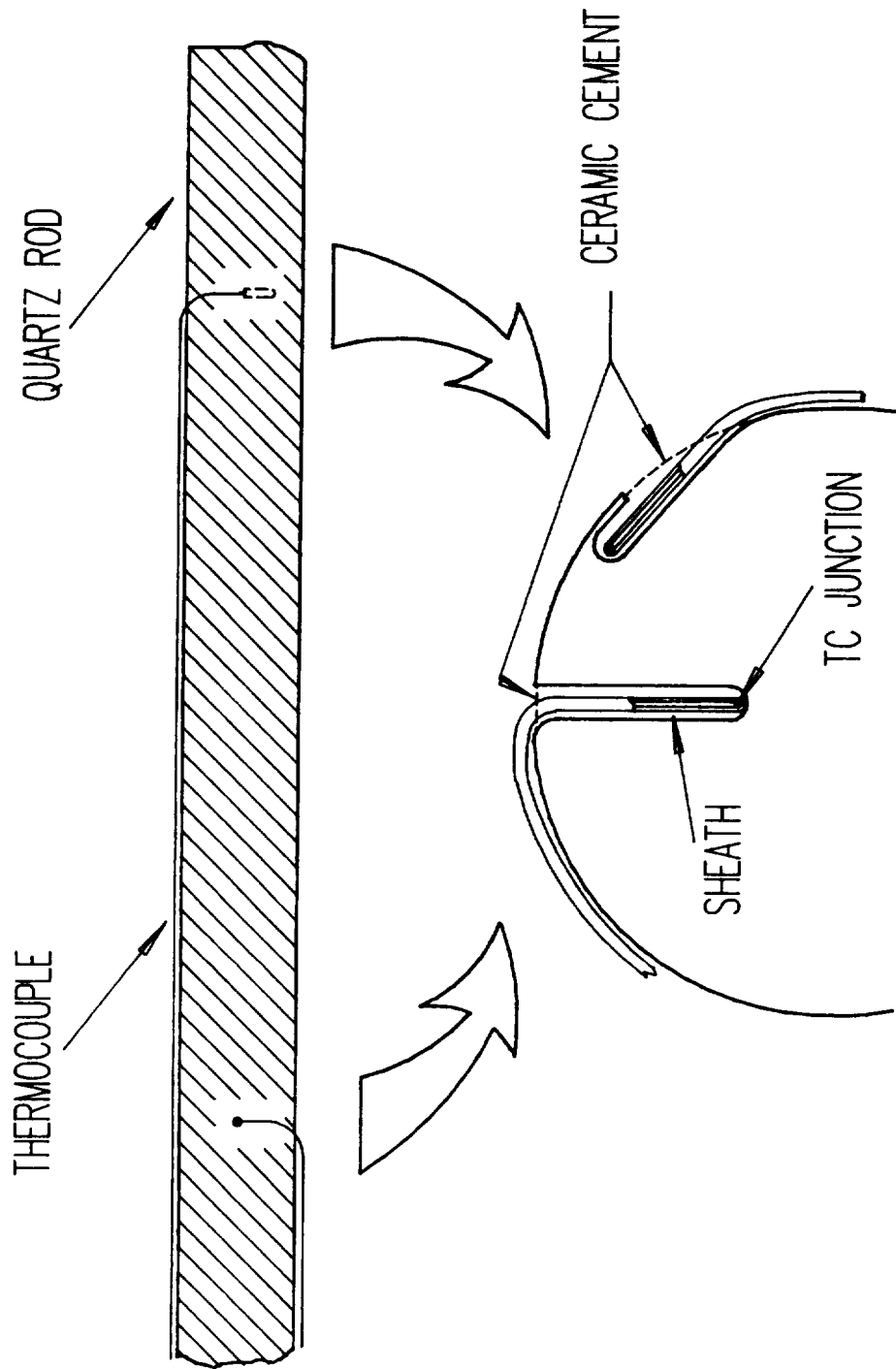


FIGURE 2. Techniques for mounting thermocouples in quartz rod.

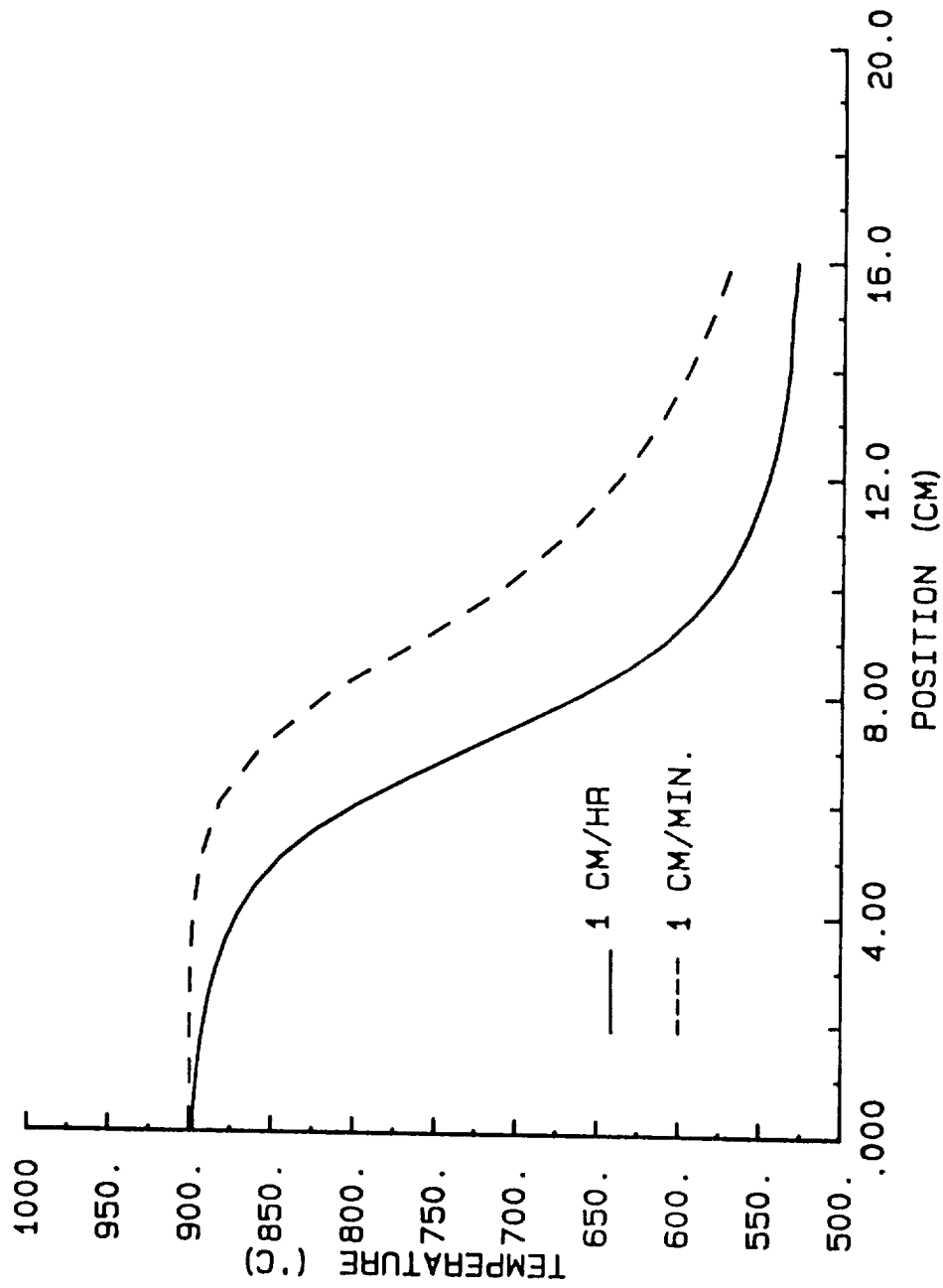


FIGURE 3. The measured temperature profile of the furnace using thermocouples attached to a quartz rod. The hot and cold zones stayed the same; only the pull rate was varied.

MICROGRAVITY NONCONTACT TEMPERATURE REQUIREMENTS AT NASA LEWIS RESEARCH CENTER

G. Santoro
National Aeronautics and Space Administration
Lewis Research Center
Cleveland, Ohio 44135

INTRODUCTION

NASA Lewis Research Center is currently supporting 66 microgravity science and applications projects. The projects consist of in-house, grant, and contract activities, or some combination of these activities, and involve the participation by personnel in the Space Experiments Division of the Space Flight Systems Directorate and the Materials Division and the Structures Division of the Aerospace Technology Directorate. The Engineering Directorate sometimes provides assistance in the design and fabrication of the in-house hardware efforts associated with these activities. The management structure is shown in figure 1. The 66 projects are separated into 23 flight projects and 43 ground-based projects.

The part of the NASA Lewis program dealing with flight experiments is divided into six areas: Combustion Science, Materials Science, Fluid Physics, Instrumentation/Equipment, Advanced Technology Development, and Space Station Multi-User Facility studies. Table I lists the flight projects and provides other pertinent information. The Advanced Technology Development, of which Noncontract Temperature Measurements is one such project, and Space Station Multi-User Facility are not science studies and will not be discussed in this presentation. For the flight projects, ground-based work is required to better define the experiment, develop and check out the flight hardware, and to provide a 1-g data base for comparison.

The part of the NASA Lewis program dealing with ground-based experiments is coincidentally also divided into six areas: Electronic Materials, Combustion Science, Fluid Dynamics and Transport Phenomena, Metals and Alloys, Glasses and Ceramics, and Physics and Chemistry Experiments. Several purposes exist for ground-based experimenting. Preliminary information is necessary before a decision can be made for flight status, the short low gravity durations available in ground facilities are adequate for a particular study, or extensive ground-based research must be conducted to define and support the microgravity science endeavors contemplated for space. Knowledge of gravity related effects in the ground-based projects (i.e., in a suborbital setting) is obtained by conducting experiments in drop tower facilities or aircraft. Low gravity durations of up to 20 sec are available using these facilities. Table II lists the ground-based projects.

Not all of the 66 microgravity science and application projects at NASA Lewis have temperature requirements, but most do. Since space allocation does not permit a review of all the pertinent projects, a decision was made to restrict the coverage to the science flight projects, flight projects minus the advanced technology development and multiuser facility efforts. Very little is lost by this decision as the types of temperature requirements for science flight projects can be considered representative of those for the ground-based projects. This paper then will

discuss the noncontact temperature needs at NASA Lewis, as represented by the science flight projects, by describing briefly the experiments themselves, by displaying an illustration of each experimental setup, and by specifying their temperature requisites.

FLIGHT PROJECTS

The 12 science flight projects are listed in table I and are separated into three areas: Combustion Science, Materials Science, and Fluid Physics. All of these projects contain temperature requirements, except for Droplet Combustion, and some have comments on desired or future temperature requirements. The Droplet Combustion project is an example where temperature requirements were deleted for lack of a ready technique to make the desired measurements.

Combustion Science

Solid surface combustion. - The overall objective of this project is to determine the mechanism of gas-phase flame spread over solid fuel surfaces in the absence of buoyancy-induced or externally imposed gas-phase flow in order to improve the fire safety aspects of space travel. To achieve this objective, measurements are made of the flame spread rate, solid and gas-phase temperature, and flame shape for steady flames spreading over paper and polymethylmethacrylate in a low gravity environment. Figure 2 illustrates the experimental hardware.

Temperatures are measured by small diameter (5 mils) type R thermocouples placed in both the gas and solid phases. Temperatures ranging from 250 to 1000 K are anticipated with a required accuracy of ± 0.5 percent.

Particle cloud combustion. - The objective of the research in this project is to determine the characteristics of flame propagation and extinction for quiescent, uniform clouds of particles. Particle clouds are of practical interest since they occur in coal mine and grain storage fires. The study of particles equal to or greater than 30 μm in normal gravity is compromised by the inability to provide the necessary stationary experimental conditions prior to combustion initiation. Even if these required experimental conditions were accessible at 1-g, free convection effects would be expected to dominate the underlying flame propagation mechanisms. However, experiments in low gravity will permit uniform, turbulence free clouds of combustible particulates to be established and maintained prior to the initiation of combustion. A low gravity environment will also permit the observation of flame propagation through and extinction by uniform particulate clouds wherein molecular conduction and radiative transport (rather than free convection) will be the dominant heat transfer mechanisms.

Only the pretest temperature will be measured to insure an uniform ambient temperature of 294 ± 6 K through each combustion tube, see figure 3. A typical propagation speed is 50 cm/sec, making temperature measurements after ignition a problem.

Droplet combustion. - The goal of this project is to determine the burning rates, disruption, and extinction mechanisms and chemical reaction rates of liquid fuel droplets burning at various oxygen concentrations and pressures under conditions of negligible buoyancy. These experiments will serve as large scale simulations of microscopic fuel droplets burning in ground based propulsion and power

generation systems. The delivery to and ignition of a test droplet at a prescribed test site is required. The droplet must be unconstrained mechanically and nearly motionless to achieve spherical symmetry while the droplet burns. Figure 4 illustrates the experimental hardware.

This project has no temperature requirements but desirable would be nonintrusive temperature determination of the gases surrounding the burning droplet. The profile is estimated to vary typically from 400 K at the droplet surface to perhaps 2300 K at the flame front. For typical droplets of 1 to 3 mm in diameter the corresponding flame front would be 5 to 20 mm in diameter. The droplets move typically from 2 to 10 mm/sec. Both the droplet and its flame front are proportionally diminishing with time by the d^2 law throughout the test. Additionally a soot shell in the region between the droplet and flame may interfere with measurements internal to the shell, yet outside the droplet. If the above temperature measurements were possible, an accuracy of just ± 50 K would suffice.

Gas jet diffusion flames. - The overall objective of this project is to gain a better fundamental understanding of the effect of buoyancy on laminar gas jet diffusion flames which will aid in defining the hazards and control strategies of fires in space environments, as well as improve the understanding of earthbound fires. To achieve this objective, measurements will be obtained from low gravity experiments that will include flame shape development, flame extinction, flame color and luminosity, temperature distributions, species concentrations, radiation, pressure, and acceleration. These measurements will be used to validate a transient numerical model which reflects current understanding of the important phenomena which control gas jet diffusion flames. See figure 5 for an illustration of the experimental arrangement and flame behavior at normal and low gravity.

Temperatures are measured by a rake of nine thermocouples arranged above the flame jet in three layers with three thermocouples per layer. These sensors are 2 cm apart within each layer with 3 cm between layers. The rake height above the flame is adjustable, but no specs were given. All nine thermocouples are 0.01 cm in diameter, and are type K (1523 K), except the one closest to the flame which is type S (1723 K). Flame temperatures are expected to range from 200 to 2000 K. Sampling rates will be 20 Hz or less.

Materials Science

Alloy Undercooling. - Undercooling of liquid metals provides the impetus for solidification. Once started, solidification will proceed with a release of the latent heat of fusion causing recalescence. The extent of undercooling and the cooling rate will influence the microstructure and the properties of a material. Heat removal is easily controlled in earth gravity through the use of mold materials and chills. Deep undercooling in metals, however, is beset with considerable difficulty, because solidification is easily nucleated by inclusions, impurities, contact with container walls and vibration. Nevertheless, it has been possible to effect some deep undercooling in earth gravity in very small droplets or in contact with a rotating chilled surface (melt spinning). In these instances, rapid heat removal has been more often than not the cause of undercooling, because it could, for a very short time interval, suppress nucleation. In microgravity it is possible to segregate the effects of the rate of heat removal and of nucleation on solidification. The desired undercooling will be obtained by levitating droplets of nickel and iron alloys, melting them by induction and then allowing them to cool and

solidify while still positioned in an electromagnetic levitator. During this process, temperature measurements and visual observations will be made. Subsequent metallographic examination will compare the microstructure of materials processed and undercooled in microgravity with materials undercooled in earth gravity. See figure 6 for an illustration of the procedure.

Data to be obtained and compared include temperature-time traces for characterization of cooling rates, recalescence and, solidification; surface and cross-sectional microstructures for nucleation sites, grain and dendrite morphologies; and high-speed photography for observation of the recalescence and progression of solidification. The levitated molten specimen will be between 5 and 8 mm in diameter. Temperature will be sensed by two color pyrometry, two spots 90° apart aligned on the center of the specimen. Temperatures will range from 700 to 2000 K and require an accuracy of 3 K.

GaAs crystal growth. - Improving the homogeneity and purity of GaAs are two major goals of current research by the GaAs crystal growth community. It has been shown that buoyancy-driven convection plays a major role in observed dopant segregation and dislocation formation in GaAs crystals. The objective of this study is to define the magnitude of the effects of buoyancy-driven convection on the quality of melt-grown GaAs. This will be accomplished by conducting a comparative study of GaAs crystals grown from melt with differing degrees of convective flow: growth of the crystal in 1-g (maximum convection), in 1-g with an applied magnetic field (damped convection), and in microgravity aboard the Space Shuttle (minimum convection). All the space and ground-based growth experiments will be performed in a specially designed growth ampoule and furnace system with an electronically-controlled gradient, see figure 7. Both doped and undoped GaAs will be grown. Two impurities, silicon dissolved from the silicon dioxide ampoule and deliberately-introduced selenium, will be studied. The important phenomena to be addressed by the characterization include the effect of convection on the nature, concentration, and homogeneity of unintentionally introduced defects and intentionally introduced dopants, as well as the effect of convection on the electrical and optical properties of GaAs. A numerical model of the fluid flow patterns in melts will be constructed.

The space-growth experiment will be flown in a Get-Away-Special canister. Two regrown boules of selenium-doped GaAs, 1 in. in diameter and 4 in. long, will be regrown during nominal 6 hr, low g periods in the gradient furnaces. Power will be supplied by self-contained alkaline batteries. Temperature will be monitored at six locations outside of each of the growth ampoules. The relationship between these temperatures and the desired temperature gradient of the crystal will be established by trial and error. A 60 K gradient will be established over the 3 in. molten zone of the crystal. The melting point of GaAs is 1511 K. The cooling rate controlling the single crystal growth will be linearized by the microprocessor control system. Temperature, acceleration and selected housekeeping data will be acquired and stored during the growth of each crystal. Nonintrusive determination of the crystal core and radial temperatures would be desirable, but are not part of this project.

Isothermal dendritic growth. - This project will test fundamental assumptions concerning dendritic solidification of molten metals and provide mathematical models describing important aspects of that process. Since virtually all industrial alloys solidify dendritically, correct models could lead to improved

earth-based industrial production of alloys such as steel and aluminum. Specifically, the project will provide precise quantitative data relating dendrite growth velocity, tip radius, and side branch spacing to melt undercooling, to material physical properties, and to acceleration (g levels). To permit direct visualization of dendritic growth, succinonitrile (SCN) will be used in the experiment. SCN is a transparent body-centered cubic crystalline material that solidifies dendritically in a manner similar to iron.

Precise temperature measurements of the isothermal test volume is required, an accuracy of ± 0.002 K. Such accuracies dictate the use of thermistors as the sensors.

Figure 8 illustrates the experimental arrangement.

Fluid Physics

EMD flow in metals. - The purpose of the Electromagnetically Driven Flow in Metals project is to develop an improved fundamental understanding of electromagnetic, heat and fluid flow phenomena in levitation melted (positioned) metallic specimens under both normal gravity and microgravity conditions. The principal components of this research are the calculation of the transient heat and fluid flow phenomena in levitation-melted specimens; the calculation and measurement of three-dimensional turbulent recirculating flow phenomena; and the prediction and measurement of pulsed flow phenomena in electromagnetically stirred melts.

Gold alloys and silver have proven to be suitable metals on which to measure electromagnetic flow. The molten spherical specimen will be about 10 mm in diameter. Temperatures in the range of 700 to 1500 K will be measured by an optical pyrometer to an accuracy of 0.5 percent of the reading. The temperature measurement rate will be 1 per second. Figure 9 schematically depicts the experimental layout.

Surface tension driven convection. - Materials processing involving solidification and crystal growth is expected to be dramatically improved in the microgravity of space. However, changes in the nature and extent of thermocapillary flows can cause deleterious fluid oscillations. Thermocapillary flow is fluid motions that are generated by the surface-tractive force induced by surface tension variation due to the temperature gradient along the free surface. Numerical modeling is not adequate to predict oscillations due to an inherent coupling among the imposed thermal signature, surface flow, and surface deformation. Therefore, to complete an understanding of the physical process and to develop an accurate numerical model, experimental data must be obtained in the extended low gravity environment. This project will supply the necessary data. The experiment consists of a container 4 in. in diameter and 2 in. deep filled with silicone fluid, see figure 10. The design can provide both a flat and a curved free surface which can be centrally heated either externally or internally. The cross section is illuminated by a sheet of light that is scattered by micron size alumina particles in the silicone oil allowing the observation of the resulting thermocapillary flows.

The liquid bulk temperature will be measured at six specified points using thermistors. The bulk temperature range will be from 298 to 473 K with a required accuracy of plus or ± 0.1 K. A full field surface temperature gradient measurement is specified using infrared thermography. The surface temperature range will be from 298 to 473 K with a required accuracy of ± 5 percent of the delta temperature (60 K). A surface temperature resolution of 1 mm^2 is needed. The desired set of temperature specifications include noncontact full field bulk measurements with

accuracies comparable to thermistors, higher resolution quantitative thermography with accuracies greater than presently available, and two color full field infrared thermography to eliminate emissivity dependence.

Critical fluid light scattering. - The proposed experiment will measure the decay rates and correlation lengths of density fluctuations in xenon at its critical density as a function of temperature. This will be achieved by using laser light scattering (correlation spectroscopy) and turbidity measurements, see figure 11. The goal of the experiment is to measure the fluctuation decay rate and correlation length at temperatures very near to the critical temperature, which could be as close as 100 μ K if the residual gravity level is low enough. Such experiments are severely limited on earth because the gravitational field causes large density gradients in the sample due to the divergence of the compressibility of the gas as the critical temperature is approached.

The experiment concept requires the automatic location, within 20 μ K, of the critical temperature of xenon at its critical density. Light transmission and fixed-angle scattering intensities will be measured at controlled temperatures, within 3 μ K, in the range 1 K to 100 μ K above the critical temperature. The control system will calculate and store the turbidity and correlation functions at each temperature. These data will be used during postflight analysis to determine the density, fluctuation decay rates and correlation lengths near the critical temperature. Temperatures within the liquid and gas phase will be measured with thermistors with lock-in amplifiers. Precision and resolution will be in the vicinity of micro Kelvin. It would be desirable, although not very feasible, to have a noncontact three dimensional point measurement device with the above precision.

Pool boiling. - The goal here is to experimentally determine the effect of heat flux and liquid subcooling on nucleate pool boiling in a long term reduced gravity environment using Freon R-113 as the test fluid. An analytical study will be made of the onset of nucleate boiling, bubble growth and collapse, bubble motion, and heat transfer characteristics. Small thermocouples or thermistors will be located at various positions within the Freon chamber to measure the uniformity of the fluid (± 0.22 K) and variations associated with the boiling process taking place on the heater surface. The test fluid temperature will range from 311 to 339 K and will need to be measured with an accuracy and a resolution of 0.06 K. Figure 12 illustrates the apparatus for this experiment.

Critical fluid viscosity measurement. - The purpose of the project is to produce archival viscosity data on xenon closer to its liquid-vapor fluid critical point than is possible in 1-g due to the strong density gradient arising from the singular compressibility of the fluid near the critical point and the hydrostatic head from gravity. The data will provide complementary results with the Critical Fluid Light Scattering project to test the mode coupling theory of critical phenomena and provide guidance to renormalization group theory development on dynamic critical point fluid behavior.

The apparatus concept (see figure 13) currently centers on a torsional viscometer with a filled 1 mm deep by 10 mm radius cylindrical fluid cavity in a bob suspended by a fine quartz fiber. The bob is excited into torsional motion by capacitance vanes and the viscous damping is recorded through amplitude decay by the same vanes. Magnetic bearings are used to eliminate nontorsional motions and maintain constant tension on the quartz fiber. The task requires a few micro Kelvin temperature controls and vibration isolation sufficient to approach the critical temperature to within 300 μ K while measuring viscosities to 0.5 percent precision.

The temperature specifications for this project are the same as with the Critical Fluid Light Scattering project and the noncontact temperature desires are also the same.

SUMMARY OF RESULTS

Although the temperature needs of none of the 43 ground-based projects have been discussed, they cover many of the same discipline areas as the flight projects so that in general the needs of one set of projects can be used to represent those of the other. Many of the temperature requirements of both sets of projects can be completely satisfied with contact devices, thermocouples and thermistors, but a need has been shown for noncontact temperature techniques. As has been shown, the temperatures range from below ambient to those generated by combustion. Accuracies and precisions vary from a few degrees to a few thousandth of a degree. Extremely accurate point measurements are required in some cases while the full field temperature is desired if not actually measured. The spectrum of conditions for temperature in microgravity experiments possesses a challenge to the designers of temperature measuring instruments. Also it has been shown that it is desirable to have noncontact temperature measuring techniques so as not to interrupt the delicately balanced processes encountered when investigating effects of microgravity. The lack of noncontact type instruments for measuring accurate temperature, point and full field, has led investigators to by-pass the problem, but at the expense of more meaningful data.

TABLE I. - FLIGHT PROJECTS

Projects	Principal investigator/ affiliation	Lewis project manager Project scientist	Carrier
Combustion science			
Solid Surface Combustion (SSCE) Particle Cloud Combustion (PCCE) Droplet Combustion (DCE) Gas Jet Diffusion Flames (GDF)	Altenkirch/U Kentucky Berlad/UCSD Williams/Princeton Edelman/SAIC	Zavesky/Olson Siegert/Ross Haggard/Haggard Stocker/Stocker	Middeck; Spacelab (a) Middeck; Spacelab GroundProgram
Materials science			
Alloy Undercooling (AUE) GaAs Crystal Growth (GaAs) Isothermal Dendritic Growth (IDGE)	Flemings/MIT Kafalas/GTE Glicksman/RPI	Harf/Harf Lauver/Lauver Winsa/Winsa	(a) GAS MSL; Spacelab
Fluid physics			
EMD Flow in Metals (EMDF) Surface Tension Driven Convection (STDC) Critical Fluid Light Scattering (CFLSE) Pooling Boiling (PBE) Critical Fluid Viscosity	Szekely/MIT Ostrach/CWRU, Gammon/U Maryland Merte/U Michigan Moldover/NBS	Harf/Harf Jacobson/Jacobson Lauver/Wilkinson Zavesky/ Chiaromonte Lauver/Wilkinson	(a) Spacelab MSL GAS MSL
Instrumentation			
Space Acceleration Measurement System (SAMS)	Chase/Lewis	Delombard/Chase	Middeck; Spacelab MSL
Advanced technology development (ATD)			
Microgravity Fluids and Combustion Diagnostics (MFCD) High-Temperature Furnace Technology (HTFT) High-Resolution, High-Framer-Rate Video Technology (HHVT) Reactionless Microgravity Mechanisms and Robotics (RMMR) Vibration Isolation Technology (VIT) Noncontact Temperature Measurement (NCTM) Laser Light-Scattering Instrument (LLSI)		Santoro/Greenberg Rosenthal Metzinger/Butcher Rohn Lubomaki Santoro Meyer	
Space station multiuser facilities			
Modular Combustion Facility (MCF) Fluid Physics and Dynamics Facility (FPDF) Modular Containerless Processing Facility (MCPF)		Thompson/Sacksteder Thompson/Salzman Glasgow	

^aTo be determined.

TABLE II. - GROUND-BASED PROJECTS

Projects	Principal investigator/ institution	Lewis project manager/ project scientist
Electronic materials		
CVD Silicon Deposition Opto-Electronic Materials Crystal Growth	Stinespring/Aerodyne Hopkins/Westinghouse Duval/Lewis	Glasgow/Santoro Glasgow/Duval Glasgow/Duval
Combustion science		
Pool Fires: Modeling Pool Fires: Preignition Process Smoldering Combustion Particle Cloud Combustion Computational Studies of Flames Fuel Droplet Vaporization Flame Spreading Over Solids in Forced Flows Flame Spreading in Liquid Pools Complementary Activities	Sirignano/UC Irvine Ross/Lewis Fernandez-Pello, Pagni/UC Berk. Berlad/UC San Diego Oran/NRL, ONR Farrell, Peters/Wisc., GM Olson/Lewis Ross/Lewis Lewis	Salzman/Ross Salzman/Ross Salzman/Olson Salzman/Ross Salzman/Ross Salzman/Stocker Salzman/Olson Salzman/Ross Salzman/Olson, Ross Salzman/Sacksteder, Stocker Salzman/Friedman
Radiative Ignition	Kashiwagi/NIST	Salzman/Friedman
Fluid dynamics and transport phenomena		
Transport Processes In-House No-Slip Boundary Condition Thermodiffusocapillary Phenomena In-House EM Driven Flow in Salts Thermocapillary Convection Pool Boiling Capillary Containment Suppression of Marangoni Convection Capillary Convection Benard Stability	Kassem, Wilkinson/Lewis; Wang/NRC Pettit/Los Alamos Chai, McQuillen/Lewis; Balasubramaniam/CWRU Szekely/MIT Neitzel, Jankowski/ U Arizona Merte/U Michigan Steen/Cornell Dressler/GWU Yang/U Michigan Koschmieder/U Texas	Salzman/Wilkinson Salzman/Wilkinson Salzman/Chai Salzman/Harf Salzman/Chai Salzman/Chiaromonte Salzman/Chai Salzman/Salzman Salzman/Chai Salzman/Salzman
Metals and alloys		
Bulk Undercooling Studies Metal Undercooling Channel Segregation Macrosegregation of Alloys Liquid-Phase Sintering Theory of Solidification Microsegregation of Alloys Whisker Growth Float Zone Modeling Mg-Alloy Composites Process Modeling	Laxmanan/Lewis, CWRU; deGroh/Lewis Perepezko/U Wisconsin Hollawell/MTU Poirier/U Arizona German/RPI Davis/Northwestern Tewari, Chopra/CSU Hobbs/GWU Young/Akron Cornie, Szekely/MIT Chait/Lewis	Glasgow/Glasgow Glasgow/deGroh Glasgow/Chait Glasgow/Chait Glasgow/Santoro Glasgow/Chait Glasgow/Glasgow Glasgow/Westfall Glasgow/Chait Glasgow/Harf Glasgow/Chait
Glasses and ceramics		
Slip Casting Colloidal Suspensions Combustion Synthesis Foaming in Glass Powder Agglomeration Phase Separation Single-Crystal Fiber Growth	Debenedetti, Russel/Princeton Behrens/LANL, Hurst/Lewis Hrma/CWRU Cawley/OSU Hyatt/Lewis Levine/Lewis	Levine/Fiser Levine/Hurst Levine/Jaskowiak Levine/Fox Levine/Levine Levine/Levine
Physics and chemistry experiments (PACE)		
Electrohydrodynamics Critical Point Viscosity Measurement Mass Transport	Saville/Princeton Moldover/NIST Dewitt/U Toledo	Salzman/Chai Salzman/Wilkinson Salzman/Chai

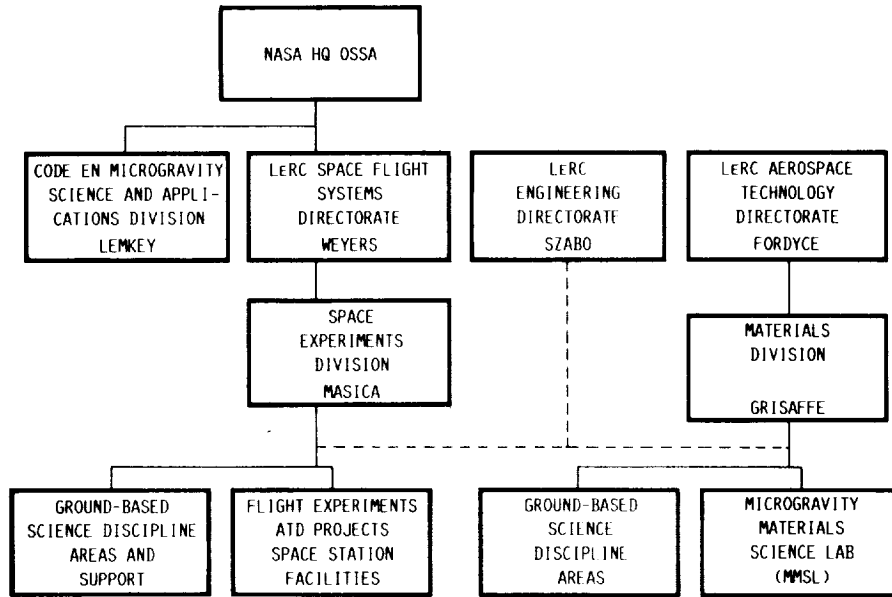
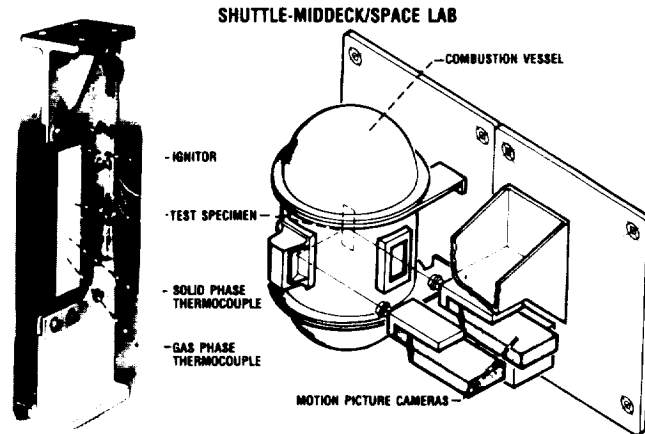


FIGURE 1. - LERC MICROGRAVITY SCIENCE APPLICATIONS PROJECT MANAGEMENT STRUCTURE.



A STUDY OF THE MECHANISMS OF GAS-PHASE FLAMES SPREADING OVER SOLID FUELS IN QUIESCENT ENVIRONMENTS.

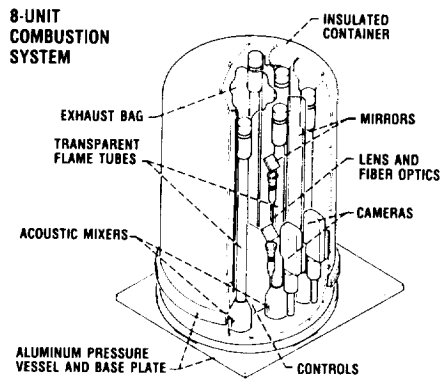
P I : PROF. ROBERT A. ALTENKORCH
MISSISSIPPI STATE UNIVERSITY

CD-88-34499

LERC CONTACTS
P S : SANDRA L. OLSON
P M : RALPH J. ZAVESKY

FIGURE 2. - SOLID SURFACE COMBUSTION EXPERIMENT.

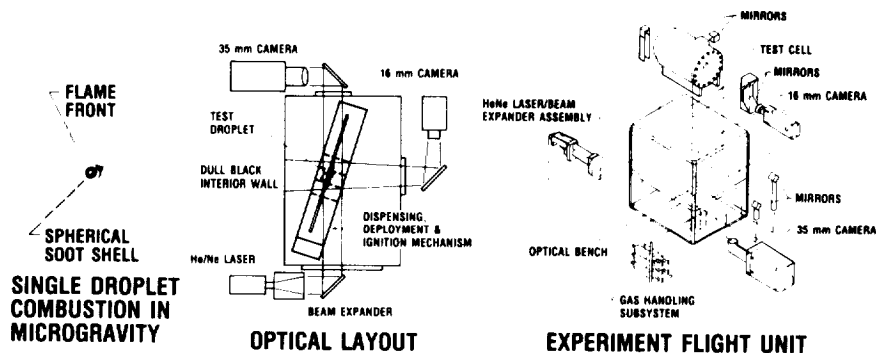
**A STUDY OF FLAME PROPAGATION AND EXTINCTION LIMITS FOR
UNIFORM AND QUIESCENT MIXTURES OF PARTICULATE FUELS IN AIR**



P.I. PROF. ABRAHAM L. BERLAD
UNIVERSITY OF CALIFORNIA-SAN DIEGO

LeRC CONTACTS
P.S. HOWARD D. ROSS
P.M. CLIFFORD E. SIEGERT
CD-88-31247

FIGURE 3. - PARTICLE CLOUD COMBUSTION EXPERIMENT - SPACE SHUTTLE-BAY.

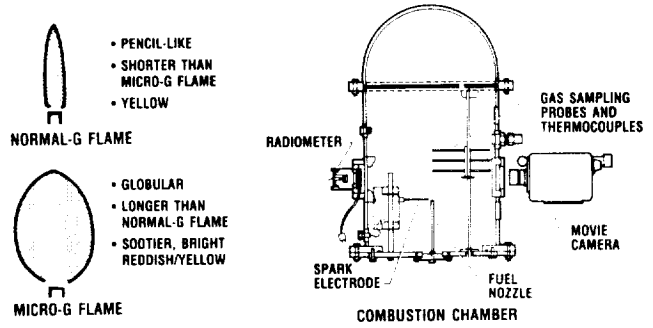


**DEVELOPMENT AND VERIFICATION OF A MATHEMATICAL MODEL FOR DROPLET
BURNING RATES AND CRITICAL DROPLET EXTINCTION DIAMETERS**

P.I.'S: PROF. FORMAN A. WILLIAMS
PROF. FREDERICK L. DRYER
PRINCETON UNIVERSITY

LeRC CONTACT:
JOHN B. HAGGARD, JR.
CD-88-31248

FIGURE 4. - DROPLET COMBUSTION EXPERIMENT - SPACE SHUTTLE-MIDDECK, SPACELAB.



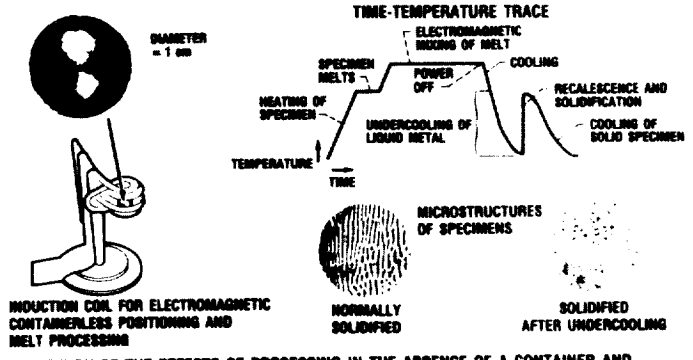
A STUDY OF FLAME-LIMITING MOLECULAR DIFFUSION PROCESSES IN THE ABSENCE OF BUOYANCY DRIVEN CONVECTION

P.I. DR. RAYMOND EDELMAN
DR. YOUSEF BAHADORI
SCIENCE APPLICATIONS INTERNATIONAL CORP.

LRPC CONTACT
DENNIS P. STOCKER

CS 88-31042

FIGURE 5. - GAS JET DIFFUSION FLAMES EXPERIMENT.



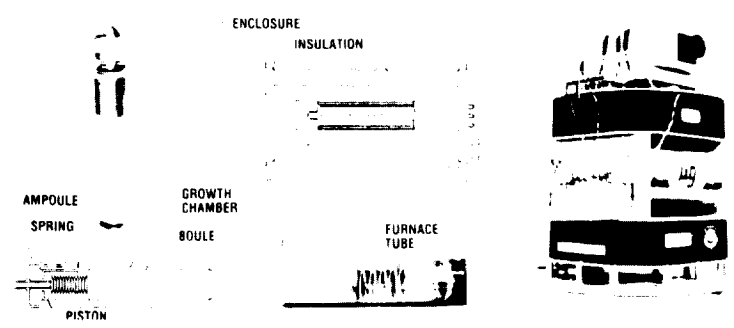
A STUDY OF THE EFFECTS OF PROCESSING IN THE ABSENCE OF A CONTAINER AND CONVECTION ON THE STRUCTURE AND PROPERTIES OF METAL ALLOYS (FIRST FLIGHT JANUARY 12-18, 1986; MSL-2, STS 61-C)

P.I. PROF. MERTON C. FLEMINGS
DR. YUH SHONARA
MASSACHUSETTS INSTITUTE OF TECHNOLOGY

LRPC CONTACT
FREDRIC H. HART

CS 88-3008

FIGURE 6. - ALLOY UNDERCOOLING EXPERIMENT - SPACE SHUTTLE-SPACE STATION.



A COMPARATIVE STUDY OF THE INFLUENCE OF BUOYANCY DRIVEN FLUID FLOW ON GaAs CRYSTAL GROWTH IN LOW-G AND SELECTED NORMAL GRAVITY ENVIRONMENTS

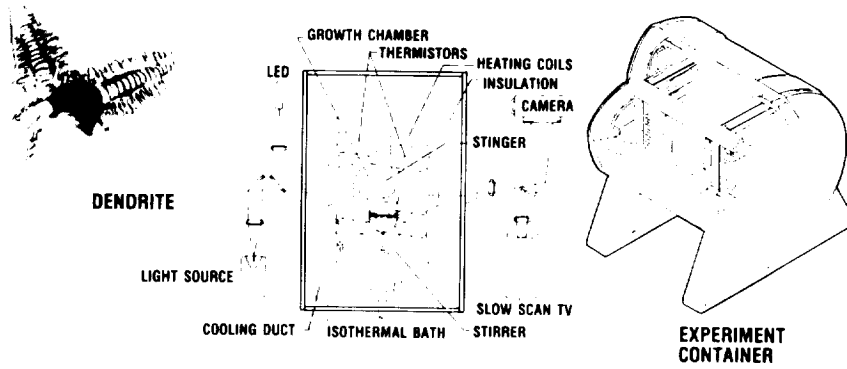
JOINTLY FUNDED: GTE, AFML, NASA

P.I. JAMES A. KAFALAS
GTE LABORATORIES, INC.

LRPC CONTACT
RICHARD W. LAUVER

CS 88-30632

FIGURE 7. - GaAs CRYSTAL GROWTH EXPERIMENT - GET AWAY SPECIAL PAYLOAD.



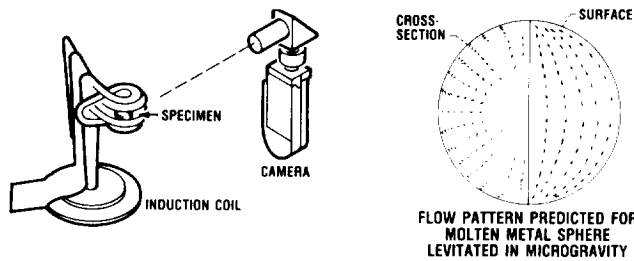
DEVELOPMENT AND VERIFICATION OF A MATHEMATICAL MODEL RELATING DENDRITE GROWTH RATES AND TIP RADII TO TIP UNDERCOOLING

P.I.: PROF. MARTIN E. GLICKSMAN
RENSSELAER POLYTECHNIC INSTITUTE

CD-88-34408

LeRC CONTACT:
EDWARD A. WINSA

FIGURE 8. - ISOTHERMAL DENDRITIC GROWTH EXPERIMENT - SPACE SHUTTLE, MSL.



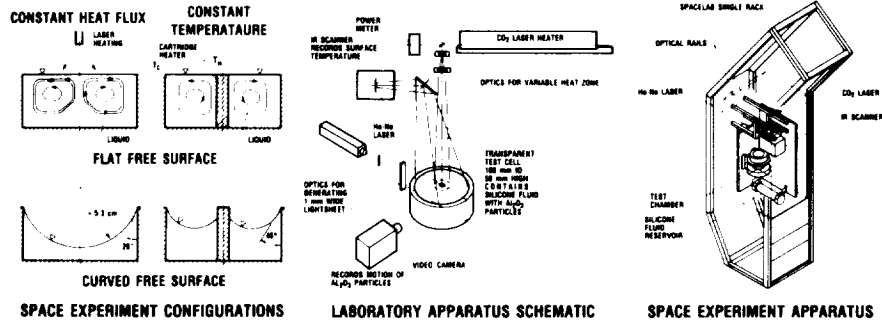
A STUDY OF THE CHARACTERISTICS OF ELECTROMAGNETICALLY DRIVEN FLOW GENERATED IN MOLTEN METALS IN THE ABSENCE OF GRAVITY INDUCED CONVECTION

P.I.: PROF. JULIAN SZEKELY
MASSACHUSETTS INSTITUTE OF TECHNOLOGY

CD-88 31043

LeRC CONTACT:
FREDRIC H. HARF

FIGURE 9. - ELECTROMAGNETICALLY DRIVEN FLOW EXPERIMENT - SHUTTLE OR SOUNDING ROCKET.



NUMERICAL DEVELOPMENT AND EXPERIMENTAL VERIFICATION OF THERMOCAPILLARY FLOW IN REDUCED GRAVITY

P.I.: PROF. SIMON OSTRACH
PROF. YASUHIRO KAMOTANI
CASE WESTERN RESERVE UNIVERSITY

CD-88 31618

LeRC CONTACT:
THOMAS P. JACOBSON

FIGURE 10. - SURFACE TENSION DRIVEN CONVECTION EXPERIMENT - SPACELAB.

Marshall Space Flight Center
Non-Contact Temperature Measurement Requirements

D. B. Higgins, W. K. Witherow

The Marshall Space Flight Center is involved with levitation experiments for Spacelab, Space Station, and drop tube/tower operations. These experiments have temperature measurement requirements, that of course must be non-contact in nature. The experiment modules involved are the Acoustic Levitator Furnace(ALF), and the Modular Electromagnetic Levitator(MEL). User requirements for the MEL are being covered separately, and will not be covered here. This paper will focus on user requirements of the ALF and drop tube. The center also has temperature measurement needs that are not microgravity experiment oriented, but rather are related to the propulsion system for the STS. This requirement will also be discussed.

The research objective of the ALF is to quantify the extent of enhancement of glass formation under containerless low-g conditions. Each experiment will involve the containerless melting and resolidification of a glass forming composition several times at numerous cooling rates. A typical experiment would involve 5 to 10 samples, melted and cooled at 5 to 10 different cooling rates ranging from $0.1^{\circ}\text{C}/\text{sec}$ to $20^{\circ}\text{C}/\text{sec}$. This cooling rate range is based on $\text{Ga}_2\text{O}_3\text{-}43\text{CaO}$. Secondary experiments will include determination of the maximum quench rate possible, and rates as high as $250^{\circ}\text{C}/\text{sec}$ will be attempted. A typical experiment timeline is outlined in figure 1. Figure 2 illustrates a hypothetical scenario in which it is discovered that glass formation is greatly enhanced under microgravity conditions.

The temperature of the ALF furnace will range from 400 to 1750°C , with temperature control accuracy of $\pm 3^{\circ}\text{C}$. The sample heating rate will be at least $2^{\circ}\text{C}/\text{sec}$, with higher rates preferred. The furnace atmospheres are nitrogen,, argon, oxygen, and mixtures of these gases.

For the critical glass formation experiment, the knowledge of the time and temperature of nucleation and crystallization is crucial. Thermocouples placed near the sample could provide near real temperature data at slow cooling rates. At higher cooling rates however, where thermal models are not as valid, radiation pyrometry will be necessary to determine the actual sample temperature. The pyrometer should operate at a wavelength that is opaque to the sample to prevent problems with variable emissivity of semitransparent materials. Refractory oxides are generally transparent at visible and near infrared wavelengths. A calibration curve for the

optical pyrometer could be obtained by running one sample with a thermocouple embedded in the sample.

Two pyrometry systems are planned for the ALF, thermal imaging pyrometry and single spot optical pyrometry. The thermal image pyrometer assumes black body conditions, and calibration will be accomplished by sample temperature measurement in duplicate flight hardware. This system will provide two orthogonal views of the sample, operate at visible wavelength, and have a temperature resolution of 1° . The absolute accuracy, assuming black body conditions, will be $\pm 5^{\circ}\text{C}$. The nominal measurement rate is 1/sec, with a fast burst rate of 10/sec for 1 second.

The single spot system will provide two orthogonal views. The wavelength will be sample dependent, but will be greater than $4.5\ \mu\text{m}$. Resolution will be 1°C , which is acceptable in the temperature range of 400 to 1750°C . The measurement rate will be up to 100/sec.

Required digital data will include process identification, sample number, processing time, furnace thermocouple temperatures, noncontact sample temperature, heating/cooling rates, gas quench flow rates, acoustic power levels, and acoustic phase information.

The drop tube is a facility at MSFC in which samples are dropped to simulate micro-g. The drop tube is 350-foot-long and samples fall in vacuum for 4.6 seconds. There are view ports every 24 feet along the length of the tube. The drops are typically opaque metallic samples filled with a gas. The gases are helium, argon, air, or mixtures of helium/hydrogen or air/hydrogen. Typically, the drop tube is run with a vacuum of 10^{-6} Torr or with a helium atmosphere with up to 6% hydrogen.

In drop tube experiments at MSFC, noncontact temperature measurements of the falling drops are required in order to determine undercooling and solidification process parameters. The drops are levitated and melted at the top of the drop tube facility. Since it is important to know the complete thermal history of the drop, the temperature is measured to determine how far above the melting point of the material it was heated, and at what temperature the drop is released. Then temperature measurements are required of the drop as it undercools during its fall and during recalescence.

The ideal instrument to measure the temperatures at the drop tube facility would have a measurement range of 800 to 3000°C with a resolution of 1°C . The optimum measurement rate would be 10^5 readings/sec.

In the propulsion area at MSFC there is a need for noncontact temperature measurement of the spatial and temporal surfaces of Space Shuttle Main Engine turbine blades for thermal model verifications. Contact measurement would interrupt the blade boundary layer, changing heat transfer rates.

These blades rotate at 600 revolutions per second, and have an initial acceleration of 600 revolutions/sec/sec. The blade environment will consist of a mixture of hydrogen and steam, but could also be locally oxygen rich during transient conditions. Steady state temperatures will range from 1000°R to 2000°R. Transient temperatures could range between 500 and 6000°R. Transient measurements should be continuous over 10 seconds. The required precision would be ± 10 to ± 50 °R depending on the thermal phase for model validation. The spatial resolution required is 0.2 inches.

For modeling and verification in propulsion research, confirming gas temperatures as well as those of components is necessary. This would be required in laboratory setting as well as in operating size systems. Temperature measurement is required for the solid propellant at room temperature to combustion products at steady state, from ambient pressure to 1200 psia.

The solid propellants burn around 6000°R, and the hybrids (usually solid fuel with liquid oxidizer) burn in the low 7000°R range. In past experiments thermocouples have melted after 4000°R, and the adhesives used for the thermocouples have melted at 400°R. Inserting probes into surrounding hardware has been attempted, but these probes also melted around 4500°R.

A typical combustion experiment would have a maximum burn time of 60 seconds. Measurements required include pressure, temperature, flowrate, and visual observation. For rocket plume measurements a spatial resolution of one percent for 10, 100, and 1000 micron and 10, 100, and 500 mm fields of view is required. Noncontact temperature measurement at these high temperatures is also needed for materials characterization studies for future generation booster systems.

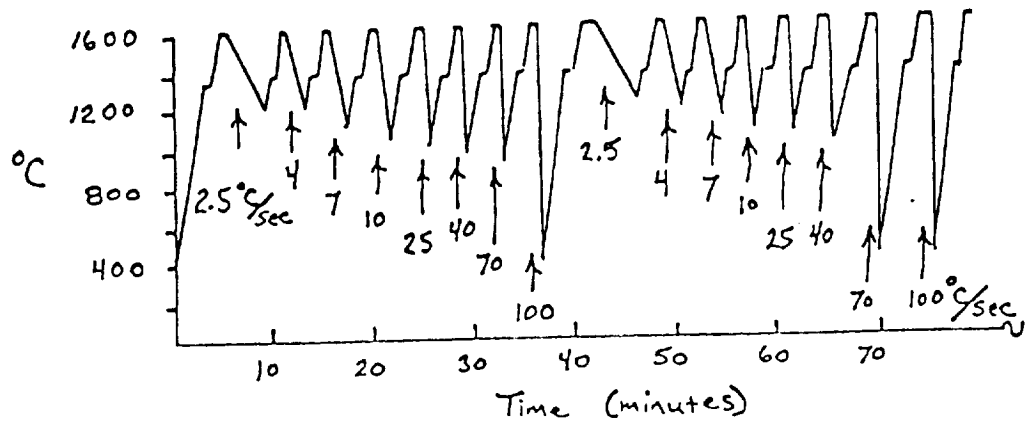
Effective noncontact temperature measurement techniques at high temperatures can therefore benefit not only the microgravity materials science disciplines, but propulsion technology as well. Those techniques developed for microgravity science may at some point be adapted to use for other technologies.

Typical Flight Experiment Timeline

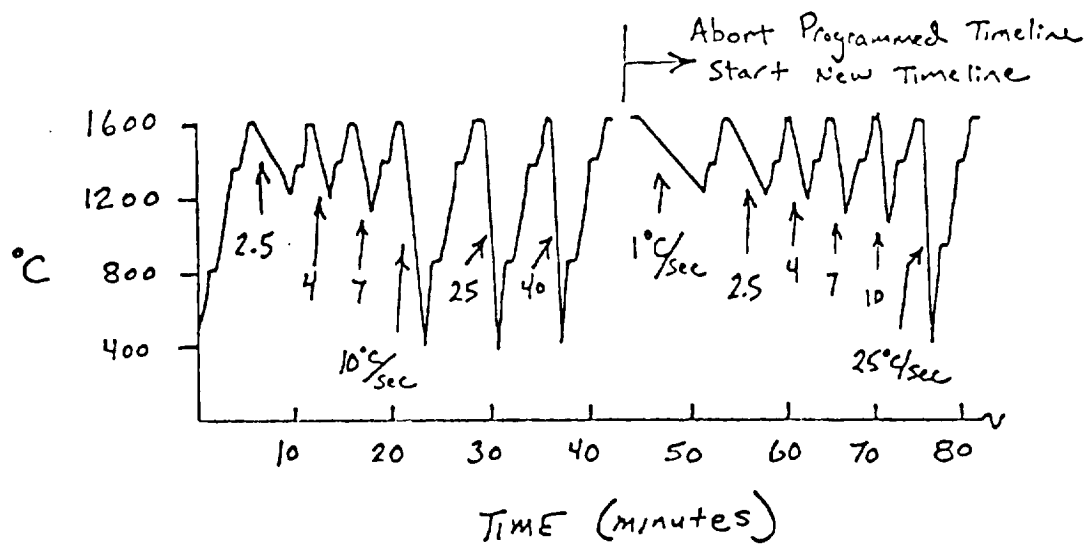
A typical hypothetical timeline for a glass formation space experiment using a reluctant glass former is shown in Figure 3 and can be summarized as follows:

1. Deploy the sample into the "cold" 400°C furnace. Initiate data collection including furnace temperature and sample temperatures at a rate of about 1 reading per second. Record the image with video having a minimum frame rate of one frame per second to verify the maintaining of containerless conditions.
2. Heat at specified heating rate (ie. 4°C/sec, 400 to 800°C, 100 sec).
3. Observe crystallization time and temperature. Video will confirm glass crystallization on heating.
4. Continue heating, past melting (which can serve as an independent temperature calibration point) to soak temperature (800 to 1600°C, 200 sec). Video sampling to confirm sample melting and containerless conditions.
5. Soak for 1 min. above critical temperature (60 sec).
6. Initiate cooling cycle. Quench at cooling rates ranging from 0.1°C/sec to 20°C/sec (faster cooling rates to 250°C/sec will be tested). Start rapid data collection (i.e. sample temperature at 1000 readings per sec.). Determine whether the sample crystallized or formed a glass from the thermal data (presence or absence of recalescence). Obtain time and temperature of crystallization from thermal data. Video is required to confirm the presence or absence of crystallization (High resolution video is desirable).
7. Either retrieve the sample or recycle the same sample again.
8. For a given sample composition perform at least 5 runs at a given cooling rate, perform 5 to 10 different cooling rates.

Figure 1



TYPICAL EXPERIMENTAL TIMELINE
HYPOTHETICAL DATA



TYPICAL EXPERIMENTAL TIMELINE, DIFFERENT HYPOTHETICAL DATA
WITH ENHANCED GLASS FORMATION, SHOWING CHANGE IN TIMELINE.

Figure 2 illustrates a second hypothetical scenario in which it is discovered that glass formation is greatly enhanced by low-g containerless processing at particular cooling rates. Telescience will allow the changing of the experimental protocol to concentrate experiments within the more useful cooling rates in order to maximize the significance of data output. In this case after a number of glass formation experiments are performed, nucleation data would be more beneficial. Effective use of telescience could greatly enhance the significance of data by concentrating on cooling rates that yield the most appropriate kinds of data.

ACKNOWLEDGMENTS:

The following individuals are gratefully acknowledged for their assistance in the preparation of this paper.

1. Edwin Ethridge, NASA/MSFC ES74, ALF requirements.
2. Ben Shackelford, NASA/MSFC EP54, propulsion requirements.
Garry Lyles, NASA/MSFC EP52, propulsion requirements.
3. Michael Robinson, NASA/MSFC ES74, drop tube requirements.
Gary Workman, University of Alabama in Huntsville, drop tube requirements.

SECTION 2

NCTM CAPABILITIES TECHNICAL PAPERS

INTRODUCTION AND NONCONTACT SCIENCE AND TECHNOLOGY

Robert R. Hale
Jet Propulsion Laboratory
California Institute of Technology

In addressing the issue of noncontact temperature measurement (NCTM), it is helpful to look at the range of science carried out in association with various wavelengths and frequencies of the electromagnetic spectrum. Table 1 illustrates approximately 22 orders of magnitude of range, both in frequency and wavelength, in which remote sensing science is presently being conducted. Many of these can be categorized as noncontact measurement methodologies to the extent that we discount electromagnetic wave interaction effects with materials as contact.

By comparison, human vision perceives only a part of one order of magnitude of this spectrum and, in fact, the early work on optical pyrometry used only a very small portion of the human visible response to electromagnetic radiation as light. This session explored many of the techniques which hold promise for NCTM, including several which are not traditionally linked to radiation pyrometry or thermometry. They include considerations of signal processing methodologies analogous to those which have been used in acoustic and photo-acoustic research; an approach utilizing magnetic resonance imaging; a concept involving thermal electron emission detection; exploratory work on the optical detection of Johnson noise; fundamental diagnostics related to interaction of lasers with fluids and particles; the utilization of ellipsometric principles for optical constant measurement to help infer temperature; and developmental approaches involving computation with improved accuracy of the thermoradiative properties of materials and the development of a multicolor imaging pyrometer.

Table 1. Examples of Science Activity vs Electromagnetic -
Wave Spectral Distribution

SPECTRAL RANGE NAME	WAVELENGTH (m)	FREQUENCY (MHz)	SCIENCE ACTIVITY	NON-CONTACT SENSING METHOD
COSMIC	10^{-13}	10^{15}		HIGHEST NATURAL RADIOACTIVE SUBSTANCE
X-RAY	10^{-9}	10^{11}	LARGEST ATOM DIAMETER	X-RAY TELESCOPE
UV	10^{-8} 10^{-7}	10^{10} 10^9	ATOMIC STRUCTURE STUDIES VISIBLE/HUMAN EYE	HUMAN VISUAL OBSERVATIONS
IR	10^{-5}	10^7	MOLECULAR STRUCTURE STUDIES	IR ROTATIONAL SPECTRA
EXPT	10^{-2}	10^4	RADIO ASTRONOMY	DOPPLER RADAR, WEATHER
TV	10^1	10^1	SPACE RESEARCH	RADIO ASTRONOMY
ULTRASONIC	10^4	10^{-2}	ELECTRON INDUCTION HEATING	SONAR
INFRASONIC	10^9	10^{-7} (0.1 Hz)	ELECTROMAGNETIC MICROPULSATIONS	

OPTICAL JOHNSON NOISE THERMOMETRY¹

R. L. Shepard, T. V. Blalock, L. C. Maxey, M. J. Roberts, and M. L. Simpson

Oak Ridge National Laboratory²

Oak Ridge, Tennessee

For Presentation to the NASA Technical Workshop on Non-Contact Temperature Measurement,
Pasadena, California, January 17-19, 1989

Abstract

A concept is being explored that an optical analog of the electrical Johnson noise may be used to measure temperature independently of emissivity. The concept is that a laser beam may be modulated on reflection from a hot surface by interaction of the laser photons with the thermally agitated conduction electrons or the lattice phonons, thereby adding noise to the reflected laser beam. If the "reflectance noise" can be detected and quantified in a background of other noise in the optical and signal processing systems, the reflectance noise may provide a noncontact measurement of the absolute surface temperature and may be independent of the surface's emissivity.

1 Work Performed for The National Aeronautics and Space Administration, The Marshall Space Flight Center under Interagency Agreement DOE No. 1281-B019-A1

2 Operated by Martin Marietta Energy Systems, Inc. for the U. S. Department of Energy under Contract No. DE-AC05-84OR21400

"The submitted manuscript has been authored by a contractor of the U.S. Government under contract No. DE-AC05-84OR21400. Accordingly, the U.S. Government retains a nonexclusive, royalty-free license to publish or reproduce the published form of this contribution, or allow others to do so, for U.S. Government purposes."

Introduction

Uncertainties in the emissivity of metal specimens cause uncertainties in the measurement of their temperature using conventional radiometric techniques. These uncertainties may be minimized by using multiple wavelength radiometry or by ancillary measurements of surface reflectivity which is related to surface emissivity. A method for absolute radiometric measurement of surface temperature that is independent of emissivity or material properties has not been developed heretofore. Such a method may result from studies of an optical analog of the electrical Johnson noise thermometer.

Conventional radiation thermometry -- and indeed, most instruments -- use intensities or dc levels for measuring the temperature of materials, and are necessarily dependent on knowledge of some physical property of the material: resistivity, emissivity, Seebeck coefficient, acoustic modulus, etc. Superimposed on these dc levels is noise that limits the precision with which the temperature can be determined. Good thermometric practice would reduce the noise to a minimum. This noise, however, contains some information that can be used to indicate some conditions of the specimen, the measuring system, or the specimen's environment.

Johnson and Nyquist⁽¹⁾ in 1928 attempted to eliminate noise from radio receivers and found that an irreducible minimum noise was produced by passive components in electrical circuits with no current flow. The magnitude of this noise depends on the absolute temperature of the component, but not on its material composition. The relationship between measured noise, the absolute temperature (T), and the ohmic resistance (R) of the component is given (for $hf/kT \ll 1$) by:

$$\overline{V_n^2} = 4 k T R \Delta f$$

$$\overline{I_n^2} = 4 k T/R \Delta f$$

$$T = \sqrt{P_n^2} / 4 k \Delta f$$

$$R_n = \overline{V_n^2} / \overline{I_n^2}$$

where, $\overline{V_n^2}$ is the open-circuit noise voltage spectral density, $\overline{I_n^2}$ is the short-circuit noise current spectral density, measured over a frequency band Δf , h is Planck's constant, k is the Boltzmann constant, and $\sqrt{P_n^2}$ is the noise power, defined as the product of the open-circuit voltage and short-circuit current. These relations ⁽²⁾ hold at frequencies up to about 100 GHz. For a 100- Ω resistor at a temperature of 300 K and noise measured over a 60-kHz bandwidth,

the noise voltage is about 0.32 μV rms, the noise current is about 3.2 nA rms, and the noise power is about 10^{-15} W.

Johnson noise is produced by the thermal agitation of the free electrons in a solid or liquid as a result of electron-phonon interactions with the lattice atoms. The noise power is independent of the resistor material and depends only on the absolute temperature. The relationship between noise power and temperature is linear.

Electrical Johnson noise thermometry has used various measurement schemes⁽³⁾, including; (a) the ratio of noise voltages produced by two resistors, one at a known temperature, where both resistances can be measured, (b) separate measurement of noise voltage and noise current on a single resistor, from which noise power can be calculated, and (c) several tuned RLC circuits from which temperature can be obtained from a noise voltage and a capacitance measurement. Signal correlation circuits have been employed to greatly reduce the noise contribution of the measuring system. Lacking a direct electrical measurement of noise power, two measurements must be made in each case to obtain temperature independent of sensor resistance. A "noise resistance" can also be obtained from the ratio of the noise voltage and noise current, which is roughly equal to a measured dc resistance.

Electrical Johnson noise thermometry has been used (a) to measure temperatures in high nuclear radiation environment⁽⁴⁾, (b) to establish an absolute thermodynamic temperature scale, (c) to perform in situ calibration of platinum resistance thermometers installed in nuclear plants⁽⁵⁾, and could be used (d) in high-pressure or high-magnetic field environments⁽⁶⁾. It is presently being engineered for long-term, high-radiation, high-temperature measurements in space nuclear reactors.

Adaptation of Johnson Noise to Noncontact Thermometry

For Johnson noise techniques to be applied to noncontact thermometry, some method of quantifying the noise power of the electrons in a specimen without making any physical contact must be devised. An approach, now being considered, is the detection of the modulation of a laser beam incident on a hot surface by the interaction of the laser photons with the surface's conduction electrons. It is proposed that an increase in the noise content of the reflected laser beam should be proportional to the noise of the electrons, depend on the surface temperature, and be independent of the surface composition and its emissivity.

Two forms of optical noise modulation may occur. The first is an amplitude modulation due to scattering of the incident laser beam. The second is a laser line-width broadening due to energy transfer between the incident photon and the surface electron. These mechanisms are shown diagrammatically in Figure 1.

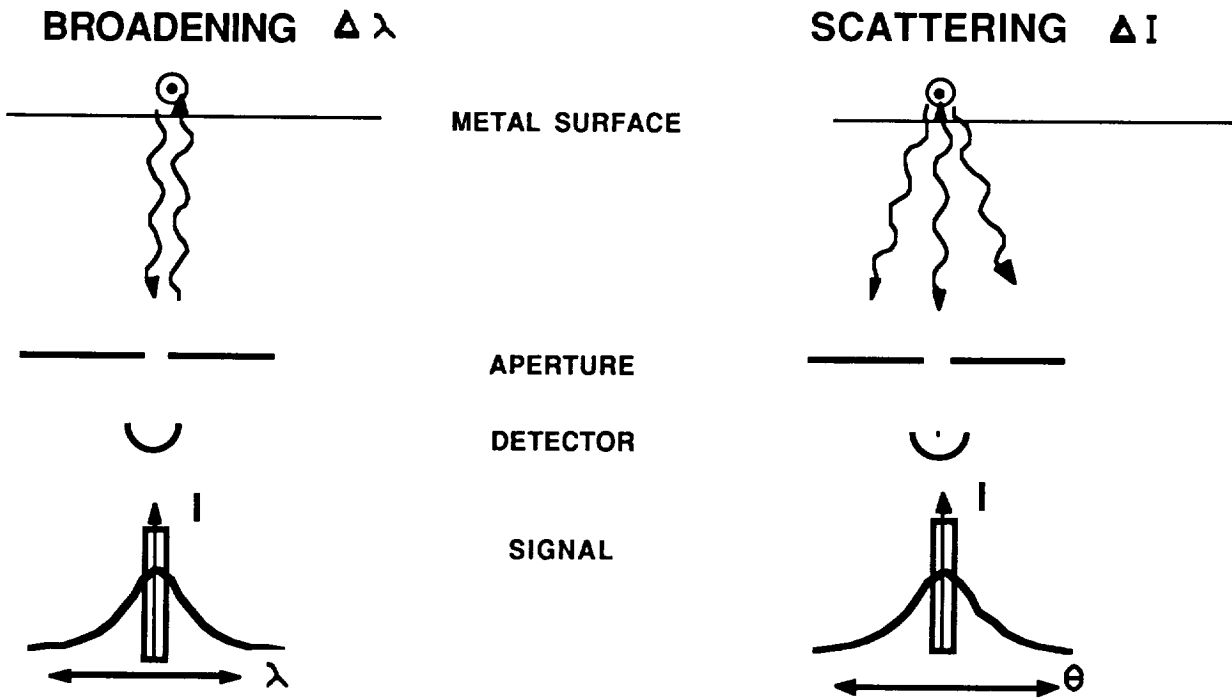


Figure 1. Simplified Mechanisms for Photon-Electron Interaction in Reflectance Noise Thermometry

If the reflectance noise modulation is directly related to the noise power spectral density of the conduction electrons, then only one type of noise measurement would be required to obtain temperature. The electrical Johnson noise measurements require two independent determinations of noise voltage and noise current (or their equivalent) to obtain noise power. The reflectance noise power could be independent of surface emissivity. If not, a second independent optical measurement such as line-broadening may be required to provide two independent measurements of surface temperature that could be combined to give a temperature independent of emissivity.

Implementation of Optical Noise Signal Processing

Various continuous (CW) lasers are available in the laboratory for evaluating these phenomena and several relevant characteristics are shown in the table.

Table 1. Lasers Evaluated for Reflectance Noise Thermometry

<u>Laser Type</u>	<u>Laser Power</u>	<u>Laser Wavelength</u>	<u>Laser Noise</u>
He-Cd	8 mW	325 nm	5%
He-Ne	3 mW	632.8 nm	0.09%
Ar Ion MultiLine	300 mW 100 mW	457-514 nm @ 488 nm	0.5%

Important considerations in selecting the laser are (1) a short wavelength and large power are desirable to minimize the relative contribution of the Planck radiation at the laser's wavelength, (2) low inherent laser noise is desirable, and (3) possible variations in the thermal noise modulation level as a function of the laser wavelength.

The illumination of the photodetectors by a hot surface and a laser beam reflected from the hot surface contains both dc (intensity) and ac (noise) components. These components and an estimate of their magnitudes are shown in Figure 2 for the He-Ne laser.

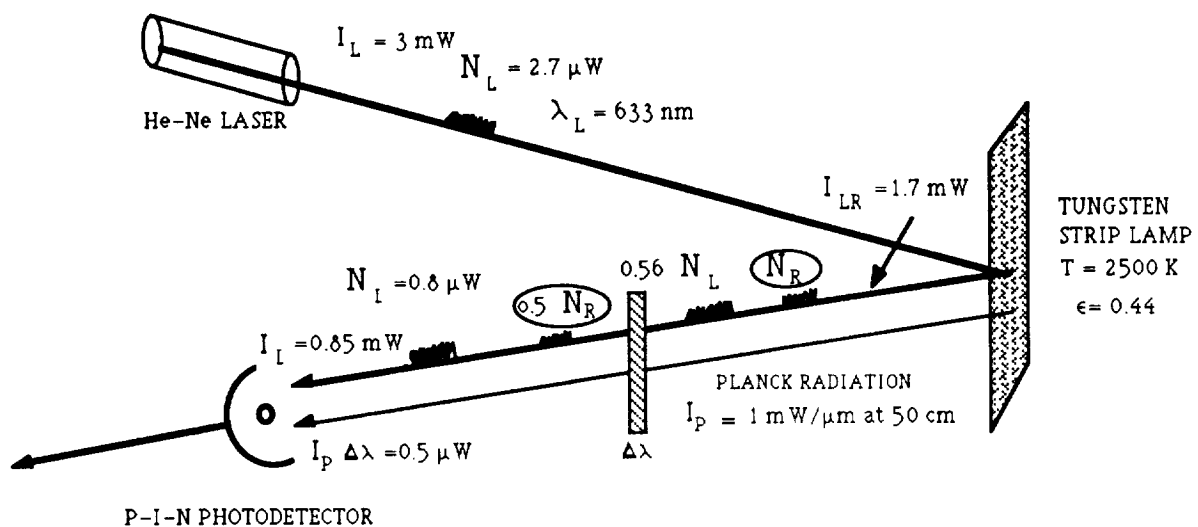


Figure 2. Laser Illumination of a Hot Surface

The dc components of the photodetector signal can be electrically separated from the ac components by filtering and signal subtraction. The dc illumination includes the reflected laser beam intensity and the Planck radiation from the hot surface. Signal channel ac gains may be balanced using high-level, low-frequency modulation of the incident laser beam. The dc levels are not used to provide information about the surface temperature. A system for signal correlation is shown in Figure 3.

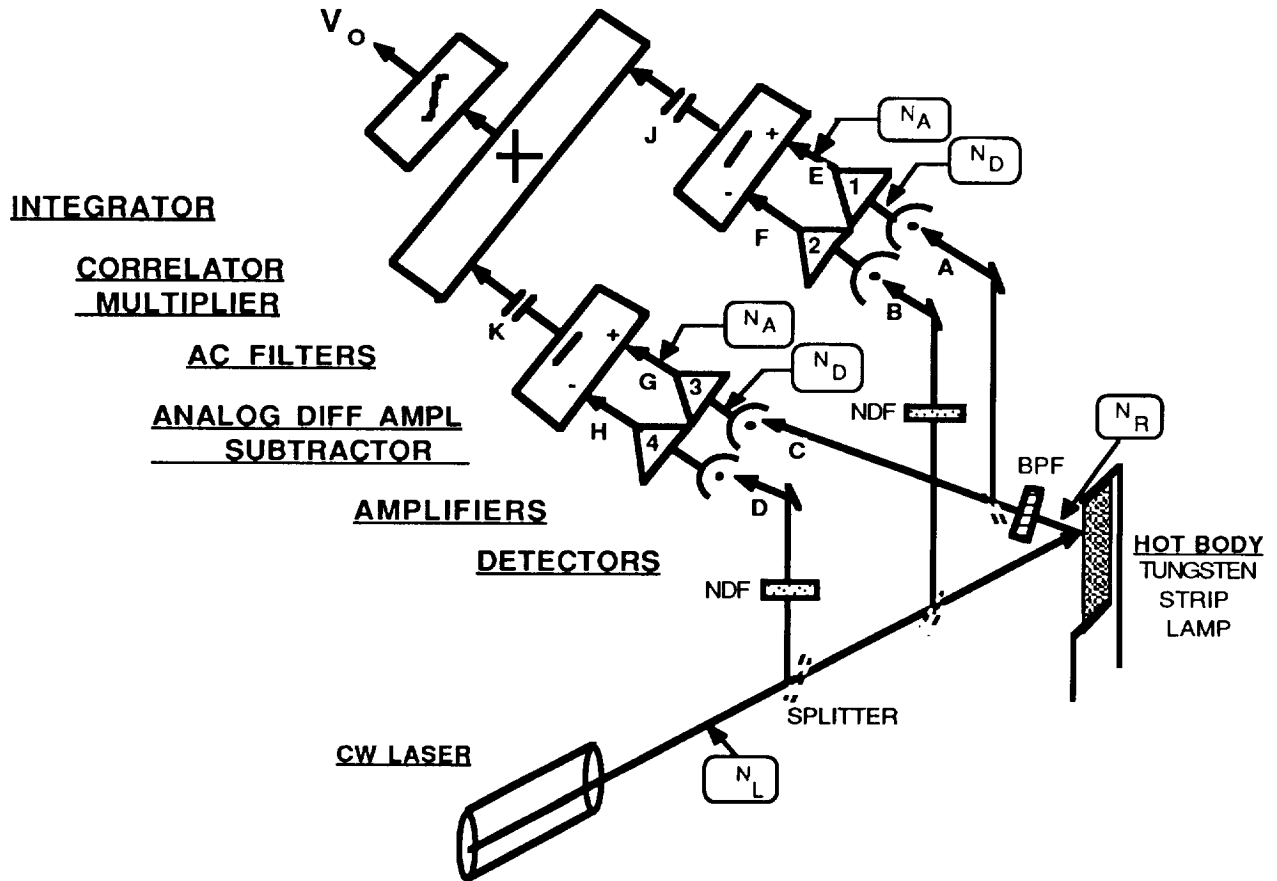


Figure 3. Signal Correlation System for Reflectance Noise Measurement

The ac components of the photodetector signal must be separated to select only the noise contributed by surface reflection of the laser beam (and possibly, the noise in the Planck radiation from the surface). Other sources of noise in the reflected beam include optical noise generated in the laser and microphonics in the optical system. Additional noise will be added in the measurement channels by shot noise generated in the photodetector and rf noise pickup. Some of the low-frequency noise components can be eliminated by high-pass filtering. The remaining wide-band noise components must be separated by signal processing and correlation,

using multichannel optical paths. The largest correlated noise signal component is the laser noise. This noise which is common to all four optical channels, can be reduced by subtraction with analog differential amplifiers. The largest source of uncorrelated noise is the shot noise of the photodetectors. The effect of these uncorrelated noise signals is reduced by the multiplier-integrator stage of the signal processor. If the differential amplifiers and the correlator completely eliminate the laser noise and the uncorrelated nonthermal noise sources, the output of the multiplier-integrator should be proportional to the remaining noise from the reflectance modulation of the laser beam by the hot surface.

Correlation System Performance and Requirements

A preliminary estimate was made of the sensitivity of our present signal processing system to detect thermal noise modulation of the laser beam. This estimate shows a minimum detectable signal of 3 nW of noise power can be detected with an uncertainty of 1%, or $1:10^3$ of the laser noise, using the helium-neon laser. The estimate assumes (a) total elimination of the uncorrelated system noise, (b) a common mode rejection ratio (CMRR) of 100 dB in the differential amplifiers, and (c) a laser noise power of 0.1%. To detect a thermal noise power of 10^{-14} W, calculated for $T=2500$ K and $\Delta f = 60$ kHz, with 1% uncertainty requires five orders of magnitude improvement in the signal processor sensitivity. This improvement may be accomplished by decreasing the laser noise contribution, increasing the CMRR of the differential amplifiers, and modifying the bandwidth of the signal processor. Adequate rejection of the shot noise in the detectors, which is the major noise contribution of the measuring system, may require unreasonably long integration times for the correlation process to reduce this noise to a level below that of the reflectance noise.

The above analysis assumes that a laser beam can be modulated by another noise source, such as the proposed hot-surface reflectance, over any bandwidth of interest. The unexplored question is whether the electron-photon power transfer process in surface-reflectance signal modulation is efficient at frequencies below 1 MHz.

No estimates have yet been made for possible noise associated with the Planck radiation from the hot surface, nor have we assessed the possibility of measuring the line broadening (see Figure 1) to determine temperature.

Further work on this program will (a) continue the development of a signal processor with

improved common mode rejection and larger bandwidth, (b) theoretical investigation of the electron-photon modulation process at a hot surface, (c) reduction of the laser noise and extraneous noise sources in the system, and (d) investigation of line broadening in hot-surface reflection.

Conclusions

A postulated phenomenon of temperature-dependent reflectance modulation of a laser beam is being investigated to determine whether it might provide a means of noncontact surface temperature measurement that is independent of the emissivity of the surface. Methods of signal processing are being developed for eliminating the nonthermal noise sources from the desired thermal reflectance noise. A preliminary estimate indicates that the signal correlation system may need to extract one part of desired noise from a background at least eight orders of magnitude larger.

References

1. Johnson, J. B., "Thermal agitation of electricity in conductors," Phys. Rev. 32, 110 (1928)
2. Borkowski, C. J. and T. V. Blalock, "A new method of Johnson noise thermometry," Review of Scientific Instruments 45(2), 151 (1974)
3. Blalock, T. V. and R. L. Shepard, "A decade of progress in high temperature Johnson noise thermometry," Temperature, Its Measurement and Control in Science and Industry, Vol. 5, Part 2, pp 1219-1237, American Institute of Physics (1982)
4. Brixy, H., R. Hecker, K. F. Rittinghaus, and H. Howener, "Application of noise thermometry in industry under plant conditions," Temperature, Its Measurement and Control in Science and Industry, Vol 5, Part 2, 1225-1241, American Institute of Physics (1982)
5. Shepard, R. L., T. V. Blalock, and M. J. Roberts, "Remote Calibration of Resistance Temperature Devices (RTDs)," Electric Power Research Institute Report EPRI NP-5537, Final Report Project 2254-1, (February 1988).
6. Garrison, J. B. and A. W. Lawson, "An absolute noise thermometer for high temperatures and high pressures," Rev. Sci. Instrum. 20, 785 (1949)

Non-contact Temperature Measurements in Support of
Microgravity Combustion Experiments

Paul S. Greenberg
NASA-Lewis Research Center
Cleveland, Ohio 44135

I. Introduction

Recent conceptual advances in the understanding of combustion science fundamentals in the context of microgravity processes and phenomenology have resulted in an increased demand for diagnostic systems of greater sophistication. Owing primarily to the severe operational constraints that accompany the space flight environment, measurement systems to date remain fairly primitive in nature. Qualitative pictures provided by photographic recording media comprise the majority of the existing data, the remainder consisting of the output of conventional transducers, such as thermocouples, hot wires, and pressure transducers. The absence of the rather strong influence of buoyant convection renders microgravity combustion phenomena more fragile than their 1-G counterparts. The emphasis has therefore been placed on nonperturbing optical diagnostics. Other factors, such as limited supplies of expendable reactants, and periods of microgravity time of sufficient duration, coupled with more fundamental questions regarding inherent length and time scales and reproducibility have favored multipoint or multidimensional techniques. While the development of optical diagnostics for application to combustion science is an extremely active area at present, the peculiarities of space flight hardware severely

restrict the feasibility of implementing the majority of techniques which are being utilized in terrestrial applications. The additional requirements for system reliability and operational simplicity have tended to promote somewhat less commonly emphasized techniques such as refractive index mapping and molecular Rayleigh scattering.

II. Refractive Index Mapping

The development of quantitative diagnostic tools for planar (2-D) measurements of temperature fields in gaseous flows is of significant interest in combustion science. For the most part, the development of 2-D measurement techniques has emphasized the application of Laser Induced Fluorescence (LIF) and molecular scattering processes (Raman and Rayleigh). These methods offer the advantages of spatial specificity (afforded by planar illumination) and species or transition specificity (with the exception of Rayleigh scattering). The relative weakness of these processes, however, places requirements on the optical source strengths which are, in many cases, incommensurate with presently envisioned spaceflight hardware. A number of tuned absorption techniques are also being pursued for this purpose, but are generally restricted to single-point realizations.

For these reasons, refractive index methods represent an attractive alternative for a number of applications. The emphasis is not being placed on interferometric techniques, however, due to their relatively severe mechanical stability requirements. In contrast, deflectometers tend to be less

complex, less sensitive to vibration and misalignment, and more readily accommodating to large fields of view. In addition, it is possible to construct systems of suitable sensitivity to accommodate the majority of applications which are currently envisioned.¹ For situations involving gasses of known composition, the refractive index data can be directly related to specific parameters of interest, such as temperature and density.² More complex compositions must be addressed on a selective basis. Because of the line-of-sight nature of refractive index measurements, the initial application will be delegated to systems of known symmetry, thus eliminating the requirement for more complex multiple angle tomographic reconstruction procedures.

The first method to be pursued is an extension of the qualitative Rainbow Schlieren system which is currently being developed for flow visualization purposes. The continuously graded color filter offers several advantages over conventional knife-edge or slit systems.³ Principal among these are a lack of stepwise discontinuities, and the use of color rather than intensity to encode deflection magnitudes. A two stage, folded catadioptric optical system has been designed to afford the desired optical performance in a fairly compact package (approximately 0.5 meters on a side). A schematic drawing of this configuration is shown in figure 1. A small zirconium arc lamp serves as the optical source. The spatial extent of the arc itself (approximately 0.010") is well matched to the corresponding dimensions of the rainbow filter, and its spectrum is relatively uniform over the

range of visible wavelengths. The primary focusing elements are off-axis paraboloidal mirrors, which provide a true diffraction limited image of the source at all wavelengths. The secondary element is an asymmetric pair of Cooke triplets operating at a conjugate ratio of 1:10 at F4.

A true three-color solid state array detector with zero pixel offset will be employed as the imaging device. This detector is read by a three channel parallel digitizer which resides in a conventional laboratory PC system. Various basis sets for color representation are being pursued. Hue, saturation, and intensity (HSI) space appears the most promising at present, and should provide roughly 0.5% accuracies of resulting deflection magnitudes. Conventional integral transform methods will then be utilized to invert the measured ray deflection fields, yielding the desired refractive distributions.⁴ The ability of the system to reconstruct specific refractive index fields will then be evaluated in the context of other previously demonstrated deflectometric methods, such as heterodyne Moire⁵ and Wollaston full-field interferometry.⁶

III. 2-D Rayleigh Scattering

The need for nonintrusive methods of determining quantitative 2-D temperatures and gas concentrations has led to the development of various planar imaging techniques. As previously described, several methods have been recently demonstrated, utilizing both spontaneous Raman and Rayleigh scattering, as well as laser induced fluorescence techniques. While Raman scattering and induced fluorescence afford the advantages of species

specificity, the requirements placed upon the optical sources are currently somewhat disadvantageous in the context of space flight applications. Raman scattering, for example, suffers from exceedingly small scattering cross sections, thus demanding unrealistically large input optical power levels. Fluorescence techniques are hindered by configurationally complex and, in many cases, inefficient conversion processes which are a necessary step in the generation of the appropriate source wavelengths. The relatively large signal strengths and wavelength independence of the source make Rayleigh scattering a potentially viable technique for these applications as rapid technological advancements begin to place new types of laser devices within reach.

2-D Rayleigh scattering methods have recently been demonstrated by a number of investigators.^{7,8,9} In general, these methods are predicated on the linear relationship between the scattered power and the local gas density (i.e. the number of available scattering centers). In isobaric systems, this number density can, in turn, be related to the local gas temperature. The removal of the elastically scattered background contribution usually involves cumbersome in-situ calibration procedures. The test chamber or ambient region surrounding the apparatus must be either evacuated, or back-filled with an atmosphere whose cross section and number density are accurately known at two or more values in order for the background contribution to the scattered intensity to be determined explicitly.

Two approaches are being explored in which the effect of background contributions to the scattered signal can be removed without a priori calibration procedures: i) simultaneous multiple wavelength scattering and ii) spectrally resolved imaging interferometry. Multiple wavelength scattering exploits the specific dependence of the Rayleigh scattering cross section on wavelength. The other scattering processes which contribute to the total measured signal do not exhibit this functional dependence, and can thus be removed via a straightforward system of N algebraic equations (where N represents the number of discrete wavelengths being employed). This approach has been demonstrated for single point measurements using the two principal lines (510 578 nm) of a pulsed copper vapor laser.¹⁰ Single point measurements of gas density to a predicted accuracy of 1.7% have been reported in a 1200^o K, 20 atm. environment. The decreased signal strengths resulting from near ambient pressure conditions will be offset by increased gate times. The initial application will operate at conventional video frame rates, which represent an increase in integration times of 2×10^2 . A split imaging system will be constructed, wherein the field of view will be simultaneously imaged onto separate portions of the imaging array (see figure 2). Narrow line interference filters will be employed to achieve adequate channel separation. Although Rayleigh scattering is only applicable to gas temperature measurements if the effective cross section of the reactants and combustion products remains constant throughout the reaction, it has been shown that a variety of gas mixtures satisfy this condition to within a few percent.¹¹ In addition,

more sophisticated models have been developed wherein the evolution of the scattering cross sections can be predicted as a function of the extent of the completion of the reaction.¹² Using such predictions, the change in cross sections can be incorporated into the data reduction procedures to achieve a more refined temperature measurement.

Spectrally resolved imaging interferometry will be employed to measure the Doppler-broadened linewidths of the scattered signal directly. The scattered linewidth depends on the temperature because the spectral broadening is caused by the Doppler shift from moving molecules. The translational velocity distribution giving rise to the observed shifts is in turn linked to temperature via the Maxwell-Boltzmann relationship. The background signal does not exhibit this broadening, and hence can be readily distinguished. The functional form of the measured spectrum is dependent on pressure. At low pressures (assuming noninteracting, randomly distributed particles) the spectrum has a Gaussian form. Higher pressure regimes require corrections to account for interparticle interactions. The association of the measured spectral width with temperature requires a knowledge of the molecular weights of the species present. As such, similar mixture tailoring procedures or additional information about the reaction chemistry are required for the total intensity measurements which have been previously discussed. Point temperature measurements using Rayleigh scattering linewidths have been previously reported,¹³ and an a priori analysis indicates that accuracies of 10° K are achievable in a

10 msec interval at 2000^o K and one atmosphere, using an input power level of 1 watt at 488.0 nm. Spectrally resolved imaging interferometry as applied to remote thermometry has been reported by several investigators,^{14,15} primarily for measuring auroral emissions. In recent years, flight-qualified versions of these instruments have been constructed, most notably for the Explorer space probe. Two methods of acquiring spectral data will be pursued. In the fringe or image mode, the spectral width is manifest by the local broadening of the fringe field. In the spectrally scanned mode, the center frequency of the interferometer is swept, yielding spectral signatures independently at each point in the pixel field.

1. Howes, W. L., Rainbow Schlieren vs. Mach-Zender Interferometer: A Comparison, Appl. Opt., Vol 24, No. 6, 1985.
2. Vest, C. M., Holographic Interferometry, Wiley, New York, 1979.
3. Howes, W. L., Rainbow Schlieren and Its Applications, Appl. Opt., Vol. 23, No. 14.
4. Sweeny, D. W., Vest, C. M., Reconstruction of Three-dimensional Refractive Index Fields from Multidirectional Interferometric Data Appl. Opt., Vol. 12, No. 11.
5. Decker, A.J., Stricker, J., Sources of Error in Heterodyne Moire Deflectometry, Appl. Opt., Vol. 27, No. 8.
6. Merzkirch, W., Flow Visualization, Academic Press, New York, 1974.
7. Escoda, M. C., Long, M. B., AIAA Journal, Vol. 21, No. 1, 1983.
8. Fourgette, D. C., Zurn, R. M., Long, M. B., Sci. and Tech., Vol 44, 1986.
9. Yip, B., Fourgette, D. C., Long, M. B., Appl. Opt., Vol. 25, No. 21, 1986.
10. Annen, K. D., Joklik, R., Final Contract Report, NAS3-24613.
11. Dibble, R. W., Hollenbach, R. E., Eighteenth Symposium on Combustion, 1981.
12. Namer, I., Schefer, R. W., Chan, M., Western States Mtg. of the Combustion Institute, 1980.
13. Killeen, T. L., et al, Appl. Opt., Vol 22, No. 22, 1983.
14. Shepherd, et al, Appl. Opt., Vol. 24, No. 5, 1985.
15. Killeen, et al, Appl. Opt., Vol. 21, No. 21, 1982.

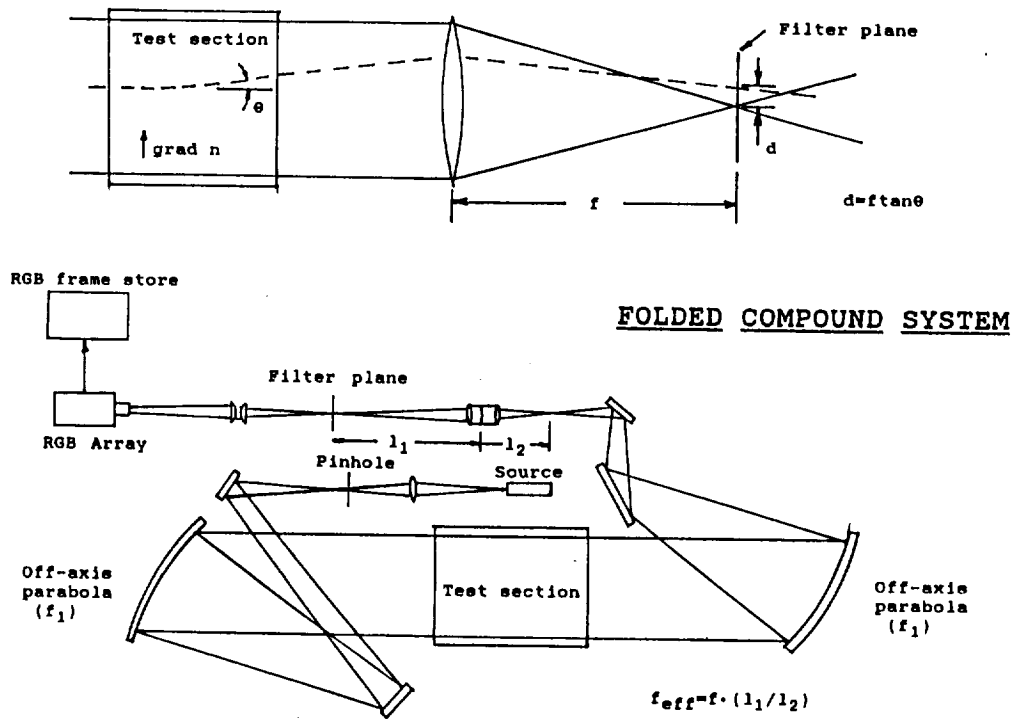


Figure 1. Operating Principle of Rainbow Schlieren

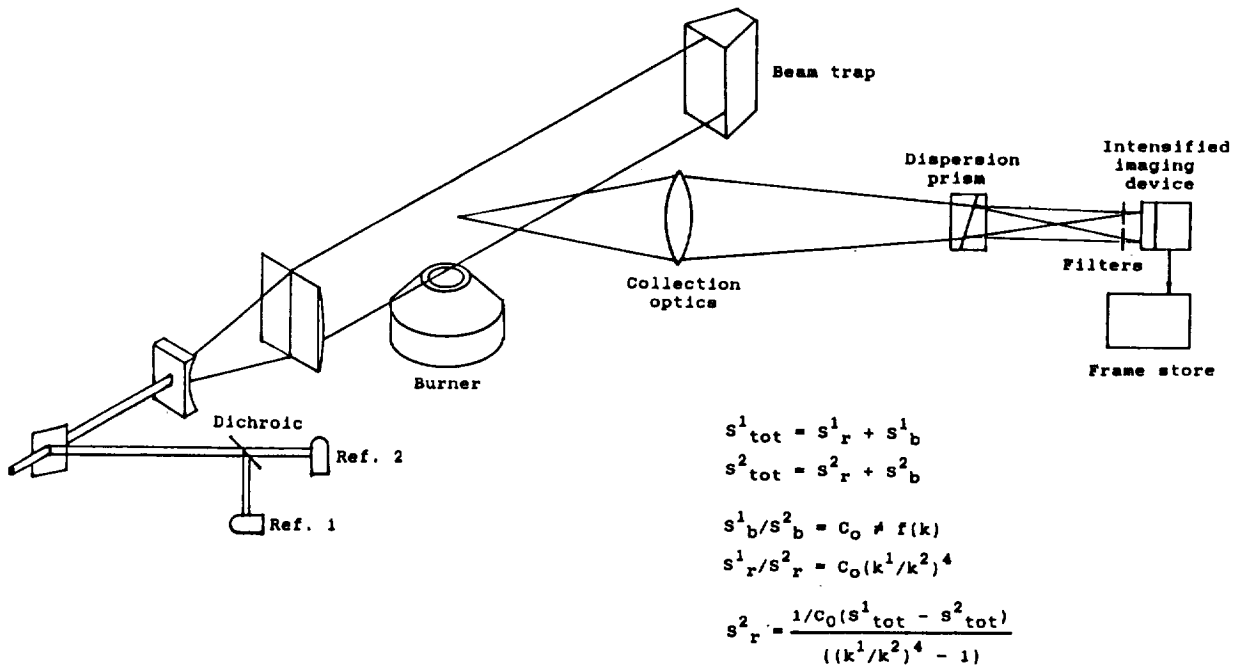


Figure 2. 2-Wavelength Rayleigh Scattering

**Solid State Lasers for Use in
Non-Contact Temperature Measurements**

**A.M. Buoncristiani
Langley Research Center
Hampton, VA 23665**

Introduction

The last decade has seen a series of dramatic developments in solid state laser technology. Prominent among these has been the emergence of high power semiconductor laser diode arrays and a deepening understanding of the dynamics of solid state lasers. Taken in tandem these two developments enable the design of laser diode pumped solid state lasers [1]. It is possible now to design solid state lasers to meet quite specific and precise criteria such as output wavelength, linewidth, beam quality, stability and tunability. Pumping solid state lasers with semiconductor diodes relieves the need for cumbersome and inefficient flashlamps and results in an efficient and stable laser with the compactness and reliability we have come to associate with solid state technology. It provides a laser source that can be reliably used in space. In this paper I shall describe how to incorporate these new coherent sources into the non-contact measurement of temperature.

The primary focus of the LaRC Solid State Laser Materials Research group is the development and characterization of new optical materials for use in active remote sensors of the atmosphere. In the course of this effort we have studied several new materials and new concepts which can be used for other sensor applications. We are interested in seeing this technology put to use for other NASA missions. We share this interest in the development of new electro-optic sensors with our colleagues at the Center for Fiber and Electro-optics at the Virginia Polytechnic Institute and have been working together in this effort. Our general approach to the problem of new non-contact temperature measurements has had two components. The first component centers on passive sensors using optical fibers; VPI has designed and tested an optical fiber temperature sensor for the drop tube at the Marshall Space Flight Center. Work on this problem has given us some insight into the use of optical fibers, especially new IR fibers, in thermal metrology. This work will be described separately by the VPI group. The second component of our effort is to utilize the experience gained in the study of passive sensors to examine new active sensor concepts. By active sensor we mean a sensing device or mechanism which is interrogated in some way by radiation, usually from a laser.

In the next section I will summarize the status of solid state lasers as sources for active non-contact temperature sensors. Then I will describe some specific electro-optic techniques applicable to the sensor problems at hand. Work on some of these ideas is in progress while other concepts are still being worked out.

Status of Solid State Laser Technology

We survey two separate laser technologies here- semiconductor laser diodes and solid state lasers. Diode lasers provide high brightness light sources which are reliable and compact. Diode lasers and diode laser arrays have been fabricated mainly from GaAlAs; the Al composition determines the bandgap and hence emission wavelength. These wavelengths can range from 700 to 900 nm with most production diodes having emission around 800 nm. The emission wavelength can be further tuned by controlling the diode temperature. The diodes can be operated in cw mode, in a short pulse mode (by, for example, Q-switching) or in a quasi-cw mode (long pulses and low repetition rates). Table 1 shows the operating characteristics of several different diode lasers and diode laser arrays as reported in a recent review article [2]. The highest power reported there is 800W in a 13 bar array operating at 35% efficiency. Efficiency of diode laser arrays is expected to reach about 50%.

Table 1.

Operating Characteristics of Semiconductor Diode Lasers and Laser Arrays

Device	Operating Mode	Peak Output Power	Efficiency
SQW-SCH 10 stripe	cw	0.75 W	50 %
SQW-SCH (high brightness laser)	cw q-cw	3.8 W 8.0 W	----- 40 %
laser bar (1 cm)	cw q-cw	12 W 100 W	40 % 30 %
3 bar array	q-cw	300 W	40 %
13 bar array	q-cw	800 W	35 %

Notation: SQW- Single Quantum Well;
SCH- Separate Confinement Heterostructure; q-cw- quasi-continuous wave (150 μ s pulse with 100 Hz repetition).

Compiled from reference [2].

Solid state lasers operate on the optical properties of individual ions doped into host material. The dopant ions may be either transition metals (Cr, Ti, Ni, ...) or lanthanide rare earths (Nd, Er, Tm, Ho, ...). Dopant transition metal ions couple strongly to their host lattice and as a result electronic transitions may be vibrationally broadened. This results in broad emission and absorption in the visible and near IR. The rare earths ions couple more weakly to the lattice and so have narrower absorption and emission and it occurs further into the IR (1 to 3 μm).

A large number of ions in various hosts have already been made to lase; we report here only the results of diode pumped lasers in Table 2.

Table 2.

Diode Pumped Rare Earth Laser Transitions to Date

Ion	Transition	Wavelength (μm)	Temperature (K)
Nd ³⁺	$4F_{3/2} - 4I_{11/2}$	1.06	300
	$4F_{3/2} - 4I_{13/2}$	1.32	300
	$4F_{3/2} - 4I_{9/2}$	0.95	300
U ³⁺	$4I_{11/2} - 4I_{9/2}$	2.61	4.2
Dy ³⁺	$5I_7 - 5I_8$	2.36	1.9
Yb ³⁺	$2F_{7/2} - 2F_{5/2}$	1.03	77
Ho ³⁺	$5I_7 - 5I_8$	2.10	300
Er ³⁺	$4I_{11/2} - 4I_{13/2}$	2.8	300
	$4I_{13/2} - 4I_{9/2}$	1.6	300
Tm ³⁺	$3F_4 - 3H_5$	2.3	300

from Reference [1].

A diode pumped Nd:YVO4 laser has demonstrated an overall efficiency of 12.5% and cw power output of 750 mW [3]. Extrapolating from this result we can anticipate that improvements in diode operation can lead to overall (electrical to optical) efficiencies exceeding 20%.

Despite the fact that laser emission in the mid-IR region occurs in well separated and narrow bands we can still expect diversity in wavelength by shifting the wavelength in non-linear crystals. Harmonic generation can translate the emission to shorter wavelengths while optical parametric oscillation will allow tunable operation from 1 to 10 μm . The cw single mode emission from a diode pumped Nd-YAG oscillator has had its emission at 1.06 μm doubled to 532 nm with 56% efficiency. This second harmonic generation was in a LiNbO3: MgO crystal external to the laser. The maximum efficiency of second harmonic generation in this system may be as high as 80% [4]. A diode laser pumped Nd:YAG oscillator, injection seeded and q-switched has been used to pump a β -Barium Borate crystal with a tuning range from 0.41 to 2.15 μm [1]. Figure 1. displays the tunable emission region for some of these ions and hosts.

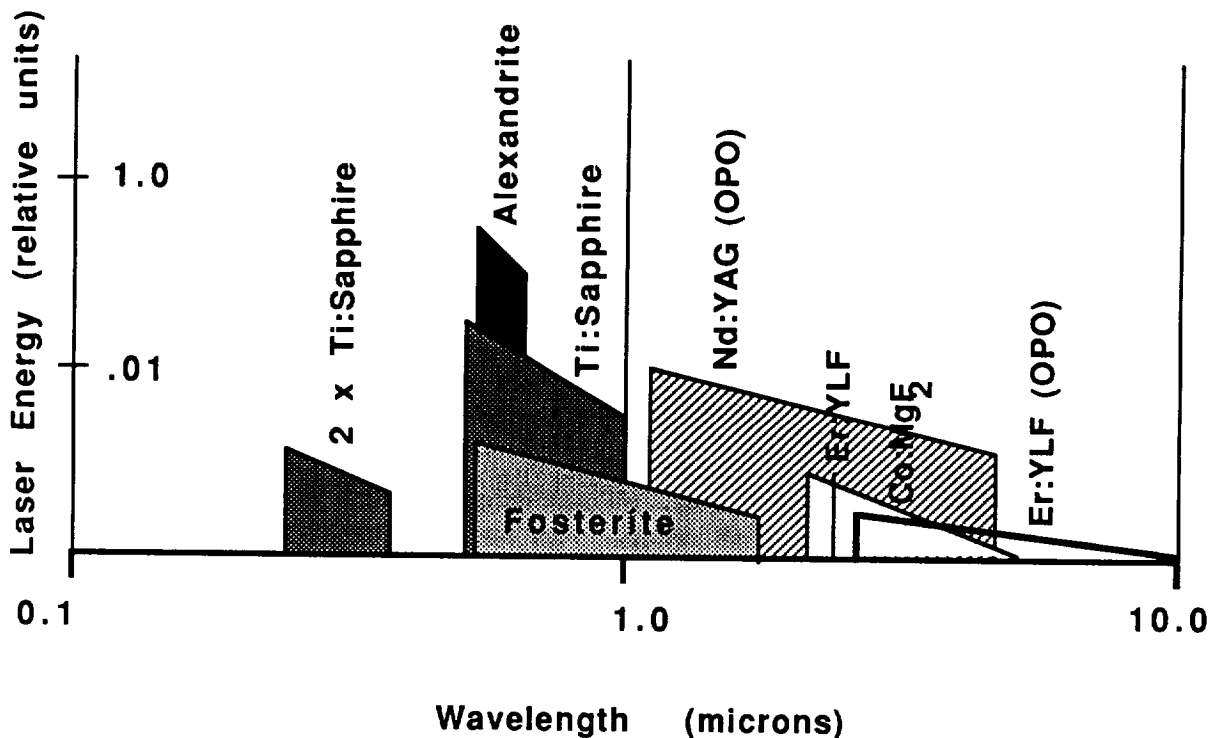


Figure 1. This figure represents the tuning ranges of some solid state laser systems. Most of the recently discovered tunable solid state lasers are represented. In order not to clutter the diagram only one example of second harmonic generation (2 x Ti:Sapphire) and two examples of wavelength shifting by optical parametric oscillation (OPO) are depicted.

This has been a short survey of recent work in diode pumped solid state lasers. It is intended to demonstrate that technology exists to design 'all solid state lasers' with high quality emission from the visible out to 10 μ m. Such lasers provide compact, efficient and reliable sources for active sensing.

Active Sensor Concepts

In this section we describe some ideas about possible non-contact temperature measurements which utilize laser sources. Research has been initiated in some of these techniques while some of the ideas have yet to be tried. An important part of these measurement schemes is their use of optical fibers to transmit and gather the optical signals. Advantages of optical fiber technology will be described more fully in the talk by Professors Claus and May of VPI.

A. Doped Crystal Fibers

Ions doped directly into crystalline or glass fibers can act as sensing elements. This idea has several realizations and I will describe one which was developed from our lab. A few years ago a new technique for the containerless growth of crystals was developed at the Center for Materials Research at Stanford University- the laser heated pedestal to growth of a crystal fiber [5]. We had developed several spectroscopic techniques using these fibers to streamline our optical characterization of new laser materials [6] when it occurred to us that that these techniques could be turned into sensors.

The optical properties of dopant ions are due to the local crystal field seen by the ion. Changes in the environment which alter this crystal field are detectable as changes in the optical properties of the ion. This provides a sensing of the environment on a microscopic scale. To illustrate the possibilities offered by this circumstance I will describe a series of experiments carried out on a Sapphire fiber. In the growth of sapphire (Al_2O_3) unintentional contamination of the crystal with Cr^{3+} ions cannot be avoided so that any sapphire fiber grown has a low concentration of Cr (this concentration was less than 10^{-16} cm^{-3} in the fibers studied). It is these Cr ions that act as sensors. The optical emission from Cr^{3+} ions in Sapphire occurs in two strong and narrow lines in the red (~ 694.3 nm), the so called R-lines. Temperature shifts in both the lifetime and intensity of this emission have been observed [7] in Sapphire fibers. Tensile stress induces a blue shift in the wavelength of the R-lines [7]. Raman spectra of each active vibrational mode of the Sapphire crystal have been observed and their temperature dependence determined. The Raman spectra are shown in Figure 2. The crystal fiber geometry provides an excellent experimental arrangement for Raman measurements since the exciting light is entrained in the fiber while the Raman shifted light is coupled out of the fiber. These results, which

are for one ion and one host crystal, may not be optimal for specific instrument needs. By varying the dopant ions, their concentration and the host it should be possible to achieve a wide range of temperature sensitivities.

The geometry of a crystal fiber favors certain experiments that would be more difficult with bulk samples. There are two basic modes of excitation and detection as shown in Figure 3. Injection of exciting radiation may be either transverse as described in Ref. [6] or longitudinal as in Ref. [7,8].

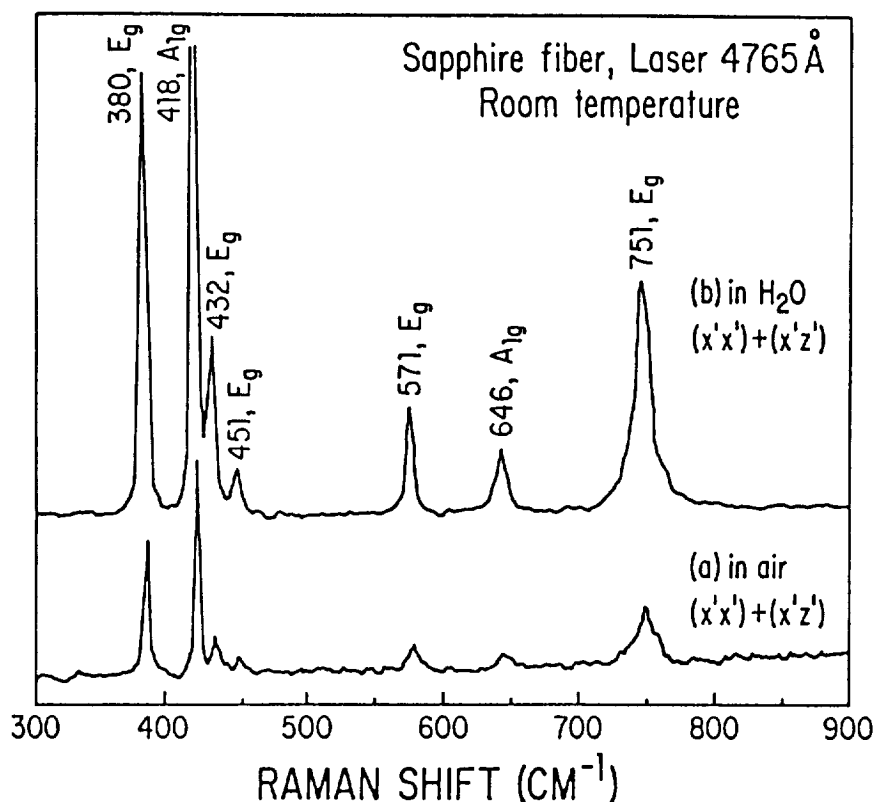


Figure 2. Raman spectra of a single crystal fiber of sapphire at room temperature observed in air and in water. The index matching fluid allows isotropically emitted light to escape the fiber while the excitation laser light, injected longitudinally, remains entrained.

A final remark about this technology. There is a rich variety to the optical properties of ions in solids; all are available for incorporation into optical sensing systems. Optical devices can provide logical operations as well as sensing elements. Furthermore, some of these devices can be optically altered. It has been demonstrated that erasable changes in the refractive index of some glasses doped with Eu can be written with laser light of one frequency and read by light of another frequency [9]. It may be possible to write holographic gratings into optical fibers and to use these gratings as filters for active multiplexing of sensor

signals. This idea is currently under investigation.

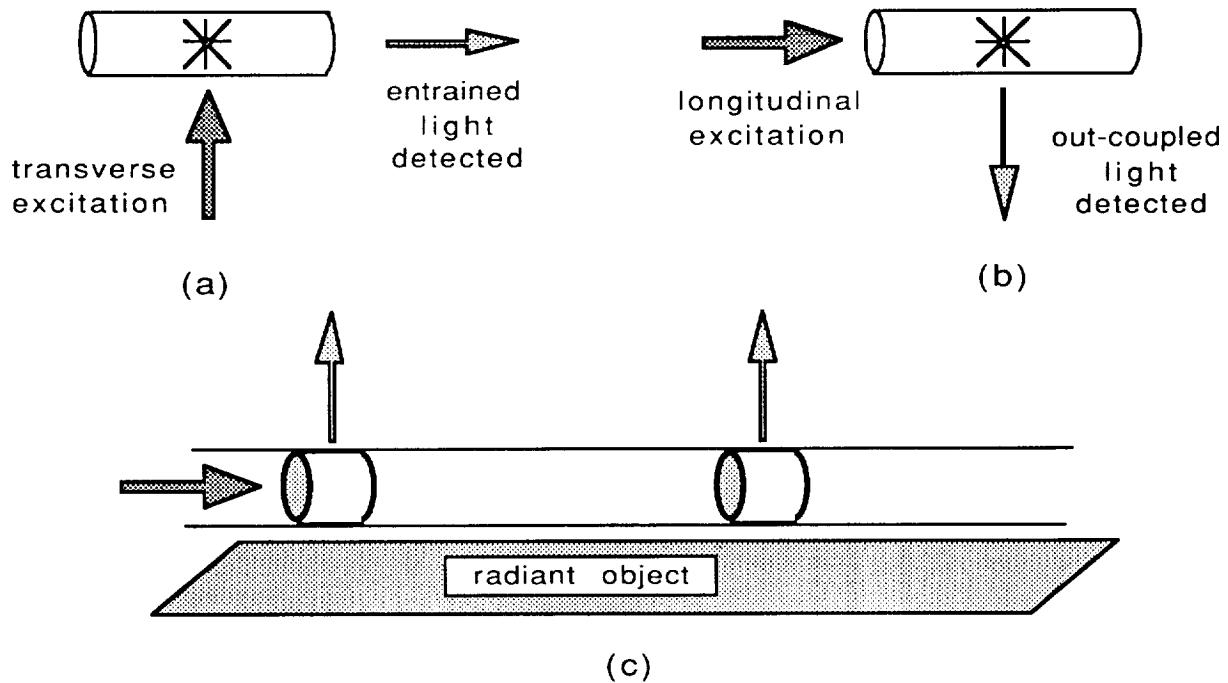


Figure 3. This figure depicts the basic excitation and detection modes for an active element of a fiber system: (a) transverse excitation with entrained light detected; (b) longitudinal excitation with detection of out-coupled light; (c) any combination of excitation and detection modes can be incorporated into a distributed sensor system.

B. Modulated Reflection Spectroscopy

This notion is an extension of a technique developed to study excitation near the band edges of semiconductor materials [10]. It depends upon the alteration of the energy band structure of a solid in the presence of intense laser light. I will describe specific work on semiconductors but the basic procedure could, in principle, be extended to dielectrics and metals. The experimental set up is described in Figure 4. It utilizes two laser beams. A pump beam at a fixed wavelength above the band gap is modulated. Its excitation of the sample surface is probed by a tunable laser through the band gap energy. Measurement of the differential reflectivity ($\Delta R/R$) of the probe beam gives an analogue signal related to the third derivative of the complex index of refraction. The complex refractive index carries information of the absorption coefficient which changes rapidly near the band edge. By fitting the measured lineshape to a simple model of the absorption coefficient the band gap energy can be determined. Thus the derivative signal isolates the band edge which, in turn, depends upon the sample temperature.

Modulated Reflection Spectroscopy

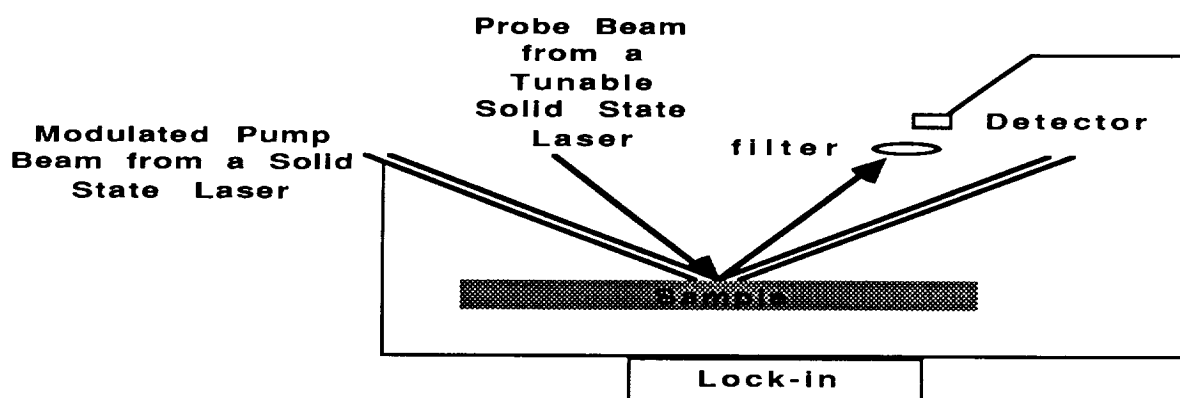


Figure 4. A modulated pump beam alters the band edge near the surface of the sample. This alteration is interrogated by the reflected light from a tunable probe beam. The differential reflectivity ($\Delta R/R$) is related to the third derivative of the complex refractive index.

Using this technique (with a broadband probe beam instead of a tunable laser) non-contact temperature measurements of GaAs up to 610 C have been made with an accuracy of ± 10 C [11]. Using a laser probe should improve the accuracy of this measurement.

This technique has several advantages. First, by measuring a derivative quantity it is insensitive to background behavior and is sensitive to the feature measured, the energy gap location. It measures a quantity which is not dependent on the emissivity. Furthermore, since it is an ac measurement other information such as the phase shift of the reflected light is available.

C. Thermal-Quantum Detectors

This idea for this measurement arose from an analysis of the thermodynamic efficiency of radiation detectors. Radiation detectors can be divided into two broad categories: thermal devices, which convert the energy of each photon absorbed to internal heat and quantum devices which count individual photons having energy above a threshold. This distinction in operation has a significant effect on the thermodynamic efficiency of each type of device when it is used to measure blackbody radiation [12].

Not all of the radiant energy emitted from a blackbody source at a constant temperature T_S and subsequently absorbed by a quantum detector at constant temperature T_R can be converted into a detectable signal (usable work in the thermodynamic sense). Some of the radiant energy absorbed by the receiver is converted to heat, some is reradiated and the remainder is converted to usable energy. The basic limitation on the amount of energy converted to usable work is a consequence of the second law of thermodynamics and it involves the flux of free energy [12]. An upper bound on

the efficiency of this conversion assuming that all of the available free energy is converted to usable energy was derived by Landsberg and Malinson [13]. This bound is given by a polynomial function of the ratio of the temperatures $x = T_R/T_S$ as

$$\eta_{\max} = 1 - \frac{4}{3} x + \frac{1}{3} x^4$$

However, in quantum devices not all of the free energy available in the radiation field can be converted into usable work because of the basic limitation of the detecting device itself. Figure 5. shows the maximum efficiency for the conversion of energy from a blackbody source by a device having a threshold energy $E_0 = h\nu$ and maintained at a temperature T_R .

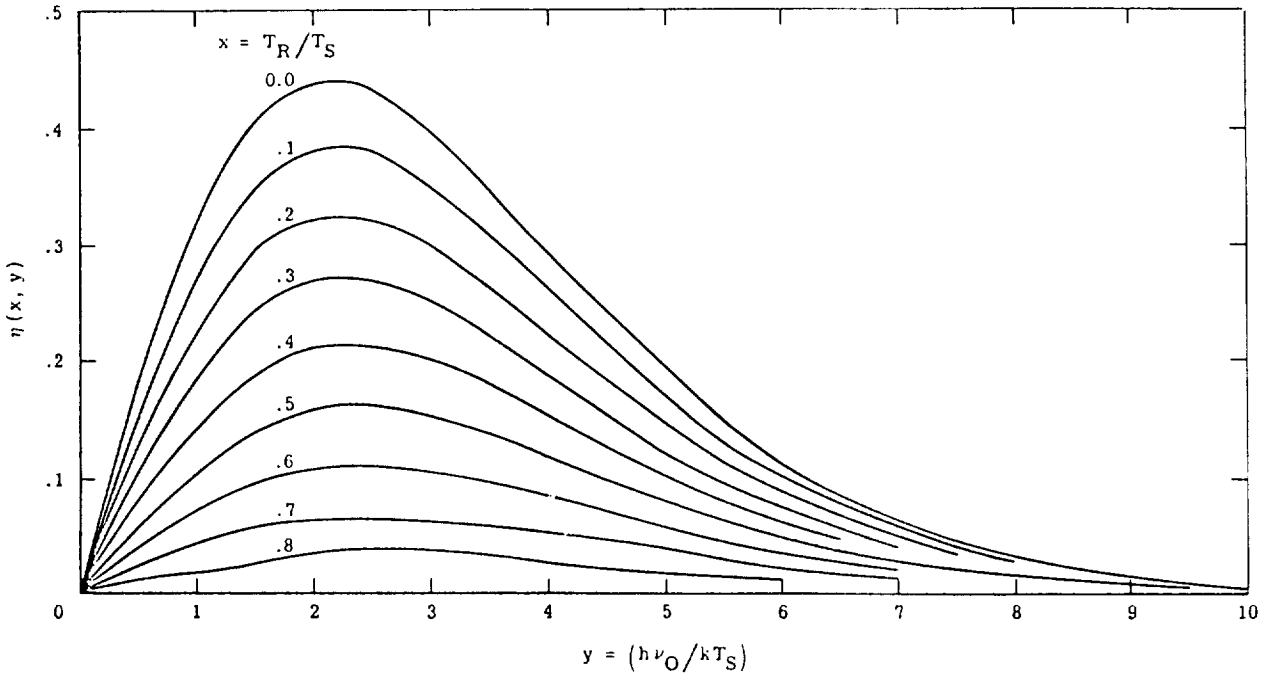


Figure 5. Maximum efficiency for the conversion of energy from a blackbody source at temperature T_S by a device having an energy threshold E_0 and maintained at a temperature T_R , η_{\max} , expressed in terms of the dimensionless parameters $x = T_R/T_S$ and $y = E_0/kT_S$.

In summary then, a thermal device converts the net radiant energy flux incident upon it into heat which is measured as the bolometer signal while a quantum device can detect only the net radiant free energy flux. The difference between these two fluxes depends on the source temperature. This suggests that by comparing the signals from a thermal detector adjacent to a quantum detector one can determine the temperature of the source.

Conclusions

Solid state laser technology is rapidly developing to the point where individual tunable solid state lasers can be designed to meet specific needs. This flexibility in the sources of coherent radiation provides an opportunity for thermal metrology. These developments parallel developments in electro-optics and optical fiber technology. Together they enable new measurement strategies to be designed. In this paper we have described the characteristics of the current generation of diode pumped solid state lasers and suggested how they may be utilized to enable new non-contact temperature measurements.

Acknowledgements

I want to acknowledge the contributions of several collaborators to this work: Dr. Charles Byvik, W.J.Schaefer Associates, Inc.; Professors Claus and May, Virginia State University; Professor Richard Powell, Oklahoma State University; Professor William Yen, University of Georgia.

References

- [1] T.Y.Fan and R.L.Byer, IEEE J. Quantum Electronics, vol. 24, no. 6, pp.895-919 (1988).
- [2] W.Streifer, D.R.Scifres, G,L.Harnagel, D.F.Welch, J.Beger and M.Sakamoto, IEEE J. Quantum Electronics, vol. 24, no. 6, pp. 883-894 (1988).
- [3] R.A.Fields et al, in Advances in Laser Science - III, Amer. Inst. of Phys. Conference Proceedings No. 172, pp20-22 (1988).
- [4] W.J.Kozlovsky, C.D.Nabors and R.L.Byer, IEEE J. Quantum Electronics vol.24, no. 6, pp. 913-919 (1988).
- [5] R.S.Feigelson, in Tunable Solid State Lasers, P.Hammerling, A.Budgor and A.Pinto, eds., Springer Series 47, p 129 (1985).
- [6] A.M.Buoncristiani, C.E.Byvik and S.Albin, J. Appl.Phys. vol. 64, no. 8, pp. 4239-41 (1988).
- [7] H.Liu, K.Lim,W.Jia,E.Strauss, W.M.Yen, A.M.Buoncristiani and C.E.Byvik et al., Optics Letters, vol. 13, no. 10, pp. 931-33 (1988).
- [8] W.M.Yen, to be published in Proceedings of the Conference on Trends in Quantum Electronics, SPIE, Bucharest , Aug. 1988.
- [9] F.M.Durville, E.G.Behrens and R.C.Powell, Phys Rev. vol. 34, no. 6, pp.4213-20 (1986).
- [10] M.R.Belic, Solid State Communications, vol. 62, no, 12, pp. 817-820 (1987).
- [11] F.H.Pollak and H.Shen, to appear in Proceedings of the United States-Japan Seminar Semiconductor Physics and Electronics, October, 1988.
- [12] A.M.Buoncristiani, C.E.Byvik and B.T.Smith, J.Appl.Phys. vol. 53, no. 8, pp. 5382-5386 (1982).
- [13] P.T.Landsberg and J.R.Mallinson, in International Colloquium on Solar Energy, pp. 27-46, (CNES, Toulouse,1976).

SIGNAL PROCESSING APPLIED TO PHOTOTHERMAL
TECHNIQUES FOR MATERIALS CHARACTERIZATION

JAMES A. ROONEY
JET PROPULSION LABORATORY
CALIFORNIA INSTITUTE OF TECHNOLOGY
PASADENA, CALIFORNIA 91109

There is a need to make noncontact measurements of material characteristics in the microgravity environment. Photothermal and photoacoustic techniques offer one approach for attaining this capability since lasers can be used to generate the required thermal or acoustic signals. The perturbations in the materials that can be used for characterization can be detected by optical reflectance, infrared detection or laser detection of photoacoustics. However, some of these laser techniques have disadvantages of either high energy pulsed excitation or low signal-to-noise ratio. Alternative signal processing techniques that have been developed at JPL can be applied to photothermal or photoacoustic instrumentation. One fully coherent spread spectrum signal processing technique is called time delay spectrometry (TDS)¹. With TDS the system is excited using a combined frequency-time domain by employing a linear frequency sweep excitation function. The processed received signal can provide either frequency, phase or improved time resolution. This signal processing technique has been shown to outperform other time selective techniques with respect to noise rejection and has been recently applied to photothermal instrumentation. The technique yields the mathematical equivalent of pulses yet the input irradiances are orders of magnitude less than pulses with the concomitant reduction in perturbation of the sample and can increase the capability of photothermal methods for materials characterization. ¹ R.C. Heyser, J. Audio Eng. Soc. 15 370 (1967).

**Radiation Thermometry at NIST: An Update of
Services and Research Activities**

G. Barry Hillard

Radiometric Physics Division
National Institute of Standards and Technology
(Formerly National Bureau of Standards)
Gaithersburg, Maryland 20899

Abstract

An overview of activities at NIST in radiation thermometry and related temperature scale research is presented. An expansion of calibration services for pyrometers will be described as well as efforts to develop calibration services for blackbody simulators. Research relevant to the realization of the new international temperature scale (ITS 90) will be discussed.

Introduction

At the last NASA noncontact temperature measurement workshop, held on 30 April - 1 May 1987, a summary of relevant activities conducted by the Radiometric Physics Division of the National Institute of Standards and Technology (NIST) was presented. Since that time, the scope of our activities has continued to expand to meet the evolving measurement needs of the user community. In addition to developing new calibration services, we are contributing to the imminent redefinition of the international temperature scale with fundamental measurements of the freezing point of gold.

Pyrometer Calibrations

The primary activities at NIST relevant to radiation thermometry have always revolved around our mandate to maintain and disseminate the national temperature scale above the temperature of freezing gold (1064.43°C). To this end, the radiance temperature scale is maintained and disseminated¹ on tungsten strip lamps calibrated in the range 800°C to 2300°C. Additionally optical pyrometers, both visual and automatic, are calibrated in their design range. These calibrations are performed in a facility which is shown schematically in figure 1. Both scale realization and lamp and pyrometer calibrations have traditionally been done near 650 nm. In our laboratory, the actual wavelength used was for many years 654.6 nm and is currently 655.3 nm.

Over the past few years, the silicon photodetector based pyrometer operating in the 0.8 to 1.2 micrometer range has become increasingly prevalent. While we have calibrated a limited number of these instruments on a special test basis, it is clear that there is sufficient demand to warrant a formal calibration service. To meet this need, the facility in figure 1 is being extensively modified. A large area blackbody has been added to accommodate the larger spot size of these instruments and the calibration pyrometer is now undergoing a redesign. These modifications are well underway and we are working to establish a calibration service.

Calibration of Ambient Temperature Blackbodies

Blackbodies operating in the 5°C - 100°C range are often used to calibrate thermal imaging systems and imaging radiometers. These are usually not cavity radiators but are most commonly in the form of flat plates having active areas of several square centimeters. In particular, Forward Looking InfraRed (FLIR) systems, used by all branches of the armed forces as well as a variety of infrared scanners, are maintained with a calibration chain based on such blackbodies. To support such devices we have for a number of years maintained a calibration facility. To meet the need for increased accuracy these facilities have been

undergoing a systematic upgrade and expansion.

The heart of the new facility is a water-bath blackbody² (WB BB) designed and built at NIST. The design goals include a large-area (ten centimeter diameter aperture) blackbody with an effective emissivity of .99 or better. It is required to operate from 5°C - 60°C with a setpoint stability of $\pm .01^\circ\text{C}$ and have a central area of the ten centimeter aperture that is uniform to $\pm .01^\circ\text{C}$. Two such systems have been incorporated into the calibration facility, shown schematically in figure 2, and verification of the design parameters is well underway.

Development of the water-bath blackbodies is continuing and a second generation design will be completed by the end of this year. Ultimately, we hope to demonstrate stability and uniformity better than $.005^\circ\text{C}$.

Calibration of Medium Temperature Blackbodies

In the past year, it was determined that sufficient need exists for the calibration of blackbodies operating in the 350°C - 1000°C range to warrant the design and construction of a dedicated facility. Shown schematically in figure 3, the facility will be built around two pressure controlled heat pipe³ furnaces modified as blackbody simulators. One furnace will cover the temperature range of 350°C - 700°C by using cesium as a working fluid while the second furnace will be sodium charged and will operate from 550°C - 1050°C. The cavities themselves will be cylindro-cones 60 centimeters deep and 5 centimeters in diameter. The use of pressure controlled heat pipes will result in stability and uniformity better than $.01^\circ\text{C}$.

The choice of radiometer for this facility has not been made. Occasional calibrations performed in the past used a scanning monochromator and were primarily in the 3 - 5 micrometer band with a limited amount of work in the 8 - 14 micrometer band. We plan to expand our working range and will investigate the feasibility of covering the entire 2 - 20 micrometer range. We are actively pursuing the possibility of using a Fourier transform radiometer to achieve this.

Temperature Scale Research

The International Practical Temperature Scale is defined in terms of a number of primary fixed points and specifications for interpolation between them. The upper fixed point on the scale, as defined in 1968 (IPTS-68), is the temperature of freezing gold (gold point). Above this point, temperature is defined radiometrically by Planck's law. In IPTS-68 the gold point was specified as 1337.58 K (1064.43°C). In the years since the scale was issued a consensus has emerged that the value is about 0.3 K too high.

In our laboratory, a unique experiment is underway⁴ to perform an absolute radiometric measurement of the gold point. Shown schematically in figure 4, this experiment measures the freezing temperature of gold by directly comparing the spectral radiance of a gold point blackbody with that of a laser irradiated integrating sphere that has been calibrated by both silicon detector standards (Si) and an electrically calibrated radiometer (ECR). Preliminary results give a temperature of 1337.32 \pm 0.36 K (3σ).

On January 1, 1990 it is anticipated that a new international temperature scale will be implemented (ITS-90). It will involve reassignments of a wide range of fixed points. (Table 1 shows the effect on radiance temperature if the downward adjustment in the gold point is 0.3 K.) In addition to these reassignments, the upper part of the new scale is expected to be defined radiometrically from the freezing point of silver, currently given in IPTS-68 as 1235.08 K. This value will be reassigned in ITS-90 and we will explore the possibility of employing the same technique used to measure the gold point to perform a silver-point measurement.

Table 1. Projected change in radiance temperature resulting from -0.3 K reassignment of the gold-point temperature from 1337.58 K to 1337.28 K.

Radiance Temperature	Quoted Uncertainty (NIST 3σ)	Change of Value
800°C	\pm 0.5°C	-0.2°C
1100	0.6	-0.3
1400	0.8	-0.5
1800	1.3	-0.7
2300	2.0	-1.1

Summary

A summary of recent and ongoing activities relevant to radiation thermometry has been presented. Because of the wide scope of the work, only a very brief overview has been possible. Anyone desiring further information concerning these or other activities of the Radiometric Physics Division or who wishes to suggest new directions we might pursue is encouraged to contact us directly.

References

1. W. Waters, J. Walker, and A. Hattenburg, Radiance Temperature Calibrations, NBS Special Publication 250-7, October 1987
2. J. Geist and J. Fowler, A Water Bath Blackbody for the 5 to 60°C Temperature Range: Performance Goal, Design Concept, and Test Results; NBS Technical Note 1228, October 1986
3. C. Busse and C. Bassani; A New Generation of Precision Furnaces, in Temperature: Its Measurement and Control in Science and Industry (American Institute of Physics, 1982) Vol 5, p 1265
4. K.D. Mielenz, R.D. Saunders, and J.B. Shumaker, Spectroradiometric Determination of the Freezing Temperature of Gold (submitted for publication)

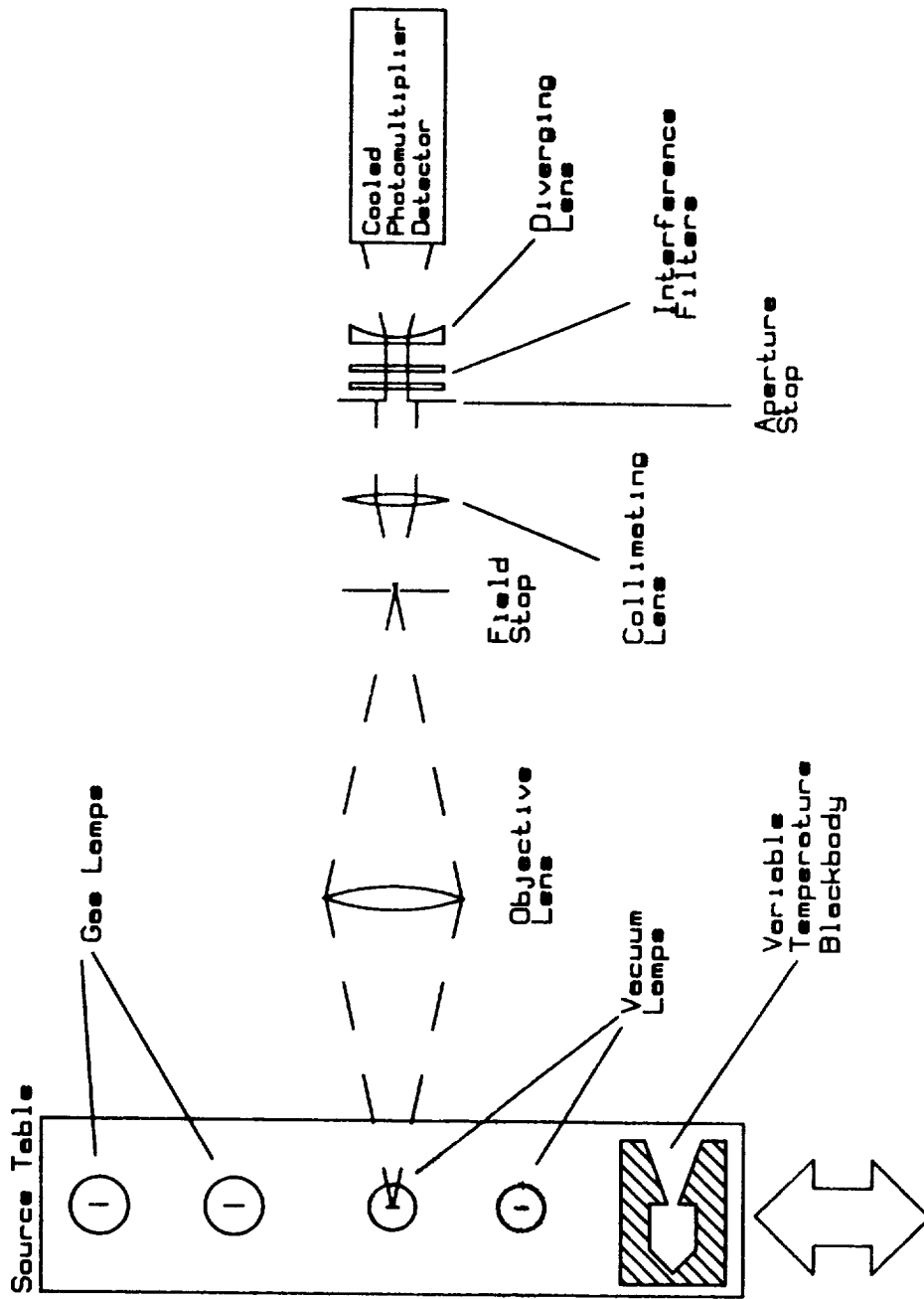


Figure 1. Schematic of the Calibration Facility based on the NIST Photoelectric Pyrometer

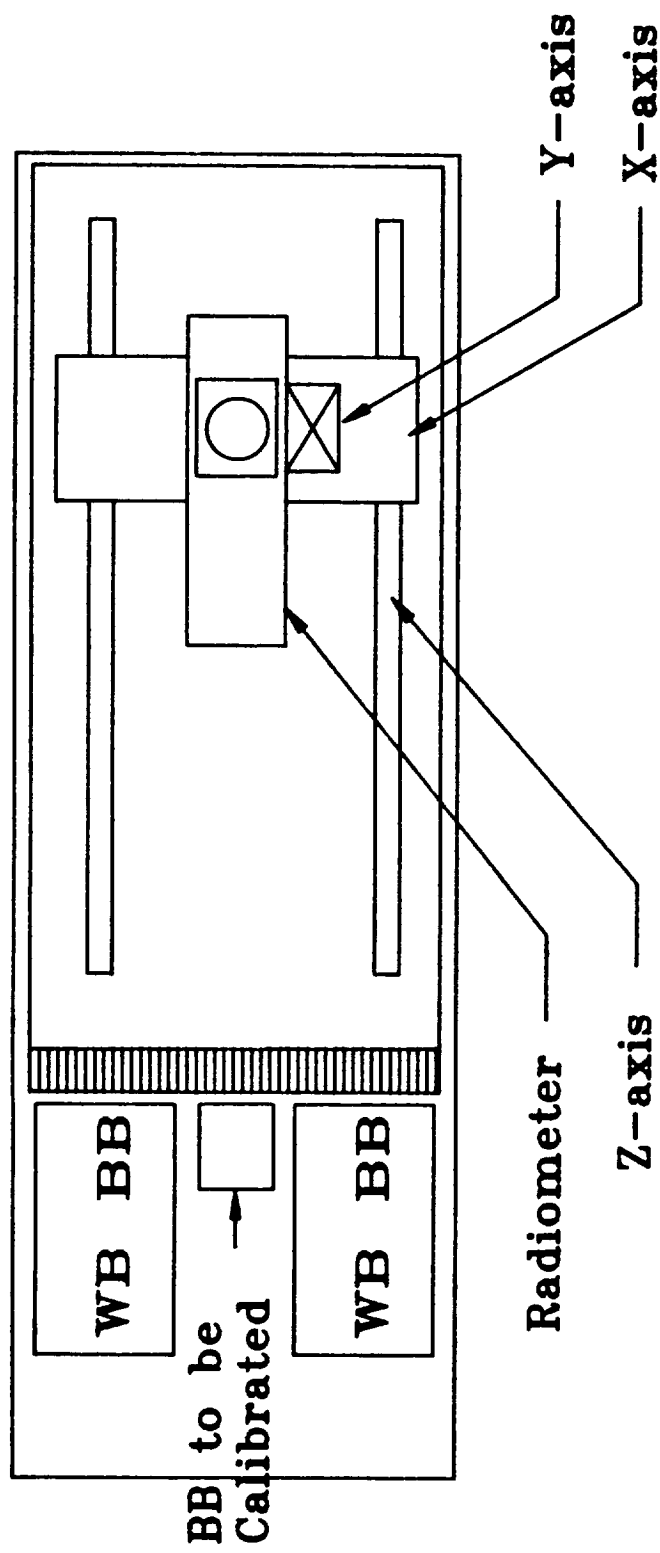


Figure 2. Simplified Schematic of the Ambient Temperature Blackbody Calibration Facility

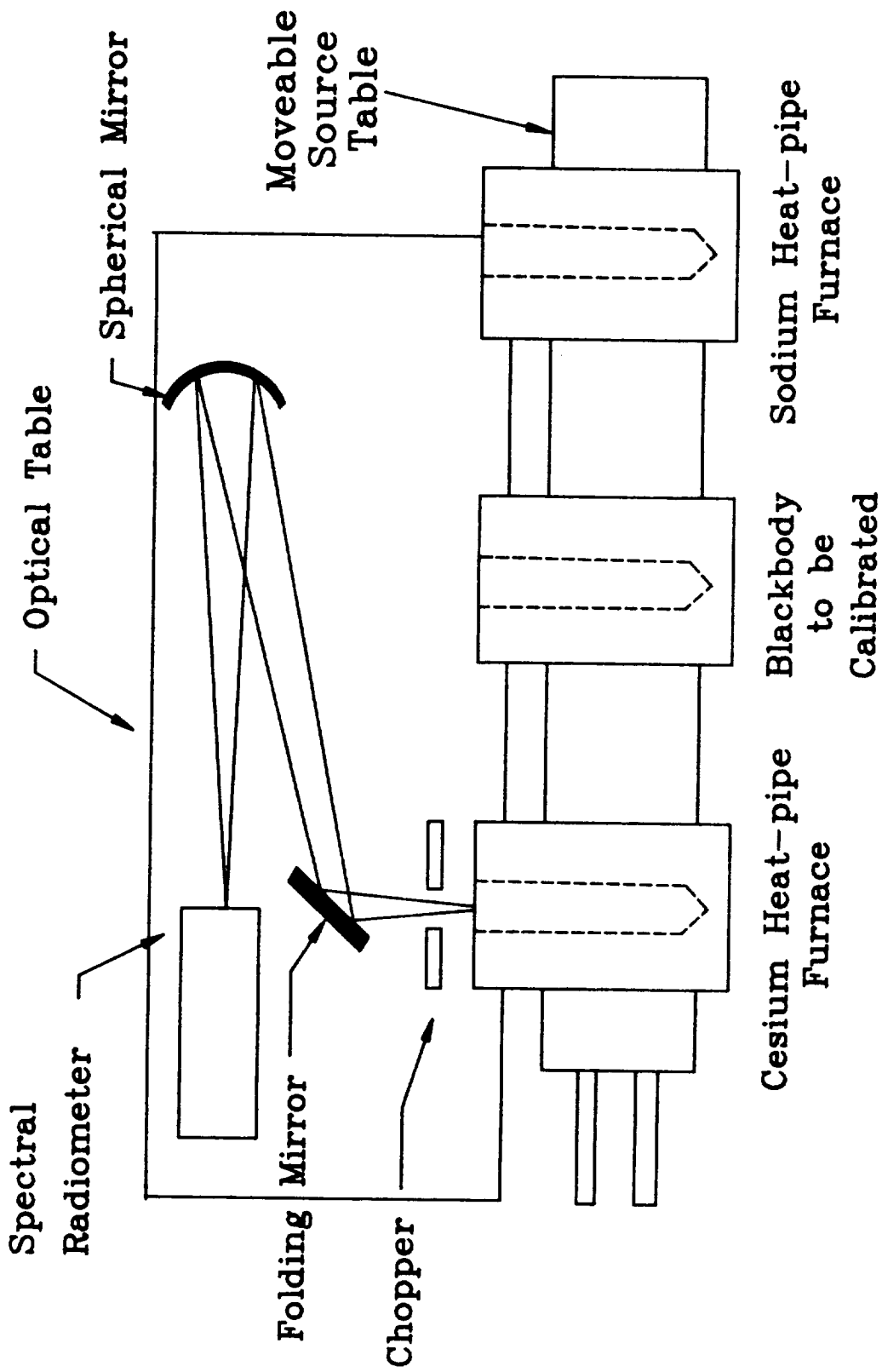


Figure 3. Simplified Schematic of the Medium Temperature Blackbody Calibration Facility

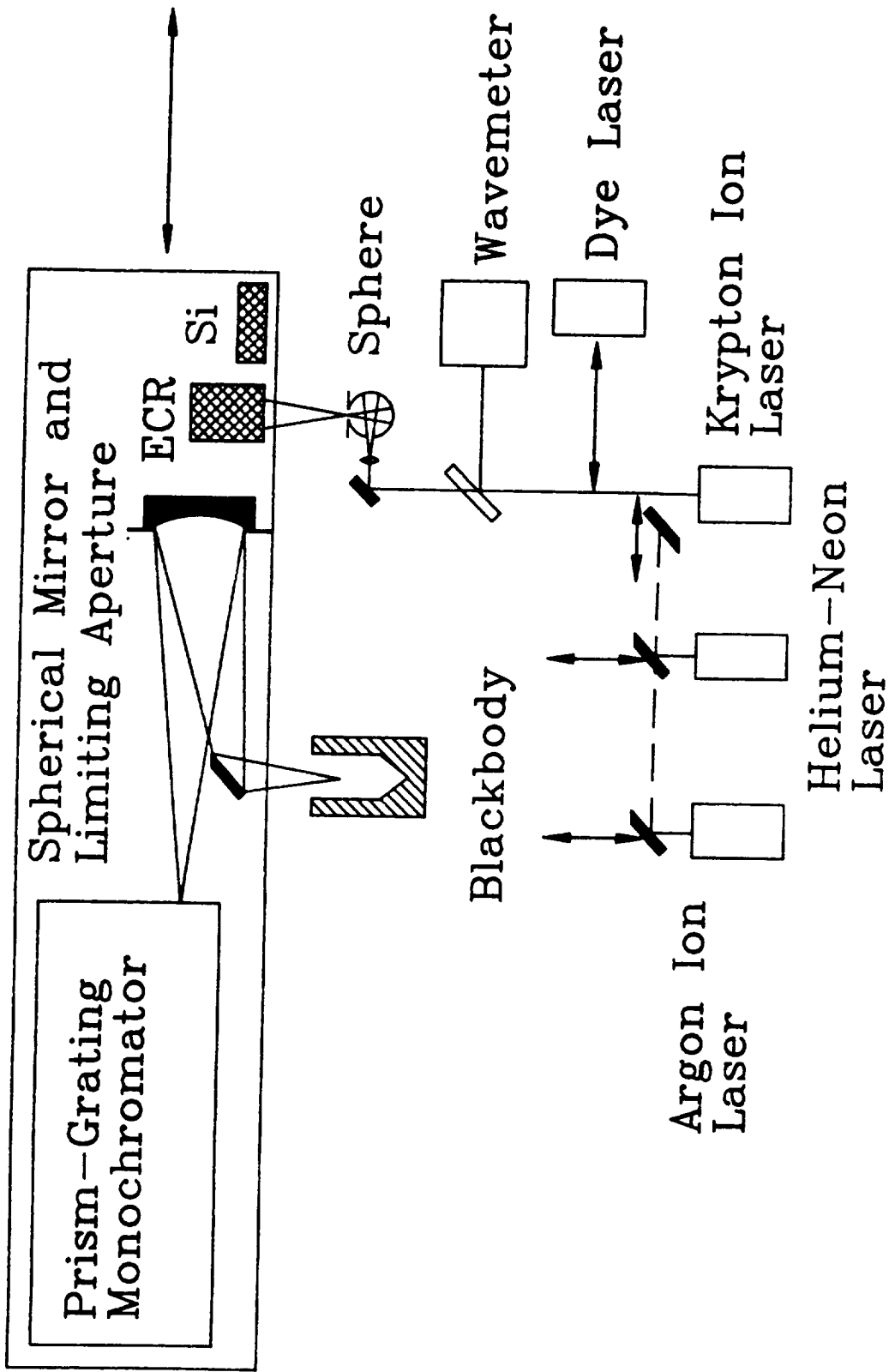


Figure 4. Radiometric Measurement of the Freezing Point of Gold

INFRARED THERMAL IMAGING FIGURES OF MERIT

Herbert Kaplan

Honeyhill Technical Company
193 East Avenue, Norwalk, Connecticut 06855Abstract

This paper will begin with a discussion of commercially available types of infrared thermal imaging instruments, both viewers (qualitative) and imagers (quantitative). The various scanning methods by which thermal images (thermograms) are generated will be reviewed.

The performance parameters (figures of merit) that define the quality of performance of infrared radiation thermometers will be introduced. A discussion of how these parameters are extended and adapted to define the performance of thermal imaging instruments will be provided.

Finally, the significance of each of the key performance parameters of thermal imaging instruments will be reviewed and procedures currently used for testing to verify performance will be outlined.

INFRARED THERMAL IMAGING FIGURES OF MERIT

Introduction

This paper deals with the performance parameters or "figures of merit" of commercially available infrared thermal imaging instruments; how they are defined, how they are specified by the potential user and how the instruments can be tested to assure compliance. From the user's point of view, there are two broad categories of imaging instruments; those that provide quantitative information, generally in terms of target (blackbody equivalent) temperature, and those that provide only a qualitative thermal image. In the discussions to follow the term *imager* will be used to describe the quantitative instrument and the term *viewer* will be used to describe the qualitative instrument.

Since many of these parameters are based on the means by which scanning is accomplished, it is appropriate to review scanning methodology, beginning with point sensing of infrared radiation from a target.

An important advantage of infrared radiation thermometers over contact thermometers is their speed of response. The measured energy travels from the target to the sensor at the speed of light. The response of the instrument can then be in milliseconds or even microseconds. This important feature has allowed the field of infrared radiation thermometry to expand into real time thermal scanning and thermal mapping. When problems in temperature monitoring and control cannot be solved by the measurement of one or several discrete points on a target surface it becomes necessary to spatially scan, that is to move the collecting beam (instantaneous field of view) of the instrument relative to the target. This can be done by moving the target with the instrument fixed or by moving (translating or panning) the instrument, but is more practically accomplished by inserting a movable optical element or elements into the collecting beam. Depending on where these elements are placed the instrument can be made to scan in object space (in front of the primary optical element) or in image space (behind the primary element). Scanning in image space generally provides better resolution uniformity over narrow scanning angles and requires shorter excursions of the scanning elements. Scanning in object space generally allows wider scanning angles and requires wider angular excursions of the scanning elements in order to accomplish this.

Rectilinear scanning

The purpose of spatial scanning is to derive information concerning the distribution of radiant energy over a target scene. Although an almost infinite variety of scanning patterns can be generated using two moving elements, the most common pattern is rectilinear, and this is most often accomplished by two elements each scanning a direction normal to the other. A typical commercially available rectilinear single detector scanner employs two rotating prisms behind the primary lens system (refractive scanning in image space). An alternate approach to scanning using two oscillating mirrors in front of the primary lens (reflective scanning in object space) is also commonly used in commercially available single detector scanners. Both image space scanners and object space scanners can employ refractive or reflective scanning elements or even combinations of both elements. Most commercially available infrared imagers use a fast scan element to scan lines and a slower scan element to scan image frames, both scanning simultaneously in synchronism.

Multidetector scanners

One of the performance limitations of single-detector scanners is that imposed on the trade-off between speed of response and signal-to-noise ratio of the detector. These instruments require high speed cooled photodetectors which are pushed to their performance limits as the desired real-time scanning rate is increased. Multidetector scanners are scanning imagers that reduce the constraints on detector performance by adding detector elements which share the temporal-spatial burden. By varying detector spacing in the focal plane, the instrument designer can accomplish interlace scanning, stepped scanning, serial scanning or various combinations. These scanning improvements allow for faster frame rates with no reduction in signal-to-noise ratio or improve signal-to-noise ratio with no decreases in frame rate.

In one commercially available instrument, the vertical scanning element is entirely eliminated, and an oscillating mirror serves as the horizontal scanning element. A linear detector array is used on which the number of detector elements equals the number of scan lines in the frame, and each detector element always scans its "assigned" line. Certain adjustments, sometimes costly, are required when conventional linear arrays are used. A preamplifier is required for each detector, and the variations in detector characteristics from channel to channel need to be corrected so that thermal response across the image is uniform. The instrument described above is used commercially as a "thermal viewer" with no absolute temperature readout requirements; this makes it quite cost-effective. Otherwise, depending on the stringency of the instrument performance requirements, the cost of the array itself can be quite high, and the requirement for multiple individually matched preamplifiers may make the cost even higher.

In recent years detector mosaics or "staring" arrays have been used successfully for military night vision FLIR (Forward Looking InfraRed) viewers. Each detector element is assigned one display picture element and mechanical scanning is eliminated altogether.

It is important to understand the basic differences between night vision viewers (non-quantitative) and most high performance commercial IR imagers from the point of view of the end user. The purpose of a night vision system is to provide the clearest possible thermal map of the target to an observer with no actual measurement requirements. The purpose of the commercial thermal imager is to provide a high resolution quantitative thermal image of the target to an observer or to a data processing control system. Neither viewers or imagers using detector mosaics are presently available commercially although one staring array viewer is expected to become available soon.

Pyrovidicon viewers

Pyrovidicon thermal viewers are basically video cameras that operate in the infrared and are worth mentioning here as possible cost-effective tools for users who do not require quantitative thermal information. Pyrovidicons are discussed in some detail in the Kaplan paper, "An Update of Commercial Infrared Sensing and Imaging Instruments" (reference 1).

SPRITE technology

Around 1980 the British introduced a new detector that performs time delay and integration within the detector material itself. The SPRITE (Signal Processing in the Element) detector and its incorporation into a high resolution thermal imager are reviewed in the Leftwich paper, "Advanced TV Compatible Thermal Imaging Using the SPRITE Detector" (reference 2). The paper explains:

"It is possible to manufacture SPRITE detector filaments which are equivalent (depending on the applied field) to about 7 to 14 discrete, high D* elements, thus significantly reducing the number of leads to the cold finger and the complexity of the array."

The first commercial imager series using SPRITE technology was introduced in 1987 and is currently available. It is discussed in reference 1.

Performance parameters of two dimensional scanners

The parameters used for assessing the performance of infrared thermal imaging scanners are complex and the methods used for testing performance have generated some controversy among manufacturers and users of these instruments. Since a thermal image is made up of a great number of discrete point measurements, however, many of the performance parameters of infrared thermal imagers are the same as those of radiation thermometers (point sensing infrared radiometers that read out in temperature). Others derive from, or are extensions of, radiation thermometer performance parameters. It should be noted that for users requiring qualitative rather than quantitative thermal images, many of the parameters discussed herein are of no importance.

The following parameters can be used to specify the performance of an infrared (one-color) radiation thermometer:

- o Temperature range: The high and low limits over which the target temperature may vary
- o Absolute accuracy: As related to the NBS (National Bureau of Standards) standard
- o Repeatability: How faithfully a reading is repeated for the same target
- o Temperature sensitivity: The smallest target temperature change the instrument needs to detect
- o Speed of response: How fast the instrument responds to a temperature change at the target surface
- o Target spot size and working distance: The size of the spot on the target to be measured and its distance from the instrument
- o Output requirements: How the output signal is to be utilized
- o Spectral range: The portion of the infrared spectrum over which the instrument will operate
- o Sensor environment: The ambient conditions under which the instrument will operate

For infrared imaging scanners, the ERIM Infrared Handbook (reference 3) provides an extensive table of terms and definitions (section 19.1.2) and a list of specimen specifications (section 19.4.1). The section of the Handbook covering infrared imaging systems does not, however, deal with the imager as a quantitative measurement instrument, and so the performance parameters related with temperature measurement need to be added. From the user's point of view, some simplifications can be made which result in some acceptable approximations. Bearing these qualifications in mind, the following definitions of the key performance parameters of infrared thermal scanners are offered:

- o Total field of view (TFOV): The image size, in terms of scanning angle. (example: TFOV=20°V x 30°H)
- o Instantaneous field of view (IFOV): The angular projection of the detector element at the target plane: Imaging spatial resolution. (example: IFOV= 2 milliradians)
- o Measurement spatial resolution: (IFOV_{meas}): The spatial resolution describing the minimum target spot size on which an accurate temperature measurement can be made. (example: IFOV_{meas} = 5 milliradians)
- o Frame Rate: The number of times every point on the target is scanned in one second. (example: Frame rate = 30/second)
- o Minimum resolvable temperature (MRT): The smallest blackbody equivalent target temperature difference that can be observed: Temperature sensitivity. (example: MRT=0.1°C @ 30°C target temp.)

It shall be seen that MRT and the terms relating to spatial resolution are interrelated and cannot be considered independently. Other parameters such as spectral ranges, target temperature ranges, accuracy and repeatability and focusing distances are essentially the same as those defined previously for infrared radiation thermometers although they may be expressed differently. "Dynamic range" and "reference level range", for example, are the terms that define the target temperature ranges for thermal imagers. (For thermal viewers parameters relating to temperature range are only applicable in the broadest sense; absolute accuracy and stability parameters are not applicable; MRT is applicable only as an approximation since stability cannot be assured; IFOV_{meas} is not applicable).

Secondary features such as field uniformity and spatial distortion are design parameters, and are assumed to be handled by responsible manufacturers.

A discussion of the significant figures of merit follows:

Temperature range, accuracy and repeatability

Temperature range and absolute accuracy will always be interrelated; for example, the instrument might be expected to measure a range of temperatures from 0 to 200°C with an absolute accuracy $\pm 2^\circ\text{C}$ over the entire range. This could alternately be specified as $\pm 1\%$ absolute accuracy over full scale. Since absolute accuracy is based on traceability to the NBS standard, it is difficult for a manufacturer to comply with a tight specification for absolute accuracy. An absolute accuracy of $\pm 0.5^\circ\text{C} \pm 1\%$ of full scale is about as tight as can be reasonably specified. Repeatability, on the other hand, can be more easily

assured by the manufacturer, and is usually more important to the user. Testing for these parameters can be accomplished quite easily using blackbody reference sources. Commercial thermal imagers are usually provided with tables of temperature calibration data and, where applicable, corrections for atmospheric and ambient conditions.

Temperature sensitivity, MRTD or MRT

Temperature sensitivity is also called "thermal resolution" or "noise equivalent temperature difference" (NETD). For a radiation thermometer, it is the smallest temperature change at the target surface which can be clearly sensed at the output of the instrument. For any given instrument, temperature sensitivity will improve for hotter targets where there is more energy available for the instrument to measure. Any requirement for temperature sensitivity, therefore, should be specified at a particular target temperature, and this should be near the low end of the range of interest. A specified temperature sensitivity of 0.25°C at a target temperature of 25°C , for example, will ensure that the sensitivity of the instrument will be at least that for targets hotter than 25°C . NETD is the minimum equivalent blackbody temperature difference which will create a signal output equal to the steady state noise present in the instrument. This is easily measured electronically on radiation thermometers, but does not provide a satisfactory assessment of imager system performance.

For an imaging system, the term "minimum resolvable temperature" (MRT) or "minimum resolvable temperature difference" (MRTD) defines temperature sensitivity but also implies spatial resolution (IFOV). MRTD is expressed as a function of angular spatial frequency. Testing for MRTD is usually accomplished by means of a subjective procedure developed by the Department of Defense community. This involves selecting the smallest (highest frequency) standard periodic test pattern (four bars, 7:1 length to width aspect ratio) that can be distinguished as a 4 bar contrast target by the observer, and recording the smallest detectable element-to-element temperature difference between two blackbody elements on this pattern. Unlimited viewing time and optimization of controls is allowed and the target is oriented with the bars normal to the fast scan (line scanning) direction. Figure 1 illustrates the setup using an ambient pattern and a heated background. The MRTD curve shown is a function of spatial frequency (cycles/mrad). Additional points on the curve are achieved by changing the pattern size or the distance to the scanner.

Spot size, instantaneous field of view (IFOV), spatial resolution, measurement spatial resolution (IFOV_{meas})

For a radiation thermometer, target spot size (also called spatial resolution) and working distance may be specified as just that; "0.25" at 2 feet" for example, or in more general terms such as field of view angle (10 milliradians, 1 degree, 2 degrees) or a field of view (spot size-to-working distance) ratio (D/15, D/30, D/75). A D/15 ratio means that the instrument measures the emitted energy of a spot one-fifteenth the size of the working distance (3" at 45" for example).

For thermal imagers the instantaneous field of view (IFOV) expresses spatial resolution for imaging purposes but not for measurement purposes. Measurement instantaneous field of view (IFOV_{meas}) expresses spatial resolution for measurement purposes. The modulation transfer function (MTF) is a measure

of IFOV. Modulation is a measure of radiance contrast and is expressed:

$$\text{Modulation} = \frac{L_{\text{max}} - L_{\text{min}}}{L_{\text{max}} + L_{\text{min}}}$$

Modulation transfer is the ratio of the modulation in the observed image to that in the actual object. For any system, MTF will vary with scan angle and background, and will almost always be different when measured along the high speed scanning direction than it is when measured normal to it. For this reason a methodology was established and accepted by manufacturers and users alike to measure the MTF of an imager and, thereby, to verify the spatial resolution for imaging (night vision) purposes. A sample procedure follows for a system where IFOV is specified at 2.0 milliradians using the same setup as illustrated in figure 1:

A standard 4 bar (slit) resolution target (7:1 aspect ratio) with a 0.060" slit width is placed in front of a heated blackbody reference surface at a distance of 30" from the primary optic of the instrument (The ratio of the 0.060" slit width to the 30" working distance is 2 milliradians). The target is centered in the scanned field and oriented so that the fast scan axis is normal to the slit, and the fast scan output signal is monitored. The analog signal value of the 4 peaks (V_{max}), as the slits are scanned, and the analog signal value of the 3 valleys (V_{min}) are recorded using the bar target surface ambient temperature as a base reference. The MTF is $(V_{\text{max}} - V_{\text{min}}) / (V_{\text{max}} + V_{\text{min}})$. If this is at least 0.35 the 2 milliradian IFOV is verified.

There are some disagreements among users and manufacturers regarding the acceptable minimum value of MTF to verify IFOV with values varying between 0.35 and 0.5 depending on the manufacturer and the purpose of the instrument. For most users a tested value of $\text{MTF} \geq 0.35$ for a slit width representing a specified spatial resolution is generally considered sufficient to demonstrate that spatial resolution for imaging purposes.

Both MRTD and MTF are functions of spatial frequency for any given system. This is illustrated in figure 2, reprinted from J.M. Lloyd, "Thermal Imaging Systems" (reference 5) for a typical system rated by the manufacturer to be 1 milliradian. The cutoff frequency is where the IFOV equals 1 cycle (one bar and one slit) so that the intersection of the two curves at the half-cutoff frequency represents the actual performance of the system for an MRTD of 1°C. MTF is seen to be about 0.22 for this system.

For measurement purposes, of course, the slit width should, ideally, be increased until the modulation reaches unity. For this reason the MTF method was found to be unsatisfactory for commercial thermal imagers where quantitative temperature measurement and control are often necessary. Another procedure called the "Slit Response Method" was developed for this purpose and is generally accepted for measuring IFOV_{meas}. In this method, illustrated in figure 3, a single variable slit is placed in front of a blackbody source and the slit width is varied until the resultant signal approaches the signal of the blackbody reference. The curve shown is the Slit Response Function (SRF). Since there are other errors in the optics and the 100% level of SRF is approached rather slowly, the slit width at which the SRF reaches 0.9 is usually accepted as the IFOV_{meas}. Figures 1 and 3 are reprinted from the Ohman paper, "Measurement Versus Imaging in Thermography" (reference 4) which provides a detailed description of the Slit Response Method, setup diagrams and a discussion of imaging and measurement spatial resolution figures of merit.

Speed of response and frame rate

Speed of response of a radiation thermometer is generally defined as the time it takes the instrument output to respond to 95% of a step change at the target surface (about 5 time constants). This parameter is not applicable for thermal imagers, where each element of the target surface is scanned so rapidly that the value for an individual element may never reach 95% of the element-to-element contrast during a single frame scan. Frame integration techniques are used to improve measurement precision (and image quality as well) where it is critical.

Frame repetition rate is the measure of data update of a thermal imager. This is not the same as field repetition rate. Manufacturers tend to use fast field rates with not all the scan lines included in any one scan, and then interlace the fields so that it takes multiple fields to complete a full frame. This produces a more flicker-free image and is more pleasing to the eye than scanning full data frames at a slower rate. Frame rate is the number of times per second every element is scanned.

Output capabilities, recording and display features

Output capabilities are generally dependent on the user's needs. For radiation thermometers a wide selection of readout indicators is usually offered. An analog output suitable for recording, monitoring and control is commonly provided. In addition, most manufacturers offer a broad selection of output functions including digital (BCD coded) outputs, high, low, and proportional setpoints, signal peak or valley sensors, sample and hold circuits, and even closed-loop controls for specific applications. Many presently available instruments, even portable hand-held units, include microprocessors that provide many of the above functions on standard models.

For thermal imagers a selection of monochrome and color display capabilities is usually available, as well as videorecording and playback accessories. Display capabilities and software-dependent features such as data and image processing features are not considered performance figures of merit. They are discussed in the Kaplan paper of reference 1.

Spectral performance

The operating spectral range of a radiation thermometer is often critical to its performance. For cooler targets, up to about 500°C, most manufacturers offer instruments operating in the 8-14 μ atmospheric window. For hotter targets shorter operating wavelengths are selected, usually shorter than 3 μ . One reason for choosing shorter wavelengths is that this enables manufacturers to use commonly available and less expensive quartz and glass optics, which have the added benefit of being visibly transparent for more convenient aiming and sighting. Another reason is that estimating emittance incorrectly will result in smaller temperature errors when measurements are made at shorter wavelengths. Spectrally selective instruments employ interference filters to allow only a very specific broad or narrow band of wavelengths to reach the detector. (A combination of a spectrally selective detector and a filter can also be used). This can make the instrument highly selective to a specific material whose temperature is to be measured in the presence of an intervening medium or an interfering background.

The spectral range of operation of a thermal imager, on the other hand, is not usually critical to the user. All commercial thermal imagers operate in either the 2-5 μ or the 8-12 μ atmospheric window, depending on the manufacturer's choice of detector. Filter wheels or slides are usually available so that users can insert special interference filters and perform spectrally selective measurements when necessary.

Despite some manufacturer's claims to the contrary, there is usually little difference in overall performance between an imager operating in the 2-5 μ band and an imager operating in the 8-12 μ band, all other parameters being equal. For a specific application, however, there may be a clear choice. One example of this would be selecting an imager operating in the 2-5 μ band to observe a target through a quartz window. Since quartz is virtually opaque in the 8-12 μ region, there would be no alternative. Another example would be selecting an imager operating in the 8-12 μ band to observe a cool target through a long atmospheric path. Since long path atmospheric absorption is substantially greater in the 2-5 μ window than in the 8-12 μ , the choice would be obvious.

Operating environment

For radiation thermometers, manufacturers offer environmental enclosures when the operating environment is expected to be hostile enough to the sensor to affect its operation. Most commercial thermal viewers are hand-held and will generally operate satisfactorily in any environment that the user can tolerate. Many thermal imagers are intended for laboratory type of operation only and published specifications illustrate this. Most manufacturers, however, package their scanners in rugged portable housings suitable for most factory and field uses. Reference 1 provides a more detailed discussion of this subject.

References

1. H. Kaplan, An Update of Commercial Infrared Sensing and Imaging Instruments, NASA Conference Publication, NCTM Workshop, Pasadena, CA, January, 1989.
2. R.F. Leftwich, Advanced TV Compatible Thermal Imaging Using the SPRITE Detector, SPIE Proceedings Vol. 371, Thermal Infrared Sensing Diagnostics (THERMOSENSE V), Detroit, MI, October, 1982, P. 216.
3. Wolfe, Zissis, "The Infrared Handbook", ERIM, ONR, Dept. of the Navy, 1978.
4. C. Ohman, "Measurement VS Imaging in Thermography, or What is Resolution?", Proceedings of the Fifth Infrared Information Exchange, New Orleans LA, 1985, Book 2, P. 65 (AGEMA Infrared Systems)
5. J.M. Lloyd, "Thermal Imaging Systems", Plenum Press, 1975

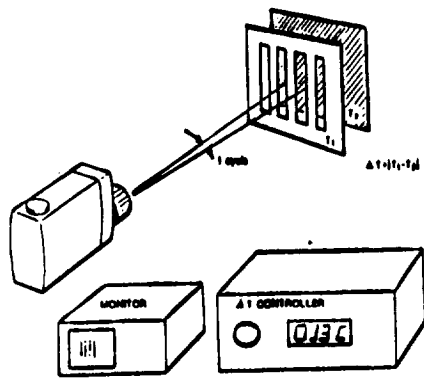


Figure 1. Minimum resolvable temperature difference

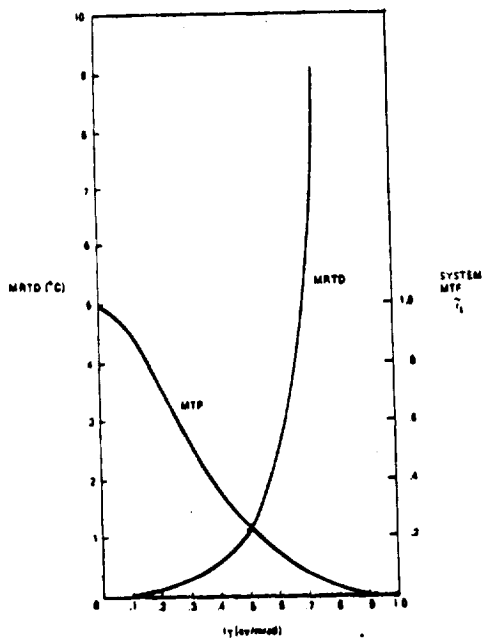
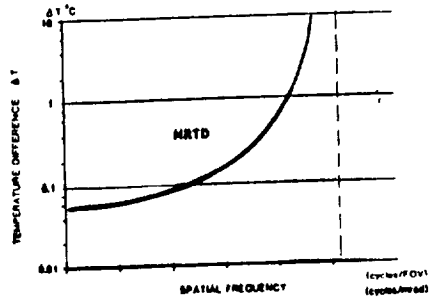
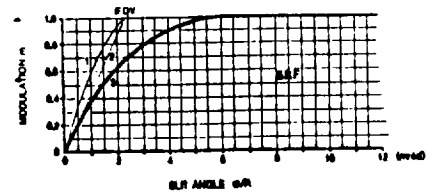
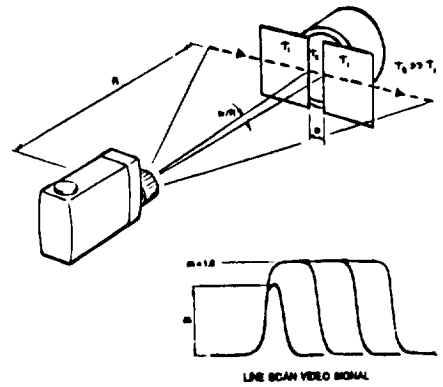


Figure 2. MRTD and MTF for the example system.



- 1) Ideal SMI for a square detector
- 2) Ideal SMI for a square detector
- 3) Typical measured SMI

Figure 3. SMI response function

A MULTICOLOR IMAGING PYROMETER

Michael B. Frish and Jonathan H. Frank

Physical Sciences Inc.
Research Park, PO Box 3100, Andover MA 01810

1. INTRODUCTION

Pyrometry is a well-established technique for determining the temperature of a material by measuring the radiation that it emits. In general, the accuracy of pyrometry suffers from the problem that there is always one parameter which must be known to determine the temperature but cannot be measured. This parameter is usually the emissivity of the material at a specific wavelength or the ratio of emissivities at two or more different wavelengths. In most materials the emissivity changes as the material is heated, and easily made measurements of the emissivity at room temperature provide little information that is useful at elevated temperatures. Therefore, an educated guess of the material's high temperature emissivity must be made. The accuracy of this guess determines the resultant accuracy of the temperature measurement.

Recently, a new technique has been developed for using pyrometry to measure elevated temperatures with a minimum of emissivity related uncertainty.¹⁻⁴ The approach utilizes an optical system that collects radiation emitted at a wavelength that is short compared to the peak of the blackbody spectrum for the temperature range of interest. In this regime the radiant power increases faster than exponentially with temperature. Because of this extreme sensitivity to temperature, the emissivity of the source plays a relatively small role in determining the emitted power. Such a pyrometer therefore provides a more accurate measurement of the temperature than one using a longer wavelength. However, because the dynamic range of the photodetector usually places rather narrow limits on the range of temperatures that can be measured at a single short wavelength, to cover a broad range of temperatures it is valuable to provide several different detectors, each sensitive to a different wavelength and to a specific temperature range. Such a device is herein called a multicolor pyrometer.

This multicolor approach has now been incorporated into an imaging pyrometer designed to measure the temperatures distributions along the surfaces of small (~2 mm diameter) moving objects subjected to radiant heating in a furnace. As reported herein, this device is capable of measuring temperatures between 1000 and 2500K with better than 0.2 percent precision and an emissivity-related temperature uncertainty which is less than 10 percent of the emissivity uncertainty. In its present configuration, the system updates the temperature map at a rate of about 10 Hz and has a spatial resolution of about 0.1 mm.

The theory underlying the design of the multicolor pyrometer is discussed in Section 2 below. This is followed by a detailed description of the imaging system in Section 3, and its operation in Section 4. Section 4 also reports the successful results of an experiment validating the pyrometer's accuracy and precision. The paper concludes with a summary in Section 5.

2. THEORY

2.1 The Accuracy of Multicolor Pyrometry

The radiant energy emitted by any object is determined by the Planck equation:⁵

$$R(\lambda)d\lambda = \frac{C_1}{\pi\lambda^5} \frac{\epsilon(\lambda,T) d\lambda}{\exp(C_2/\lambda T) - 1} \quad (1)$$

where $R(\lambda)d\lambda$ is the radiant flux per steradian per unit area of emitter surface in the wavelength interval $[\lambda, \lambda + d\lambda]$, $C_1/\pi = 1.191 \times 10^{-12}$ W-cm²/sr, $C_2 = 1.44$ cm-K, T is the temperature, and $\epsilon(\lambda,T)$ is the spectral emissivity of the material at wavelength λ . In a typical pyrometer, a portion of the heated target's surface is imaged by a group of lenses and mirrors onto a photodetector which converts the incident radiation into a measurable electrical quantity. The optical path generally contains several windows, mirrors, beam splitters or filters, each of which has a wavelength dependent transmittance or reflectance, $t_i(\lambda)$. They, together with the solid angle Ω subtended by the optical collection system, and the surface area, A_S , of the radiant target, determine the radiant power which reaches the detector,

$$P = \frac{A_S \Omega C_1}{\pi} \int_0^\infty \frac{\prod_{i=1}^n t_i(\lambda) \epsilon(\lambda,T) d\lambda}{\lambda^5 [\exp(C_2/\lambda T) - 1]} \quad (2)$$

where n is the number of components in the optical train. By using a narrow bandpass optical filter to select a particular wavelength (i.e., color) at which to measure the radiance, the emissivity of the target and the transmittance or reflectance of other optical components are essentially constant over the bandpass. These

variables can therefore be removed from the integral in Eq.(2) and, if the transmission curve of the filter is known, the integral may be evaluated, as

$$P = \epsilon_{\lambda} D_{\lambda} \int_{\lambda_1}^{\lambda_2} \frac{t_f(\lambda) d\lambda}{\lambda^5 [\exp(C_2/\lambda T) - 1]} \quad (3)$$

where ϵ_{λ} is the emissivity at the central wavelength of the filter, D_{λ} is a constant (independent of temperature) determined by the optical system which may be evaluated by calibration, t_f is the (known) transmission function of the filter, and λ_1, λ_2 are the bandpass limits of the filter. When the photodetector is operated such that it generates a voltage signal which is proportional to the energy incident on its surface during a period of time τ , Eq. (3) may be written as

$$V(T) = \epsilon_{\lambda} B_{\lambda} F_{\lambda}(T) \quad (4)$$

where $F_{\lambda}(T)$ is a known thermal response function proportional to the integral in Eq. (3), and

$$B_{\lambda} = G D_{\lambda} \eta_{\lambda} \tau \quad (5)$$

where G (volts/coulomb) is the responsivity of the photodetector and its associated amplification circuitry, and η_{λ} (coulombs/joule) is proportional to the quantum efficiency of the detector.

Unfortunately, in addition to its dependence on temperature, the radiant emission from a heated object at a given wavelength depends on its emissivity, an intrinsic property of the material. Furthermore, as indicated in Eq. (1), the emissivity may be a function of both wavelength and temperature. It may also change with time as a material suffers changes in its transparency, reflectivity, or surface structure due to phase changes, chemical reaction, ablation, etc. Thus, the wavelength and temperature dependences of the emissivity are often unknown, and precise pyrometric measurement of the true temperature in such situations is generally accepted as being essentially impossible.

By always operating the pyrometer at a wavelength such that $\lambda T \ll 1$ cm-K, the multicolor technique described herein provides the best possible estimate of the true temperature under the difficult circumstances of unknown and unmeasurable emissivities which vary wildly and unpredictably with wavelength, temperature, and time. Eq. (1) shows that, at these short wavelengths, the radiant power emitted by a heated surface increases faster than exponentially with temperature, but is only linearly dependent on emissivity. Thus, a large uncertainty in emissivity causes only a small error in temperature. Mathematically, this is seen by solving Eq.(4) for temperature. The function $F_{\lambda}(T)$ may be easily evaluated by approximating the transmission function of the narrow bandpass filter by a rectangle of height t_{λ} and width $\Delta\lambda = \lambda_2 - \lambda_1$. Defining

$$F_{\lambda}(T) = \{\exp(C_2/\lambda T) - 1\}^{-1} \quad (6)$$

and

$$B_{\lambda} = \frac{A_s \Omega t_{\lambda} \eta_{\lambda} \tau G C_1 \Delta\lambda}{\pi \lambda^5} \prod_{i=1}^n t_i \quad (7)$$

and solving Eqs. (4) through (7) for temperature yields

$$T = \frac{C_2}{\lambda \ln\{(B_{\lambda} \epsilon_{\lambda} / V) + 1\}} \quad (8)$$

Differentiating with respect to ϵ_{λ} gives the temperature accuracy as

$$\frac{\Delta T}{T} = [1 - \exp(-C_2/\lambda T)] \frac{\lambda T}{C_2} \frac{\Delta \epsilon_{\lambda}}{\epsilon_{\lambda}} \quad (9)$$

which is plotted in Figure 1 for several wavelengths using $\Delta \epsilon_{\lambda} / \epsilon_{\lambda} = \pm 0.25$. Although the temperature uncertainty increases with temperature for all wavelengths, it is clear that, by selecting a sufficiently short wavelength for operation of the pyrometer, uncertainties of less than two percent can be achieved.

2.2 Practical Considerations

On the basis of Eqs. (8) and (9), it would appear that a single color pyrometer could be used to measure any temperature below a predetermined value to any degree of accuracy simply by selecting a sufficiently short wavelength. Although this is true in principle, either detector sensitivity or shot noise places a lower limit on the temperature sensitivity for any particular wavelength and optical collector combination. In addition, there is a maximum temperature to which a particular system will be sensitive, fixed by the onset of detector saturation. Photodetectors used in typical imaging systems have a dynamic range of only about two orders of magnitude. However, at 370 nm, where the temperature accuracy is $\pm 40K$ when the true temperature is 2500K and the emissivity error is ± 25 percent, the radiant power spans a dynamic range exceeding ten orders of magnitude as the temperature increases from 1000 to 2500K. A single imaging pyrometer operating at this

wavelength is clearly unsuitable for measurements over this entire temperature range. Longer wavelengths cannot be used at the higher temperatures without sacrificing accuracy. However, if use of this short wavelength is limited to temperatures between about 2250 and 2500K, the dynamic range required of the detector is less than 10. An additional detector operating at 420 nm and otherwise having the same sensitivity and dynamic range is able to measure temperatures between 1970 and 2250K while retaining the accuracy of the shorter wavelength detector. Thus, by using several individual different-color pyrometers, the entire temperature range of interest can in principle be measured with high accuracy, assuming only marginal knowledge of the emissivity. Thus, a multicolor pyrometer is considered here to be a group of single color pyrometers of which only one is used at a time. As described next, we have utilized this approach to assemble a multicolor imaging pyrometer.

3. MULTICOLOR IMAGING PYROMETER

3.1 Description

The imaging pyrometer was designed to measure surface temperature distributions of objects having diameters of at least 2 mm moving within a spherical volume of about 1 cm diameter. As illustrated schematically in Figure 2, radiation emitted by the heated sample is collected by a 360 mm focal length objective lens which, since the sample is located within the focal plane of the objective, projects a nearly collimated beam into a color separator. Six different-color images are then projected onto a single charged-coupled-device (CCD) photodetector array.

The color separation is accomplished using a series of dichroic beamsplitters, of which three are shown in Figure 2. The first beamsplitter ideally reflects all radiation at wavelengths greater than λ_1 while transmitting all shorter wavelengths. The second beamsplitter similarly reflects all radiation at wavelengths longer than λ_2 (of which there is ideally none longer than λ_1) and transmits the rest, which is reflected by the third mirror. The three reflected beams are transmitted through interference filters, which select the desired narrow bands of wavelengths from the relatively broad bands reflected by the beamsplitters, and thence through 100 mm focal length lenses which image the sample onto the CCD array located at the focal plane of the lenses. To provide all six images, a fourth dichroic beamsplitter is inserted ahead of the three shown. It reflects a band of wavelengths upwards to a second row of beamsplitters. The reflections from this second layer are projected similarly onto the CCD, as illustrated by the side view of Figure 3. The optical collection efficiency of the system is limited by the 25 mm diameter imaging lenses to about F/14. To reduce optical aberrations, it is preferable to place a stop at the objective lens limiting the speed to F/18. When operating at this speed there is no vignetting of objects moving within the field of view. The overall system magnification of 0.28 is determined by the ratio of the focal lengths of the objective lens to the imaging lenses.

The six optical paths are aligned so that the centers of the images are positioned on the CCD as illustrated in Figure 4. Each center is 1.5 mm from its neighbors, meaning that objects $1.5/.28 = 5.3$ mm in diameter can be observed without the images overlapping each other. Since the image centers are also at least 1.5 mm from the edge of the detector, each image is a projection of the full 1 cm field of view.

The CCD detector divides the images into an array of 610 x 244 pixels, each of which can be considered to be an individual photodetector. The associated electronics, incorporated into a Sierra Scientific Model 4032 camera, convert the irradiance incident on each pixel during a fixed exposure period into a voltage value, and transmits the voltage values sequentially in an RS-170 video format. That is, each horizontal line of pixels is transmitted during a 63.5 μ s period, and all 244 lines are transmitted every 1/60 s, thereby comprising a video field. A unique feature of this camera is its capability to alter the exposure time to any value between 1 and 1000 ms while maintaining the RS-170 format. Each video field is acquired by a Data Translation Model 2851 frame grabber, which digitizes the transmitted data with 8-bit accuracy, stores it in an on-board buffer or transfers it to the Compaq 286 personal computer memory, and displays it on a video monitor. The computer and frame-grabber, functioning together, are programmed to select which one of the six available images contained within the frame provides data that is suitable for conversion to temperature values, performs the conversion, and displays the results as a false color temperature map. The map can be updated 10 times per second, and the data can be stored on videotape for post-test analysis.

3.2 Wavelength Selection

The six wavelengths used in the pyrometer have been selected to provide high measurement precision while spanning a temperature range from less than 1000K to greater than 2500K. The longest wavelength provides measurement of the lowest temperature possible with this system, determined as follows: The minimum temperature detectable at any given wavelength is that which, during the exposure time, generates a signal equal to the detector's rms noise. In general, as the wavelength increases the associated minimum detectable temperature decreases, and conversely as the temperature decreases the optimum wavelength for measuring it increases. However, at long wavelengths the quantum efficiency of the detector decreases with increasing wavelength, resulting in the existence of a temperature below which no signal can be detected regardless of the wavelength. This is the minimum measurable temperature and, for our system, has been calculated to be 888K at a wavelength of 930 nm assuming an exposure time of 50 ms. The maximum temperature observable at this wavelength, i.e. that which saturates the detector, is 1302K.

All of the other colors were chosen to provide a precision better than 0.2 percent during a 16.67 ms exposure at a minimum temperature equal to the maximum temperature observable with the next longest wavelength. The precision of the temperature measurement is, in essence, determined by the 8-bit precision of the video frame grabber, in which the minimum resolvable change in signal is $1/(2^8-1) = 1/255$ of the signal at saturation. Each 1-bit signal change is called a gray level. Because the signal generated at a specific wavelength increases much more rapidly than linear with increasing temperature, the precision of the measurement also increases with temperature. That is, at higher temperatures a smaller change in temperature is required to produce an incremental step in the gray level than at lower temperatures. Thus, the minimum temperature at which a specified precision can be achieved may correspond to a gray level greater than unity,

and therefore is higher than the minimum detectable temperature. Each color therefore has both a wavelength and a minimum gray level specified for optimum precision. The selected colors, the range of temperatures spanned by each color while providing a measurement precision of 0.2 percent, and the ranges measurable regardless of precision are shown in Table 1. The ratio of temperature uncertainty to the emissivity uncertainty at the peak temperature of each color is also tabulated.

TABLE 1

Wavelength (nm)	High Temp. (K)	Low Temp. @ 0.2 % Precision	Minimum Detectable Temperature	$\Delta T/T$ ---- $\Delta \epsilon/\epsilon$
930	1302	1119	888	0.08
750	1506	1298	1050	0.08
590	1728	1505	1244	0.07
480	1971	1726	1445	0.07
420	2249	1970	1650	0.07
370	2562	2243	1878	0.07

The temperature ranges shown in Table 1 assume a sample emissivity of 0.5. Figure 5 graphically displays the range of temperatures measurable with 0.2 percent precision at each of these wavelengths as a function of emissivity. The minimum temperature measurable at the longest wavelength regardless of precision is also shown. In the shaded regions the upper range of one filter overlaps with the lower range of the filter of next shorter wavelength. The overlap has been designed to be only a few degrees at each transition, but can be enhanced by decreasing the lower temperature limits of each color, either by increasing the integration time, or by decreasing the precision. Thus, through the use of the computer controlled variable integration time camera and these filters, wide flexibility in the the operation of the system is possible.

4. PYROMETER OPERATION

4.1 Data Acquisition and Processing Algorithms

Four steps are required for each update of the temperature map acquired and displayed with the pyrometer: 1) acquiring a field of data; 2) subtracting the dark signal from that field; 3) selecting the appropriate one of the six available images for analysis; and 4) converting the radiance data in the image to temperature values. The last step assumes, of course, that the system has been precalibrated so that the correspondence between measured radiance and temperature is known.

Acquisition of the video field is performed by straightforward programming of the frame grabber. The video signal is digitized and stored in one of the on-board frame buffers. To convert this information into accurate temperature data, the dark signal is subtracted from each field of data. Each pixel in the field has a unique dark signal that is a function of the integration time and is measured simply by blocking the pyrometer's entrance aperture, adjusting the integration time to the desired value, and averaging a sequence of 100 frames. Average values of the gray level at each pixel are then stored in an auxiliary frame buffer and called up as required for background subtraction.

As described above, the pyrometer projects six non-overlapping images onto the CCD array simultaneously, but only one image provides data suitable for reduction to temperature. All of the other images are either bright enough to saturate the frame grabber, or dim enough to be undetectable. Selection of the correct image is accomplished by scanning predetermined portions of the video field to locate pixels which have non-zero but unsaturated gray levels. To this end, an algorithm has been developed that locates the centroid of the longest wavelength image, and checks to determine whether it is saturated. If it is saturated, then the center of the image corresponding to the next longest wavelength, located 1.5 mm away from the first image, is checked for saturation. This procedure is repeated until an unsaturated image is found, which, by design, must be the one that provides valid data.

The pyrometer is calibrated by placing a source (such as a blackbody) of known temperature and emissivity in the object plane, measuring the most probable gray level of the image at the appropriate wavelength, determining the calibration constant defined by Eq. (4), and finally using the Planck equation to generate a lookup table relating each of the 256 available gray levels within the image to a corresponding temperature. The lookup table is stored for use during data acquisition.

The temperature measurement procedure combines all of the steps described above. A video field containing the six images of the hot moving object is acquired and stored in a frame buffer. The appropriate image is then located and the background subtracted. The result is passed through an output lookup table which displays on the video monitor a false color image corresponding to the temperature distribution in the object. This lookup table may be the one created during the calibration procedure, or it may be a modified version that accounts for any user knowledge of the object's emissivity. In addition to displaying a temperature map, the algorithm finds the maximum temperature within the object and displays this value in numerical form. This value may also be used in a feedback loop to actively control the temperature.

4.2 Demonstration

A breadboard version of the multicolor imaging pyrometer has been used to measure the temperature of a low emissivity surface, namely molten aluminum contained in a clear quartz crucible, subjected to radiant

heating within a kiln and observed through a small port in the kiln's wall, as illustrated in Figure 6. Under these conditions, the radiation seen by the pyrometer is a combination of the radiation emitted by the aluminum and that emitted by the kiln walls at temperature T_V and reflected from the aluminum surface at T_S :

$$R(\lambda)d\lambda = \frac{c_1}{\pi\lambda^5} \left[\frac{\epsilon_s(\lambda, T_S)}{\exp(c_2/\lambda T_S) - 1} + \frac{1 - \epsilon_s(\lambda, T_S)}{\exp(c_2/\lambda T_V) - 1} \right] \quad (10)$$

The second term, which accounts for the reflected radiation, depends on the background temperature and the sample emissivity. This is simply a result of energy conservation, which requires the sum of the monochromatic reflectivity, transmittivity and absorptivity of a material to equal unity, and Kirchoff's law which, in a simple form, states that the absorptivity of a material, at a given wavelength, is equal to its emissivity. Thus, $1 - \epsilon_s(\lambda, T_S)$ is equal to the reflectivity of the aluminum and is the proper factor to use for incorporating the background radiation effects.

In these experiments, because the heating rate is slow, the aluminum and the walls of the kiln are at roughly the same temperatures, i.e. $T_V = T_S$. As a result, the radiation observed is approximately that of a blackbody at T_S . The pyrometer was therefore programmed to assume an emissivity of unity. The temperature of the aluminum, as it heated from room temperature to about 1000C, was monitored by the pyrometer. A thermocouple was suspended within the crucible to measure the aluminum's temperature directly. Figure 7 is a comparison of the average temperature observed by the pyrometer with that of the thermocouple. The agreement is essentially perfect within the precision of the pyrometer's measurement capabilities.

5. SUMMARY

A multicolor imaging pyrometer has been designed for accurately and precisely measuring the temperature distribution histories of small moving samples. The device projects six different color images of the sample onto a single CCD array that provides an RS-170 video signal to a computerized frame grabber. The computer automatically selects which one of the six images provides useful data, and converts that information to a temperature map. By measuring the temperature of molten aluminum heated in a kiln, a breadboard version of the device has been shown to provide high accuracy in difficult measurement situations. It is expected that this pyrometer will ultimately find application in measuring the temperatures of materials undergoing radiant heating in a microgravity acoustic levitation furnace.

References

1. M.B. Frish, "Measurement of High Temperature Thermophysical Properties with Electron Beam Heating," AIAA Paper No. 84-1784 (1984).
2. M.B. Frish, M.N. Spencer, N.E. Wolk, J.S. Werner and H.A. Miranda, "Multi-Color Pyrometer for Materials Processing in Space", Proc. of the Noncontact Temperature Measurement Workshop, NASA Conf. Pub. 2503 (May 1987).
3. P.C. Nordine, "The Accuracy of Multicolor Optical Pyrometry", High Temperature Science, 21, (1986).
4. D.P. DeWitt and R.E. Rondeau, "Evaluation of a Method for Measuring Front-Face Surface Temperatures and Spectral Emissivities During Irradiation", AIAA Paper No. 87-1565 (1987).
5. Siegel, R. and Howell, J.R., Thermal Radiation Heat Transfer, McGraw-Hill (1981).

Acknowledgment

Support for this work from the NASA Jet Propulsion Laboratory, under SBIR contract NAS7-1002, is gratefully acknowledged.

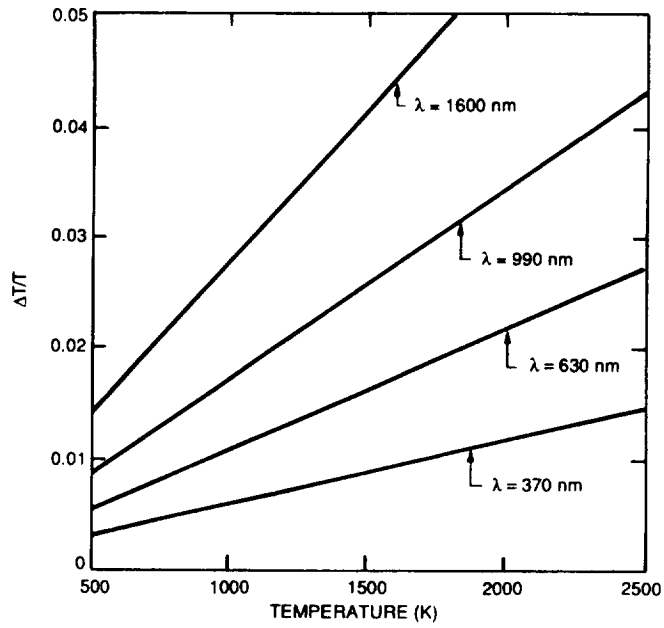


Figure 1. Temperature uncertainties resulting from an emissivity uncertainty of $\Delta\epsilon/\epsilon = \pm 0.25$ at several wavelengths.

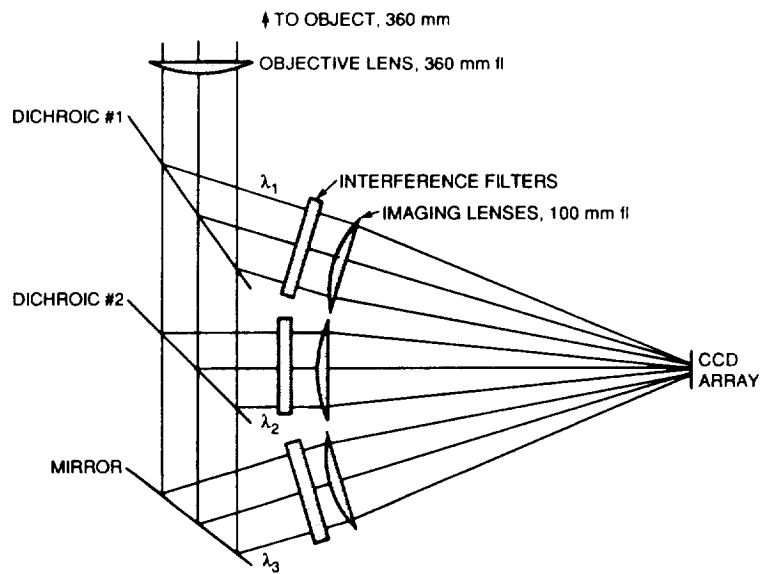


Figure 2. Schematic illustration of multicolor pyrometer optical configuration.

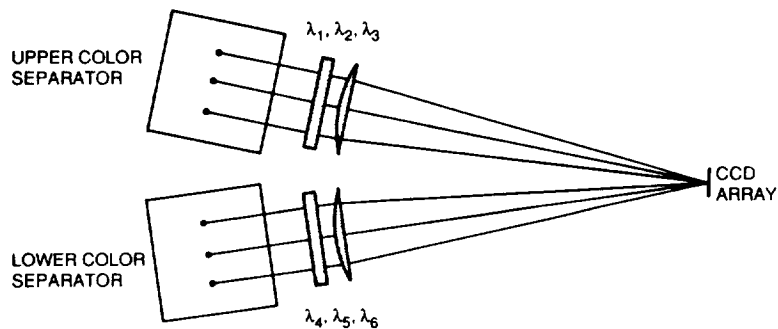


Figure 3. Side view of pyrometer optical configuration.

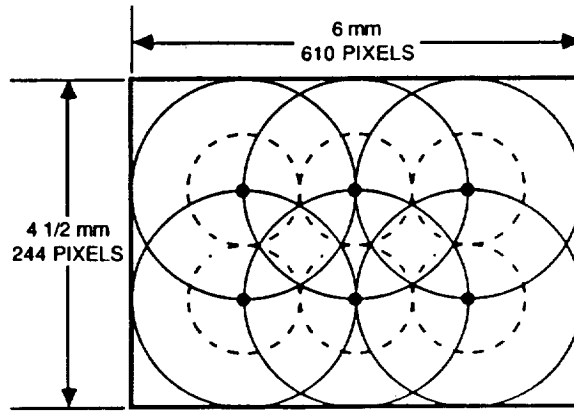


Figure 4. Arrangement of six images on CCD array. Solid circles enclose the area used to project onto the detector the entire field-of-view seen by each image. Dashed circles indicate the maximum size of a moving object that can be observed without suffering image overlap.

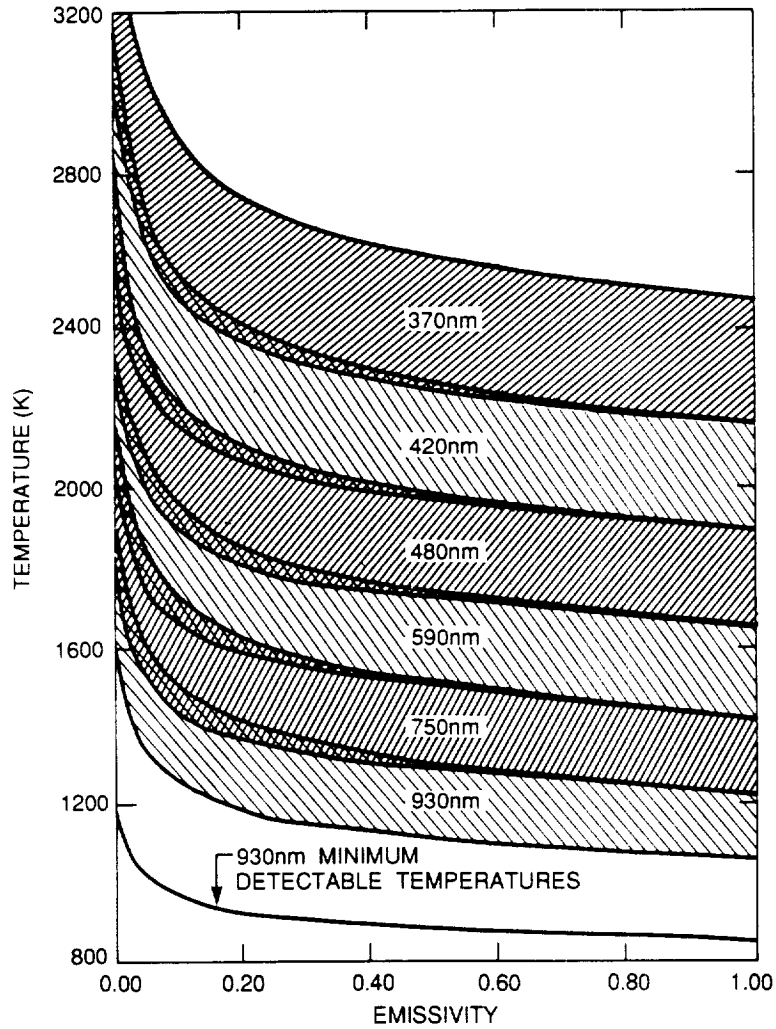


Figure 5. Temperature ranges observable at each wavelength as a function of sample emissivity.

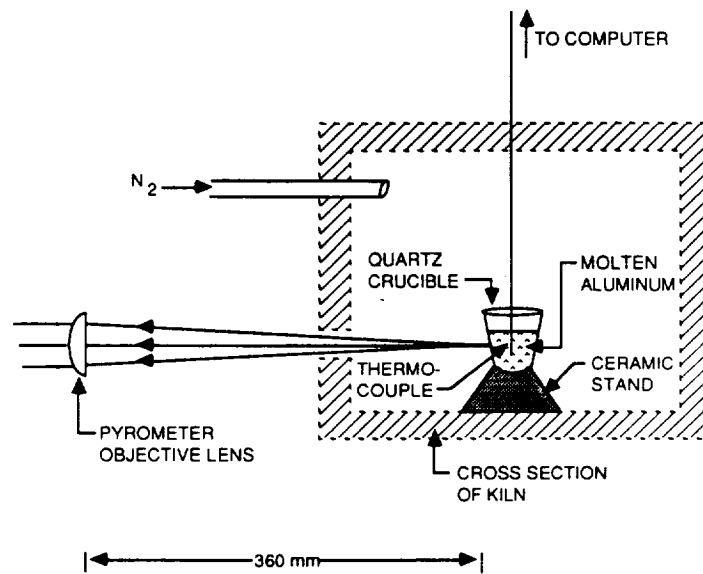


Figure 6. Illustration of pyrometer demonstration experiment.

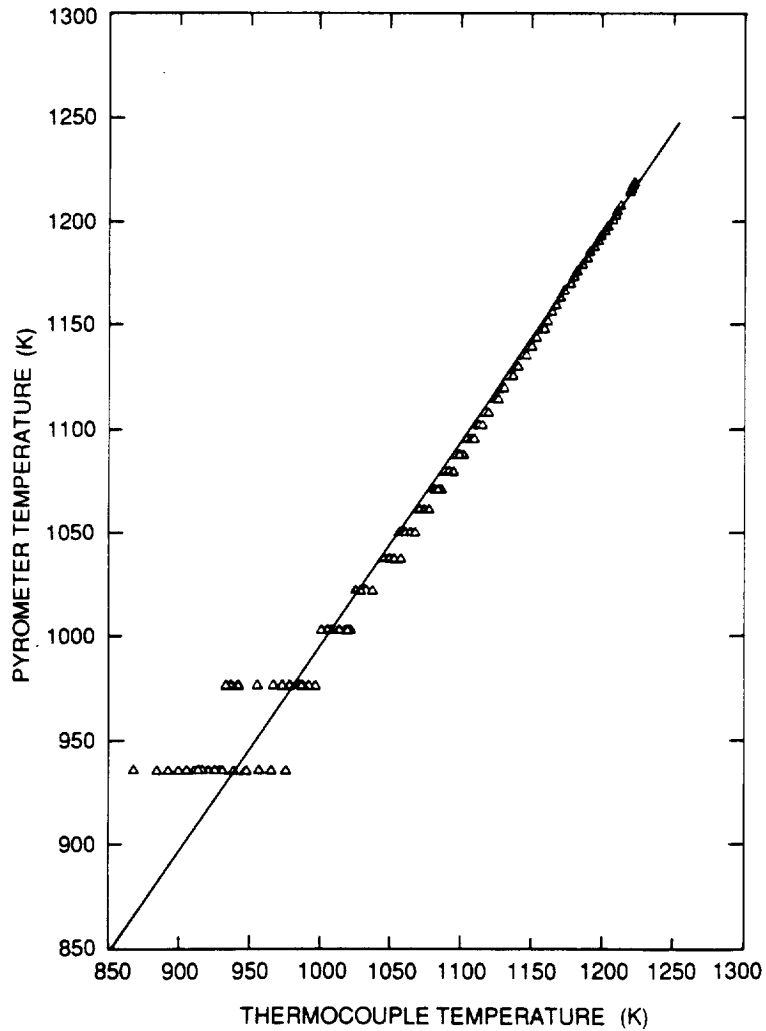


Figure 7. Comparisons of temperatures measured by a multicolor pyrometer vs those measured by thermocouple for molten aluminum heated in a kiln.

NON-CONTACT TRUE TEMPERATURE MEASUREMENTS IN THE MICROGRAVITY ENVIRONMENT

MANSOOR A. KHAN

Wyman Gordon Co., 244 Worcester St., N. Grafton, MA 01536

CHARLY ALLEMAND AND THOMAS W. EAGAR

MIT, 77 Massachusetts Ave., Cambridge, MA 02139

INTRODUCTION

The accurate measurement and control of temperature can be of great importance in most materials manufacturing and processing applications. With present-day technology such measurement almost always requires either physical contact with the subject or an extensive calibration procedure. In many cases contact is either not desirable, because such contact may significantly alter the temperature or other characteristics of the subject, or is not possible because the subject is moving, is too far away, is too hot or is in an otherwise hostile environment. Similarly calibration may not be possible if the characteristics change too much.

Multiwavelength pyrometry can help solve some of these problems by providing a reliable method for emissivity independent noncontact true temperature measurements.

BASIC THEORY

All bodies above absolute zero radiate thermal energy. The most efficient thermal radiator is a black body, which is defined as an object that will absorb all incident radiation. The emitted radiance per unit wavelength or spectral radiance of such a body is given by the Planck radiation law:

$$N'_\lambda = C_1 \lambda^{-5} (\exp(C_2/\lambda T) - 1)^{-1} \quad (1)$$

where λ is the wavelength, T is the absolute temperature and C_1 and C_2 are the Planck constants. Figure 1 is a plot of N'_λ vs. λ at various temperatures. The dotted curve depicts Wiens law (as opposed to Wiens approximation which is discussed later) which relates the peak of the Planck curves to wavelength.

A real body however emits only a fraction of what a black body emits at any given temperature. The spectral radiance of a real body is given by a modified form of the Planck radiation law:

$$N_\lambda = \epsilon_\lambda C_1 \lambda^{-5} (\exp(C_2/\lambda T) - 1)^{-1} \quad (2)$$

The term ϵ_λ is called the emissivity and is defined as the ratio of what a real body emits at a given temperature to what a black body emits at that temperature (i.e. $\epsilon_\lambda \leq 1$). In general emissivities of real bodies are functions of wavelength, temperature and surface condition. For fast measurements, though, the emissivity can be considered to be a function only of wavelength. The

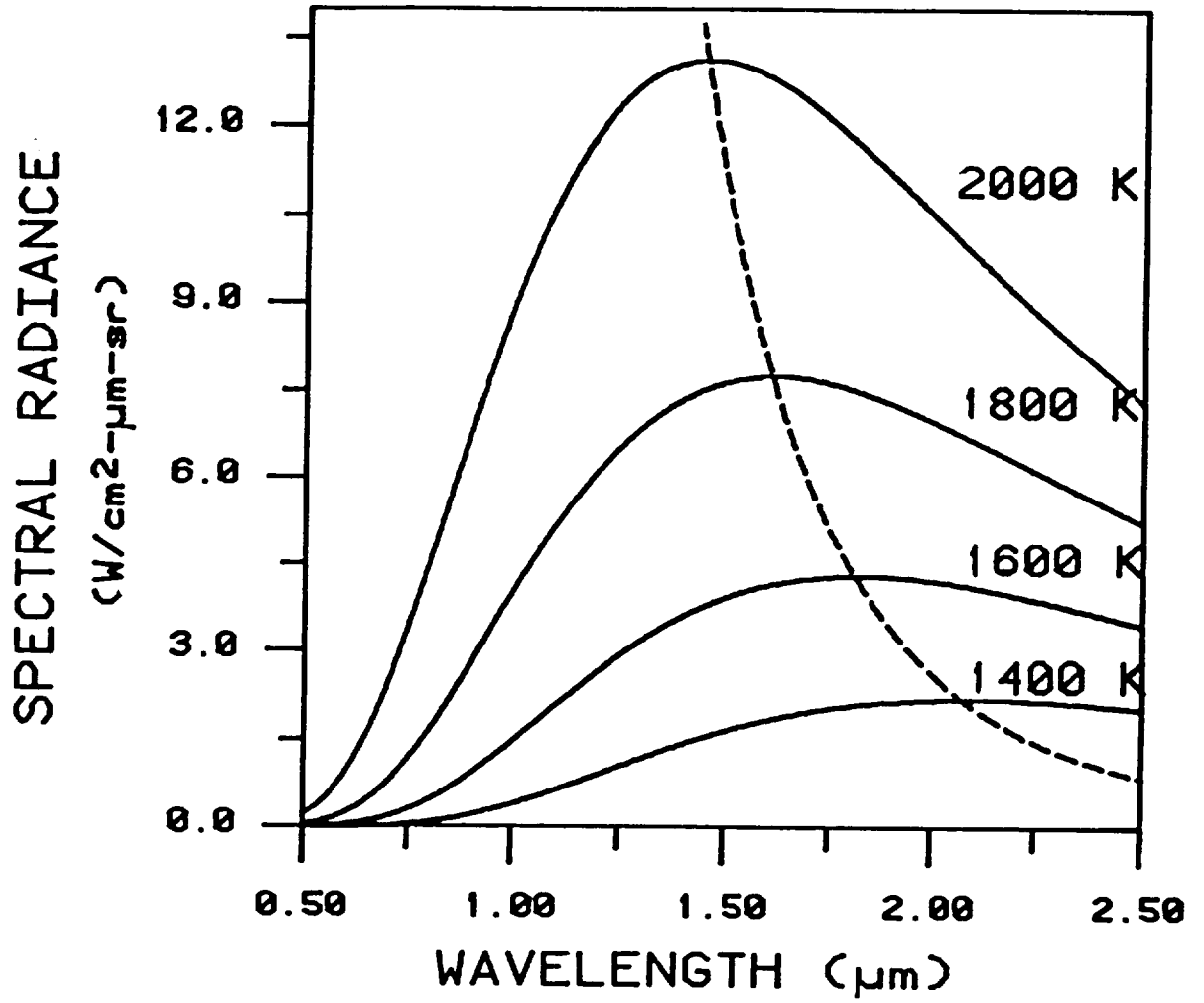


Figure 1 - Spectral radiance curves at different temperatures, as predicted by the Planck radiation law.

emissivity of these bodies can easily vary by 10% over fairly small wavelength ranges. Therefore, any pyrometer that does not take emissivity changes into account can produce significant errors. Additionally because emissivity is rarely known for a given set of circumstances it must be either measured or calculated separately if an accurate temperature determination is to be made.

STATE OF THE ART

The most sophisticated technique of noncontact temperature measurement available today is Ratio or two-color pyrometry [1]. This method uses an approximation of the Planck relation called the Wien radiation relation:

$$N_{\lambda} = \epsilon_{\lambda} C_1 \lambda^{-5} \exp(-C_2/\lambda T) \quad (3)$$

The Wien relation can be solved for temperatures at two different wavelengths to give:

$$T = C_2 \frac{(\lambda_2 - \lambda_1)}{\lambda_1 \lambda_2 \{5 \ln(\lambda_2/\lambda_1) - \ln(N_1/N_2) + \ln(\epsilon_1/\epsilon_2)\}} \quad (4)$$

If the wavelengths λ_1 and λ_2 are chosen such that gray body behavior can be assumed (i.e. $\epsilon_1 = \epsilon_2$) then the emissivity term drops out and the temperature measurement is straight-forward. The assumption of gray body behavior becomes more valid as $\Delta\lambda = (\lambda_1 - \lambda_2) \rightarrow 0$ but as $\Delta\lambda \rightarrow 0$ any errors in the radiance measurements become more significant. Increasing the separation of the wavelengths reduces the effects of radiance measurement errors but the gray body assumption becomes less valid.

References [1-3] provide a thorough analysis of the errors associated with this technique.

MULTIWAVELENGTH THEORY

To increase the accuracy of the temperature measurement farther, the emissivity must be modeled better. This can be achieved by measuring the spectral radiance at a larger (>2) number of wavelengths. The term multiwavelength pyrometry refers to a set of techniques that measure radiance at n different wavelengths and then fit this data to a model that has m undetermined parameters ($m < n$), to calculate both the temperature and the emissivity simultaneously. The fitting model consists of the modified Planck function (Eq. 2) with a relation containing the m-1 undetermined parameters for the emissivity. The primary strength of multiwavelength pyrometry is that it makes only one assumption about the emissivity, namely, that the spectral emissivity has a smooth first derivative.

There are three solution techniques that fall under the heading of multiwavelength pyrometry, namely, interpolation based, linear least squares (LLS) and nonlinear least squares. Due to the limited nature of this communication we shall limit our discussion to the LLS technique. For a more detailed account of all these techniques see [2,3].

LLS imposes one further limitation on the emissivity model function i.e. that it must be linear in the undetermined parameters. Additionally we are restricted to using Wiens approximation (eq. 3) rather than Plancks law.

The LLS method works by minimizing the error between a model function and the measured data. The model function contains m undetermined parameters which are assumed to have achieved their true value at this minimum. If the model function is linear with respect to the undetermined parameters, the LLS method will yield an analytical solution (it cannot be used if the model function is nonlinear in these parameters). In matrix notation we describe the technique as the problem of minimizing ρ , when

$$\rho = \|AX - B\|. \quad (6)$$

Here B is an n-dimensional vector containing the measured data, X is an m dimensional vector containing the undetermined parameters and A is an n x m coefficient matrix. The symbol $\|C\|$ refers to the square root of the sum of the squares of the terms of C and is called the 2-norm of C.

Khan [3] has shown that the relative error in the parameter estimation is limited by the following relation

$$\text{Relative Error} < K * (\text{relative random noise in the data}) \quad (7)$$

This equation says that *the error or the uncertainty in the calculation of the undetermined parameters is always less than some multiple of the perturbation of the radiance data due to the measuring instrument.* The perturbations of the radiance data can be either systematic or random in nature. The systematic variations can be caused by systematic nonlinearities in the measuring radiometer and/or by an incorrect calibration of the radiometer. These variations are not too troublesome if they are not too large, as would be the case for any reasonably designed radiometer. The random variations introduced into the radiance data due to random variations or electrical noise in the radiometer, however, are more troublesome. These appear as an uncertainty in the estimated values of the parameters after being amplified by some factor 'K', i.e. a 1% random variation in the radiance data would appear as a K% uncertainty (error) in the parameter solution.

K is a function of the wavelength range and the specific function chosen to model the emissivity. For example K is approximately equal to 7 for a constant emissivity and about 130 for a linear exponential emissivity.

COMPUTER SIMULATIONS

A computer model was developed to test the ability of the aforementioned techniques to predict temperatures, emissivities and the associated errors. The following flow chart describes the simulation procedure.

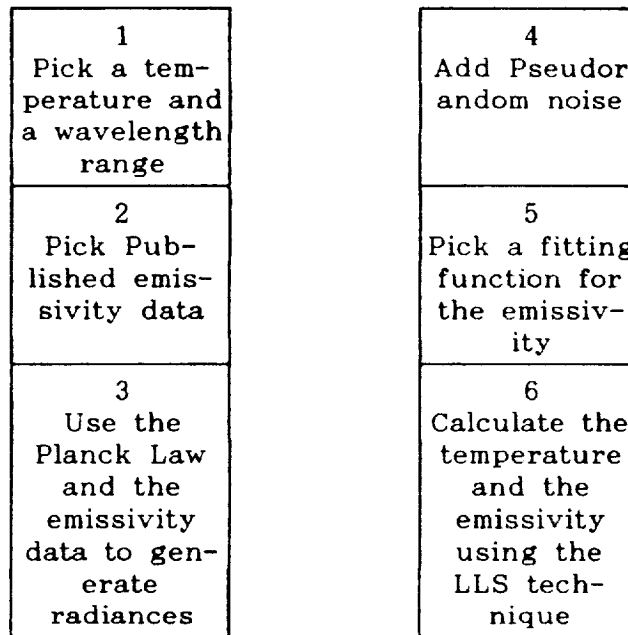


Figure 2 - Flowchart describing the simulation procedure

Figure 3 depicts some of the emissivity data (curve fit to cubic polynomials) used for these simulations. The data were extracted from the literature [4,5]. Figure 4 presents the results of some of the simulations for Iron, Platinum and Molybdenum at 1600 K and for two noise levels. The figure shows that the theory is indeed capable of predicting the error in the parameter estimation. Although at the higher noise levels the theoretical predictions are very conservative.

A large number of these simulations were performed for different materials and at various temperatures and noise levels.

EXPERIMENTAL VERIFICATION

The instrument constructed to test the theory presented here, (known as the MITTMA) consists of a personal computer and a commercial spectrograph that is portable and is about the size and weight of a video camera. This system was configured to measure radiances at 135 wavelengths simultaneously. These radiance data were calibrated for detector and optics variations using a Black Body Radiance source and then passed to the temperature calculation routines.

The minimum temperature accurately (within 1%) measurable using the MITTMA in its present configuration is around 1200 K. This lower limit is imposed by the detector sensitivity. At present the system uses silicon photodiodes which are useful in the .5 to 1.1 micron wavelength range. The low temperature limit could be easily extended by going to a detector which is sensitive further out into the infrared spectrum, such as InSb.

Table 1 lists the results of some of the experiments performed using the MITTMA. As can be seen from the data in table 1, these techniques can measure temperatures with an accuracy similar to that of thermocouples if a sufficiently noise free signal is available.

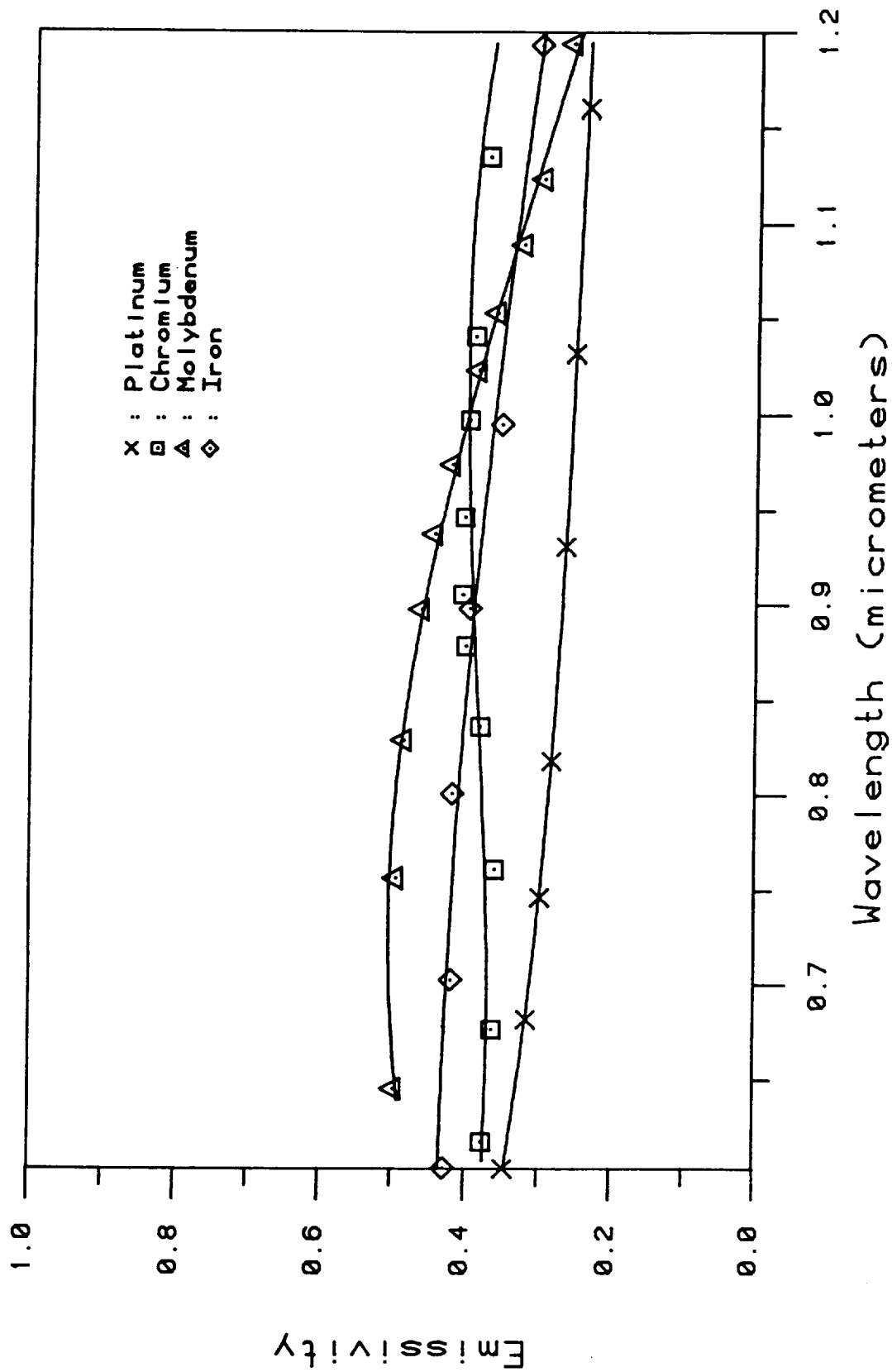


Figure 3 - Emissivity data from the literature and the approximating polynomials.

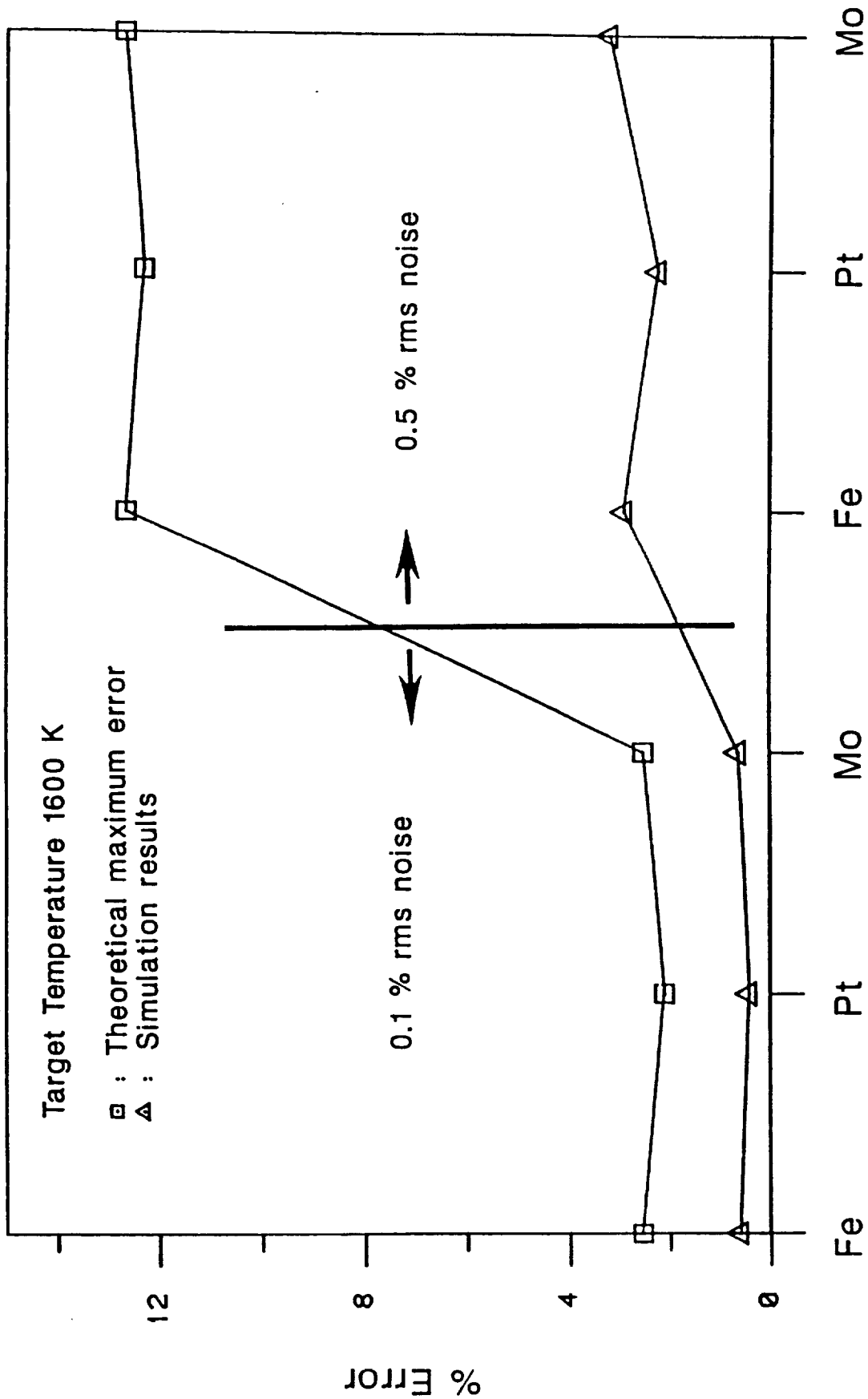


Figure 4 - Simulation results for Iron, Platinum and Molybdenum at 1600 K. This figure shows the effect of an increase in the measurement noise (from 0.1% to 0.5% rms) on the uncertainty in the parameter estimation.

Source	Thermocouple Temperature (K)	MITTMA Temperature (K)	% Difference
Tungsten Strip	2625	2617	0.3
Black Body with Filter A	1234	1241	0.6
Black Body with Filter B	1233	1251	1.5
Platinum Strip	1255	1251	0.32
Platinum Strip	1121	1155	3.0
Platinum Strip	913	970	6.24

Table 1. Results of the experiments on different sources.

In order to simulate the effects of a changing emissivity at a constant temperature the temperature of a black body, viewed through different filters, was measured. The results of two of these experiments are presented in table 1. The two filters used are identified here as A and B and their transmissivities are shown in figure 5. This filter combination can be thought of as simulating the effects of oxidation of a surface, where the material goes from having a shiny, low emissivity surface (filter B) to a dark high emissivity surface (filter A). It should be pointed out here that filter B gives worse results because the shape of its transmissivity curve somewhat resembles that of the Planck curve thereby causing the curve fitting techniques to become confused between the effects of temperature and emissivity. This phenomenon is referred to as 'correlation' and is discussed in detail by Khan [3]. Nonetheless it can be seen from these results that accuracies of better than one percent are achievable using these techniques.

Figure 6 presents a comparison between the theoretical and experimental error in the temperature estimation for the platinum strip source. This figure plots the percent difference between the MITTMA predicted temperature and the thermocouple temperature for a number of measurements of this source at a constant temperature versus the measurement number. This figure also plots the theoretically predicted error (eq. 7) versus the measurement number. Again

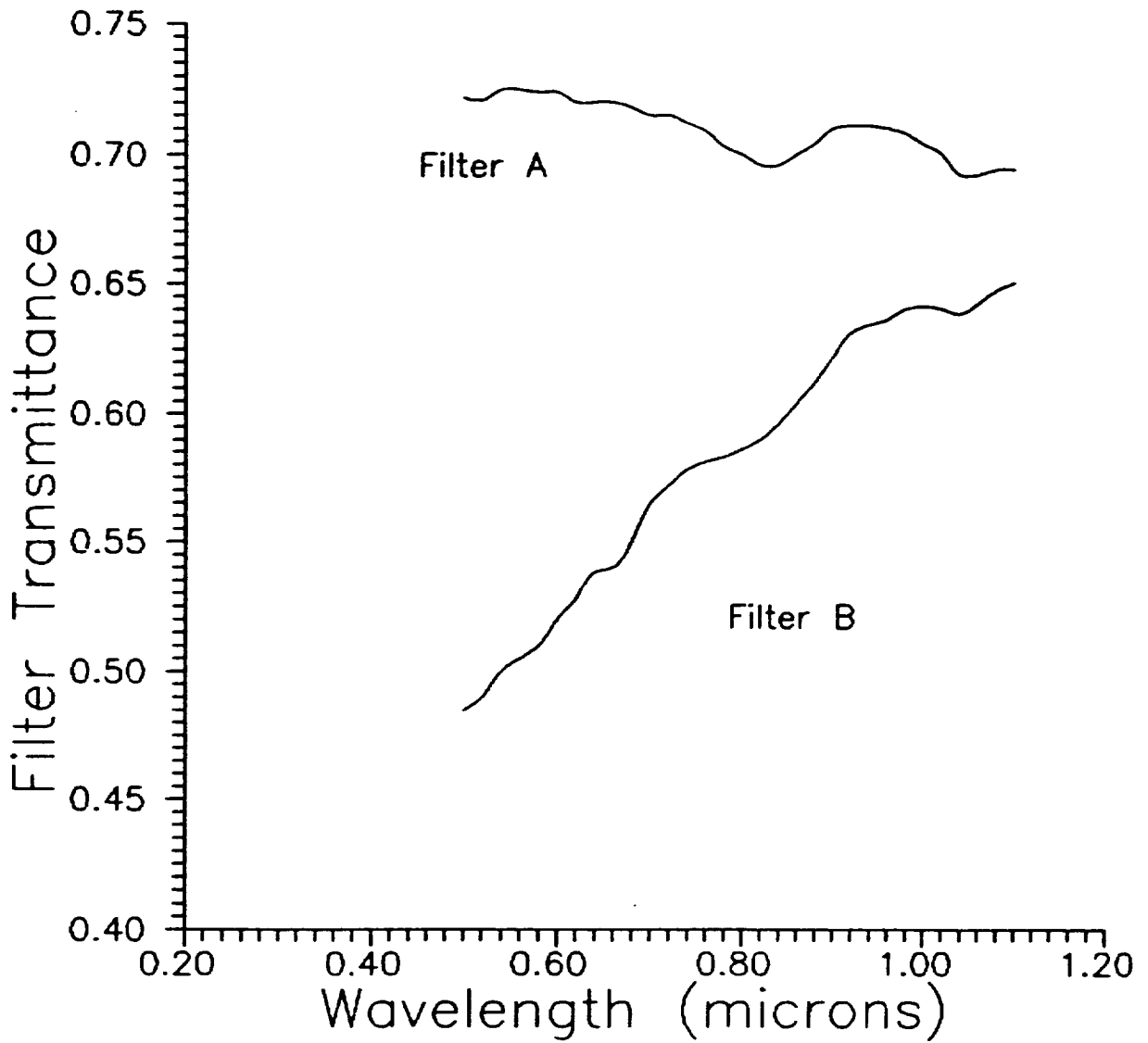


Figure 5 - Transmissivities of the filters used to simulate the effects of oxidation of a surface.

Platinum Strip at 1228 K

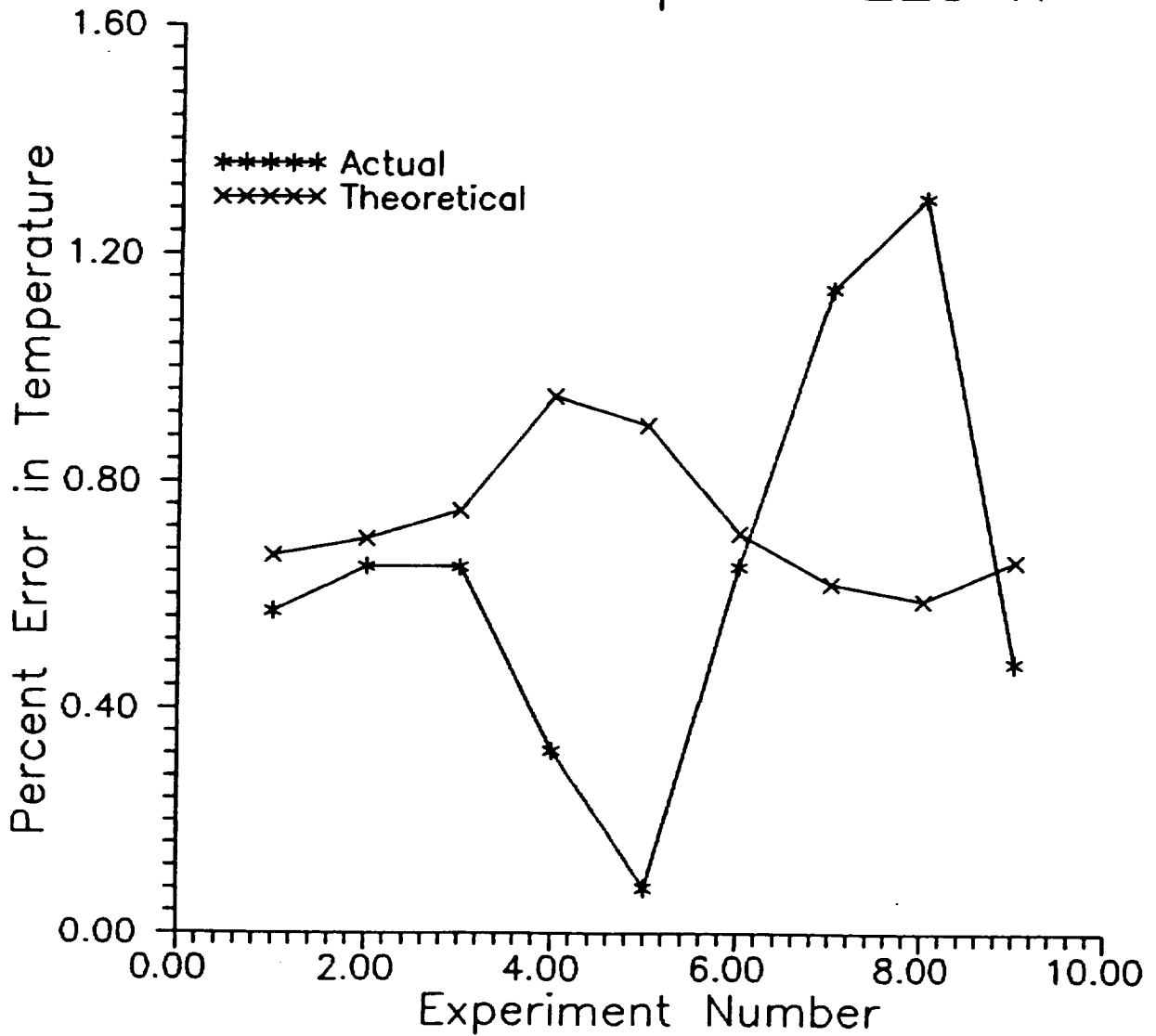


Figure 6 - Comparison of the experimental and theoretically predicted errors in the estimation of temperatures for the platinum strip source.

we find that the MITTMA temperature has an average difference of only .8 percent from the thermocouple temperature and, just as importantly, the error predicted by equation 7 is also about .7 percent. We therefore have reliable a method of estimating the accuracy of our temperature calculations.

The multiwavelength techniques presented here and in [3] have the additional advantage that they can be used to calculate the emissivity of the surface as well as the temperature from the same set of measurements. Figure 7 presents the results of four of these calculations for the platinum data of figure 6. Specifically these emissivity vs. wavelength curves correspond to measurements number 4, 5, 6 and 8 with errors of +4, -1, -8 and -16 K respectively. Due to the nature of these techniques it can be shown [3] that the relative error in the emissivity estimation is much greater than the relative error in temperature estimation for a given set of data. Figure 8 bears out this observation in that the variation from measurement to measurement is high as fifty percent and it is extremely unlikely that the emissivity actually changed by fifty percent during these measurements. Nonetheless if the techniques really are performing as well as is claimed here then one would expect that the real emissivity of platinum would lie somewhere between the two emissivity curves corresponding to the -1 and +4 K errors. An examination of the published emissivity data [5] for clean platinum strip shows that this is indeed true to within the accuracy of that data.

CONCLUSIONS

The theory developed here has been shown to be capable of calculating true temperatures of any material from radiance measurements at a number of different wavelengths. This theory has also been shown to be capable of predicting the uncertainty in these calculated temperatures.

An additional advantage of these techniques is that they can estimate the emissivity of the target simultaneously with the temperature. This aspect can prove to be very important when a fast method of generating reflectivity vs. wavelength or emissivity vs. wavelength data is required. It is presently both difficult and time consuming to generate such data.

Experiments performed on various materials over a range of temperatures and experimental conditions have been used to verify the accuracy of this theory.

REFERENCES

- 1) P.M. Reynolds, Brit. J. Appl. Phys., 15, 1964, pp.579-589
- 2) P.B. Coates, Metrologia, 17 (3), 1981, pp. 103-109
- 3) M.A. Khan, Non-contact Temperature Measurement, Sc.D. Thesis, MIT, Cambridge, MA, (1988)
- 4) S. Roberts, Physical Review, 114 (1), April 1 1959, pp. 104
- 5) G.G. Gubareff, J.E. Janssen, R.H. Torborg, Thermal Radiation Properties Survey, Honeywell Research Center, Minneapolis, Minn., 1960

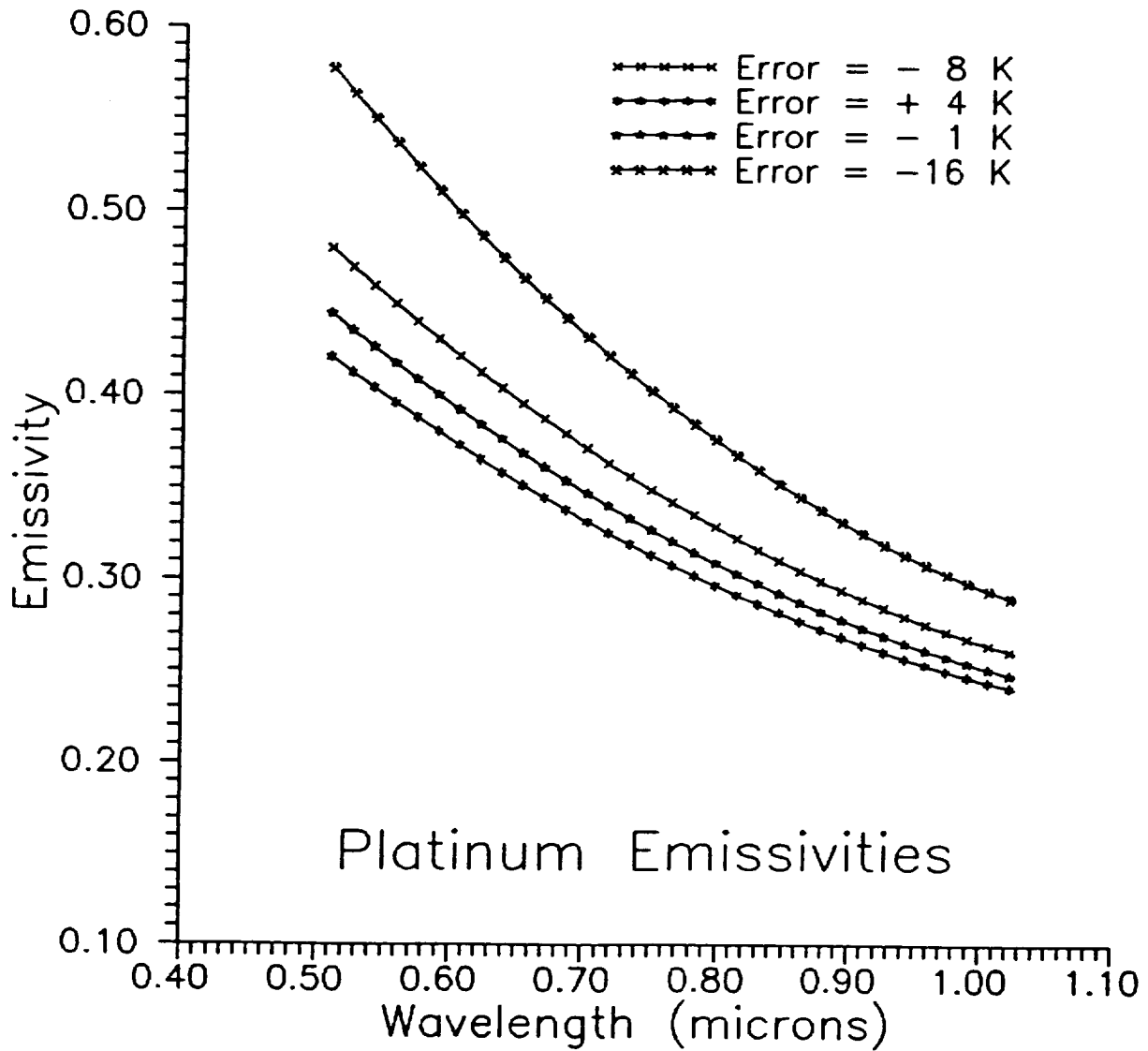


Figure 7 - Calculated spectral emissivities for platinum. The four curves correspond to four separate measurements and therefore to four distinct temperature errors. The true emissivity of platinum would lie between the curves corresponding to the -1 and +4 K errors.

Spectral Emissivities and Optical Constants of
Electromagnetically Levitated Liquid Metals as
Functions of Temperature and Wavelength

S. Krishnan

Intersonics, Inc., Northbrook, IL

and

R.H. Hauge, and J.L. Margrave

Houston Area Research Center and

Rice University

ABSTRACT

The development of a unique, non-contact, temperature measurement device utilizing rotating analyzer ellipsometry is described. The technique circumvents the necessity of spectral emissivity estimation by direct measurement concomitant with radiance brightness. Using this approach, the optical properties of electromagnetically levitated liquid metals Cu, Ag, Au, Ni, Pd, Pt, Zr were measured *in situ* at four wavelengths and up to 600 K superheat in the liquid. The data suggest an increase in the emissivity of the liquid compared with the incandescent solid. The data also show moderate temperature dependence of the spectral emissivity. A few measurements of the optical properties of undercooled liquid metals were also conducted. The data for both solids and liquids show excellent agreement with available values in the literature for the spectral emissivities as well as the optical constants.

1. INTRODUCTION

The behavior of the spectral emissivity of liquid metals at elevated temperatures has not received much attention. However, it assumes fundamental importance when it becomes necessary to carry out radiation thermometry with only an assumed emittance. The questions addressed in this study are; 1) How does the spectral emissivity depend on temperature above the melting point? 2) How do spectral emissivities vary as a function of wavelength? and 3) Is the temperature dependence different at different wavelengths?

The emissivities of liquid metals at elevated temperatures have been measured previously by several methods: 1) comparison of the measured brightness temperature of the liquid at the accepted fusion temperature¹⁻³; 2) comparison of the measured radiances by a two-color pyrometer with a single color pyrometer, and assuming the measurement of the first is independent of emissivity⁴; and, 3) having the sample in thermal contact with a substrate of known temperature, measuring the radiance brightness temperature of the sample and comparing the two temperatures⁵.

There are several difficulties associated with each of these techniques. For example, in the case of melting-point brightness measurements, the question arises as to whether the measured emissivity corresponds to the liquid, solid, or a mixture of both. If the measurement is made precisely at the melting point, equilibrium is established between the liquid and solid, so the measurement corresponds to a mixture. Even assuming one is making the measurement on the liquid, the errors resulting from brightness measurement can be substantial. Bonnell, et. al.,³ have calculated a possible error of 5-6% resulting from a 10K uncertainty in brightness temperature, in estimating a 0.30

value of emissivity at 2000 K. If the temperature being measured is higher, where the brightness-temperature uncertainty is greater, the measured emissivity can be in error by more than 10%. Several workers have pointed out the difficulties associated with two-color pyrometry as a technique for deriving thermodynamic temperatures⁶⁻⁹. The third approach is limited by container contact interactions which can cause uncertainty in temperature. It is also unlikely to provide reliable emissivity estimates due to the chemical reactivity and solubility properties of liquid metals at high temperatures (> 1800 K).

The use of ellipsometry for measurement of the optical properties of metals and alloys is not new¹⁰⁻¹⁸. However, the use of this technique for emissivity measurements on very refractory liquid metals and alloys as a function of temperature above the melting point is certainly novel. In this paper, some results of optical property measurements, including spectral emissivity, as functions of temperature at wavelengths of 488, 514.5, 632.8 and 1064 nm for a number of electromagnetically levitated liquid metals including Cu, Ag, Au, Ni, Pd, Pt, and Zr are presented. The data includes measurements on liquids, solids and undercooled liquids. Perhaps, the most significant outcome of this work is that a technique has been developed to measure accurately the optical constants, and thus temperatures, of levitated liquid materials where sample contact is unnecessary. This is of enormous importance for containerless processing technologies.

1.1. THEORETICAL BACKGROUND

According to Wien's approximation to Planck's law, the flux distribution from a black body per unit solid angle can be written as a function of wavelength, λ , and temperature, T:

$$W(\lambda, T) = C_1 \pi^{-1} \lambda^{-5} \exp\left(-\frac{C_2}{\lambda T}\right), \quad (1a)$$

where C_1 and C_2 are the first and second Planck constants, respectively. Equation 1a has been shown to be accurate⁶ to within 1% for $\lambda T < 2897.8 \mu\text{K}$. A useful form of Wien's approximation is obtained by taking the ratio of the real-body radiation at wavelength, λ , to that of a blackbody at the same wavelength:

$$\frac{1}{T_{\text{TH}}} - \frac{1}{T_{\text{B}}} = \frac{\lambda \ln(E_{\lambda})}{C_2}, \quad (1b)$$

where T_{B} is the measured brightness temperature, T_{TH} the thermodynamic (blackbody) temperature, and E_{λ} is the normal spectral emissivity of the real body at the wavelength, λ .

Assuming the liquid metal surface is specular, Kirchoff's law can be stated as:

$$E_{\lambda} + R_{\lambda} = 1, \quad (2)$$

where R_{λ} is the reflectivity and E_{λ} is the spectral emissivity. The subscript denotes the wavelength dependence of these quantities. Equation 2 holds for any angle of incidence or emission.

ϵ_1 and ϵ_2 , the real and imaginary parts of the dielectric constant, are related to the refractive index, n , and extinction coefficient, k , through the relations:

$$\epsilon_1 = n^2 - k^2, \text{ and} \quad (3a)$$

$$\epsilon_2 = 2nk. \quad (3b)$$

If ϵ_1 and ϵ_2 are experimentally determined, then the remaining optical constants of the material in question can be obtained for the wavelength, λ .

The normal incidence reflectivity is calculated from the Beer equation:

$$R_{\lambda} = \frac{(n-n_0)^2 + k^2}{(n+n_0)^2 + k^2}, \quad (4)$$

where n_0 is the refractive index of the ambient, transparent medium. Using Eq. 2, the spectral emissivity is determined. Simultaneous measurement of radiance brightness at normal incidence provides the thermodynamic temperature from Eqs. 1b, 2 and 4.

When light, plane polarized with an initial azimuth Ψ_0 to the plane of incidence is reflected from a metal surface, the P and the S components of the incident electric vector experience different phase changes and different reflectivities, producing a new azimuth Ψ . If $\Psi_0 = \frac{\pi}{4}$, then the complex reflectance ratio, ρ , is:

$$\rho = \frac{r_p}{r_s} = \tan(\Psi) e^{i\Delta}, \quad (5)$$

where, r_p and r_s are the amplitude reflection coefficients of the P and S components, respectively, Ψ is the restored azimuth and Δ the relative phase difference between the two components of the reflected electric vector ($\Delta = \delta_{rp} - \delta_{rs}$). If the reflected intensity is measured at four azimuths (obtained at two positions of an analyzer) - I_1 (90°), I_2 (0°), I_3 (45°), I_4 (135°), then the fundamental ellipsometric parameters ψ and Δ are given by¹⁴:

$$\tan(\Psi) = \left(\frac{I_2}{I_1}\right)^{1/2}, \text{ and} \quad (6a)$$

$$\cos(\Delta) = \frac{1}{2} \left[\left(\frac{I_2}{I_1}\right)^{1/2} + \left(\frac{I_1}{I_2}\right)^{1/2} \right] \times \left[\frac{(1 - I_4/I_3)}{(1 + I_4/I_3)} \right]. \quad (6b)$$

The real and imaginary parts of the dielectric constant are then calculated from ψ , Δ , and

Θ using³¹:

$$\epsilon_1 = \sin^2\theta \tan^2\theta \frac{\cos^2 2\psi - \sin^2 2\psi \sin^2 \Delta}{(1 + \cos \Delta \sin 2\psi)^2} + \sin^2\theta, \quad (8a)$$

and

$$\epsilon_2 = \frac{2 \sin 2\psi \cos 2\psi \sin \Delta}{(1 + \cos \Delta \sin 2\psi)^2} \sin^2\theta \tan^2\theta, \quad (8b)$$

where Θ is the angle of incidence. Once ϵ_1 and ϵ_2 are obtained, one calculates n and k . Then, the normal incidence reflectivity is obtained from Eq. 4. It is important to note that the entire measurement essentially consists of two ratio measurements ($\frac{I_2}{I_1}$ and $\frac{I_4}{I_3}$). Thus, systematic errors tend to cancel.

2. EXPERIMENTAL

Figure 1 shows the experimental arrangement used to make emissivity measurements by RAE on electromagnetically levitated materials. A chopped (2000 Hz), focussed, plane polarized laser beam impinged on the sample at 67.5° angle of incidence. The laser used at the 488 and 514 nm wavelengths was a Lexel (Model 95) 2 watt Argon-Ion laser that was lasing multi-line. The measurements at 633 nm were carried out using the Aerotech 5 mW He-Ne laser while the measurements at 1064 nm were carried out using an ALC 1064-50P (Amoco Laser Corporation) diode-pumped YAG laser with an output of 50 mW polarized light. The experiments that were performed at the YAG and He-Ne wavelength required the laser to be focussed while no focussing was needed for measurements with the Argon-Ion laser. The plane of polarization of the beam was rotated 45° (clockwise for a viewer looking at the sample from the laser) with respect to the plane of incidence (plane of the figure). Also shown in the figure is a laser shutter

positioned between the chopper and the sample chamber. Closure of this shutter allowed measurements of radiance brightness of the sample without error due to the laser. A Leeds & Northrup, Automatic Optical Pyrometer was used to monitor the brightness temperature of the sample via another port on the chamber situated at 67.5° from the incident laser port. The thermodynamic temperatures of the liquid were calculated using Wien's approximation to Planck's law and using values of spectral emissivity measured at $\lambda = 633\text{nm}$. Additionally, thermodynamic temperatures were also obtained using the radiance detector situated on the ellipsometer based on measured brightness and the optical constants measured by the ellipsometer. This was accomplished by recomputing a spectral emissivity from the measured dielectric constants at this oblique angle and then using Wien's approximation to Planck's law. The second measurement was not feasible in the blue and green regions of the spectrum since samples usually emitted very little light.

Light from the sample (radiated and reflected) was imaged on an aperture by a lens. A second lens and aperture generated parallel light from this image. The f number of the second lens and aperture fixed the maximum solid angle from which light was collected at about 1° . Since the study involved several wavelengths, spectral discrimination was achieved using laser line interference filters obtained from Corion and Ealing. Light that passed through the hole was then analyzed by a beam-splitting Thompson calcite prism that was rotatable around the beam axis.

Shown in Fig. 1 is the flow diagram for the data acquisition system. The outputs of the polarization detectors were monitored individually with separate lock-in amplifiers which were phase-locked with the reference signal from the chopper. The lock-in

amplifiers were obtained from EG&G PARC and had 20 KHz bandwidths. The outputs of the lock-in amplifiers were monitored continuously by the computer, as were the outputs of the radiance detector and the Leeds & Northrup pyrometer.

In a previous paper³⁰, the dynamics of electromagnetically levitated liquid metals and alloys at elevated temperatures were described. These results showed that the levitated liquid metal droplets underwent rotations, shape oscillations, and translations in the coil. This behavior causes oscillations in the intensity of the emitted as well as reflected light from the sample.

It was necessary to minimize the effect of these surface perturbations by carrying out long-time signal averaging. Since the perturbation frequencies from previous studies were established to be on the order of 50-200 Hz, the output time constant on the lock-in amplifiers was set at 0.1 seconds. The outputs of the lock-in amplifiers were monitored for 10-20 seconds, until a reliable mean value could be extracted. The analyzer was then rotated for the second set of measurements and the signal averaging repeated. Finally, the signal intensities were compared for the two analyzer positions and the criterion of validity elucidated by Beattie¹⁵, was verified. Any data not meeting this criterion were rejected. A detailed description of the calibration procedure for the optics and electronics has been presented elsewhere³¹ and will not be presented here.

All samples used had purities in the range 99.9 to 99.999%. The samples were cut from rod or bar stock and had masses in the range 0.5-1.5 gms. After melting in the levitation coil, residual oxide surface contaminants were allowed to vaporize and be removed from the chamber before the measurements were started.

The experiments were performed at pressures on the order of 1 atmosphere and gas flow rates of 10 - 20 cc/min. The gases used were argon and helium with 3% hydrogen added to inhibit surface oxide formation. Temperature control was achieved to a limited extent by regulating the gas mixture and flow rate. Helium, with the higher thermal conductivity, was used to achieve the lower temperatures, including the undercooled state, while argon was used to obtain the higher temperatures. The upper temperature limit for each sample was set by the vaporization rate of the metal. At higher temperatures, vapors near the metal surface scattered the reflected laser light which resulted in much larger measurement errors.

3. RESULTS

Tables 1 to 4 give a summary of some of the results of the experiments reported here. In these values are given of the dielectric constants, and spectral emissivities of Cu, Ag, Au, Ni, Pd, Pt, and Zr over wide ranges of superheat of the liquid at the four wavelengths respectively. Since much of the data reported here showed moderate to strong temperature dependence, an interpolated value based on a linear regression to the data is provided. For each element, a common temperature was chosen to interpolate towards. A value of the confidence interval is listed in the parenthesis below each of the tabulated values. These intervals correspond to a confidence level of 95% for the data listed in the table. Also listed parenthetically below the temperature range is the number of determinations of the optical properties over the range. The temperatures for the interpolation (in some cases, extrapolation) were chosen on the basis of the temperature range over which most of the data were acquired. The interpolation temperatures were: Copper at 1400 K, Silver at 1300 K, Gold at 1400 K, Nickel at 1800 K, Palladium at 1925 K and

Platinum at 2250 K. The data for liquid zirconium represents an average of the optical properties as is the case with the data for solid palladium. Correspondingly, the values in those parenthesis represents a standard deviation and not a standard error of estimate. In a few cases, extrapolation of the data to the chosen temperature was necessary, and consequently the error bars were slightly higher.

Since the chosen temperatures were at least 100 degrees or more above the melting point, some disagreement with available literature data is expected. Each of these four tables corresponds to measurements at a single wavelength. The three noble metals Cu, Ag, and Au, and the three transition metals Ni, Pd, and Pt were studied at all four wavelengths while Zr was studied only at the He-Ne wavelength. A salient feature of the data listed in Tables 1 - 4 is that almost all spectral emissivities were measured with an error of ± 0.01 corresponding to the 95% precision limits of the data.

Table 5 is a compilation of emissivity data found in the literature, together with the data obtained in this study, to illustrate the changes in emissivity as a function of temperature. In this table we list emissivity data for these metals at room temperature (RT), incandescent temperatures (IT) and in the liquid regime. The spectral emissivities calculated from the data reported by Miller²¹ and our study have been obtained at a photon energy of 1.97 eV ($\lambda = 0.63 \mu\text{m}$) while the other emissivity data pertaining to the elevated temperatures were measured at $\lambda = 0.65 - 0.665 \mu\text{m}$ (1.91 - 1.87 eV). The room temperature emissivity data were obtained at 1.97 eV. It can be seen that the agreement of the present results with data found in the literature is excellent in all cases except perhaps in the case of liquid zirconium where there appears to be a large discrepancy in the literature data. The lack of spectral emissivity data in the literature at the other

wavelengths made a similar compilation at other wavelengths impossible.

To illustrate the overall wavelength dependence of the spectral emissivity, the spectral emissivities of the copper and nickel groups are plotted in Figs. 2 and 3 respectively. The spectral emissivity data used for these plots are the same data that are listed in Tables 1 - 4. The error bars in Figs. 2 and 3 correspond to a 95% confidence interval. The spectral emissivities correspond to the previously listed interpolation temperatures. In these two plots, it is seen quite clearly that the spectral emissivity increases gradually as the wavelength decreases, until the blue region where a sharp rise is seen. The behavior of Cu and Au are similar while silver does not show such a dramatic rise. The corresponding plot in Fig. 3 for the nickel group has two points of interest. Firstly, all three metals behave identically in the visible region of the spectrum. Secondly, they seem to show very little dependence between the red and green regions of the spectrum and then show a rise in the blue. They also converge to almost the same value of spectral emissivity in the blue.

In order to illustrate the temperature dependence of the spectral emissivity, we have selected the results for liquid gold, nickel and platinum as examples.

The optical constants of liquid gold were measured in the temperature range 1270-1980 K ($0.98 - 1.48 T_m$), where T_m is the melting point. Measurements of spectral emissivity and optical properties at the four wavelengths were conducted in this temperature range. These data include three measurements on the undercooled liquid (He-Ne wavelength).

Figure 4 is a plot of the spectral emissivity of liquid gold in the above temperature range at the 4 wavelengths. The solid lines in the figure represent the results of a least

squares fit to the data at each of the wavelengths. The results of the least squares fit, $a + bT$, are also shown in the figure. Since raw data are directly plotted and fitted in the plots shown, the least squares fit tends to be weighted somewhat to those regions where a large numbers of data are present. In many cases, several data points overlapped since the temperature was not constantly varied. A small increase in spectral emissivity is seen in the blue while there is a very large decrease in the green. The spectral emissivity in the green close to the melting point is 0.47 while at 1900 K it decreases to about 0.40. This corresponds to about 12.5% decrease in spectral emissivity. The spectral emissivity is constant in the red and has a small positive slope in the infra-red.

The spectral emissivity (at 1400 K) in the blue is 0.52 and compares well with that calculated from the data of Miller²¹ (0.52). The spectral emissivity is 0.40 in the green and is a little lower than that of Miller. The emissivity of liquid gold in this range for the He-Ne wavelength was determined to be 0.30. This value is in agreement with that computed from the data of Miller²¹, but is higher than that reported by Burgess and Waltenburg⁴⁹. There appear to be no data available in the infra-red for liquid gold and the value reported here is 0.12.

The optical constants and spectral emissivities of liquid nickel were measured in the temperature range 1776-2143 K ($1.03 - 1.24 T_m$) at $\lambda = 488, 514.5, 632.8,$ and 1064 nm. Figure 5 is a plot of the spectral emissivities of liquid nickel as a function of temperature at the four wavelengths. There is non-linear but monotonic increase in emissivity with decreasing wavelength. That is, there is an initial rapid increase in emissivity from 1064 to 632.8 nm. The values at 632.8 and 514.5 nm are close, but the difference between 514.5 and 488 nm is again substantial.

The mean values of spectral emissivity (at 1800 K) for liquid nickel agree reasonably well with literature. The value of spectral emissivity in the blue is 0.49 and is 0.41 in the green. The values calculated from the data of Miller⁶ are lower in the blue and higher in the green than the values measured in this study. The agreement at the He-Ne wavelength with the literature data is good as can be seen in Table 5. The spectral emissivity in the infra-red is 0.31.

The optical properties and spectral emissivities of liquid platinum were measured in the temperature range 2000-2650 K ($0.98-1.30 T_m$). The data obtained in this range included 6 measurements on the undercooled liquid (for the He-Ne wavelength). Figure 6 is a plot of the spectral emissivity of liquid platinum as a function of temperature at the four wavelengths together with the results of a least squares fit to the data at each of the wavelengths. It is seen quite clearly that the spectral emissivity decreases with increasing temperature in the blue, green and in the infra-red while it appears to increase in the red. It must be pointed out that the data in the green would probably fit better with a curve rather than a straight line although no such fit was attempted. An unusual feature of the data in the green was the dramatic change in the values of the dielectric constants in the neighborhood of 2550 K.

Since most of the data for liquid platinum were measured at temperatures substantially higher than the melting point, extrapolation of the data to temperatures close to the melting point would result in larger errors. Therefore, the temperature of interpolation was chosen as 2250 K which is about 200 K above the melting point. The spectral emissivity in the red was determined as 0.38 and compares very well with the data in the literature (see Table 5). The spectral emissivity of undercooled platinum in the red was

measured as 0.36. The mean values in the blue, green and infra-red were determined as 0.48, 0.45, and 0.30 respectively. It was not possible to assess the agreement with literature data since such data were not available at these wavelengths.

4. DISCUSSION

One of the goals of this work was the development of a pyrometric technique by which one could measure both spectral emissivities and true temperatures of liquid metals *in situ*, since an error is introduced in temperature measurement of incandescent solids or liquids when spectral emissivities are only estimated. Also, the paucity of emissivity data for liquid metals at temperatures above the melting point has made reliable temperature measurement in that regime difficult. As a result, thermophysical property data such as specific heats, expansion coefficients, etc., have always been subject to this uncertainty. In order to measure accurately the thermodynamic temperature of these high temperature liquids, it is necessary to know the surface spectral emissivity as a function of temperature and independent of radiance brightness measurements.

Two important results reported here are the observations that the spectral emissivities at the four wavelengths of the metals in the Ni and Cu groups show a moderate temperature dependence in the liquid over the temperature ranges studied and that the spectral emissivities of the liquids are *higher* than those of the corresponding solids. Furthermore, in those liquid metals where moderate supercooling was observed, the measured spectral emissivities of the supercooled liquid were essentially the same as the those of the liquid above the melting point. Corrections may need to be made to thermophysical data obtained previously which have made the assumption of constant emissivity. For instance, Bonnell³⁶ observed an anomaly in measurements of the specific heat, $C_p(l)$, of

liquid zirconium at elevated temperatures. He attributed the behavior to either a real change in C_p (l) or a monotonic decrease in emissivity. The latter would compensate for the non-linear rise in total enthalpy, $H(T) - H(298)$, making C_p (l) constant. The few measurements on liquid zirconium suggested a constant spectral emissivity at $\lambda = 633\text{nm}$. At the present time it appears that the data of Bonnell³⁶ may not need to be corrected therefore suggesting that C_p (l) does increase but only further work can confirm this observation.

The possibility that spectral emissivities change appreciably with temperature has been suggested by Nordine³⁷ and Margrave³⁸, but never really established. However, indirect support for such an observation can be found in the literature. For instance, the contributions to C_p (l) in the range 3000-5000 K due to expansion coefficients, compressibility factors, and electronic parameters have been studied using exploding wires by Cezariliyan³⁹ and by Gathers, et. al.,⁴⁰ and significant deviations from the classical 3R value have been observed. Similar variations in spectral emissivities can be expected, especially at temperatures of 3000 K and higher.

The second point concerns the increase in emissivity on melting of the metal. In these experiments, measurements of the spectral emissivities of solid copper and palladium were performed just below their melting point by allowing them to freeze within the levitation coil. The emissivity measured for solid copper was 0.10, while for palladium the value was 0.32 (for the He-Ne wavelength). These are 15-20 % lower than the emissivity of the corresponding liquids. A similar increase of about 13% was observed in the green for palladium. This increase in emissivity on melting was observed previously for these metals by others^{3,5}, but no explanations have been forthcoming. Intuitively,

one expects the smoother, liquid surface, to have a lower emissivity than the solid. This would be the case if factors affecting emissivity were the macroscopic physical and chemical structure of the surface; however, the optical properties are also governed by the electronic properties of the material. Factors which affect the electronic properties will play a role in determining the spectral emissivity of the material. For example, significant destruction of the long range order of the lattice occurs on melting. This will significantly modify the band structure and may provide at least part of the basis for the changes observed in the optical properties upon melting of these metals.

Further, some measurements of the optical properties of undercooled liquids were carried out in this study (palladium, platinum, gold). These data reveal that the spectral emissivities of the undercooled liquids are virtually the same as that of the liquid above the melting point, although they are just slightly lower. Since large undercoolings were not attained, the extension of this behavior to larger undercoolings must be performed with caution.

5. CONCLUSIONS

Rotating analyzer ellipsometry has been used successfully to measure the optical constants of Cu, Ag, Au, Ni, Pd, Pt and Zr and extract normal incidence spectral emissivities at 488, 514.5, 632.8, and 1064 nm over a large range of superheat in the liquid state. The technique was adapted as a non-contact diagnostic method to our electromagnetic levitation system, and it was possible to extract the dielectric functions and complex indices of refraction data for liquid metals at elevated temperatures.

The spectral emissivities at 633 nm of the liquid metals obtained in this study agreed well with most of the data available in the literature. In the cases of palladium and copper, the emissivities were also measured in the solid state with the sample levitated. The data for all metals studied showed that the spectral emissivities of the liquids were higher than those of the solids. Additionally, the spectral emissivities of all the metals studied here showed moderate to strong temperature dependence in the liquid over large temperature ranges. This fact therefore suggests that corrections may need to be made to thermophysical property measurements that have been based on the assumption of constant emissivity.

Comparisons of the dielectric functions and complex index of refraction data with those available in the literature showed excellent agreement. Since only data for the low melting materials were available, it was not possible to compare the results for liquid Pd, Pt, and Zr.

6. ACKNOWLEDGEMENTS

This work was supported by the National Aeronautics and Space Administration.

REFERENCES

1. F.O. Jones, A.G. Knapton, and J. Savill, *J. Less Comm. Met.*, 1, 80 (1959).
2. J.A. Treverton and J.L. Margrave, *Proc. 5th Symp. Thermophysical Properties*, ASME, Boston, Mass., 1970, pp. 489-494.
3. D.W. Bonnell, J.A. Treverton, A.J. Valerga, and J.L. Margrave, *Presented at 5th Symp. on Temperature*, Washington D.C., 1971, pp. 483-487.
4. R.R. Koch, J.L. Hoffman, and R.A. Beall, *Rep. Inv. # 7743, U. S. Dept. of Interior, Bureau of Mines*, Washington D.C., 1973.
5. G.K. Burgess, and R.G. Waltenburg, *Bureau of Standards Scientific Paper # 242, 1914*, pp. 591-605.
6. D.L. McElroy, and W. Fulkerson, *Temperature Measurement and Control*, John Wiley & Sons, Inc., New York, *Techniques of Metals Res.*, vol. 1, pt. 1, , 1968, Ed. R.F. Bunshah, p. 489.
7. P.B. Coates, *Metrologia*, 17, 103 (1981).
8. P.C. Nordine, *High Temp. Sci.*, 21, 97 (1986).
9. G.D. Nutter, *in Applications of Radiation Thermometry*, ASTM STP 895, Eds. J.C. Richmond and D.P. DeWitt, pp. 3-24.
10. O. Hunderi, and R. Ryberg, *Surf. Sci.*, 56, 182 (1976).
11. H.G. Liljenvall, A.G. Mathewson, and H.P. Myers, *Phil. Mag.*, 22, 243 (1970).
12. N.V. Smith, *Phys. Rev.*, 183, 634 (1969).
13. W. Budde, *Appl. Optics*, 1, 201 (1962).

14. M.P. Givins, *Solid State Physics*, Eds. F. Seitz and D. Turnbull, Vol. 6, pp. 313-353.
15. J.R. Beattie, *Phil. Mag.*, 46, 235 (1955).
16. P.S. Hauge and F.H. Dill, *IBM J. Res. Dev.*, 14, 472 (1973).
17. P.S. Hauge *Surf. Sci.*, 56, 148 (1976).
18. R.M.A. Azzam and N.M. Bashara, *Ellipsometry and Polarized Light*, North Holland, Amsterdam, 1987, pp. 1-267.
19. E.T. Arakawa, T. Ingaki, and M.W. Williams, *Surf. Sci.*, 96, 248 (1980).
20. N.R. Comins, *Phil. Mag.*, 25, 817 (1972).
21. J.C. Miller, *Phil. Mag.*, 20, 1115 (1969).
22. L.G. Schulz, *ADV. Phys.*, 6, 102 (1957).
23. J.N. Hodgson., *Phil. Mag.*, 5, 272 (1960).
24. J.N. Hodgson., *Phil. Mag.*, 6, 509 (1961).
25. J.N. Hodgson., *Phil. Mag.*, 4, 183 (1959).
26. J.N. Hodgson., *Phil. Mag.*, 7, 229 (1962).
27. J.N. Hodgson, *Proc. Phys. Soc. B*, 68, 593 (1955).
28. N.V. Smith, *Adv. Phys.*, 16, 629 (1967).
29. J.M. Ziman, *Phil. Mag.*, 6, 1013 (1961).
30. G.P. Hansen, S. Krishnan, R.H. Hauge, and J.L. Margrave, *Met. Trans.*, 19A, 1939 (1988).
31. Handbook of Optical Constants, Ed., E.D. Palik, Academic Press, 1985, pp. 275-368.

32. G.P. Hansen, S. Krishnan, R.H. Hauge, and J.L. Margrave, *Met. Trans.*, 19A, 1889 (1988).
33. A.G. Worthing, *Phys. Rev.*, 28, 174 (1926).
34. B.T. Barnes, *J. Opt. Soc. Am.*, 56, 1546 (1966).
35. M. Otter, *Z. Phys.*, 161, 539 (1960).
36. D.W. Bonnell, *Ph.D. Thesis*, Rice University, 1972.
37. P.C. Nordine, *Personal Communication*.
38. J.L. Margrave, *Personal Communication*.
39. A. Cezariliyan, *High Temp. High Press.*, 11, 9 (1979).
40. G.R. Gaithers, J.W. Shaner, and W.M. Hodgson, *High Temp. High Press.*, 11, 529 (1979).

TABLE 1
Optical Constants of Liquid Metals at 488 nm

METAL	TEMP. RANGE(K)**	ϵ_1	ϵ_2	E_λ
Copper	1499-1877 (13)	-4.92 (0.13)	7.63 (0.12)	0.45 (0.01)
Silver	1398-1552 (17)	-9.28 (0.38)	1.78 (0.31)	0.11 (0.01)
Gold	1420-1907 (16)	-2.77 (0.28)	7.57 (0.62)	0.522 (0.018)
Nickel	1789-2109 (24)	-2.66 (0.35)	13.17 (0.30)	0.486 (0.007)
Palladium (s)	1424-1699 (11)	-5.66 (0.24)	12.23 (0.31)	0.43 (0.01)
Palladium (l)	1911-2120 (27)	-3.47 (0.39)	13.51 (0.65)	0.468 (0.004)
Platinum	2266-2646 (33)	-1.86 (0.66)	15.72 (0.90)	0.48 (0.01)

* Confidence interval for 95% limits of the data is listed parenthetically below each value.

The number of determinations is listed parenthetically below the temperature range.

**Temperatures chosen for interpolation of optical constant values are: Cu (1400 K), Ag (1300 K), Au (1400 K), Ni (1800 K), Pd (1925 K), and Pt (2250 K). Pd (s) and Zr values represent mean values.

TABLE 2
Optical Constants of Liquid Metals at 514.5

METAL	TEMP. RANGE(K)**	ϵ_1	ϵ_2	E_λ
Copper	1361-1903 (19)	-8.81 (0.16)	7.11 (0.42)	0.30 (0.01)
Silver	1452-1541 (17)	-10.86 (0.52)	0.84 (0.14)	0.05 (0.01)
Gold	1449-1903 (20)	-6.34 (1.08)	8.07 (0.47)	0.47 (0.02)
Nickel	1776-2063 (31)	-6.35 (0.39)	15.42 (1.20)	0.412 (0.008)
Palladium (s)	1486-1810 (11)	-11.63 (0.37)	13.68 (0.26)	0.32 (0.005)
Palladium (l)	1869-2134 (25)	-7.83 (0.42)	16.95 (0.83)	0.381 (0.006)
Platinum	2307-2649 (19)	-2.46 (0.37)	25.44 (0.60)	0.45 (0.01)

* Confidence interval for 95% limits of the data is listed parenthetically below each value.

The number of determinations is listed parenthetically below the temperature range.

**Temperatures chosen for interpolation of optical constant values are: Cu (1400 K), Ag (1300 K), Au (1400 K), Ni (1800 K), Pd (1925 K), and Pt (2250 K). Pd (s) and Zr values represent mean values.

TABLE 3
Optical Constants of Liquid Metals at 633 nm

METAL	TEMP. RANGE(K)**	ϵ_1	ϵ_2	E_λ
Copper	1315-1727 (27)	-14.11 (0.45)	3.83 (0.39)	0.13 (0.01)
Silver	1291-1481 (41)	-16.31 (0.36)	3.34 (0.44)	0.086 (0.01)
Gold	1270-1932 (37)	-9.58 (0.79)	8.20 (1.36)	0.30 (0.01)
Nickel	1822-2143 (21)	-6.60 (0.90)	18.55 (1.24)	0.40 (0.01)
Palladium (s)	1297-1577 (11)	-12.12 (0.43)	19.35 (0.39)	0.32 (0.005)
Palladium (l)	1807-2126 (23)	-7.32 (0.72)	18.93 (0.73)	0.38 (0.01)
Platinum	2006-2475 (33)	-6.04 (1.38)	25.20 (1.63)	0.38 (0.01)
Zirconium	2175-2402 (3)	-4.81 (0.87)	21.7 (2.46)	0.41 (0.005)

* Confidence interval for 95% limits of the data is listed parenthetically below each value.

The number of determinations is listed parenthetically below the temperature range.

**Temperatures chosen for interpolation of optical constant values are: Cu (1400 K), Ag (1300 K), Au (1400 K), Ni (1800 K), Pd (1925 K), and Pt (2250 K). Pd (s) and Zr values represent mean values.

TABLE 4
Optical Constants of Liquid Metals at 1064 nm

METAL	TEMP. RANGE(K)**	ϵ_1	ϵ_2	E_λ
Copper	1434-1729 (11)	-33.19 (1.25)	11.18 (1.02)	0.085 (0.008)
Silver	1236-1489 (12)	-38.13 (1.60)	7.68 (0.44)	0.06 (0.005)
Gold	1417-1976 (10)	-34.82 (1.88)	14.25 (1.02)	0.12 (0.01)
Nickel	1888-2031 (9)	-12.71 (1.33)	15.31 (0.92)	0.31 (0.016)
Palladium	1947-2073 (5)	-15.21 (2.05)	7.91 (1.08)	0.23 (0.01)
Platinum	2106-2386 (10)	-12.05 (1.62)	13.44 (2.80)	0.298 (0.006)

* Confidence interval for 95% limits of the data is listed parenthetically below each value.

The number of determinations is listed parenthetically below the temperature range.

**Temperatures chosen for interpolation of optical constant values are: Cu (1400 K), Ag (1300 K), Au (1400 K), Ni (1800 K), Pd (1925 K), and Pt (2250 K). Pd (s) and Zr values represent mean values.

TABLE 5
Comparison of Normal Incidence Spectral Emissivities
with Selected Literature Values for $\lambda = 650$ nm

Metal	RT*	REF.	IT*	REF.	Liquid	REF.	
Copper	0.08	32	0.10	This work	0.13	This work	
	0.12	31	0.10	5	0.13 0.14	21 3	
Silver	0.03	32	0.05	5	0.086	This work	
					0.08		3
					0.09		21,23
Gold	0.17	31	0.15	5	0.30	This work	
			0.22	33	0.31		21
					0.22		5
Nickel	0.35	32	0.36	5	0.40	This work	
			0.38	33	0.35		3
					0.37		5
Palladium	0.23	This work	0.32	This work	0.38	This work	
			0.32		5		0.37
Platinum	0.32	32	0.30	31	0.38	This work	
	0.27	31	0.30	34	0.39		1,4
					0.38		5
Zirconium			0.32	5	0.41	This work	
					0.30		5
					0.47		4
					0.32		3

* RT represents room temperature data; IT represents incandescent temperatures.

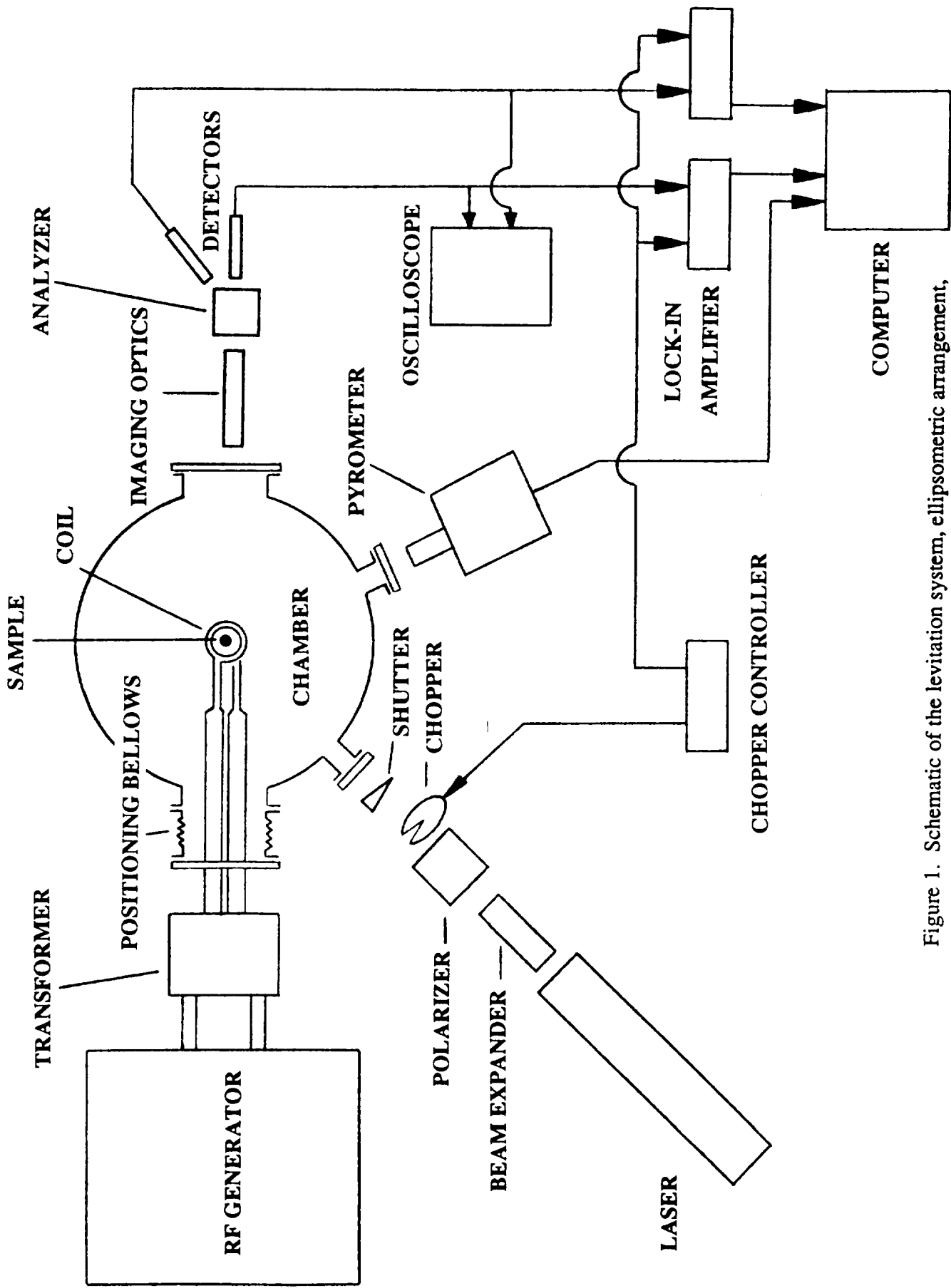


Figure 1. Schematic of the levitation system, ellipsometric arrangement, data acquisition and temperature measurement.

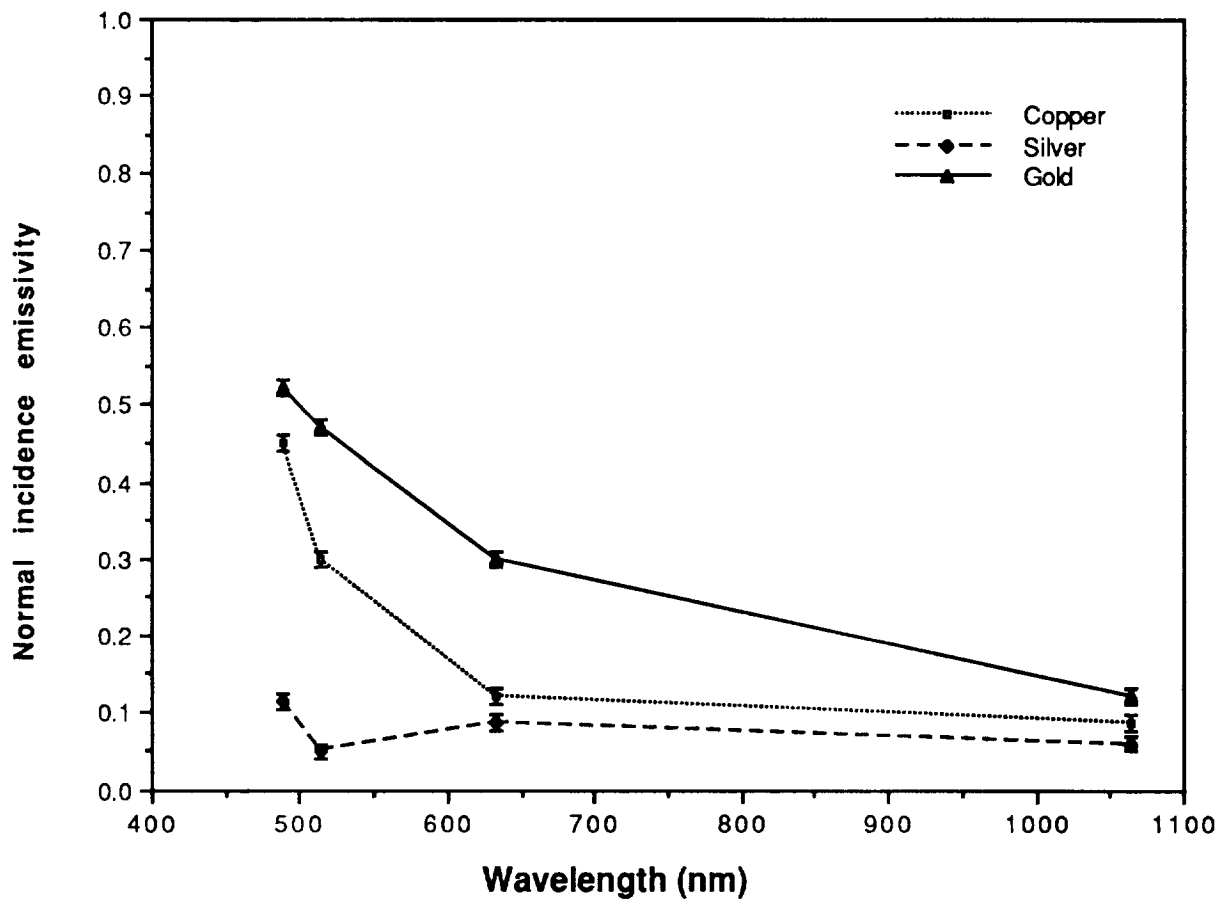


Figure 2. Spectral emissivities of liquid metals in the copper group as a function of wavelength.

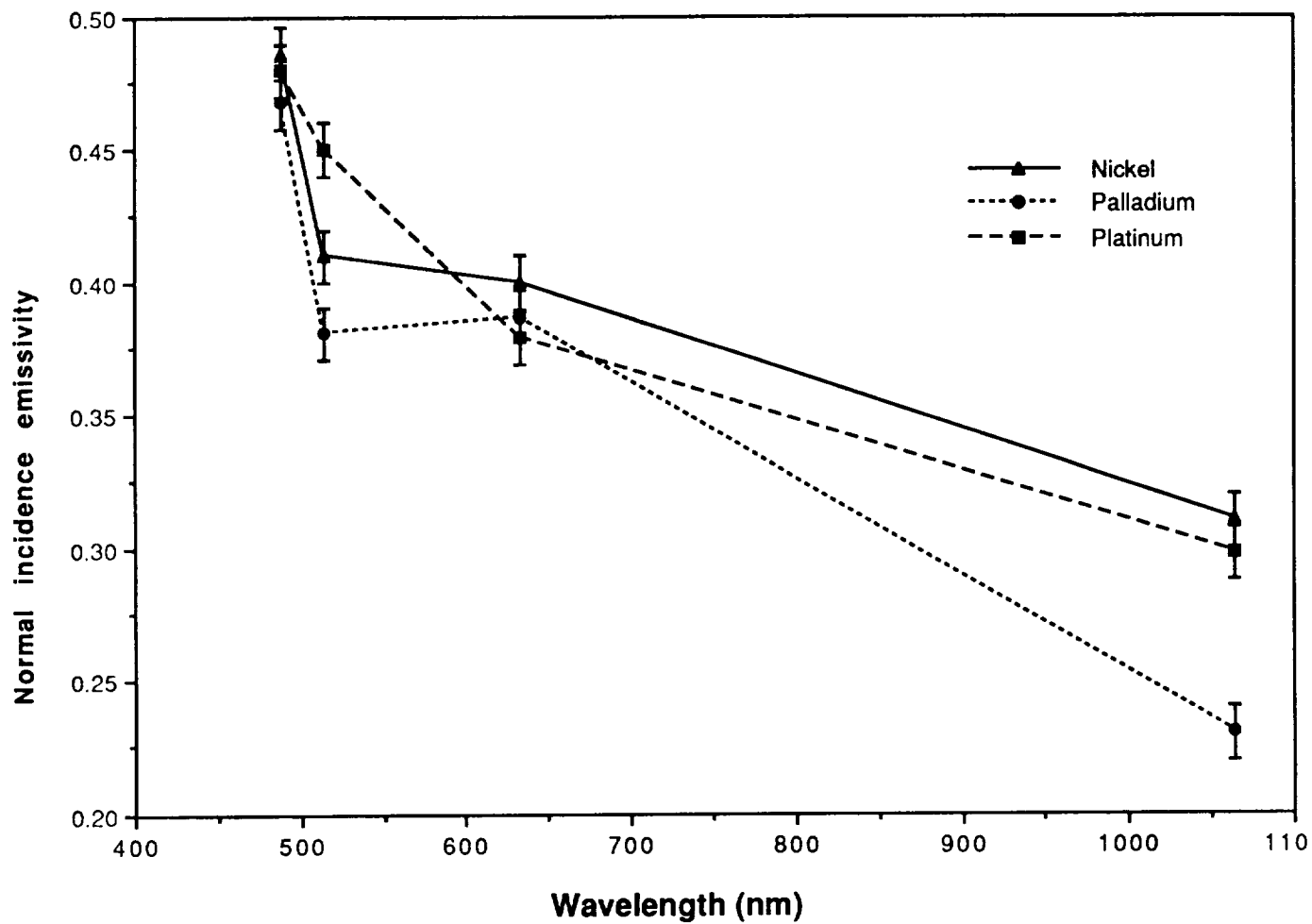


Figure 3. Spectral emissivities of liquid metals in the nickel group as a function of wavelength.

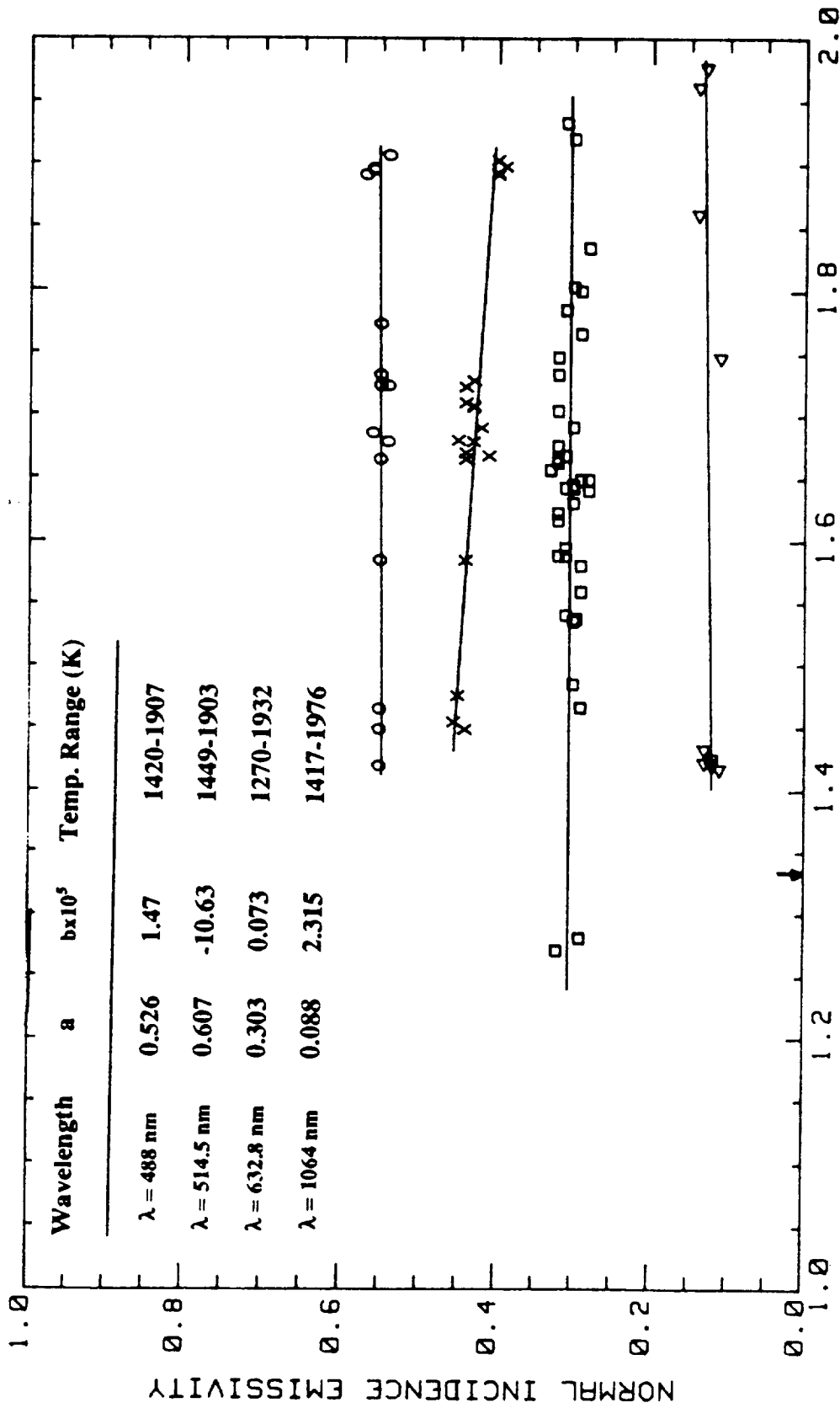
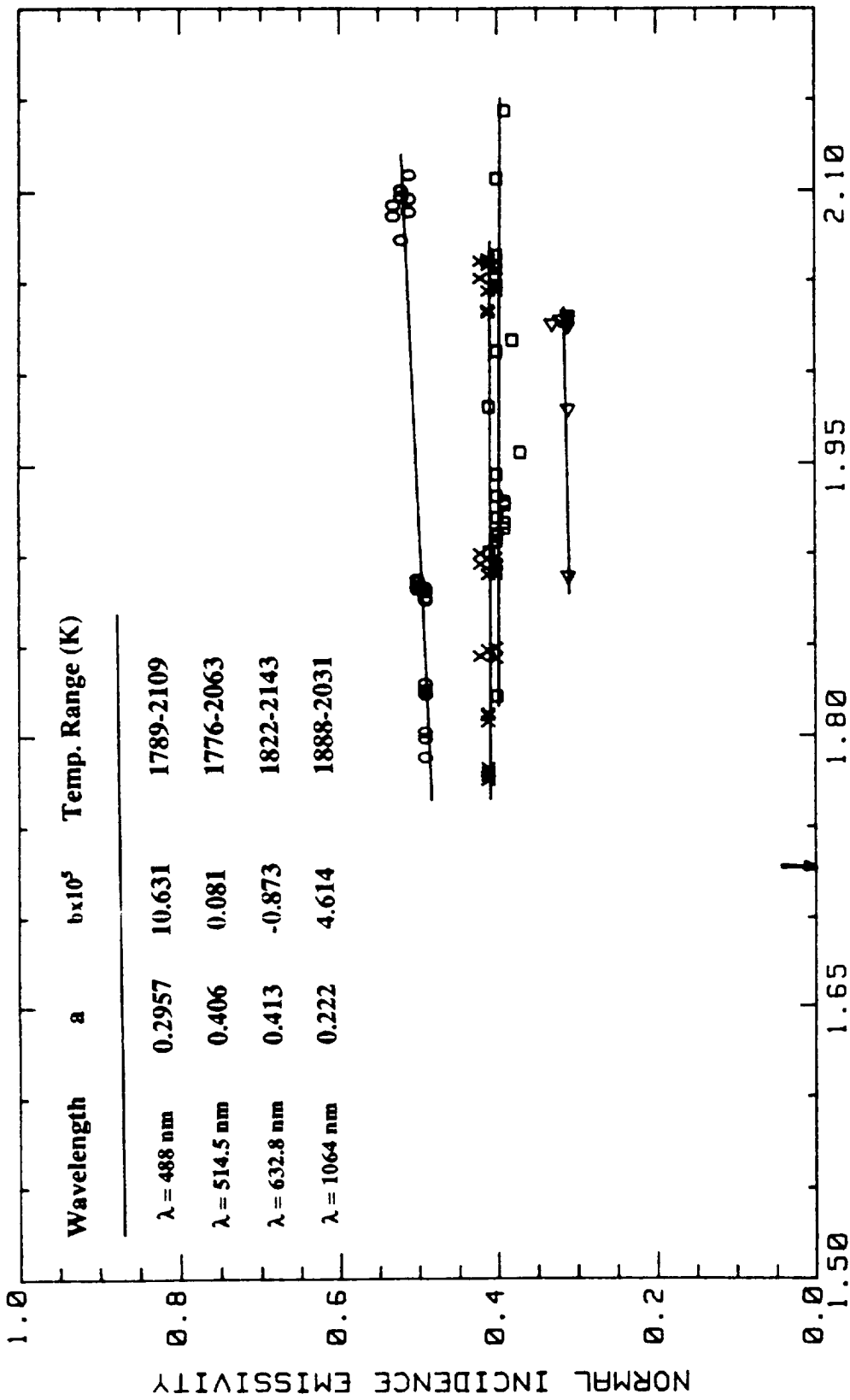


Figure 4. Normal incidence spectral emissivity of liquid gold as a

function of temperature at 1064 (\triangleright), 632.8 (\square), 514.5 (\times), and

488 nm (\circ). Solid line represents the least squares fit to the data.

Melting point indicated by arrow. The results of the fit ($a + bT$) are indicated on the plot.



TEMPERATURE (K) / 10³

Figure 5. Normal incidence spectral emissivity of liquid nickel as a

function of temperature at 1064 (▷), 632.8 (◻), 514.5 (x), and

488 nm (o). Solid line represents the least squares fit to the data.

Melting point indicated by arrow. The results of the fit ($a + bT$) are

indicated on the plot.

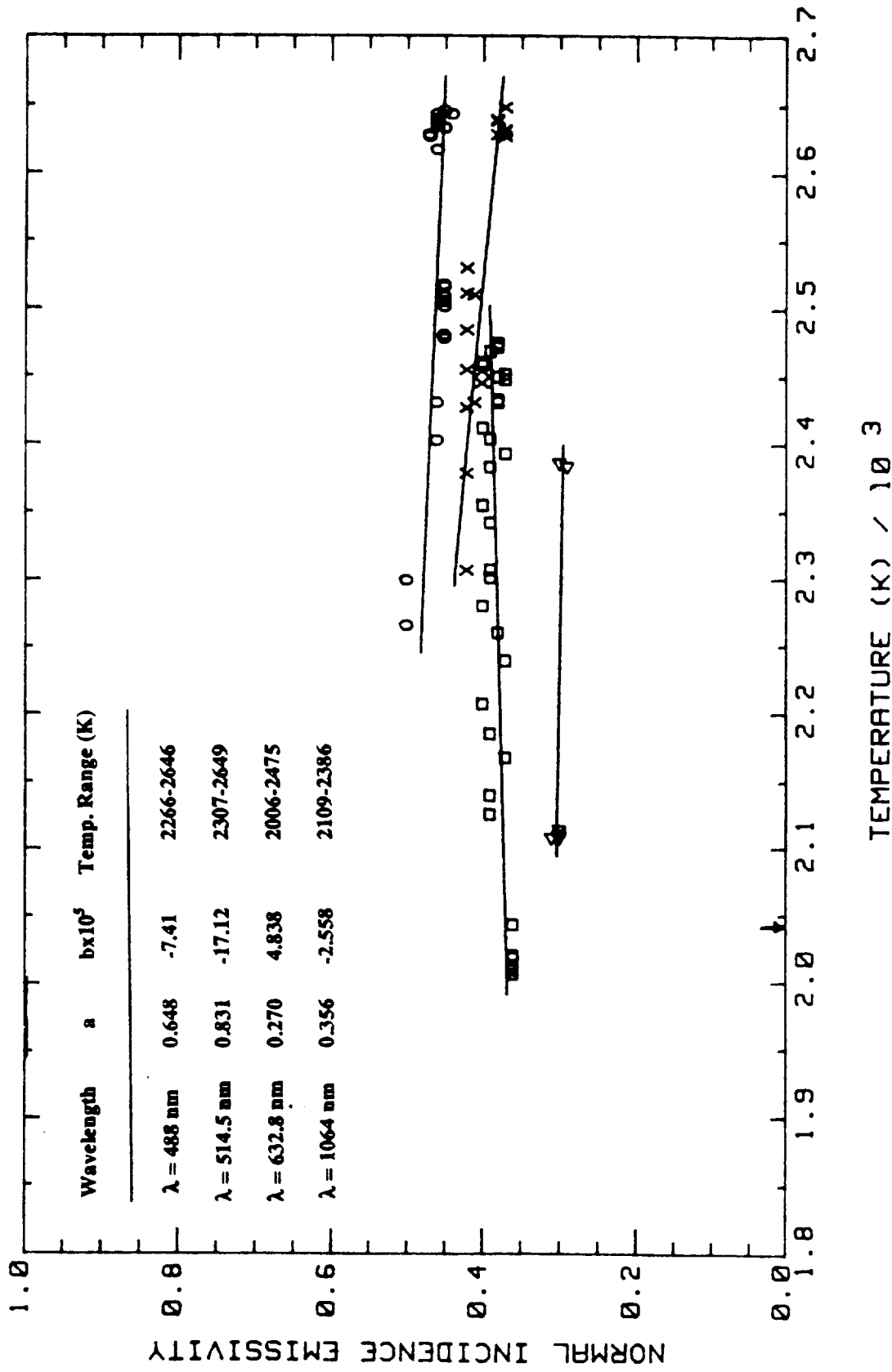


Figure 6. Normal incidence spectral emissivity of liquid platinum as a function of temperature at 1064 (\triangleright), 632.8 (\square), 514.5 (x), and 488 nm (o). Solid line represents the least squares fit to the data. Melting point indicated by arrow. The results of the fit ($a + bT$) are indicated on the plot.

**A POTENTIAL NUCLEAR MAGNETIC RESONANCE IMAGING
APPROACH FOR NONCONTACT TEMPERATURE MEASUREMENT**

Stanley L. Manatt
Applied Sciences and Microgravity
Experiments Section
Jet Propulsion Laboratory

Abstract - It is proposed that in a nuclear magnetic resonance (NMR) imaging experiment that it should be possible to measure temperature through an extended volume. The basis for such a measurement would depend upon sensing a temperature dependent NMR parameter in an inert, volatile molecule (or fluid) filling the volume of interest. Exploratory work suggest that one suitable candidate for such a purpose might be CH₃Cl. Possible parameters, other inert gases and feasible measurement schemes that might provide such temperature measurement will be discussed.

Introduction - For non-contact temperature measurement the predominate approach that has been exploited for many decades has been pyrometry of various sorts. Only now after years of research does it seem that people are finally coming to grips with all aspects of the problem (1). However, the range over which accurate and precise temperature measurements can be made by pyrometry techniques seems to be above about 800K. For the lower temperature region of about 200K to 600K, we would like to suggest a new approach that utilizes the nuclear magnet resonance (NMR) effect.

Some facts about NMR are listed in Figure 1. A great many atomic nuclei are NMR active. The parameters that can be extracted from NMR spectra in many cases reveal fundamental molecular structure data that can only be obtained from other techniques by much more work (2).

The precedent for proposing that temperature measurements can be accomplished in an NMR experiment exists in the multitudes of examples of temperature dependent NMR parameters that have been reported in the last thirty years (3). In Figure 2 are given just two examples. Both these examples were reported sometime ago so that the precision of the exhibited data could probably be improved substantially with present day instrumentation. These examples show that smooth or linear relationships exist for certain NMR parameters over some useful range of temperature (200-500K).

Next let us consider where the NMR effect arises (4). When a mass of NMR active nuclei are placed in a magnet field, a macroscopic magnetization vector results. This vector can be manipulated by radio frequency pulses whose B_1 fields are orthogonal to the B_0 , the main magnetic field. This situation is exhibited and explained in Figure 3. A typical block diagram of a pulse NMR imaging system is shown in Figure 4 (5). In many cases the transmitter and receiver coils are one and the same. In the right side of part a) of the left side of Figure 5 is shown the time dependent signal that would be obtained if the sample contained one chemical type of NMR active nucleus. Fourier transformation of this signal leads to a single line in frequency space. Part b) of this figure shows the situation when there are two chemical types in the sample being studied. In the right side of Figure 5 the principal of how spatial information can be encoded in an NMR experiment by imposing a linear magnetic field gradient is illustrated. The extension of this one dimensional example to two dimensions and three dimensions leads to magnetic resonance imaging (MRI) of a slice or multislices through the sample being investigated. Figure 6 illustrates a typical MRI pulse sequence which involves switching of the three magnetic field gradients and more than one RF pulse (6). The first RF pulse, P4, is a tailored selective $\pi/2$ pulse and the second, P2, is a non-selective π pulse. This pulse sequence is usually repeated during about 120 increments of the Y-gradient. Image reconstruction processing (either Fourier or back-projection) (7) will yield a slice image that exhibits the two dimensional intensity map of some NMR parameter. If the magnitude of the NMR parameter being sensed is temperature dependent then the image maps the temperature in the slice under study.

In the top part of Figure 7 are listed a number of temperature dependent NMR parameters that could be the basis of MRI temperature measurement schemes. In Figure 8 is depicted a possible experimental configuration about a levitation chamber for such a temperature measurement. Although the non-contact temperature scheme needs that prompted this proposal for temperature measurement were in connection with possible deployment about a levitation chamber in zero-g, there are substantial potential applications for such an approach for temperature mapping in all sorts of ground based vessels and pipes containing fluids and gases.

In the bottom part of Figure 7 are listed a few examples of molecules that might be potential candidates on which to base such an MRI temperature measurement scheme. Shown in Figure 9 are some exploratory results with the various chlorinated methanes and some properties of the isotopes $^{35}\text{C}1$ and $^{37}\text{C}1$. It appears that perhaps $\text{CH}_3\text{C}1$ might be a possible candidate as a temperature reporting molecule. The NMR spectra of this molecule were

investigated both in the liquid and gas phases but only at one temperature (about 20° C). It should be noted that there is a significant difference between the linewidths in the two phases and also between the ^{35}Cl and ^{37}Cl nuclei. From other work with some other nuclei (8) it is expected that the linewidths of the ^{35}Cl and ^{37}Cl resonances will exhibit changes with temperature. These changes are probably due to modulation of the coupling of the nuclear quadrupole moment with the magnetic dipole moment. The next step in this exploratory work is to characterize in detail the latter temperature dependences both for the liquid and gas phases. There is little data even now on such NMR temperature dependent changes for quadrupolar nuclei. There is even less data on the NMR of gases and their temperature dependencies. Thus, there is a lot of exploratory work to be done before suitable candidates for useful NMR temperature probes can be identified. It is the intention of work in progress to identify several such molecules that will be useful in the temperature range of 200-600K.

In Figure 10 are listed other considerations that bear on the development of this new non-contact temperature approach. The accuracy and precision of ± 3 degrees is a conservative estimate as right now temperature dependent NMR experiments are being done where differences as small as ± 0.5 degrees affect spectra. An important point is that one probably doesn't need high resolution to provide useful temperature mapping. It is usual to acquire NMR images with resolution of 256 x 256 pixels whereas for temperature mapping, grids of 10 x 10 to 50 x 50 may in many cases be totally adequate. There is a tradeoff with resolution and imaging time so lower resolution maps can be obtained with a great saving of time. Another important point is that really high magnetic fields are not necessarily needed to accomplish useful MRI. Excellent proton images are now being obtained at fields as low as 600-2000 gauss. (9,10) Whether satisfactory S/N can be achieved for quadrupolar nuclei with less NMR sensitivity than protons needs to be explored in detail, especially in the gas phase.

Conclusion - A new approach for non-contact temperature measurement has been described above which in the temperature range of 200-600K has the potential to meet the needs of some microgravity and containerless processing experiments. In contrast to the decades of research and development work that have been put in on pyrometry approaches, which have not resulted in many useful instruments for the above mentioned temperature range, it would seem that this new approach has the potential for development into practical protocols and instruments in a period of several years.

References

1. For a recent summary see the contributions in "Noncontact Temperature Measurement," NASA Conference Publication 2503, M.C. Lee Editor, March 1988 and other papers in the present proceedings.
2. See for example, M. L. Martin, J.-J. Delpuech and G. J. Martin, "Practical NMR Spectroscopy," Heyden & Son Ltd, London, 1980.
3. See many examples discussed by J. I. Kaplan and G. Fraenkel in "NMR of Chemical Exchanging Systems," Academic Press, New York, 1980.
4. For a more detailed discussion see reference 2.
5. Figure adapted from P.A. Bottomley, Rev. Sci. Instrum., 53, 1319 (1982).
6. Reference 5 discusses a number of other pulse sequences.
7. For a review of these techniques see G. T. Herman, "Image Reconstruction from Projections," Academic Press, New York, 1980.
8. S. L. Manatt, unpublished work on ^{14}N and ^{11}B NMR linewidths.
9. H. Lotz, L. Ekelund, S-O. Hietala and G. Wickman, J. Comput. Assist. Tomography, 12, 1006 (1988).
10. R.E. Sepponen, J.T. Sipponen and A. Sivula, ibid., 9, 237 (1985).

SOME FACTS:

- FORM OF RADIOFREQUENCY SPECTROSCOPY WITH ATOMIC NUCLEI POSSESSING SPIN (^1H , ^{13}C , ^{31}P , ^{23}Na , ^{15}N , ^2H , ^{17}O , ^{19}F , ETC.)
- REQUIRES MAGNET, R.F. TRANSMITTER-RECEIVER AND DATA ACQUISITION SYSTEM
- AREAS OF NMR SIGNALS ARE USUALLY DIRECTLY PROPORTIONAL TO NUMBER OF NUCLEI SEEN BY PROBE RECEIVER COIL
- FOR A LONG TIME VERY IMPORTANT RESEARCH TECHNIQUE IN BIOLOGY, CHEMISTRY AND PHYSICS AND NOW IMPORTANT IN BIOMEDICINE
- NMR EXPERIMENT CAN BE DONE MANY DIFFERENT WAYS AND CAN YIELD A NUMBER OF DIFFERENT PARAMETERS DIRECTLY RELATED TO MOLECULAR STRUCTURE AND DYNAMICS

Figure 1. Nuclear Magnetic Resonance (NMR): Some Facts

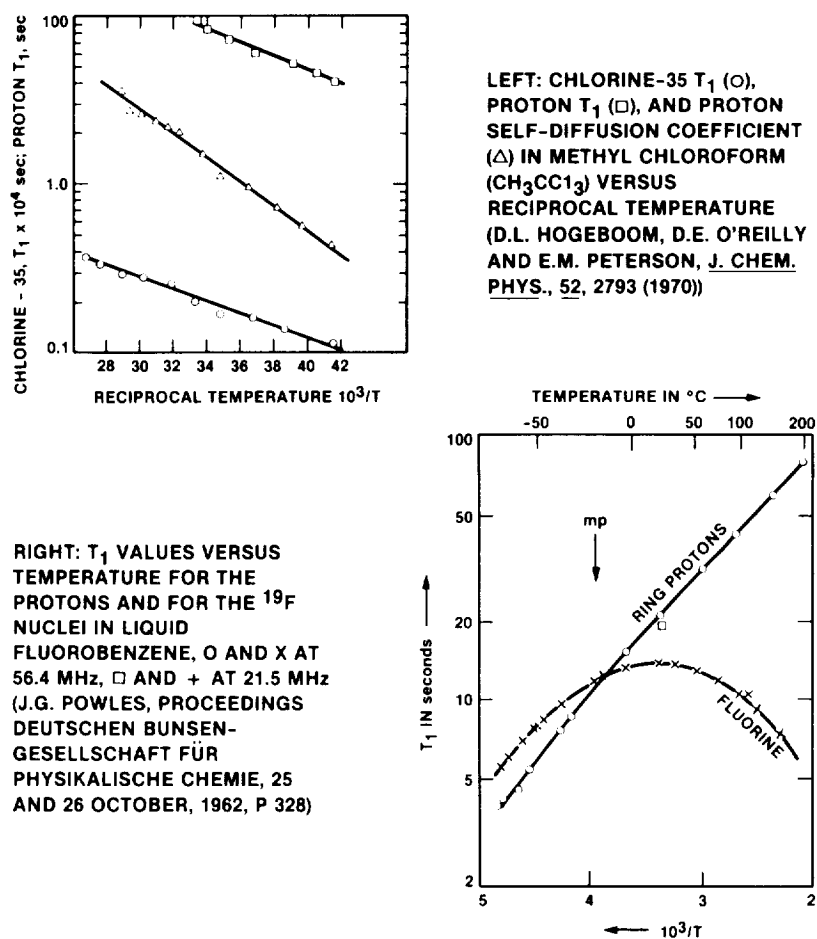


Figure 2. Two Literature Precedents for Proposed NMR Temperature Measurement Approach

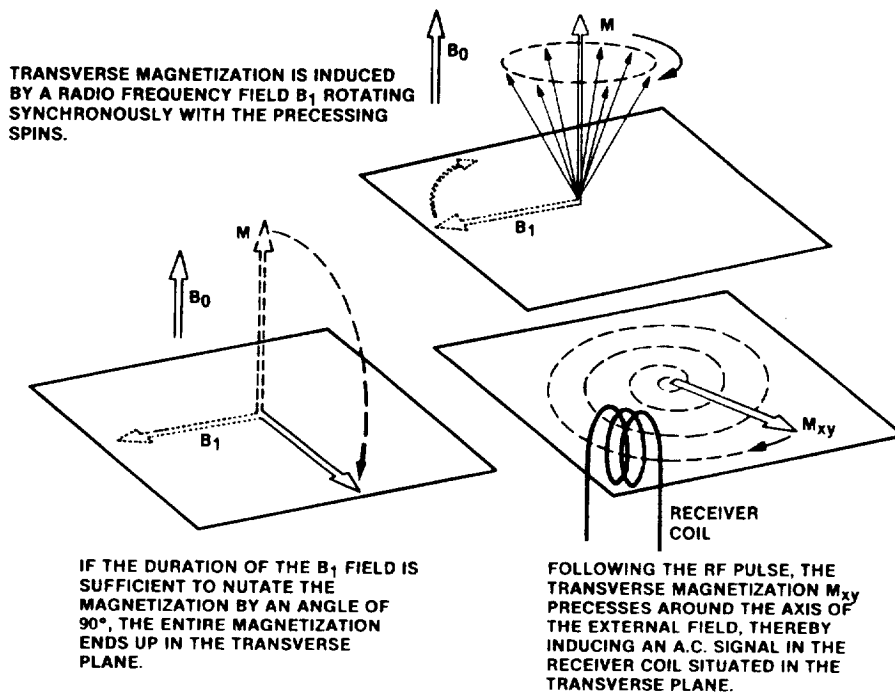


Figure 3. Illustration of How Magnetization Gives Rise to NMR Signal

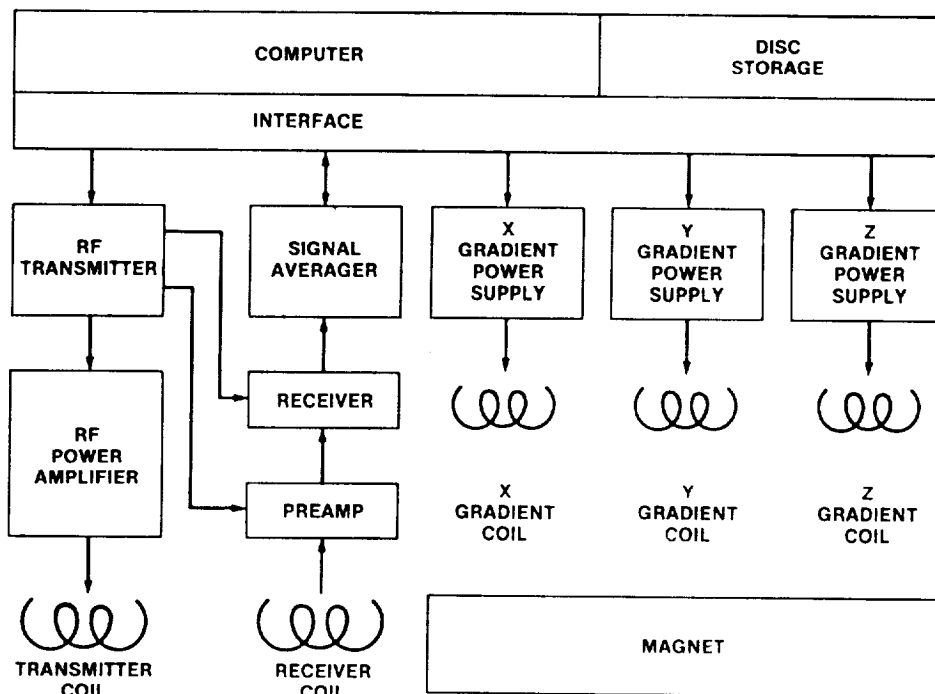


Figure 4. Simplified Block Diagram of a Typical Computer-Based NMR Imaging System; adapted from P. A. Bottomley, *Rev. Sci. Instrum.*, **53**, 1219 (1982)

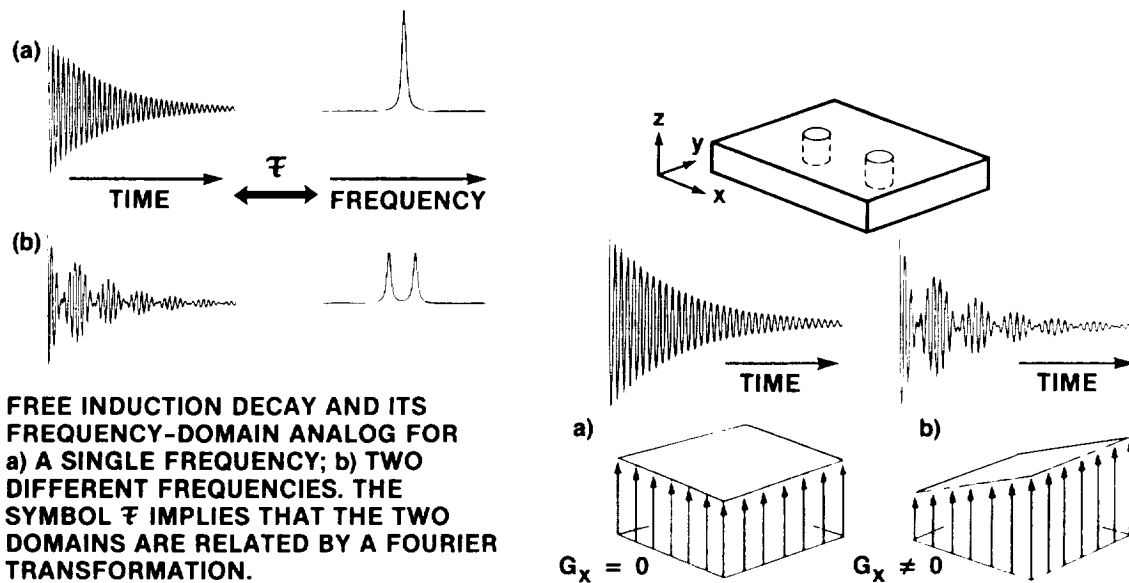


Figure 5. Typical Output From NMR System and Encoding Of Spatial Information By Field Gradient in NMR Experiment

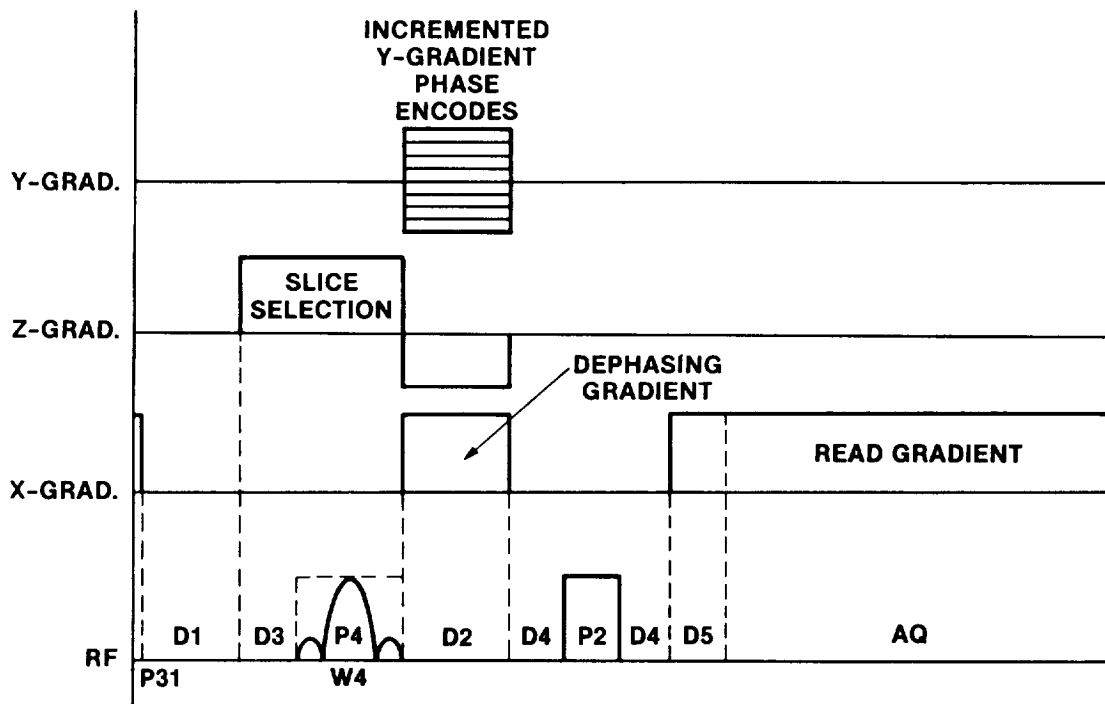


Figure 6. Line Scan Imaging Sequence

NMR PARAMETERS

- T₁-SPIN LATTICE RELAXATION TIME
- T₂-SPIN-SPIN RELAXATION TIME
- FOR SPIN > 1 NUCLEI, QUADRUPOLEAR RELAXATION CHANGES
- SLOW MOLECULAR CONFORMATION CHANGES
- COUPLING CONSTANT CHANGES
- CHEMICAL SHIFT CHANGES
- CHEMICAL EXCHANGE EFFECTS

INERT MOLECULES

- CClH₃ (³⁵C1 AND ³⁷C1 RESONANCES)
- CClF₃ (¹³C, ¹⁹F, ³⁵C1 AND ³⁷C1 RESONANCES)
- ¹²⁹Xe AND ¹³¹Xe (IN NATURAL ISOTOPIC ABUNDANCES)
- (CH₃)₃ N (¹³C AND ¹⁴N)
- CH₃OCH₃ (¹⁷O, ENRICHED)
- CFD₃ (²H, ¹³C AND ¹⁹F)

Figure 7. Potential Temperature Dependent NMR Parameters and Some Potential Inert Molecules

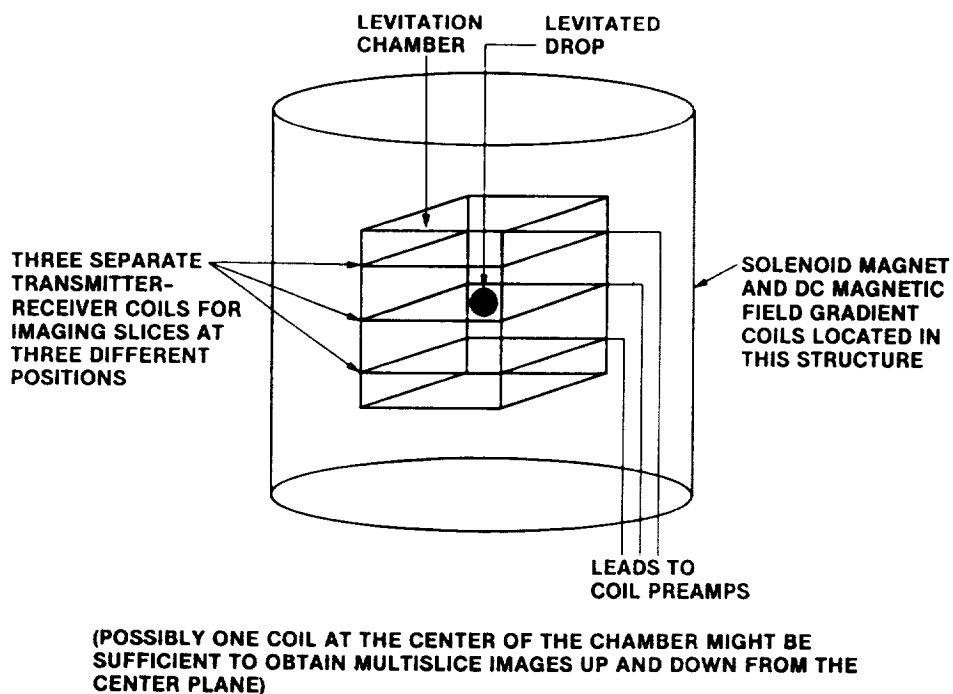


Figure 8. Experimental Configuration

- LINE WIDTHS OF C1 IN CC1₄, CC1₃H, CC1₂H₂ AND CC1H₃ MEASURED
- RATIONAL FOR WORK: PERHAPS TEMPERATURE DEPENDENCE OF LINE WIDTH OF ONE OF THESE MOLECULES MIGHT FORM BASIS FOR TEMPERATURE SCALE

- PROPERTIES OF C1 ISOTOPES

	³⁵ C1	³⁷ C1
SPIN 3/2 ABUNDANCE	75.53%	24.47%
SENSITIVITY RELATIVE ¹ H	4.7 x 10 ⁻³	2.71 x 10 ⁻³
QUADRUPOLE MOMENT	-7.89 x 10 ⁻²⁶ cm ²	-6.21 x 10 ⁻²⁶ cm ²

- RESULTS AT 19.60 MHz FOR ³⁵C1 AND 16.31 MHz FOR ³⁷C1 IN 46.98 x 10³ GAUSS FIELD

	³⁵ C1	³⁷ C1
CC1 ₄	9400 Hz (ℓ)	4400 Hz (ℓ)
CC1 ₃ H	7400 Hz (ℓ)	3700 Hz (ℓ)
CC1 ₂ H ₂	4300 Hz (ℓ)	2300 Hz (ℓ), 3000 Hz (g)
CC1H ₃	1900 Hz (ℓ)	1000 Hz (ℓ), 1500 Hz (g)

- CONCLUSIONS: LINE WIDTHS OF CC1₄, CC1₃H, AND CC1₂H₂ TOO BROAD; CC1H₃ POSSIBLE CANDIDATE FOR DETAILED TEMPERATURE DEPENDENT STUDIES

Figure 9. Preliminary ³⁵C1 and ³⁷C1 NMR Work

- RANGE OF NMR TEMPERATURE MEASUREMENT FROM ABOUT 200-600°K WITH AN ACCURACY OF ± 3 degrees
- PROBABLY ONLY NEED 10 x 10 TO 20 x 20 SLICE IMAGES FOR ADEQUATE TEMPERATURE PROFILES
- ALTHOUGH S/N FOR VARIOUS CANDIDATE GASES AT 1 atm. ARE CALCULATED TO HAVE ADEQUATE S/N FOR MODEST FIELDS, NEED TO EXPLORE SITUATION AT LOWER FIELDS
- MAGNETIC FIELD DOES NOT NEED TO BE HIGH AS GOOD IMAGES HAVE RECENTLY BEEN OBTAINED AT LOW FIELDS (600-2000 GAUSS)
- GROUND-BASED NMR TEMPERATURE PROFILE MEASUREMENT IN CHAMBERS TO BE USED IN SPACE PROCESSING MIGHT BE USEFUL IN ITSELF

Figure 10. Other Considerations

IR Optical Fiber-based Noncontact Pyrometer for Drop Tube Instrumentation

R.G. May, S. Moneyhun, W. Saleh, S. Sudeora, and R.O. Claus
Virginia Polytechnic Institute and State University, Fiber and Electro-Optics Research Center,
Blacksburg, VA 24061

A. M. Buoncristiani
NASA Langley Research Center, Hampton, 23665

ABSTRACT

The design of a two-color pyrometer with an infrared optical fiber bundles for collection of the infrared radiation is described. The pyrometer design is engineered to facilitate its use for measurement of the temperatures of small, falling samples in a microgravity materials processing experiment using a 100-meter long drop tube. Because the samples are small and move rapidly through the field-of-view of the pyrometer, the optical power budget of the detection system is severely limited. Strategies for overcoming this limitation are discussed.

INTRODUCTION

Optical fibers have been applied to the measurement of temperature since 1980¹. Methods may be broadly divided into intrinsic and extrinsic techniques. Intrinsic techniques include those in which light propagating in an optical fiber sensing element remains within the fiber; light in an extrinsic sensor instead interacts directly with the environment. Noncontact methods are inherently extrinsic because a physical separation between the fiber and the material to be evaluated is required. Noncontact optical fiber-based temperature measurement systems are typically two or three-wavelength pyrometers which utilize several optical detectors at several discrete wavelengths^{2,3,4}. The remote end of the optical fiber is aligned so that the hot material is within the fiber's field of view. Radiation which enters the fiber is split by an in-line coupler which independently feeds each of several optical filter/detector assemblies. As the temperature of the material to be sensed changes, the outputs of the different detectors also change, and via consideration of graybody radiation curves, the temperature of the material can be determined.

An application of the described research is the determination of temperatures of falling particles in the Microgravity Materials Processing drop tube facility at the NASA Marshall Space Flight Center in Huntsville, AL. The drop tube is a 100 meter tall evacuated cylinder into which molten samples of metals or metallic binary alloys are dropped. During free-fall, the samples cool and solidify, yielding metallurgical structures that are not influenced by the earth's gravity. For a typical experiment, a sample is magnetically levitated at the top of the drop tube, and heated to melting by an RF induction furnace. The magnetic field is then turned off, and the sample is dropped. As the sample cools and solidifies during the drop, it undergoes recalescence due to the heat of fusion during the phase change. The temperature of the sample during the drop is calculated from heat transport equations, given the initial temperature (measured by an optical pyrometer adjacent to the RF induction furnace) and the elapse of time from release to recalescence (determined by a silicon photodetector at the bottom of the drop tube). Experimental confirmation of the calculated temperature requires the use of noncontact measurement techniques that are independent of the usually unknown emissivities of the materials.

MODELED PERFORMANCE OF FIBER OPTIC PYROMETER INPUT CONDITIONS

The free fall of the heated pellet in the drop tube results in a limited time within the field-of-view of the fiber. Consequently, the amount of radiant flux incident on the fiber face is very small. A mathematical model was derived to determine the amount of radiant flux incident on the fiber face. Using this model a computer program was written to yield numerical values representative of the proposed measurement system.

The following assumptions were made:

- (1) The pellet is falling through the geometric center of the drop-tube.
- (2) The pellet is spherical in shape.
- (3) The fiber face area is negligible compared to the pellet surface area.
- (4) The radiation emitted by the pellet towards the fiber, as it is in the process of 'entering' and 'leaving' the field-of-view of the fiber, is neglected. In other words, the radiation when the pellet is in the field-of-view is considered to be constant from point (1) to point (2), as shown in figure (1).
- (5) The radiation from the fiber towards the pellet is neglected.
- (6) The velocity of the pellet within the field-of-view of the fiber is constant.
- (7) The temperature of the pellet within the field-of-view of the fiber is constant.

One of the mathematical difficulties in treating radiative transfer between surfaces is accounting for the geometric relations involved in how the surfaces view each other. A method of accounting for the geometry is introduced in the form of a quantity called the "geometric configuration factor", greatly simplifying the analysis.

The configuration factor of the system is derived by considering the geometry as shown in Figure 1. Figure 2 shows the fiber face area as a differential element dA_1 , and the pellet as a sphere of surface area A_2 . The

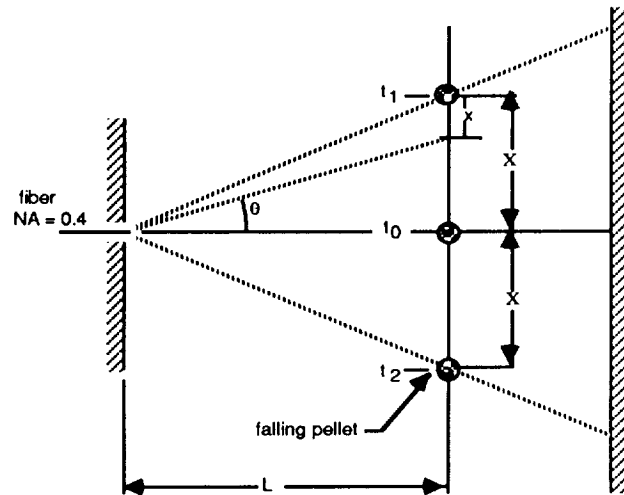


Figure 1. Geometry for radiative transfer model.

orientation is such that the normal to the center of the differential element passes through the center of the sphere. The standard result of the configuration factor of the system shown in Figure 2 is:

$$F_{d1-2} = \left[\frac{r_2}{h} \right]^2 \quad (1)$$

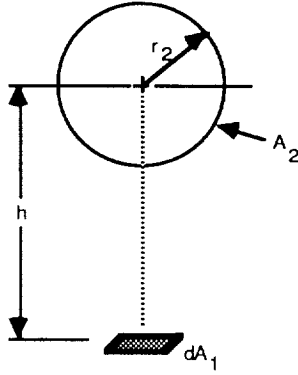


Figure 2. Geometry for configuration factor.

For the case when the pellet is directly in front of the fiber as shown in Figure 1, equation (1) becomes:

$$F_{d1-2} = \left[\frac{r_2}{L} \right]^2 \quad (2)$$

where L = radius of the drop tube.

Since we are considering the flow of radiant flux from A_2 to dA_1 , it is necessary to find dF_{2-d1} (the configuration factor needed for calculating energy flow from A_2 to dA_1). The 'reciprocity relation' between a differential element and a finite area states that

$$A_2 dF_{2-d1} = dA_1 F_{d1-2}$$

or

$$dF_{2-d1} = \frac{dA_1}{A_2} F_{d1-2} \quad (3)$$

where,

dA_1 = area of fiber face
 A_2 = surface area of the pellet.

Then equation (3) can be written as

$$F_{2-d1} = \frac{\pi r_1^2}{4\pi r_2^2} \left[\frac{r_2}{L} \right]^2 \quad (4)$$

The relation in equation (4) assumes that the normal to the fiber face passes through the center of the spherical pellet. Therefore, in order to consider for the cases when the pellet is at some angle, the component of the fiber face

area is taken which is such that the normal to the component always passes through the center of the spherical pellet.

Therefore equation (4) becomes,

$$F_{2-dl} = \frac{[\pi r_1^2] \cos \theta}{4\pi r_2^2} \left(\frac{r_2}{L}\right)^2 \quad (5)$$

Now, θ is a function of "x", as shown in Figure (1):

$$\cos \theta = \frac{L}{\sqrt{L^2 + (X-x)^2}} \quad (6)$$

In equation (6), the quantities "L" and "X" are constant and "x" varies with time "t". Writing "x" in terms of "t", we get:

$$x = \left(\frac{2X}{\Delta T}\right) t \quad (7)$$

where,

$$\begin{aligned} \Delta T &= t_1 - t_0 \text{ Time for which the pellet is in the field-of-view.} \\ 2X &= \text{Total vertical distance traveled through the field-of-view.} \end{aligned}$$

and "t" varies from t_1 to t_2 as shown in Fig. (1).

Now, equation (6) becomes,

$$\cos \theta = \frac{L}{\sqrt{L^2 + \left\{X - \left(\frac{2X}{\Delta T}\right) t\right\}^2}} \left(\frac{r_2}{L}\right)^2 \quad (8)$$

Substituting (8) in (5), we get

$$F_{2-dl} = \frac{[\pi r_1^2]}{4\pi r_2^2} \frac{L}{\sqrt{L^2 + \left\{X - \left(\frac{2X}{\Delta T}\right) t\right\}^2}} \left(\frac{r_2}{L}\right)^2$$

Canceling the like terms from the numerator and denominator, we get:

$$F_{2-d1} = \frac{r_1^2}{4L} \frac{1}{\sqrt{L^2 + \left\{ X - \left(\frac{2X}{\Delta T} \right) t \right\}^2}} \quad (9)$$

To get the total incident radiant flux on the fiber face, we use the following equation:

$$dQ_{2-d1} = \sigma K^4 dF_{2-d1} A_2 \quad (10)$$

where,

dQ_{2-d1} = Flux incident on the fiber face.

σ = Stephan - Boltzmann constant = 5.66961×10^{-8} W/m²K⁴

K = Temperature of pellet (source)

A_2 = Surface area of the pellet.

As it is assumed that the temperature of the pellet remains constant during the short interval of time the pellet is in the field-of-view of the fiber, we find that equation (10) has all the terms constant except F_{2-d1} , which varies with time.

Equation (9) is integrated between " t_1 " and " t_0 " and the result doubled to account for the time from " t_0 " to " t_2 "

$$\begin{aligned} [F_{2-d1}]_{t_1, t_0} &= \int_{t_1}^{t_0} \frac{r_1^2}{4L} \frac{1}{\sqrt{L^2 + \left\{ X - \left(\frac{2X}{\Delta T} \right) t \right\}^2}} dt \\ &= \frac{r_1^2}{4L} \int_{t_1}^{t_0} \frac{1}{\sqrt{L^2 + X^2 + \left(\frac{2X}{\Delta T} \right)^2 t^2 - \left(\frac{4X^2}{\Delta T} \right) t}} dt \end{aligned} \quad (11)$$

Let

$$A = L^2 + X^2$$

$$B = - \left(\frac{4X^2}{\Delta T} \right)$$

$$C = \left(\frac{2X}{\Delta T} \right)^2$$

Substituting A,B and C in equation (11), we have

$$[F_{2dl}]_{t_1, t_0} = \frac{r_1^2}{4L} \int_{t_0}^{t_1} \frac{1}{\sqrt{A + Bt + Ct^2}} dt \quad (12)$$

Using the standard result for

$$\int \frac{1}{\sqrt{X}} dx = \frac{1}{\sqrt{c}} \log \left[\sqrt{X} + x\sqrt{c} + \frac{b}{2\sqrt{c}} \right]$$

for $c > 0$ and where $X = a + bx + cx^2$.

Then equation (12) becomes

$$[F_{2dl}]_{t_1, t_0} = \frac{r_1^2}{4L} \left[\left\{ \frac{1}{\sqrt{C}} \log \left(\sqrt{A + Bt_0 + Ct_0^2} \right) + t_0\sqrt{C} + \frac{B}{2\sqrt{C}} \right\} - \left\{ \frac{1}{\sqrt{C}} \log \left(\sqrt{A + Bt_1 + Ct_1^2} \right) + t_1\sqrt{C} + \frac{B}{2\sqrt{C}} \right\} \right] \quad (13)$$

Now,

$$[F_{2dl}]_{total} = 2 [F_{2dl}]_{t_1, t_0} \quad (14)$$

Substituting equation (14) in equation (10), we get the total radiant flux incident on the fiber face.

NUMERICAL SIMULATION

The model for radiative transfer was coded into a FORTRAN computer program, yielding the resulting incident radiant flux in watts for different pellet temperatures. For these calculations the pellet was assumed to be 3 mm in diameter, and the single fiber was assumed to have a core diameter of 200 μm and NA of 0.4. Also, the drop tube radius was taken to be 6 inches.

The results show that the radiant flux incident on a 200 μm fiber (with NA of 0.4), 10 meters down the drop-tube and at temperature 773K is 0.45×10^{-11} Watts. This number decreases further down the drop tube (e.g. at 190

meters down the drop-tube it falls down to 0.5×10^{-13} Watts). Further, at higher temperatures, we find that the amount of incident radiant flux increases. At a temperature of 3773 K and 10 meters down the drop-tube, the value becomes 0.25×10^{-8} Watts. These numbers represent the ideal case as the falling pellet is assumed to be a blackbody. These numbers will further decrease if the falling pellet is considered to be a gray body and other effects (such as spectral attenuation of the fiber, inclusion of an anti-reflection coating, or stray reflections from the inside wall of drop-tube) are taken into account.

The field-of-view and hence the transit time of the pellet in the field-of-view can be increased by orienting the fiber at an angle with respect to the vertical wall of the drop tube. This approach is shown in Figure (3). Here β , the angle by which the fiber is tilted, is assumed to be less than θ , where $\theta = \sin^{-1}(NA)$, NA being the numerical aperture of the fiber. The configuration factor was adapted to account for the tilted fiber, and coded into a FORTRAN program. The results showed that the tilting of fiber increased the time in which the pellet remained in the field-of-view of the fiber, which, in turn, increased the radiant flux incident on the fiber-face. They indicate that the radiant flux incident on the fiber-face, 10 meters down the drop-tube, when it is tilted at an angle of 20° with respect to the horizontal reference time is 0.87×10^{-9} Watts which corresponds to a 17.6% increase in the incident radiant flux. Similarly, at 190 meters down the drop-tube, with the fiber tilted at 20° with respect to the horizontal reference line it becomes 0.1×10^{-10} Watts which corresponds to a 12.4% increase in the incident radiant flux.

As shown by the results of the above programs that as we move down the drop-tube, both the time in which one pellet remains in the field-of-view and the incident radiant flux decrease appreciably. This implies that it will be necessary to increase the tilt angle β as we move down the drop-tube, to compensate for the loss in the incident radiant flux.

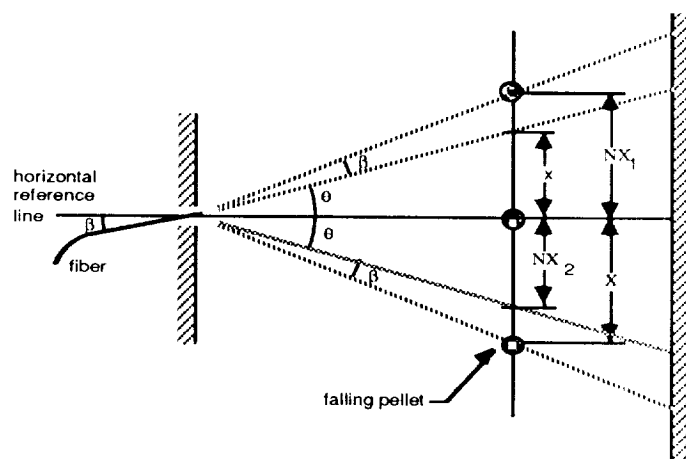


Figure 3. Geometry for tilted fiber.

IMPLEMENTATION OF PYROMETER

To augment the radiant flux incident on the detectors, an experimental pyrometer is being assembled with a six inch long, 0.125 inch diameter bundle of $200 \mu\text{m}$ diameter core, $250 \mu\text{m}$ diameter clad zirconium fluoride fibers. The bundle of approximately 120 fibers will increase the optical power budget at the detectors by about 20 dB over the case for the single fiber analyzed in the configuration factor study, and will mount to the drop tube through a $2 \frac{3}{4}$ inch flange. The bandpass filter center wavelengths will be chosen depending on the estimated initial temperature of the sample (different materials are typically heated to different initial temperatures in the induction furnace). Barium fluoride infrared lenses will be used to focus the outputs onto two cryogenically cooled indium antimonide detectors. Following amplification of the detector outputs, the ratio of the two signals are taken and the temperature derived.

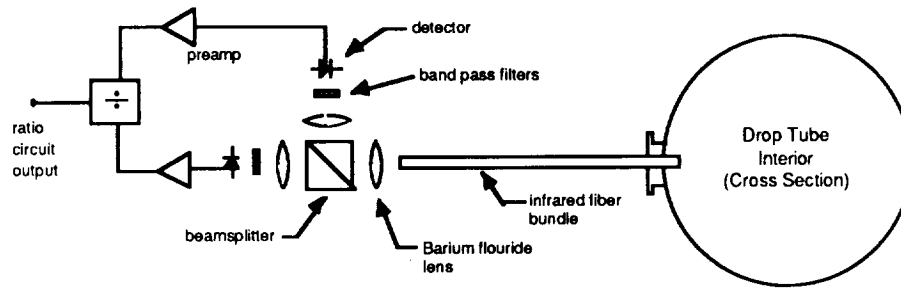


Figure 4. Pyrometer design

CONCLUSIONS

The work reported focused on determining the feasibility of employing an optical pyrometry approach using infrared optical fibers to measure the temperature of falling particles in the NASA Marshall Space Flight Center drop tube. A mathematical model based on radiative transfer principles was derived, and key parameter values representative of the drop tube system, such as particle size, tube diameter and length, and particle temperature, were used to determine an estimate of the radiant flux that will be incident on the face of an optical fiber used to collect radiation from the incandescent falling particle. The results indicate that the total power collected will be on the order of picowatts. An extension of this work examined the advantage of inclining or tilting the collecting fiber to increase the time that the falling particle remains in the fiber field-of-view. Those results indicate that increases in total power collected of about 15% may be realized by tilting the fiber. Current work is proceeding towards implementing an experimental pyrometer utilizing the design principles discussed.

REFERENCES

1. R.O. Claus and J. Cantrell, Proc. IEEE Region 3 Conference, April 1980.
2. R. Vanzetti, "The role of fiber optics in remote temperature measurement," NASA Noncontact Temperature Measurement Workshop, April 30, 1987, Washington, DC.
3. K.A. Wickersheim and M.H. Sun, "Fiberoptic thermometry and its application," J. Microwave Power, 1987, p 85-93.
4. P.B. Coates, "Multiwavelength pyrometry," Metrologia 17, p. 103, 1981.

Use of Anomalous Thermal Imaging Effects for Multi-Mode Systems Control During Crystal Growth

**Michael J. Wargo
Massachusetts Institute of Technology
Cambridge, MA 02139**

Abstract

Real time image processing techniques, combined with multitasking computational capabilities are used to establish thermal imaging as a multi-mode sensor for systems control during crystal growth. Whereas certain regions of the high temperature scene are presently unusable for quantitative determination of temperature, the anomalous information thus obtained is found to serve as a potentially low noise source of other important systems control output. Using this approach, the light emission/reflection characteristics of the crystal, meniscus and melt system are used to infer the crystal diameter and a linear regression algorithm is employed to determine the local diameter trend. This data is utilized as input for closed loop control of crystal shape. No performance penalty in thermal imaging speed is paid for this added functionality. Approach to secondary (diameter) sensor design and systems control structure is discussed. Preliminary experimental results are presented.

Introduction

Real time thermal imaging has been found to be a powerful tool for passively measuring the effects of applied magnetic fields on the temperature distribution of encapsulated high temperature semiconductor melts during the crystal growth operation. A complete description of the thermal imaging system's design and capabilities is available in [1]. Advanced image processing techniques are employed to reduce or eliminate temporal as well as spatial high frequency noise from the image. In this way spurious perturbations, such as bubbles entrained within the encapsulating liquid glass layer, do not effect the quantitative determination of the local temperature distribution. (See figures 1 and 2 for photographic and schematic descriptions of the thermal imaging process and apparatus.) However, certain attributes of the optical path related to the geometry of the high temperature scene introduce anomalous light intensity information which is not directly related to the temperature at that position in the image.

A typical example of this behavior is illustrated in figure 1 reproduced from [1]. The horizontal line across the 512 x 512 digitized image (8 bit, 256 gray level) is user input using a mouse-type pointing device. In this case, the line was selected to cross the encapsulated melt as well as the meniscus region located at the edge of the growing crystal. The light intensity data (directly related to the temperature of the melt) is read from this line and dynamically superimposed on the image. The information has been subjected to a linear convolution to reduce the effects of high frequency spatial noise. The peaks in optical intensity associated with the meniscus region (at the edge of the crystal) are unrelated to the local temperature since the temperature of the melt in contact with the crystal must be at the melting point of the material being solidified (in this case, GaAs). This behavior is currently interpreted as a measure of the radiation from the hot crucible walls which is reflected by the curved meniscus (non-normal to the CCD imaging camera, see figure 3 for details). However, this anomolous thermal information provides for an indirect measurement of the evolving crystal shape since the distance (in pixels, 0.3 mm/pixel) between peaks is proportional to the diameter. This difference data is used as input to a closed loop proportional controller for control of the crystal diameter during growth. The system input which is changed by the proportional controller is the heater temperature ramp rate. The temperature of the heater is monitored by a thermocouple situated in close proximity to an element of the heater and controlled using a digital PI (proportional/integral) controller. (See section on **Control Algorithm Development and Experimental Results** and figure 8.)

Experimental Approach

A conventional silicon puller (Hamco CG-800) was modified for the low pressure growth of GaAs by LEC (Liquid Encapsulated Czochralski) pulling. A thermal imaging system based on real time image processing techniques has been developed and is operational on the puller. All control inputs (motor rates, temperature control etc.) are activated via digital to analog conversion (D/A) of operator chosen or predetermined feedforward trajectory values (figure 4).

The systems architecture of the thermal imaging system is given in figure 2, from [1]. The melt is viewed in near normal incidence by a charge coupled device (CCD, 512 x 512 pixels) camera. The resulting monochromatic image (due to a 1 nm wide filter centered on 633 nm) is digitized (8 bit / pixel) and processed using a pipelined pixel

processor operating at an effective 40 million operations per second. The images are held in digital storage units which appear as extended dual ported memory on the bus of the main CPU. In this way image data is accessed in parallel by both the vision engine (real time image processing hardware and software) and CPU with its related floating point and array processors, permitting significant filtering of both spatial and temporal noise while maintaining real time (30 frames per second) imaging performance. The diameter inference is obtained as described above. A significant advantage to this measurement of crystal diameter is that it is insensitive to even a substantial degradation of the optical path (e.g. 'fogging' of the windows by evaporated arsenic). This is due to the measurement of the position of the peaks in intensity not the value of the peak intensity.

Control Algorithm Development and Experimental Results.

Initial experiments were carried out using a pure diameter error signal ($\text{Diameter}[\text{desired}] - \text{Diameter}[\text{measured}]$), with no image filtering, for feedback to the heater temperature using a conventional proportional/integral (PI) digital control algorithm. This approach to active diameter control gave results during growth which indicated two fundamental limitations. First, without temporal and spatial filtering of the image the diameter measurement signal contained fluctuations associated with perturbations caused by the presence of entrained bubbles in the liquid encapsulant which caused the temperature controller to change the diameter in a monotonic mode, i.e. the diameter either was reduced to zero (The crystal pulled off.) or it increased to the crucible wall (The melt surface froze.). Second and related, this approach did not take into account the dynamic changes in heater temperature required during pulling to respond to the batch nature of the process: the process is transient.

The effect of temporal filtering in obtaining a reduced noise representation of crystal diameter is shown in figures 5, 6 and 7. The thermal imaging of a crystal growth experiment was archived on a professional video tape recorder (Sony BVU-800) and used post experiment to determine the crystal diameter with and without the use of a temporal averaging algorithm. Diameter sensing in figure 5 employed no digital filtering (temporal or spatial) while the data in figure 6 was obtained with the application of a temporal filtering algorithm with a 4 second time constant. (120 images [4 s x 30 images/s] were averaged.) The post growth measurement of the actual

crystal diameter is given in figure 7. Further optimization of this filtering procedure is in progress.

The current control algorithm is a combination of feedforward and feedback components (figure 8). During growth, the diameter is measured (as described above) from images processed with both temporal and spatial filters. In five minute increments the latest diameter data (taken at 10 s intervals) is analyzed by linear regression to obtain the local diameter trend. This is compared with a set point which is no longer the absolute diameter but rather a pre-selected (and changeable) diameter slope (diameter as a function of time or distance grown). Any deviation of the measured diameter slope from the setpoint diameter slope is used as an error signal to modify using a simple proportional controller, not the absolute heater temperature, but the rate of temperature reduction of the heater (the heater temperature trajectory). The error and new heater trajectories are calculated as follows:

$$\text{error} = \text{diameter slope [desired]} - \text{diameter slope [measured]} \quad [\text{eq. 1}]$$

$$\text{new heater temperature trajectory} = \text{old trajectory} - P * \text{error} \quad [\text{eq. 2}]$$

Where P = proportional constant for controller.

This approach to automatic diameter control was used during low pressure LEC pulling of GaAs. The results are shown in figure 9. The ADC algorithm was initiated 5 cm following seeding. The setpoint (diameter slope) was initialized at 6 mm/hr. With the rate of pulling set at 1.3 cm /hr, the resulting diameter rate setpoint was 0.46 mm / cm of growth. The superposition of this slope on the crystal shape is in qualitative agreement with the trend in diameter as grown. The cyclic nature of the response indicates that the sensor did register the changes in diameter and the controller did respond in such a way so as to reverse adverse trends. The amplitude of these changes indicate the lack of controller tuning and the effects of residual diameter signal noise. It is important to note that control action was not characterized by a limit cycle response. The controller was not responding alternately between its upper and lower limits. Work is in progress in both areas.

Discussion

Closed loop diameter control during LP-LEC pulling of GaAs using thermal imaging based diameter sensing has been accomplished. A simple proportional controller is used to maintain a diameter slope setpoint by modifying the heater temperature trajectory. Noise in the diameter signal associated with video transmission noise and temporal perturbations within the high temperature scene (e.g. bubbles) have been reduced by real time spatial and temporal averaging algorithms. Residual noise in the diameter signal (for example, from 'stationary' bubbles) still causes perturbations in the control action. The solution to this problem will be sought by sensing the diameter from multiple regions of the thermal image (at various angles around the crystal) and using the 'best' data as determined from comparison with previously established good data values. An optimized value of the proportional constant will be determined both from feedforward response of diameter to heater temperature trajectory as well as from experimental experience.

Acknowledgements

The author is indebted to the Defense Advanced Research Projects Agency and the National Aeronautics and Space Administration for their support of this work. The stimulating technical discussions with Prof. August F. Witt, Dr. Douglas J. Carlson, Prof. S. Motakef and Prof. M. Gevelber contributed significantly to this effort.

Bibliography

- 1.) M.J. Wargo, "Real Time Thermal Imaging of High Temperature Semiconductor Melts", NASA Conference Publication 2503, Proceedings of a workshop held at NASA Headquarters Washington, D.C., April 30 – May 1, 1987, Published 1988, p. 384.

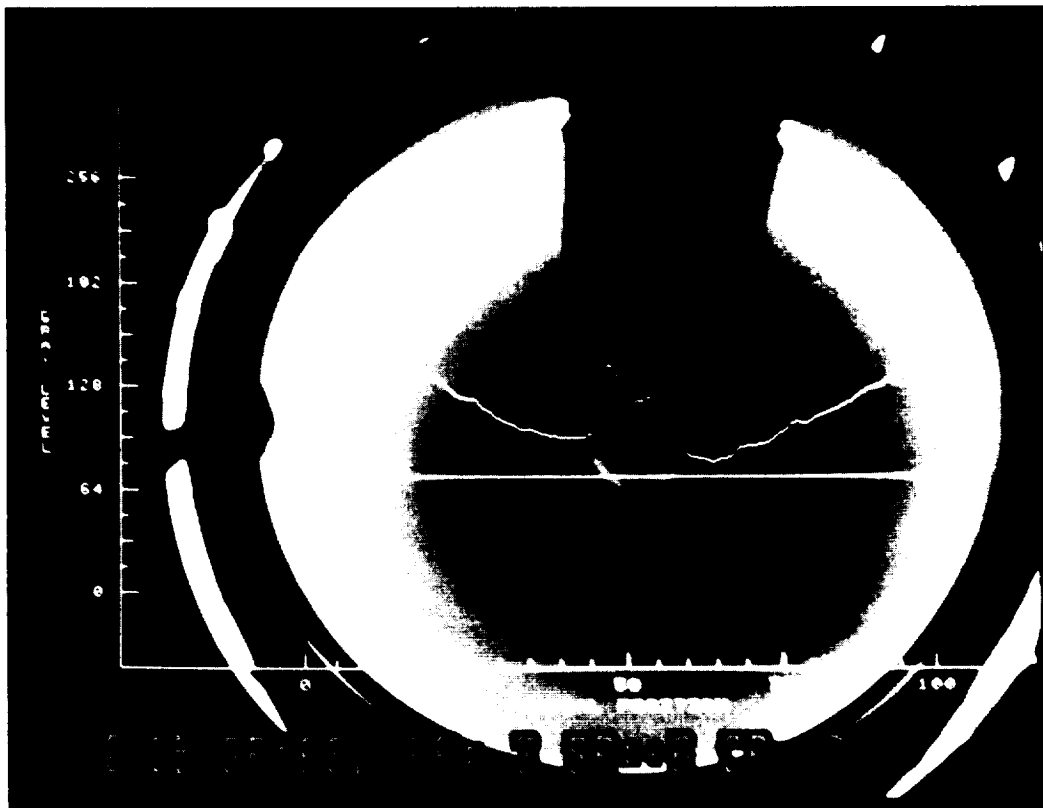


Figure 1. From [1]. Thermal image acquired during LEC growth of GaAs. The anomalous behavior of the measured thermal image in the meniscus region is used to infer the evolving shape (diameter) of the growing crystal.

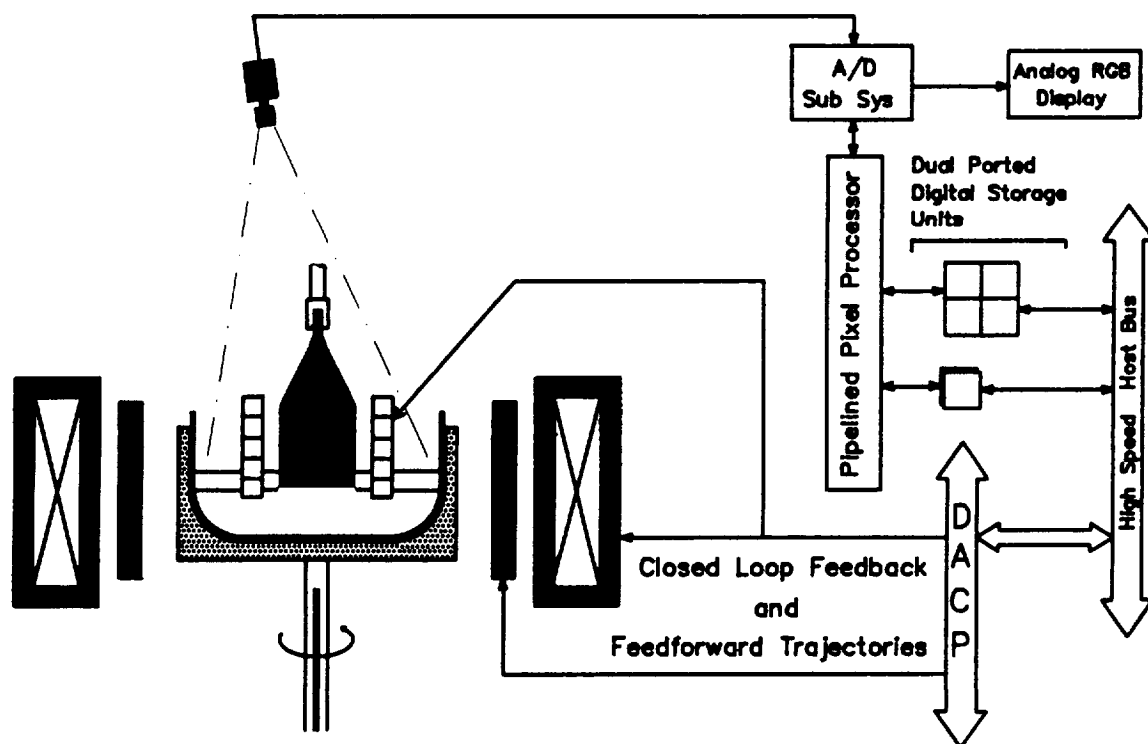
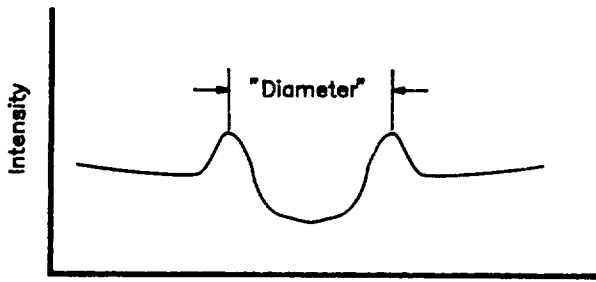


Figure 2. From [1]. Thermal imaging architecture and control structure for LEC growth of GaAs. Details can be found in [1].



1. Advanced Sensor With Spatial and Temporal Filtering
2. Insensitive To Changes In Optical Path
3. Feedforward and Feedback Components
4. Linear Regression Based Error Determination

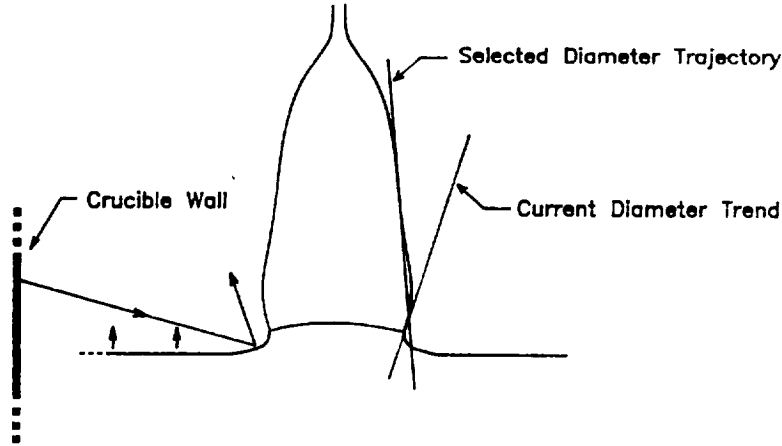


Figure 3. Inference of the crystal diameter during growth is made from anomolous thermal imaging information in the region of the meniscus formed between the crystal in contact with its melt. The large peaks in intensity measured in this area are currently interpreted as due to the radiation emitted from the high temperature crucible walls which is subsequently reflected from the curved surface of the meniscus.

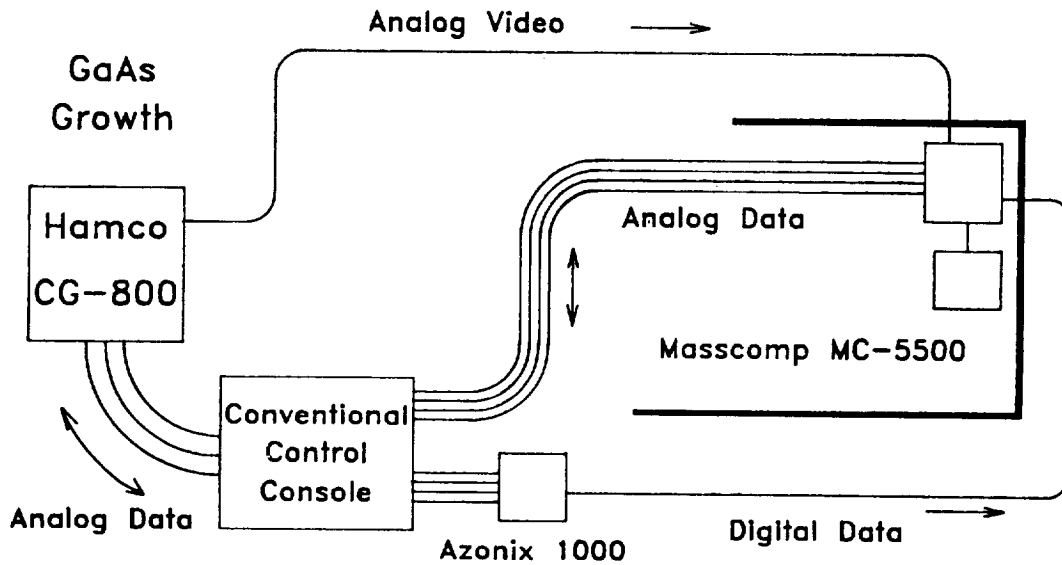


Figure 4. Data management for thermal imaging and growth control. Analog sensing and control information is exchanged with the growth system by A/D and D/A conversion within the Masscomp MC-5500. The analog video information (for thermal imaging and diameter inference) is digitized by the analog front end of the real time vision engine incorporated in the Masscomp MC-5500. (See [1] for details.) The Azonix 1000 provides 18 bit resolution direct digitization of the thermocouple sensor used to determine heater temperature.

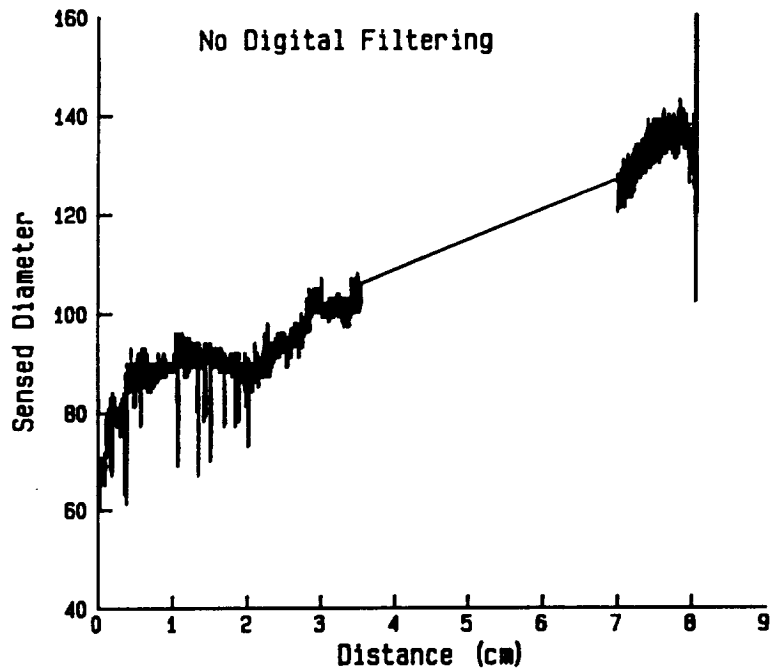


Figure 5. Crystal diameter (in pixels) inferred from archived thermal imaging information. No image processing algorithms (temporal or spatial) were applied to the video information.

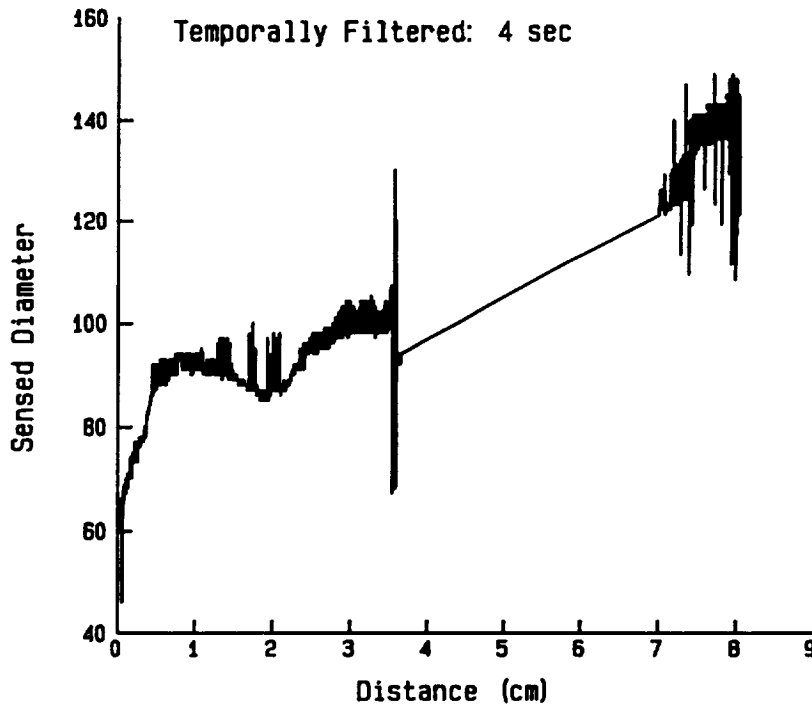


Figure 6. Crystal diameter (in pixels) inferred from archived thermal imaging information. A temporal averaging algorithm was used to reduce the effect of perturbations (e.g. entrained bubbles in the encapsulant). See text.

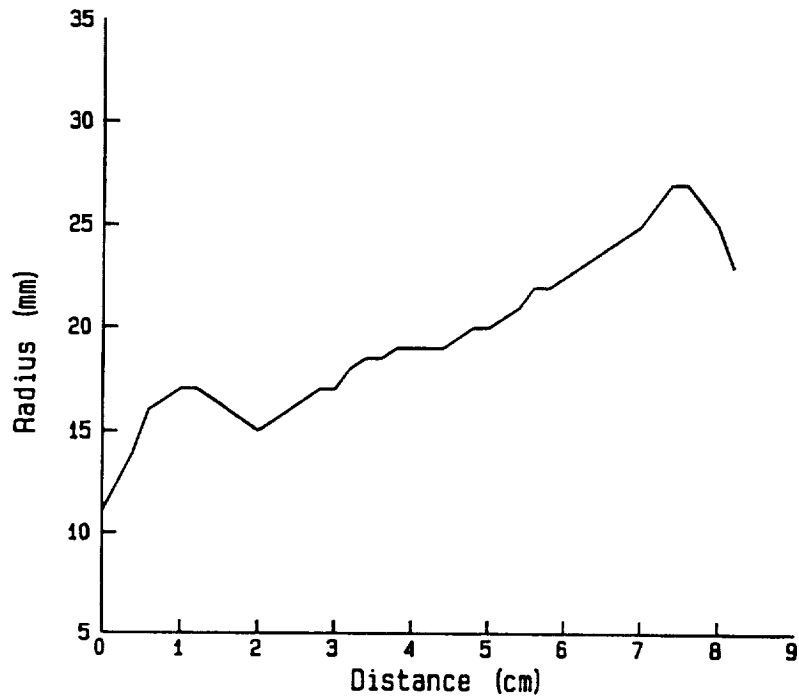


Figure 7. Actual measured diameter of the crystal analyzed in figures 5 and 6.

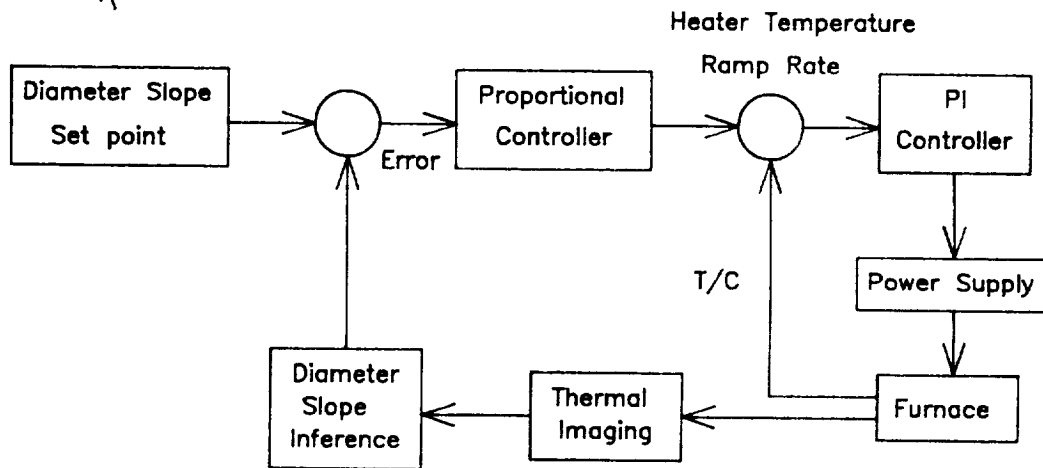
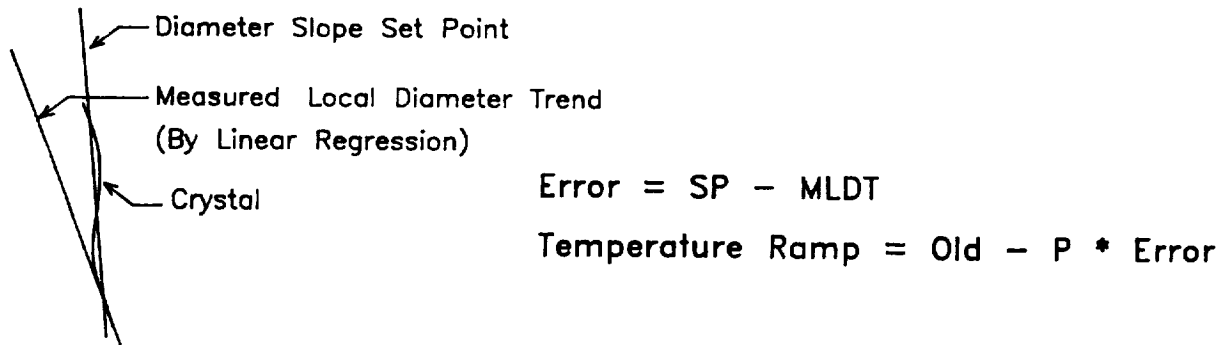


Figure 8. Control structure and algorithm used for closed loop control of crystal shape using a diameter signal inferred from anomalous thermal imaging information.

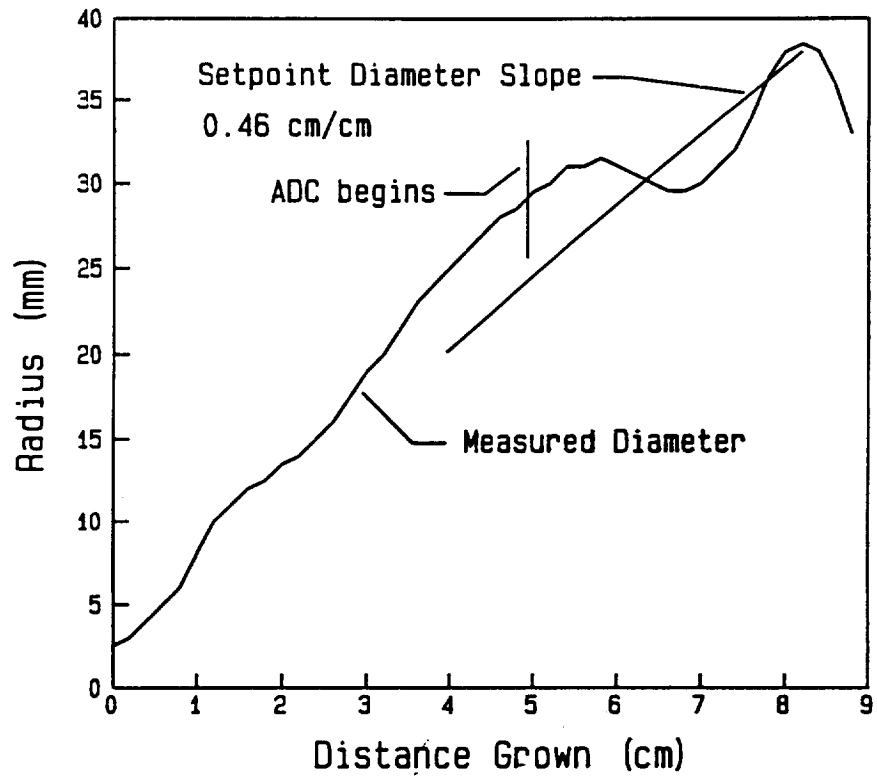


Figure 9. Preliminary experimental results of closed loop control action based on the structure and algorithm given in figure 8. See text for details.

SECTION 3

MICROGRAVITY MATERIALS SCIENCE THERMAL REQUIREMENTS

03

**COMMENTS ON CONTAINERLESS BULK CRYSTAL GROWTH
AND EPITAXY IN SPACE AND ON THEIR IMPLICATIONS
REGARDING NON-CONTACT TEMPERATURE MEASUREMENTS**

Klaus J. Bachmann

Department of Materials Science and Engineering
and
Department of Chemical Engineering
North Carolina State University
Raleigh, NC 27695-7907

1. Introduction

Variations in the diffusion layer thickness during the growth of single crystals from a supersaturated nutrient phase (liquid or vapor) cause striations in the concentrations of the segregating components. These striations follow the contours of the solid-nutrient interface and can be revealed for post-growth analysis by staining techniques or x-ray topography. Wafers cut perpendicular to the growth direction of a crystal, produced in a thermal geometry that results in a non-planar interface, thus exhibit a variation of the local concentrations of the segregating components (impurities, alloy components)¹. This is particularly detrimental in applications which require uniform local properties over large distances on the wafer surface as for example in the fabrication of planar integrated circuits. Therefore, the control of the diffusion layer thickness during crystal growth is a technologically important topic. Since one of the causes for the modulation of the diffusion layer thickness is the uncontrolled variation in buoyancy driven convective flow of the nutrient, experimentation in the microgravity environment of space can contribute to the understanding and control of fluid dynamics problems in crystal growth. It is a well established component of

NASA's materials science in space program which is reviewed in more detail in the paper by Archibald Fripp in these proceedings².

In this paper, the aim is at containerless methods of bulk crystal growth and epitaxy which thus far are a less visible component of materials science in space efforts. In the opinion of the author, this is an anomaly which ought to be corrected, because container interactions are a major problem in earth bound materials processing, including crystal growth, and can be avoided or at least significantly reduced in space. Clearly non-contact methods of temperature measurements are essential for containerless processes. In processes requiring an ultra high vacuum they are also easier to implement in space than on the ground because of the absence of windows in the path of light beams that may change their intensity and polarization due to the clouding of the windows and strain, respectively. In view of the restrictions on the length of this presentation we focus on one example each from the areas of bulk crystal growth and epitaxy to discuss more specific requirements.

2.Containerless Bulk Crystal Growth

There exist two ways of implementing the directional solidification of contained congruently melting materials: 1. The motion of the container with the charge relative to a stationary position of the melting point isotherm (Bridgman method). 2. The motion of the position of the melting point isotherm relative to a stationary charge by slow cooling (gradient freezing method). Although appearing primitive at first glance, the gradient freezing method has been developed into a viable method for the industrial fabrication of large single crystals of III-V compounds with exceptional control of the interface shape³. Since this control is achieved by careful design of passive elements, and the method requires only minimum operator attention for reproducible results, it is well worth being considered in the context of remotely controlled use in space.

To relate this to containerless processing, consider a molten charge held in a stationary position in a microgravity environment by a variable levitation force, e.g. electrostatic, electromagnetic or acoustic levitation, as illustrated in figure 1. The preferred choice of the levitation method depends on the requirements regarding the surrounding atmosphere and melt composition. Providing for an appropriate axial temperature gradient and attaching a seed crystal to this melt at the point of minimum temperature on the surface of the melt, in principle, should permit one to initiate crystal growth in a controlled manner. For shaping of the crystal and the interface it may be advantageous to provide for a relative motion of the position

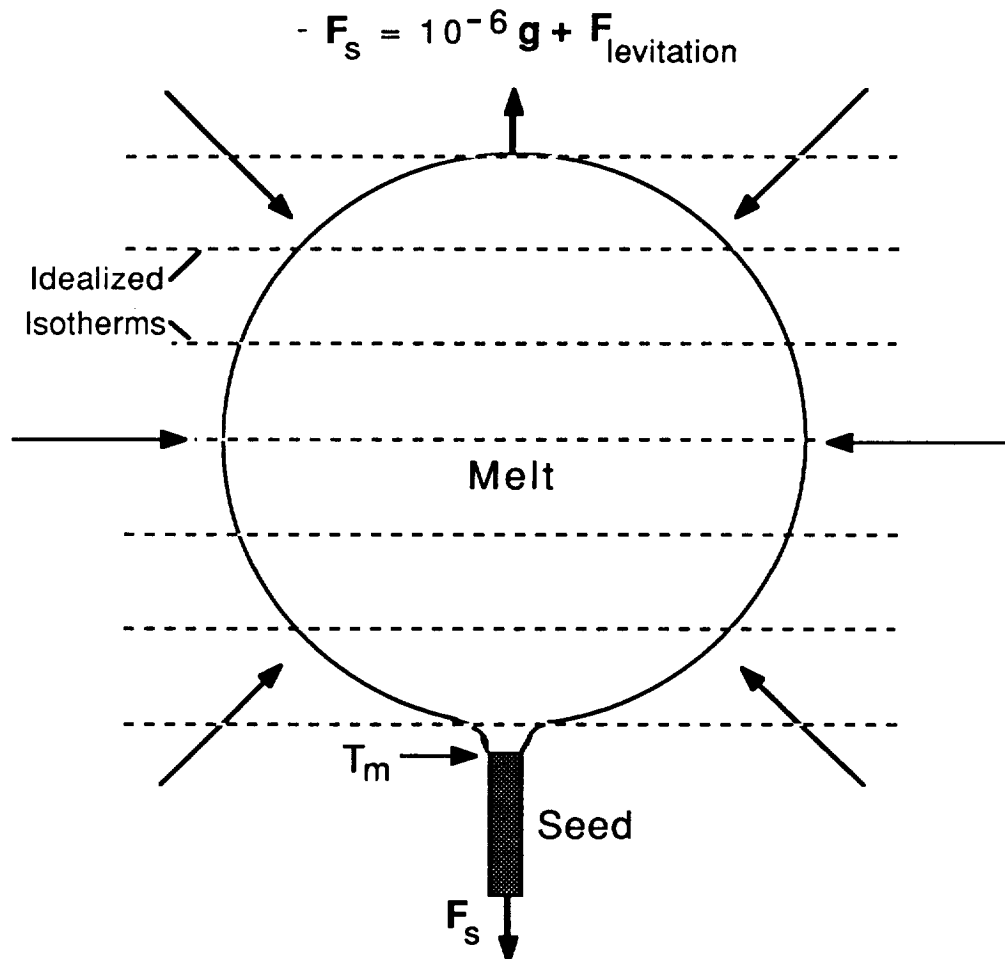


Figure 1. Schematic representation of seeded directional solidification of a melt confined to a stationary position by levitation forces

of the energy well and the seed, but not to the extent of the conditions of Czochralski pulling at 1g since slow cooling at nearly stationary position of the molten charge is the most desirable mode of crystal growth. The potential of the above method must be compared to alternative methods available on the ground, in particular float zoning and skull melting. In the opinion of the author, the above described floating drop method provides probably for greater flexibility in the control of the interface shape than the alternatives and benefits from the absence of density gradient driven convection. Therefore, it deserves evaluation by modeling and by initial experiments concerning the directional solidification of levitated melts on the ground. The method can be altered slightly for solution growth initiating nucleation by a pulse of a cold Helium jet at the point of lowest temperature on the surface of the solution followed by slow cooling.

Since the temperature distribution in the interior of the melt can be unequivocally derived from the temperature at the surface if the thermal conductivity and emissivities of the solid and liquid are known in the temperature range of interest, thermal imaging reading out a sufficient number of pixels for interface modeling will be important for the optimization of the control of the heat input into the melt, its position and the heat extraction at the seed. Fiberoptics guided sensors will be least intrusive and will permit the design of a thermal geometry that minimizes radial temperature gradients in the melt. The axial temperature gradient will depend on the material. The most interesting materials to be studied would be highly reactive compounds and elements that melt at high temperatures and that have thus container problems without solutions on earth. At present the restrictions to the power available for space experimentation make the pursuit of such crystal growth tasks unrealistic, but should not deter an evaluation of more manageable model systems, e.g. directional solidification of low melting point/low density metals and solution growth of materials that are currently in particular demand for research tasks which can be done with small crystals, but that require standards of perfection and purity unattainable by conventional methods. An example, is the growth of pure untwinned

single crystals in the systems $\text{Cu}_3\text{Ba}_2\text{YO}_{7-\delta}$ where Y stands for one of the rare earth elements. Regardless of the technological potential of these compounds, in the opinion of the author, studies of their fundamental properties would benefit from access to more perfect single crystals and warrant the effort to design appropriate crystal growth methods. Of course, if these methods address general problems of crystal growth technology which are bound to remain a challenge for future advanced materials developments in general, they deserve attention irrespective of special materials needs.

3. Containerless Epitaxial Crystal Growth

In view of the increasing demands for advanced ICs incorporating optoelectronic devices, sensors and novel switching elements, e.g. based on resonant tunneling, the combination of different classes of materials on a monolithic chip is presently under intense investigation. The methods that provide for optimum resolution are molecular beam epitaxy (MBE) and (OMCVD). Currently organometallic molecular beam epitaxy (OMMBE) is being explored in several laboratories which aim at combining the best features of the two methods, i.e. high uniformity (OMCVD), atomic resolution and flexibility in the control of the surface kinetics by the independent manipulation of individual ballistic source beams and UHV in-situ diagnostics (MBE). Figure 2 shows a schematic cross-section of the process chamber of an OMMBE system built by the author at NCSU.

Fluid dynamics problems are absent under the conditions of these methods, but memory effects are a serious impediment to the combination of several important classes of materials in high quality heteroepitaxial structures. These memory effects are caused by the accumulation of precursor molecules and products of the surface reaction at the substrate on the walls of the vacuum chamber and pumps. If these materials have sufficient vapor pressure at operating conditions to introduce in an uncontrolled manner dopants into subsequent epilayers clearly the achievement of high quality hetrostructures is foiled. For example, the group IIB elements are

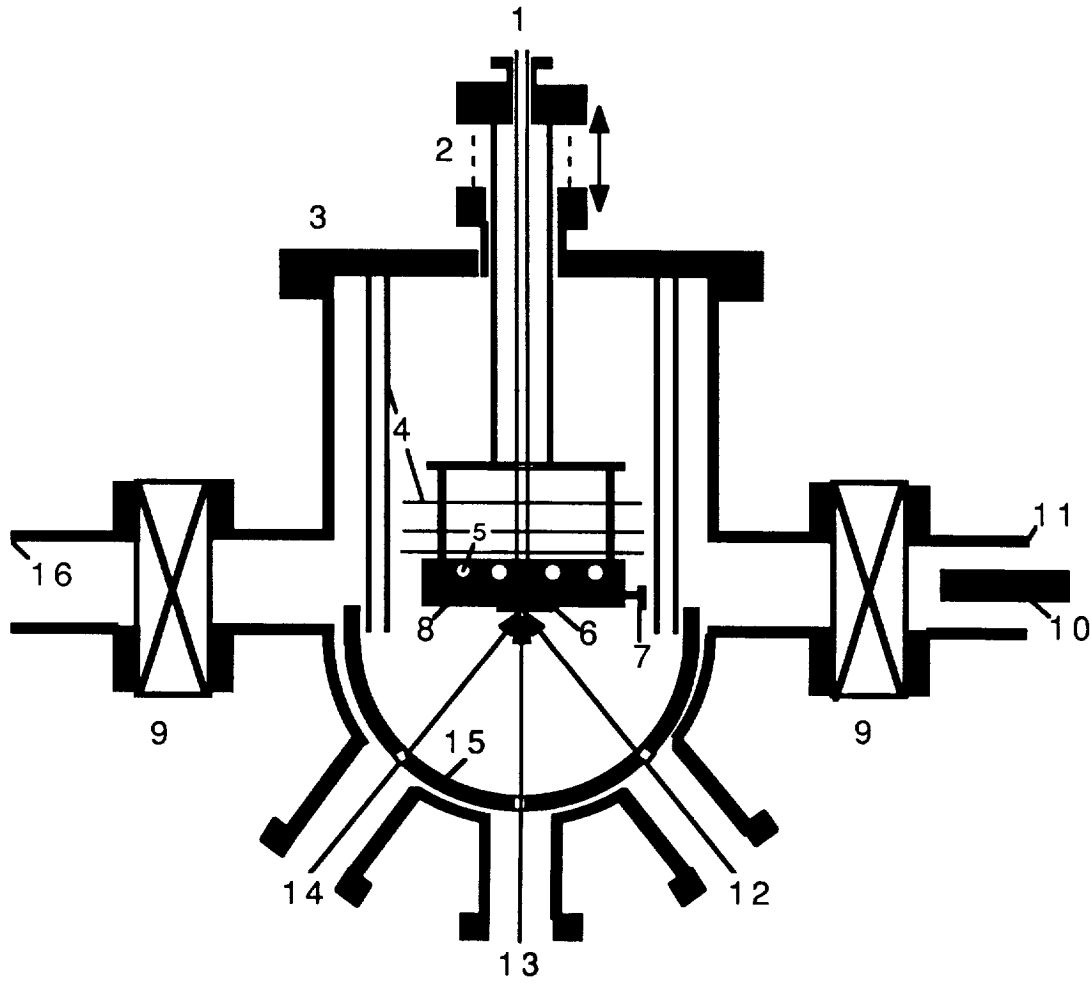


Figure 2. Schematic representation of a cross section of the process chamber of an OMMBE system⁴. 1. Thermocouple for temperature control of heaterblock 8; 2. Linear motion feedthrough; 3. Top Flange; 4. Heat shields; 5. Heater elements; 6. Substrate mounted with indium on Mo substrate carrier; 7. Key on substrate carrier engaging into pick-up tool on magnetic transfer rod 10; 9. Gate valve; 11. Tube connection to load-lock; 12.-14. Multiple OM source beam ports; 15. Cryo-shroud; 16. Tube connection to bypass pump.

notorious in this regard making the combination of II-VI and III-V compounds in monolithic structures extremely difficult. Similar difficulties are encountered in the growth of high resolution II-IV-V₂/III-V structures^{5,6} and other classes of materials combinations

for the fabrication of multilayer structures where sample transfers through gate valves prevent the maintaining reproducible growth conditions and almost certainly assure cross contamination. Therefore, the utilization of the infinite pumping rate of the space vacuum eliminating pumps and a major part of the enclosing structure of ground based UHV systems offers unique possibilities.

Non-contact temperature measurements are of particular interest in this context for the monitoring of the absolute temperature of the surface of the substrate which is a general problem in UHV. Given the drive towards low temperature processing, which is a necessity to limit reactions and interdiffusion processes at the interfaces of high resolution heterostructures, spectroscopic methods of non-contact temperature measurements become increasingly feasible. For example, photoreflectance spectroscopy is feasible in the currently preferred range of substrate temperatures, $500\text{K} \leq T \leq 800\text{K}$ ⁷. It is based on the modulation of the field at the surface of a semiconductor due to the photogeneration of carriers in a modulated laser beam that strikes the surface at the same location as the unmodulated reflected probe beam of frequency ω . Structure in $\Delta R(\omega)/R(\omega)$ is observed in the vicinity of singularities in the dielectric function which occur at wave vectors \mathbf{k} where $\nabla_{\mathbf{k}}(E_c - E_v) = 0$. This is illustrated in figure 3 for GaAs⁸. The opportunity for utilizing the method for non-contact temperature measurements arises because the bands shift with temperature. The associated shift in the positions of the various transitions is for GaAs $10^{-4} \leq \partial \Delta E / \partial T \leq 10^{-3} \text{ eV/K}$ ^{7,8}.

The accuracy of the method is limited by the line shape which depends on the defect density in the material. Figure 4 shows the photoreflectance spectra for the E_0 transition of a series of $\text{Cd}_x\text{Mn}_{1-x}\text{Te}$ crystals of different alloy composition $0 \leq x \leq 0.59$. Note the abrupt change in the line broadening at $x \geq 0.2$ which is due to a steep increase in the microtwinning and line defect density in the alloys with larger Mn concentrations. Also, note that the position of the photoreflectance signal shifts with the alloy concentration so that the error in the determination of the alloy composition adds to the error in the temperature measurement. Generally the alloy composition is well controlled in heterostructures employing semiconductor

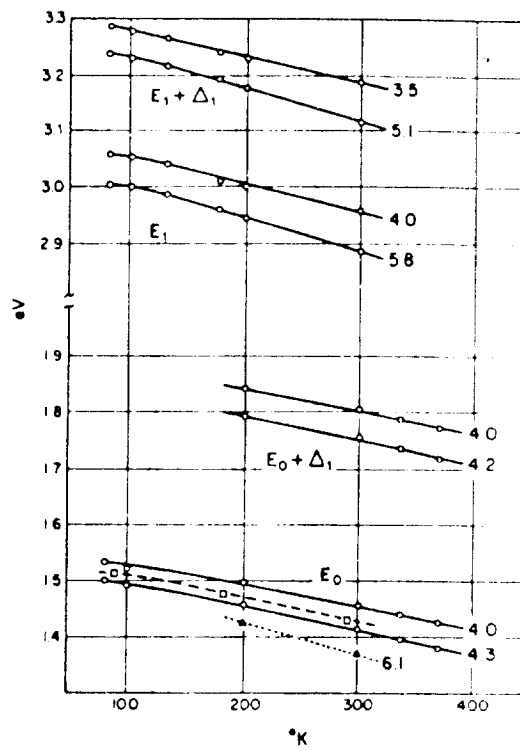
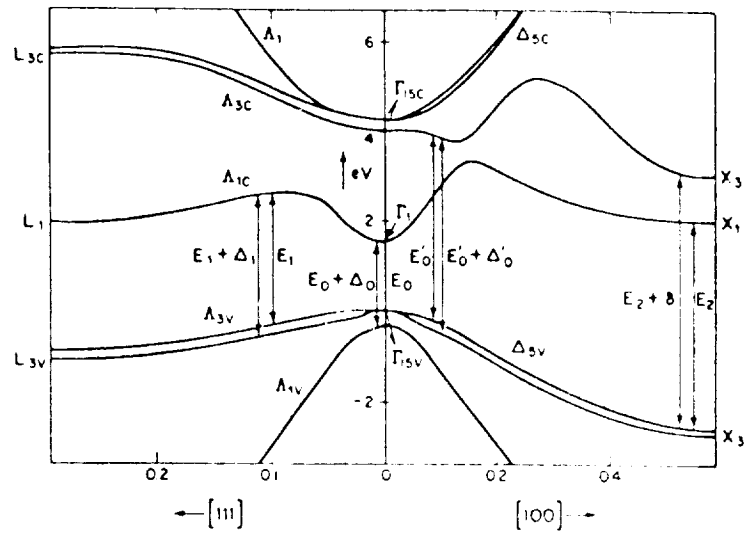


Figure 3. Positions of the interband transitions of GaAs where $V_k(E_c - E_v) = 0$ (top) and temperature dependence of these transitions determined by modulation spectroscopy (bottom)⁸.

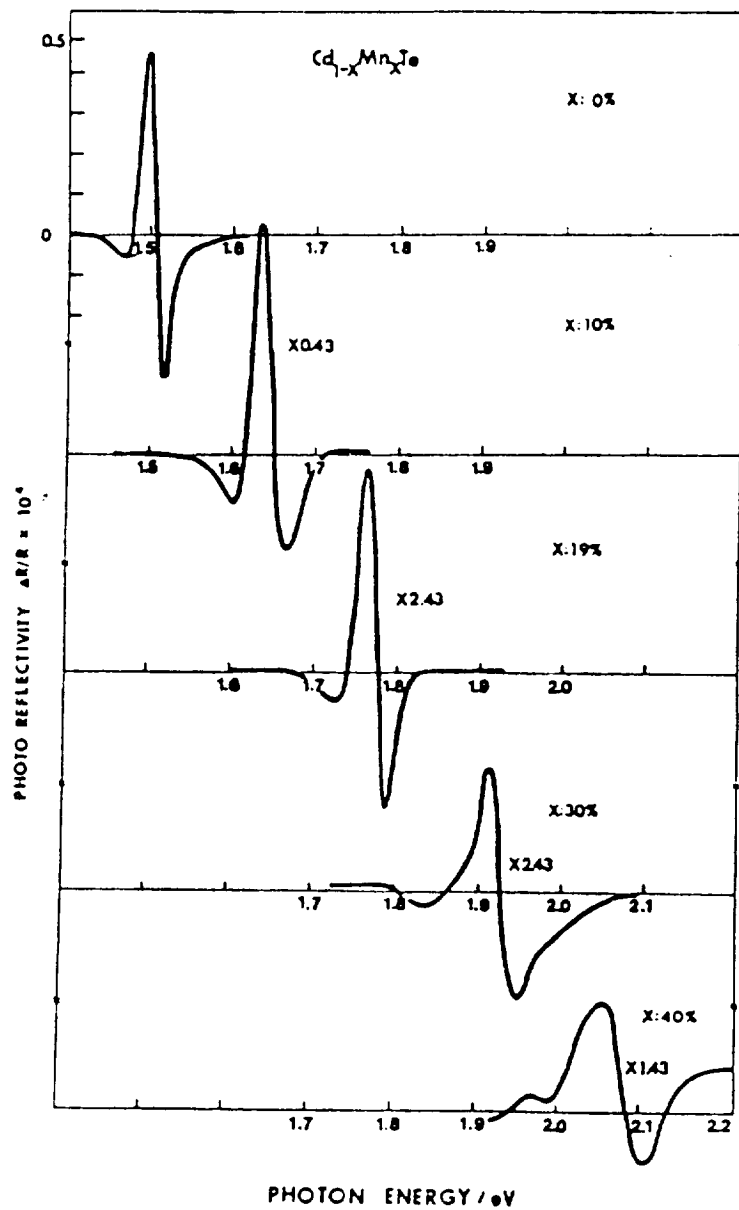


Figure 4. Photoreflectance spectra at room temperature of $\text{Cd}_{1-x}\text{Mn}_x\text{Te}$ crystals obtained at room temperature for various compositions⁹

alloys so that this error is small. It can be measured on-site without removing the wafer from the substrate stage by a variety of surface analysis methods.

An added advantage of the utilization of spectroscopic methods of non-contact temperature measurement, such as photoreflectance, is the simultaneous provision of valuable information on the success of the process and on radiation damage events that may occur by the collision of energetic particles with the semiconductor surface. Part of this problem is alleviated by the sweeping action of the wake shield in a space ultrahigh vacuum facility (SURF). However, light mass/high velocity particles could enter into the volume behind the wake shield and hit the substrate. This is not necessarily a problem since the growth proceeds under self annealing conditions. Both the damage and annealing could be followed by the signature provided by the photoreflectance signal. Figure 5 shows the line broadening and annealing of the radiation damage introduced into crystals of CdTe and $Cd_{1-x}Mn_xTe$ by the same dose of 3 KeV $Ar^{+10,11}$. Even more detailed information on the type of damage and sophisticated quality control regarding the finished heterostructures can be provided without need for retrieval of the wafer by optical spectroscopies with high spatial resolution at space ambient temperature.

In summary, there exists a need for containerless processing both with regard to bulk crystal growth and epitaxy. The space environment is unique in solving some of these problems, e.g. memory effects in the integration of different classes of materials in high resolution multilayer heterostructures by MBE or OMMBE. Spectroscopic methods of non-contact temperature measurements exist that could be developed in this context. The error in the absolute temperature measurement achieved by these techniques decreases with decreasing substrate temperature and supplements thus pyrometric measurements that are better suited for high temperature measurements. The spectroscopic methods cover a continuous range of temperatures from space ambient to a few hundred K. They provide, in addition to temperature data, valuable information on the quality of heteroepitaxial growth and on radiation damage and annealing processes without need for the retrieval of the wafer. The justification for developing these methods for use in space is predicated by the seriousness of the commitment to the

development of the SURF without which no meaningful R&D program is possible.

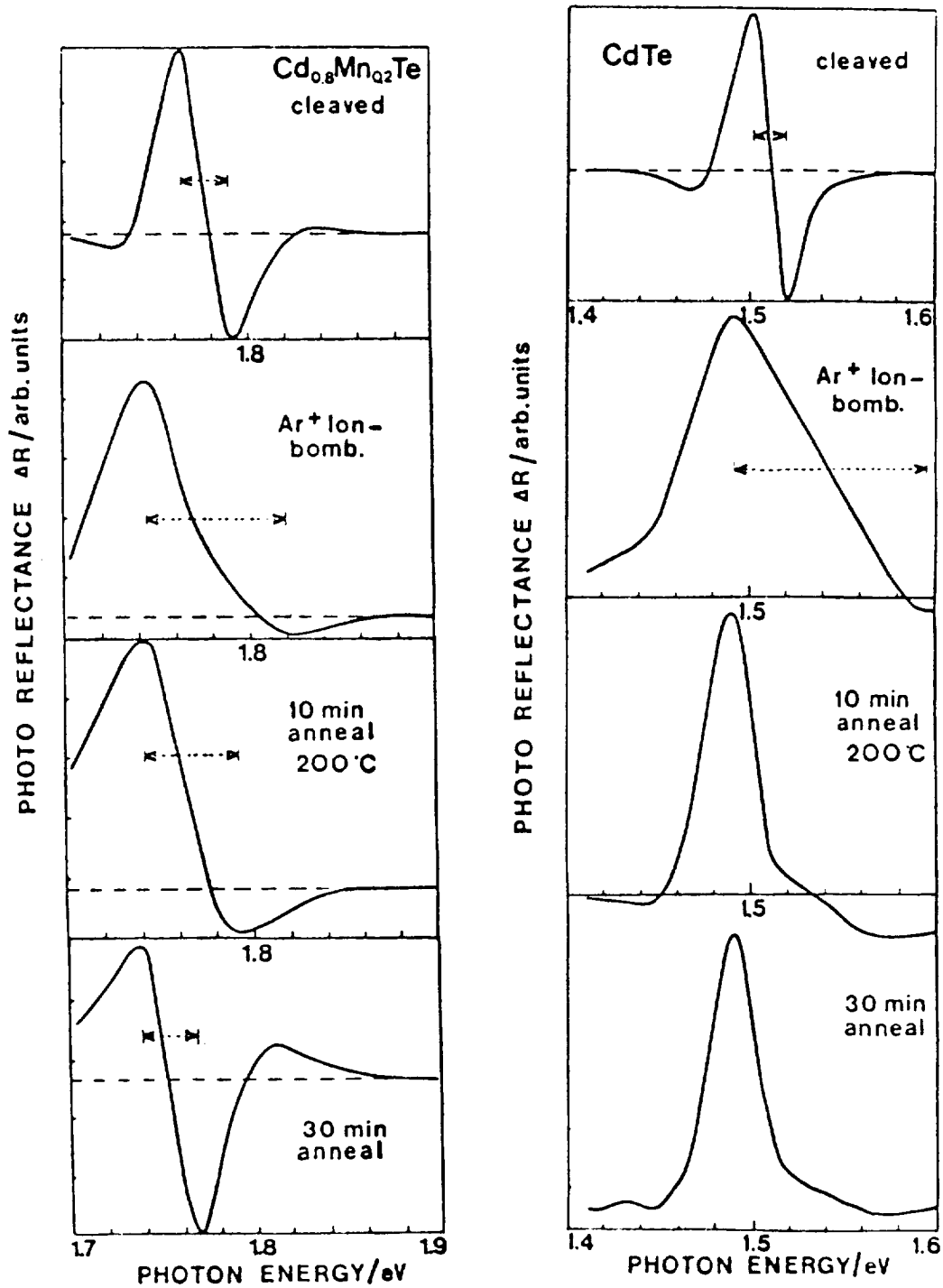


Figure 5. Line broadening and recovery of the photoreflectance signal after radiation damage and annealing of CdTe and $Cd_{1-x}Mn_xTe^{10}$

REFERENCES

1. J.R. Carruthers and A.F. Witt, Crystal Growth and Characterization, Proc. ICCG Spring School Japan 1974, R. Ueda and J.B. Mullin, eds., North Holland Publishing Company, Amsterdam, 1975, p.107
2. A. Fripp, This Volume p.
3. W. Gault, E.M. Monberg and J.E. Clemans, J. Crystal Growth 74, 491 (1986)
4. K.J. Bachmann, unpublished design
5. G.C. Xing, J.B. Posthill, G. Solomon, M. Timmons and K.J. Bachmann, J. Crystal Growth 1988, in print
6. G.C. Xing, K.J. Bachmann, J.B. Posthill, G.L. Solomon and M. Timmons, in Heteroepitaxial Approaches in Semiconductors: Lattice Mismatch and Its Consequences, A. Macrander, ed., The Electrochemical Society, Pennington, N.J., 1989, in print
7. H. Shen, Z. Hang, SH. Pan, F. H. Pollack and J.M. Woodall, Appl. Phys. Lett. 52, 2058 (1988)
8. B.O. Seraphim, J. Appl. Phys. 37, 721 (1966); J.I. Pankove, Optical Processes in Semiconductors, Prentice Hall, Englewood Cliffs, NJ, 1971
9. K.Y. Lay, H. Neff and K.J. Bachmann, phys. stat. sol. (a) 92, 567 (1985)
10. H. Neff, K. Y. Lay, B. Abid, P. Lange and K. J. Bachmann, J. Appl. Phys., 60, 151 (1986).
11. H. Neff, K.Y. Lay and K.J. Bachmann, Surface Science 189/190, 661, (1987)

NON-CONTACT TEMPERATURE MEASUREMENT OF A FALLING DROP

William Hofmeister and R.J. Bayuzick
Center for the Space Processing of Engineering Materials
Vanderbilt University
Nashville, TN 37235

M.B. Robinson
NASA Marshall Space Flight Center
Huntsville, AL 35812

ABSTRACT

The 105-meter drop tube at the Marshall Space Flight Center has been used in a number of experiments to determine the effects of containerless, microgravity processing on the undercooling and solidification behavior of metals and alloys. These experiments have been limited, however, because direct temperature measurement of the falling drops has not been available. Undercooling and nucleation temperatures are calculated from thermophysical properties based on droplet cooling models. In most cases these properties are not well known, particularly in the undercooled state. This results in a large amount of uncertainty in the determination of nucleation temperatures. If temperature measurement can be accomplished then the thermal history of the drops could be well documented. This would lead to a better understanding of the thermophysical and thermal radiative properties of undercooled melts. An effort to measure the temperature of a falling drop is under way at Vanderbilt and Marshall Space Flight Center. The technique uses two-color pyrometry and high speed data acquisition. The approach will be presented along with some preliminary data from drop tube experiments. The results from droplet cooling models will be compared with non-contact temperature measurements.

1. INTRODUCTION

Deep undercooling and the subsequent rapid solidification of metals and alloys leads to possible metastable phase formation and microstructural refinement. For this reason undercooling processes are of great interest to the materials scientists. Containerless processing techniques are used to obtain large undercooling below the equilibrium freezing temperature in liquid metals by eliminating sample/crucible interactions since the crucible is often an energetically favorable nucleation site for the solid phase. Drop tubes are used to provide a containerless as well as a microgravity environment for metals processing.

The 105-meter drop tube at Marshall Space Flight Center in Huntsville, Ala., has been used for a number of years to investigate containerless, microgravity processing of refractory metals and alloys [1-6]. A schematic of the Marshall drop tube is shown in Figure 1. The facility is instrumented with an Ircon two-color pyrometer at the top to measure the release temperature of a drop, and a series of silicon photovoltaic detectors are used to record the time after release at which solidification and recalescence occur. From this data the undercooling prior to solidification is calculated. The research reported herein represents the first attempt to measure the drop temperature by non-contact pyrometry and thereby provide an independent check on the undercooling calculations.

The experiments were performed in a 10^{-5} torr or better vacuum. Drops of approximately 730 mg were melted from 1.57 mm diameter MARZ grade niobium wire (Materials Research Corporation) in an electron beam furnace. Details of the experimental technique can be found in references 1, 4, and 6.

2. DROP COOLING MODEL

With knowledge of the drop release temperature and the free fall time to solidification, the temperature at which nucleation occurs and the undercooling of the drop can be calculated. Undercooling is the difference between the equilibrium freezing temperature and the actual solid

phase nucleation temperature. The radiative heat loss of a sphere is given by [7]:

$$Q = -\epsilon\sigma A(T^4 - T_0^4) \quad (1)$$

where Q is the rate of heat loss, ϵ is the total hemispherical emissivity, σ is the Stefan-Boltzman constant, T is the temperature of the drop and T_0 is the ambient temperature. In the cooling calculations Q was calculated as a function of temperature and sample mass for time increments (Δt) of 0.001 s; hence, the total heat loss (ΔQ) for n increments is given by:

$$\Delta Q = \sum_{q=1}^n Q_q \Delta t \quad (2)$$

The heat loss is equal to the change in enthalpy (ΔH) of the sample so that the temperature at the end of any time increment can be calculated by solving the integral of the liquid heat capacity from the initial temperature (T_i) to the unknown temperature at the time n :

$$\Delta Q = \Delta H = (m/Z) \int_{T_i}^T C_p dT \quad (3)$$

where C_p is the molar heat capacity of the liquid, m is the sample mass and Z is the atomic number. By assuming a constant heat capacity the expression is easily integrated and solved for temperature:

$$T = (\Delta H Z / m C_p) + T_i \quad (4)$$

The assumptions involved in this analysis are that the drop is spherical (since the area is calculated from the mass and liquid density) and isothermal, the heat capacity is constant and there is no radiation exchange between the drop and the walls of the tube. Radiation exchange between the drop and the tube was evaluated according to the method of Incropera and DeWitt [8] and found to be negligible. Deviations from sphericity are negligible in drop tube samples. The Biot number for these samples is on the order of 10^{-2} so the thermal gradient is less than 10 K from the center to the surface.

The uncertainty in cooling calculations can be assessed using the method of Kline and McClintok [9]. The estimated errors in liquid heat capacity (C_p), the total hemispherical emissivity (ϵ), and initial release temperature (T_i) are found to govern the uncertainty of undercooling calculations. Uncertainty due to the computation of area from mass and liquid density and the uncertainty in the cooling time are small by comparison and can be ignored. The uncertainty in nucleation temperature (ω_T) can be expressed as:

$$\omega_T = [\omega_{T_i}^2 + [(T_i - T) \left(\left[\frac{\omega_\epsilon}{\epsilon} \right]^2 + \left[\frac{4\omega_{T_i}}{T_i} \right]^2 \right)^{1/2}]^2 + [(T_i - T) \frac{\omega_{C_p}}{C_p}]^2]^{1/2} \quad (5)$$

where ω is the uncertainty of a subscript value. A detailed derivation of this equation can be found in Reference 6.

The total hemispherical emissivity of solid niobium is given as [10]:

$$\epsilon = -0.144 + 2.88 \times 10^{-4}T - 4.46 \times 10^{-8}T^2 \quad (6)$$

This value was used for the emissivity of the liquid with an assumed uncertainty of ± 0.03 . The liquid heat capacity of niobium is $40.4 \pm 2 \text{ J}\cdot\text{mol}^{-1}\cdot\text{K}^{-1}$ [11]. An Ircon two-color pyrometer was used to measure the release temperature of the drops to $\pm 30 \text{ K}$. The estimated uncertainty in undercooling calculation from this data is $\pm 50 \text{ K}$.

3. THEORY OF NON-CONTACT TEMPERATURE MEASUREMENT

Temperature measurement of a falling drop presents many scientific and technical problems. Small sample sizes (2-8 mm diameter), the acceleration of a free-falling drop, and drop drift away from the tube centerline make tracking of the droplet an extremely difficult task. Reflections from the tube walls add to apparent sample brightness. Consequently, quantitative measurement of radiant flux from the droplet through a narrow bandpass filter is problematic. Because of this, continuous single color pyrometry during free fall is considered

difficult to implement for reliable drop tube temperature measurements. Some hope, however, can be found in the theory of two-color pyrometry.

The principles of two-color pyrometry have been elucidated by numerous authors [12-14] and the theory will not be derived here. The following simplification of the radiometer measurement equation is taken from G.D. Nutter [15]. For a measurement in a narrow spectral band, $\delta\lambda$, centered about λ where the spectral radiance, L_λ varies slowly with direction, the signal from a photodetector, S , is:

$$S = A_{n,d} \Omega_d R(\lambda) \tau(\lambda) \delta\lambda L_\lambda(\lambda, T) \quad (7)$$

where $A_{n,d}$ is the projection of the field defining aperture area normal to the optical axis and Ω_d is the solid angle of radiant flux incident on that aperture. $R(\lambda)$ is the responsivity of the detector and $\tau(\lambda)$ is the transmittance of the optics. The output of an ideal radiometer is then directly proportional to the spectral radiance and the first five terms can be expressed as a constant for a given detector monitoring a given wavelength. Thus:

$$S_\lambda = K(\lambda) L_\lambda(\lambda, T) \quad (8)$$

For a two color pyrometer we have:

$$\frac{S_1}{S_2} = \frac{A_{n,d} \Omega_d R(\lambda_1) \tau(\lambda_1) \delta\lambda_1 L_\lambda(\lambda_1, T)}{A_{n,d} \Omega_d R(\lambda_2) \tau(\lambda_2) \delta\lambda_2 L_\lambda(\lambda_2, T)} \quad (9)$$

If a beam splitter is used such that the aperture and solid angle are equal for both detectors, then the equation can be simplified to:

$$\frac{S_1}{S_2} = \frac{K'(\lambda_1) L_\lambda(\lambda_1, T)}{K'(\lambda_2) L_\lambda(\lambda_2, T)} \quad (10)$$

with $K'(\lambda)$ given by $R(\lambda)\tau(\lambda)\delta\lambda$. $K'(\lambda_1)/K'(\lambda_2)$ is therefore the instrument constant and can be

determined by calibration. From the definition of spectral emissivity, ϵ_λ , we have:

$$\frac{S_1}{S_2} = \frac{K(\lambda_1) \epsilon_{\lambda_1} L_{\lambda b}(\lambda_1, T)}{K(\lambda_2) \epsilon_{\lambda_2} L_{\lambda b}(\lambda_2, T)} \quad (11)$$

where $L_{\lambda b}(\lambda)$ designates the black body spectral radiance.

The important factor from this discussion is that if a beam splitter is used after the field defining aperture then the ratio of signals is independent of the sample distance. The signal ratio depends only on the spectral radiance ratio and instrument constant. If the ratio of spectral emissivities is known and the instrument calibrated, the equation can be solved for temperature. Since the measurement is independent of distance, it is a great advantage for drop tube temperature measurements, because the technique alleviates the tracking problem.

4. DROP TUBE PYROMETER

In order to test the concept of ratio pyrometry in the drop tube a simple instrument was constructed and is shown schematically in Figure 2. Radiant energy from the drop falls on a two inch diameter front surface concave reflector and is reflected onto the end of a one inch diameter fused silica light pipe. The mirror has a 200 mm focal length and is aluminum coated with a magnesium fluoride overcoat. The light pipe is Suprasil(R) with flat, polished ends and a circumference polished to 0.05 micron diamond paste. Light exits the pipe to an Inconel coated 50/50 non-polarizing beam splitting cube. The filters are Oriel interference filters centered at 900 nm (10 nm bandwidth at half peak) and 655 nm (70 nm bandwidth). This combination was selected so that the detector signal levels would be similar in the temperature range of interest. EGG HUV-2000B photodiode/op-amp detectors with an active area of 23.4 mm² and a 200 M Ω feedback resistor were used. The signal from the detectors was collected sequentially at 10 kHz with a SOLTEC data acquisition system of 12-bit resolution with a sample and hold time of 250 ns.

5. EXPERIMENTAL PROCEDURE

The instrument was placed in the drop tube at the eleventh level, 32 m from the furnace. In previous tests niobium was found to undercool consistently to a calculated value, ΔT , of about 480 K (± 12 K at one standard deviation, ± 50 K uncertainty). At this level of undercooling the total solidification time is on the order of 0.5 s for the drop sizes used in this experiment. Therefore, after the initial rapid recalescence the drop will remain at the equilibrium freezing temperature for this period of time, and the signal ratio should remain constant. The instrument was tested in this manner.

6. EXPERIMENTAL RESULTS

6.1 TWO-COLOR RESULTS

A total of 12 drops was recorded. Figure 3 shows the signal ratio calculation for one of the better experiments. The sharp increase at about 90 ms is due to recalescence. The mean signal ratio at the melting temperature for all 12 drops was 1.163 ± 0.05 (one standard deviation). There was a slight decreasing trend of ratio with distance from the pyrometer. Correcting for this factor the instrument was able to measure the freezing temperature to ± 50 K (one standard deviation).

As can be seen in Figure 3, the ratio decreases sharply at 280 ms where the drop should maintain a constant temperature until about 600 ms. In addition a consistent dip in the ratio and a rise in both channels at 650 ms past the pyrometer, which corresponds to the position of a flange in the drop tube, was observed. This flange causes the 900 nm wavelength signal to increase more than the 650 nm wavelength. It is clear from these results that spectral reflections in the drop tube prevent accurate temperature determination with two-color pyrometry. Therefore, the drop tube must be coated with a non-reflecting surface before the two-color technique can be exploited. More consistent results were found when the data was evaluated using each channel as a single color pyrometer.

6.1 SINGLE COLOR DATA EVALUATION

The radiometer measurement equations (7 & 8) allow the evaluation of the instrument constant $K(\lambda)$ for observation of an object of known spectral radiance. Since $A_{n,d}$ and Ω_d are different for each drop's position, K and the signal level are now a function of an adjustable geometric parameter (x) and equation 8 must be modified. We now have:

$$S_i = K_i(\lambda, x_i) L_\lambda(\lambda, T) \quad (12)$$

where x_i corresponds to a particular geometric configuration or drop position. This factor changes with distance and radial position in the tube.

A GE 20A/T24/2 tungsten strip lamp calibrated at NBS in 1980 for radiance temperatures at 655 nm was used for pyrometer calibration. Fused silica condenser and focusing lenses were used to image the desired portion of the filament on a 1 mm aperture. The pyrometer assembly including the mirror was calibrated at seven distances from the aperture to the mirror (0.9 to 1.9 meters, corresponding to signal levels in the linear range of the detector assembly) and nine spectral radiance temperatures at each distance. This procedure is accurate (± 5 K) for $\lambda = 655$ nm since the strip lamp was calibrated for blackbody spectral radiance at that wavelength. To determine the spectral radiance at $\lambda = 900$ nm the tungsten emissivity data of DeVos [16] was used with a contributing error of ± 15 K.

From the laboratory calibration data it is possible to define seven instrument constants for the seven calibration distances at 655 and 900 nm. Instrument constants for each temperature agreed to better than 0.5% at a given distance (or geometrical configuration) and wavelength. Since the detector response is linear with incident power, K_i at constant λ and T vary linearly with signal level and can be described to better than 1% by a single slope. With knowledge of the radiance melting temperature of pure niobium, K_i for a particular x_i can be uniquely defined by the signal level at the melting point of niobium in the drop tube.

Figure 4 shows a typical trace of data from one channel. The time of nucleation is designated as t_n . Rapid recalescence occurs after nucleation and continues for approximately 200-400 μ s. Recalescence can be distinguished from reflections in the tube because of the

rapid rise time. Reflections occur over tens of milliseconds. At one millisecond after nucleation the drop is close to the melting temperature and the data from t_n+1 ms to t_n+2 ms was averaged and taken as the signal level at the melting point. This is used to define K_i for the drop position, x_i , at this time. The drop is moving at about 25 m per second and in 2 ms moves only 5 cm away from the detector, and its radial position has negligible change. Hence, the geometrical configuration factor x_i and K_i are very close to the same just before and just after t_n . Therefore, the instrument constant can be used to determine the radiance temperature at nucleation. The instrument constants derived from the niobium equilibrium melting point data in the drop tube are a function of free fall time. By plotting K_i as a function of t_n it was found that the correction to nucleation temperature determination due to the 2 ms of free fall was less than 3 K. In this manner the nucleation radiance temperature at 655 nm and 900 nm was measured for each drop.

6.2 SINGLE COLOR RESULTS

The data used in calculating the nucleation radiance temperature is listed in Table 1. It is interesting that the scatter in the nucleation radiance temperature data (± 4 K, one standard deviation) is much less than the scatter in the calculated undercooling (± 12 K, one standard deviation). A plot of the melting and nucleation radiance temperature data is shown in Figure 5.

If the melting temperature of niobium is taken as 2741 K then the spectral emissivity at 655 nm and 900 nm can be calculated at the melting temperature from the melting radiance temperature data [17]. These values are $\epsilon_{655} = 0.355$ and $\epsilon_{900} = 0.321$. If these spectral emissivities are used for the undercooled liquid to calculate the true nucleation temperature from pyrometer measurements we have 2341 K indicated for 655 nm and 2329 K for 900 nm, which correspond to undercoolings of 400 K and 412 K, respectively.

7. DISCUSSION OF RESULTS

The single color drop tube pyrometry data indicates there is an 80 K discrepancy between the measured nucleation temperature and the nucleation temperature calculated using the drop cooling model. This difference is greater than the combined uncertainty of either technique, indicating that problems may exist with the drop cooling model. It is significant that the scatter in nucleation temperatures is less with the non-contact measurement. Nucleation, whether homogeneous or heterogeneous, is expected over a range of temperatures depending on the activation energy barrier and pre-exponential term in the nucleation rate expression [18]. Previous drop tube experiments using the drop cooling model have shown the range to be 20-30 K for pure metals, but the non-contact temperature measurement data from this experiment indicate the spread is much narrower.

7.1 PYROMETRY MEASUREMENT

The nucleation radiance temperature measurement at 655 nm has a high confidence level. The calibration of the 20A/T24 strip lamp at 655 nm is unfortunately eight years old. The lamp has had 30 hours use in that time and drift of 1°C per 10 hours has been reported [19]. The measurement, however, relies on a relative change in radiance, the true reference being the melting temperature of pure niobium. The true temperature of a drop 1-2 ms after nucleation can be estimated by modeling the heat flow during rapid recalescence of undercooled metallic droplets, which has been done by Levi and Mehrabian [20]. The external heat flow from the drops in this experiment is less than $10^3 \text{ W}\cdot\text{m}^{-2}\cdot\text{s}^{-1}$ so that recalescence effects are considered independent of the surrounding heat flow. At undercooling levels of 400 K approximately 60% of the drop will solidify in the initial rapid recalescence phase. Using the Levi and Mehrabian models for a single nucleation event and plane front solidification the average drop temperature would be 12-15 K below the melting temperature after rapid recalescence, and large thermal gradients exist between the solid and remaining liquid. These drop tube samples, however, solidify dendritically with tip velocities around $20 \text{ m}\cdot\text{s}^{-1}$ [21]. This

increases the interfacial area by orders of magnitude over the plane front model and has an effect on temperature distribution similar to Levi and Mehrabian's model for multiple nucleation primarily because of the decreased thermal diffusion distance. These models predict drop temperatures within 2-3 K of the melting temperature after recalescence. Thus, the true temperature of the drop in the drop tube is very close to the melting temperature after rapid recalescence. Departures from the melting temperature in the drop after recalescence will slightly underestimate the degree of undercooling using single color pyrometry as described.

Given the excellent linearity (<1.0% deviation) of the detector/op-amp combination and the consistent K_j evaluations at different wavelengths, distances and temperatures (better than 1.0%), it is reasonable to assume a 2% accuracy in 655 nm spectral radiance measurements at the nucleation temperature. This corresponds to ± 5 K in radiance temperature determination at 655 nm. The 900 nm radiance temperature determination has greater uncertainty since a secondary source was not available for calibration at this wavelength. Calculation of the true nucleation temperature from the nucleation radiance temperature measurement requires an assumption for spectral emissivity values at the nucleation temperature. This is problematic, since no data exist for the spectral emissivity of undercooled liquid niobium. The change in spectral emissivity from the melting temperature to the nucleation temperature should be small and somewhat lower than the value at the melting temperature. Using the spectral emissivity values at the melting temperature for calculation of the true nucleation temperature will result in a slight overestimation of the undercooling. Considering all the above factors, the measured true undercooling (ΔT) is:

$$\Delta T = 400 \text{ K} \pm 15 \text{ K}$$

With this confidence in the temperature measurement the cooling calculation must be viewed with some skepticism.

7.2 DROP COOLING MODEL

The release temperature accuracy was quoted as ± 30 K. We have seen that the scatter in calculated undercooling is three times the scatter in measured undercooling. Since heat capacity and total emissivity estimates in the calculations do not change, the increased scatter is probably due to inaccuracies in release temperature measurement. Thermal gradients within the drop in the furnace limit the ability to determine the starting enthalpy. One known boundary condition is the solid wire-liquid drop interface which must be at the melting temperature. Also, reflections from the tungsten filament may cause overestimation of release temperature. These two facts, however, would cause the drop enthalpy to be overestimated and shift the drop cooling calculation toward lesser values of undercooling. It is clear that the enthalpy of the drop at release should be measured independently by drop calorimetry.

The use of equation 6 for liquid total emissivity is probably an overestimation of emissivity because of the decrease in surface roughness of a liquid drop. The magnitude of this overestimation is not clear. A decrease of 20% would be required for agreement with measured undercooling. The assumption of constant liquid heat capacity could also be in error [22]. Little data exists for undercooled heat capacities, but some models suggest that liquid heat capacity does increase with undercooling [23]. The quoted uncertainty in the liquid heat capacity was 2.5%. A constant heat capacity 20% higher than the value used would be necessary for agreement between calculated and measured values. Possibly, a combination of the above difficulties results in the discrepancy between drop cooling calculations and measured values from single color pyrometry.

8. CONCLUSIONS

While two-color pyrometry of falling drops appears feasible, the technique cannot be demonstrated because of reflections in the drop tube. This problem is being addressed by the installation of a non-reflecting sleeve in a portion of the drop tube. The nucleation temperature of undercooled niobium can be measured, however, by using single color techniques. This

measurement has revealed discrepancies between the previously calculated and observed undercooling. These problems cannot be resolved without continuous temperature measurement during the experiment. This may be accomplished by two-color pyrometry in the drop tube if reflections can be eliminated. Continuous temperature measurement of drops cooled by radiation could provide insight into the thermophysical properties of undercooled liquid metals and should be pursued.

9. ACKNOWLEDGEMENTS

The authors are grateful for the support of NASA under Grant NAG8-536 and the Center for Space Processing of Engineering Materials at Vanderbilt under NASA Grant NAGW-810. Mr. Tom Rathz of the University of Alabama at Huntsville provided valuable help with the drop tube experiments. The use of preliminary radiance melting temperature measurements by A. Cezairliyan is appreciated.

Table I

RESULTS OF SINGLE COLOR DATA EVALUATION FOR TWELVE NIOBIUM DROPS

<u>Wavelength (nm)</u>	<u>Radiance Temperature (K)</u>		<u>Standard Deviation of Nucleation Temperature</u>
	<u>Melting [17]</u>	<u>Nucleation</u>	
655	2427.5	2108	4
900	2294.5	1998	4

REFERENCES

1. L.L. Lacy, M.B. Robinson, and T. Rathz, *J. Crystal Growth* 51:47 (1981).
2. N.D. Evans, W.H. Hofmeister, M.B. Robinson, and R.J. Bayuzick, *Met. Trans.* 17A:973 (1986).
3. W.H. Hofmeister, N.D. Evans, R.J. Bayuzick, and M.B. Robinson, *Met. Trans.* 17A:1421 (1986).
4. W.H. Hofmeister, M.B. Robinson, and R.J. Bayuzick, *J. Appl. Phys.* 49(20):1342 (1986).
5. W.H. Hofmeister, M.B. Robinson, and R.J. Bayuzick, *Mat Res. Soc. Symp. Proc.* 87:149 (1987).
6. W.H. Hofmeister, Ph.D. Dissertation, Vanderbilt University, May 1987.
7. M.W. Zemansky, *Heat and Thermodynamics*, (McGraw-Hill, 5th edition, 1968).
8. F.P. Incropera and D.P. DeWitt, *Fundamentals of Heat Transfer*, (John Wiley & Sons, New York, 1985).
9. S.J. Kline and F.A. McClintok, *Mech. Eng.* (Jan. 1953), p. 3.
10. A. Cezairliyan, *J. Res. Nat. Bur. Stand.* 75A:565 (1971).
11. D.W. Bonnell, A.J. Valerga, and J.L. Margrave, *Abs. Am. Chem. Soc. Mtn.*, (Washington, D.C., 1971).
12. P.J. Beckwith and K.C.A. Crane, *Rev. Sci. Instru.* 53:871 (1982).
13. G.M. Foley, M.S. Morse, and A. Cezairliyan, 6th Int. Temp. Symp. (American Institute of Physics, New York, 1982), p. 447.
14. K. Nhuyen and M.C. Branch, *Rev. Sci. Instru.* 56(9):1780 (1985).
15. G.D. Nutter, *ASTM STP 895* (1985).
16. J.C. DeVos, *Physica* 20:690 (1954).
17. A. Cezairliyan, *NBS Preliminary Data* (Aug. 1987).
18. V.P. Skripov, *Current Topics in Materials Science: Crystal Growth and Materials*, Vol. 2, E. Kaldis and H.J. Scheel, eds. (North Holland Publishing Co., 1977), p. 328.
19. W.R. Waters, J.H. Walker and A.T. Hattenburg, *NBS Special Publication*, 250-7.
20. C.G. Levi and R. Mehrabian, *Met. Trans.* 11B:21 (1980).
21. M.B. Robinson, W.H. Hofmeister and R.J. Bayuzick, to be published.

22. J.L. Margrave, Colloque Int. sur l'etude des Transformations a Haute Temperature au-dessus de 2000K, Odeillo, France, 1971, (editions du Centre National de la Recherche Scientific, 71, Paris, France, 1971).
23. J.H. Perepezko and J.S. Paik, J. Non-Cryst. Sol. 61,62:113 (1984).

$$W_T = \left\{ W_{Ti}^2 + \left[(T_i - T) \left(\left[\frac{W_\epsilon}{\epsilon} \right]^2 + \left[\frac{4W_{Ti}}{T_i} \right]^2 \right)^{\frac{1}{2}} \right]^2 + \left[\frac{(T_i - T) W_c}{C_p} \right]^2 \right\}^{\frac{1}{2}}$$

FOR CLARIFICATION OF EQ. 5

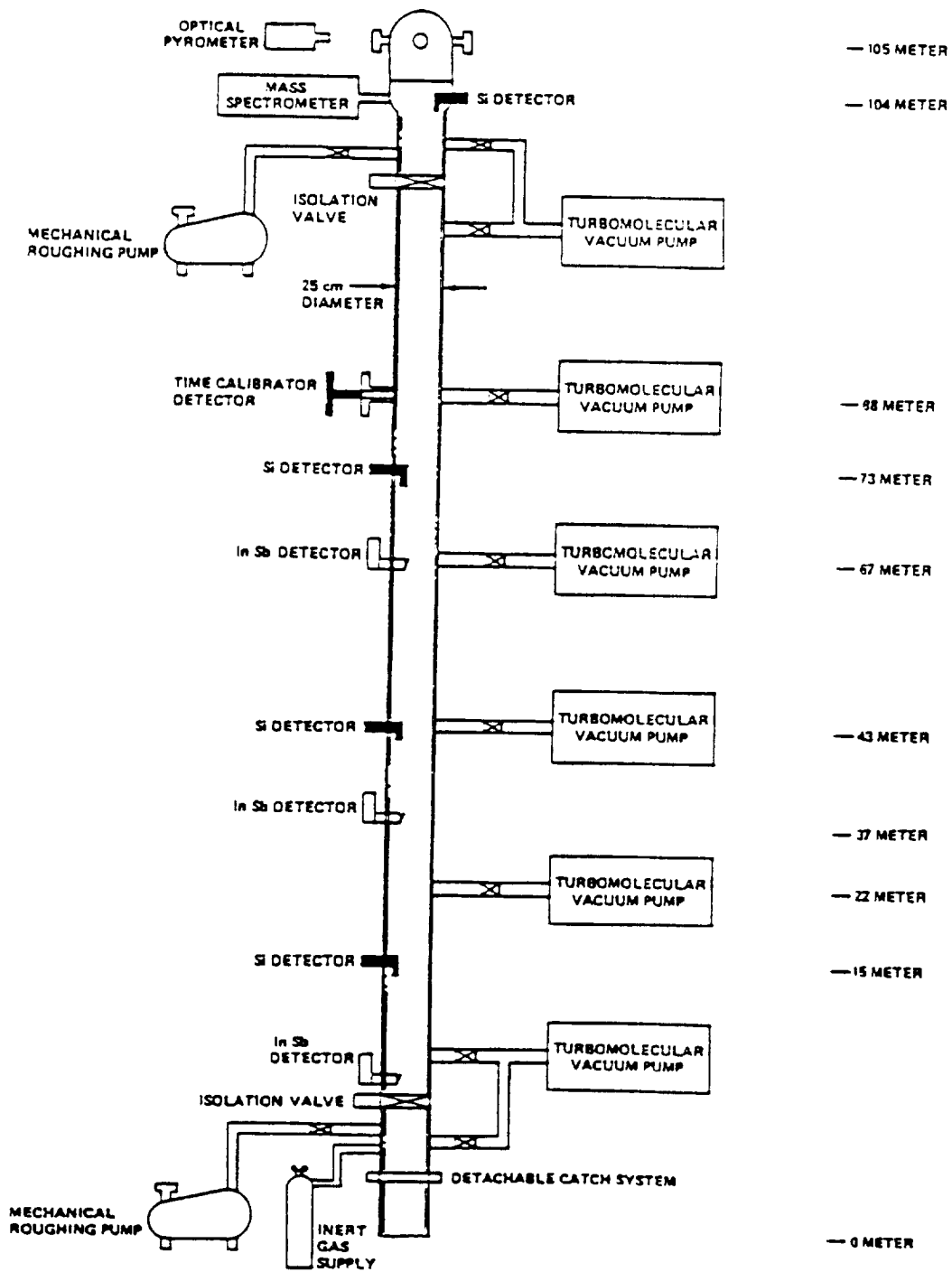


Figure 1. Schematic of the 105-m drop tube at Marshall Space Flight Center.

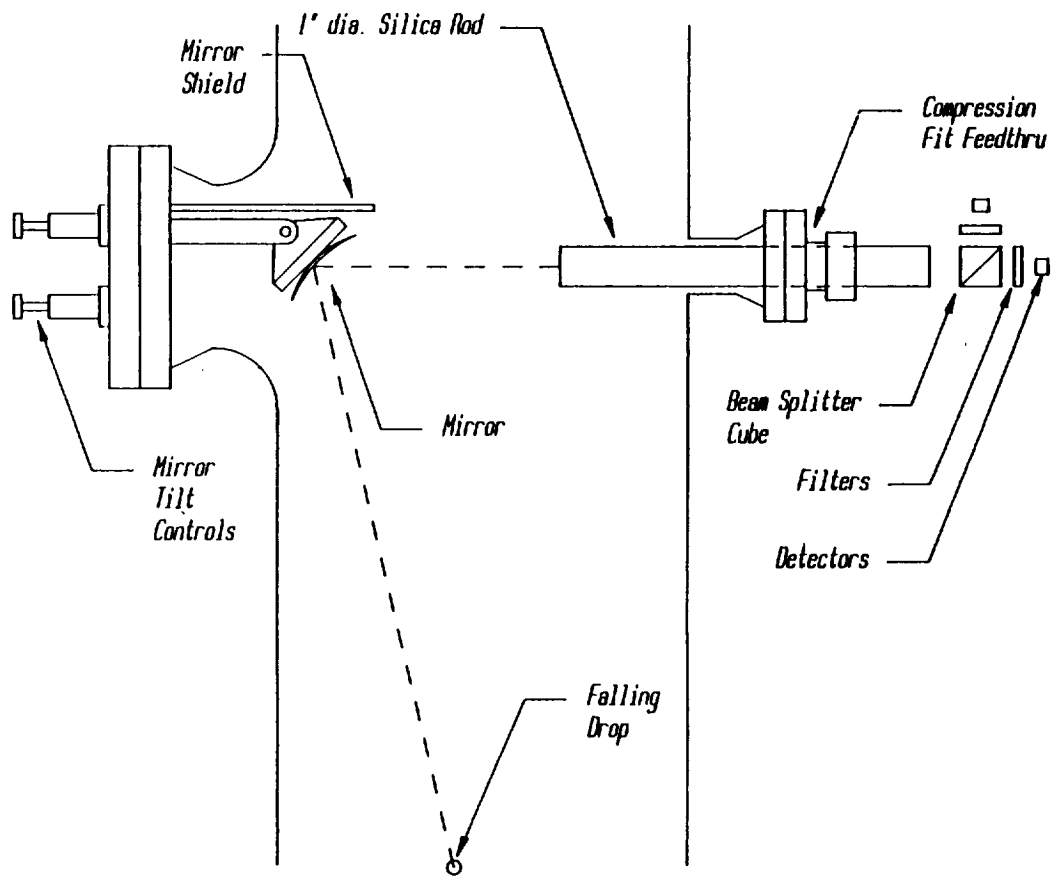


Figure 2. Schematic of the two-color pyrometer as installed in the Marshall Drop Tube.

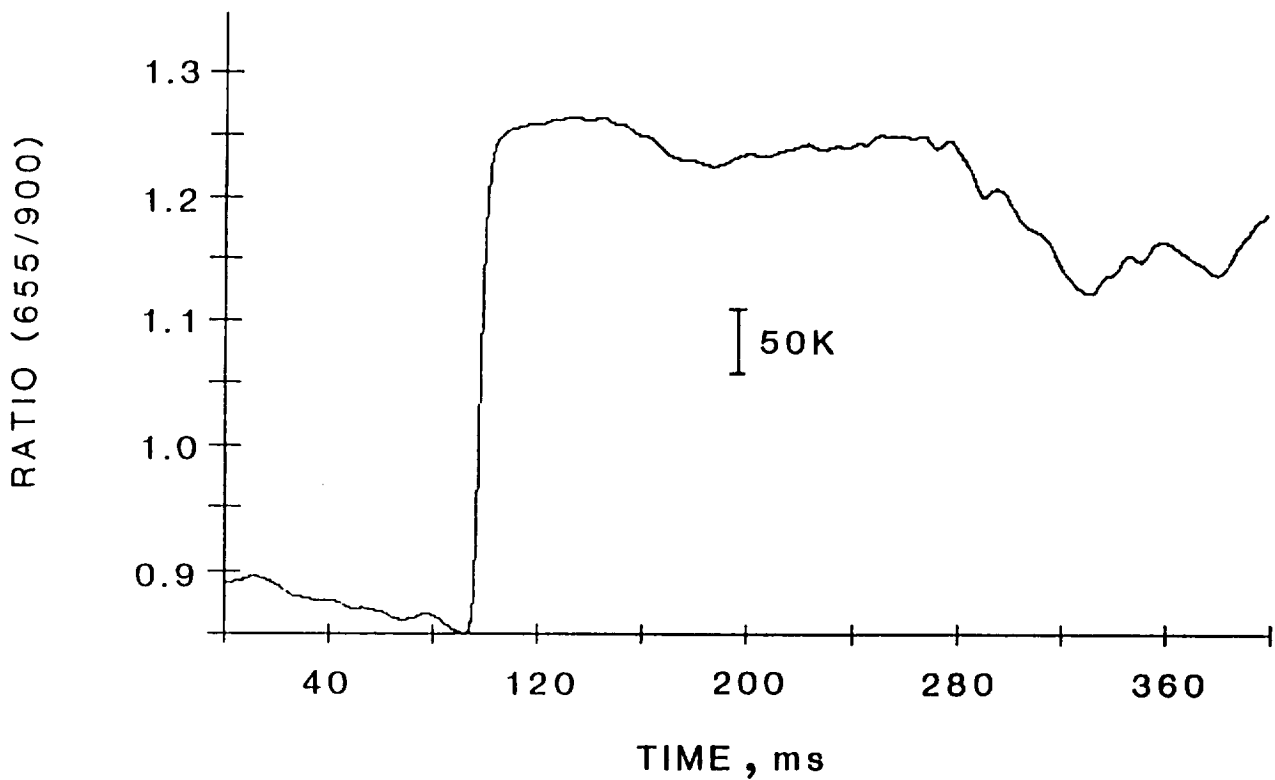


Figure 3. A typical plot of signal ratio data vs. time after passing the mirror assembly. The rise in signal at 100 ms is due to solidification.

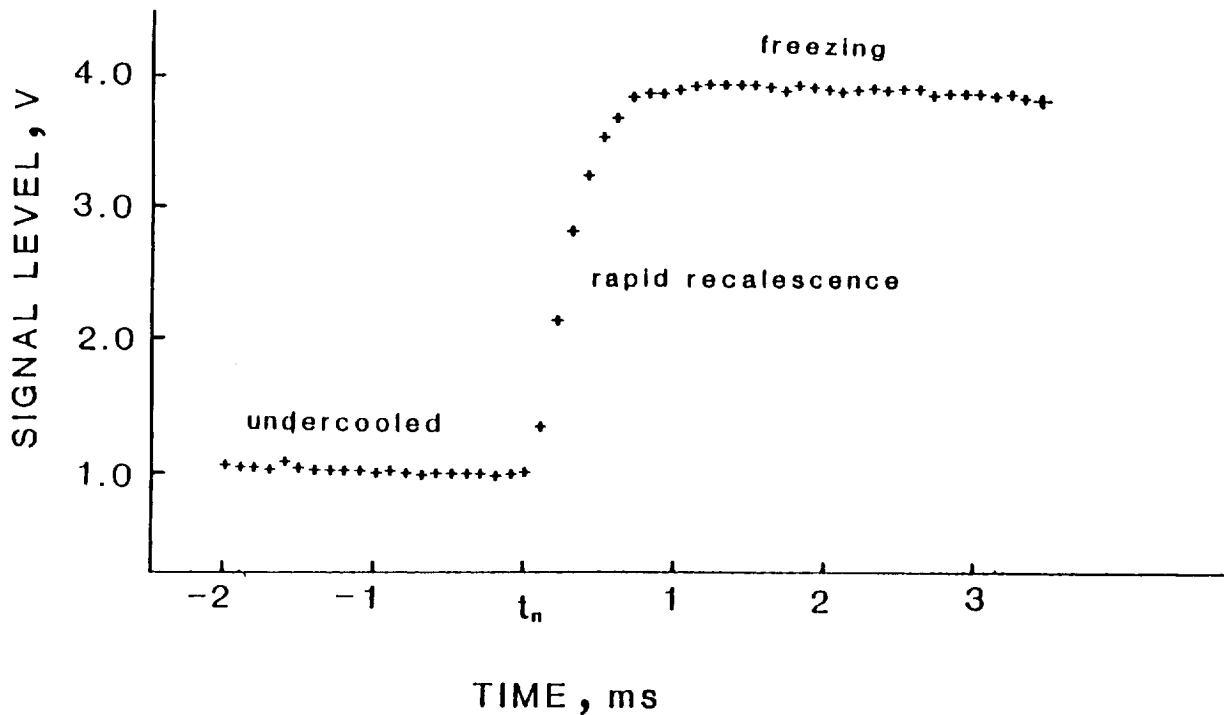


Figure 4. Single channel data at 655 nm near the nucleation temperature, t_n . Data points are taken every 100 μ s.

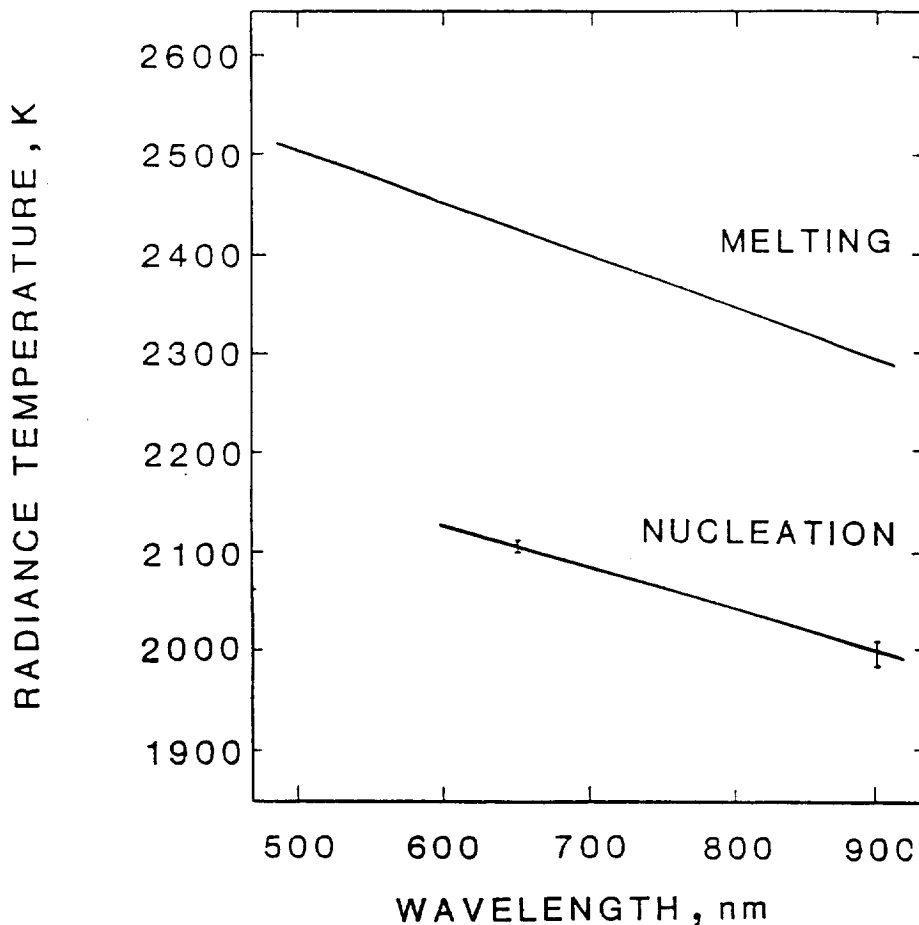


Figure 5. Nucleation radiance temperature as a function of wavelength is plotted with melting radiance temperature data from reference 17.

POLYMERIC MATERIALS SCIENCE IN THE MICROGRAVITY ENVIRONMENT

Daniel R. Coulter

Jet Propulsion Laboratory
California Institute of Technology
Pasadena, California 91109

1. INTRODUCTION

While the utilization of polymers and polymeric composites for coatings, optical components and even structural materials in space is becoming very widespread¹, relatively little attention has been given to basic polymeric materials science in this unique environment. Polymers are a very diverse class of materials that are in many ways unlike their low molecular weight organic and inorganic counterparts, metals, inorganic glasses, proteins and other materials that have been studied in space. The properties of polymers are intimately related, not only to their composition, but also to their "history". Samples with the same chemical composition may exhibit radically different physical, chemical, mechanical and optical properties due to different molecular weight distributions, different thermal histories, different processing conditions, etc.² Since the properties of these materials are so strongly tied to their history, and thus their processing environment, it is evident that a whole new area of polymeric materials science may be opening up with the coming access to the microgravity environment.

Because of the immaturity of this field at this time, it is only possible to use "broad strokes" in painting a picture of the potential for polymeric materials science in the microgravity environment. Undoubtedly, many new and exciting areas of research will emerge in the coming years as polymer scientists become more familiar with the nature of the research opportunities in space. In this paper, however, only three general areas of potential activity will be discussed: studies of solventless polymerization chemistry, studies of the polymeric solid state, and studies of polymer composite processing. In each case, an attempt will be made to give a brief background, to outline some of the relevant materials issues and to describe typical conditions under which studies might be of interest.

2. POLYMER CHEMISTRY

A typical polymerization reaction is shown schematically in figure 1. In the terrestrial laboratory, polymerization of monomers frequently is carried out in a suitable solvent at a moderately elevated temperature

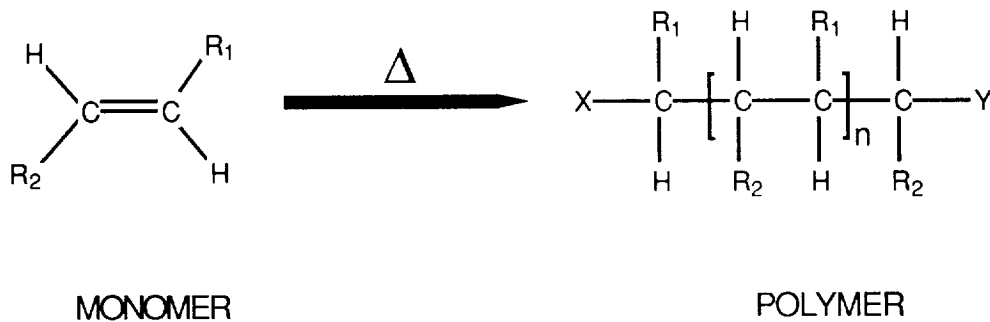


Figure 1. Typical polymerization reaction.

(usually $<100\text{ }^{\circ}\text{C}$). The polymerization may be promoted either by the thermal energy itself or by the use of chemical initiators, catalysts or ionizing radiation.³ In such reactions, n may reach a value of 10^5 or more with molecular weights surpassing 10^6 .

For many applications of polymeric materials it is desirable to achieve as high a molecular weight as possible. Low molecular weight polymers are typically inferior with respect to properties such as mechanical strength, modulus, processability, etc. In terrestrial polymerization reactions, the achievable molecular weight is many times limited by solubility of the high polymer in the reaction solvent. Polymerization in the gas phase, in the absence of solvent, might be one route to higher molecular weight materials. However, on earth gravity or diffusion to the walls of the reaction vessel would cause the growing polymer chains to be removed from the reaction zone and would thus limit the ultimate achievable extent of reaction.

Utilization of a containerless processing facility in the microgravity environment for polymerization in the gas phase could alleviate the problems arising from gravity and diffusion and might lead to new very high molecular weight polymers. The reaction could be initiated by UV irradiation of the monomer vapor. Conditions required in

the reactor would be fairly mild. Temperatures of 20-100 °C with a stability of +/- 5 °C would be desirable. Heating and cooling rates would be in the range of 1-10 deg/min and hold times at temperature would be in the range of minutes to hours.

3. STUDIES OF THE POLYMERIC SOLID STATE

Polymeric materials may be categorized in three general classes according to the nature of their solid state, including glassy polymers, semicrystalline polymers and crystalline polymers. In most cases, the state of a given sample is controlled by the processing history. For example, a thermoplastic polymer may be heated to its molten state and then cooled at various rates. If the melt is quenched, that is, cooled very rapidly by immersion in cold water or liquid nitrogen, a glassy material may result. Such totally amorphous glasses are in a nonequilibrated state. These materials "age" and their properties change with time as the glass relaxes toward the ideal equilibrium state. The exact nature of the glass depends on the cooling rate and other conditions existing at the time of formation. An example of a volume-temperature plot for a glassy polymer cooled from the melt at various rates is shown in figure 2. It is seen that the specific volume of the glass is clearly a function of the cooling rate. During formation of the glass "free volume" is incorporated into the matrix. Once the glass is formed, the aging process mentioned above begins and proceeds at a rate which depends on the aging temperature, the amount of "free volume" and any external forces acting on the materials. The aging results from reorientation of the polymer chains in the glass and results in significant changes in many properties. It is possible that the microgravity environment might have significant effects on the nature of the glasses that can be formed or on the rates of their relaxation. For example, possibly highly uniform polymer glasses could be fabricated. Furthermore, the physical aging properties of such materials in the space environment are largely unknown. Investigation of this process in the absence of gravity could yield valuable information on the nature of the relaxation processes and the prediction of behavior of polymers in space.

With some materials, if the polymer melt is cooled very slowly in a controlled manner, a highly crystalline material with high order may be achieved. If the melt is cooled at some intermediate rate, various degrees of crystallinity may be incorporated into the matrix along with amorphous regions resulting in the formation of a, so called, semicrystalline solid.

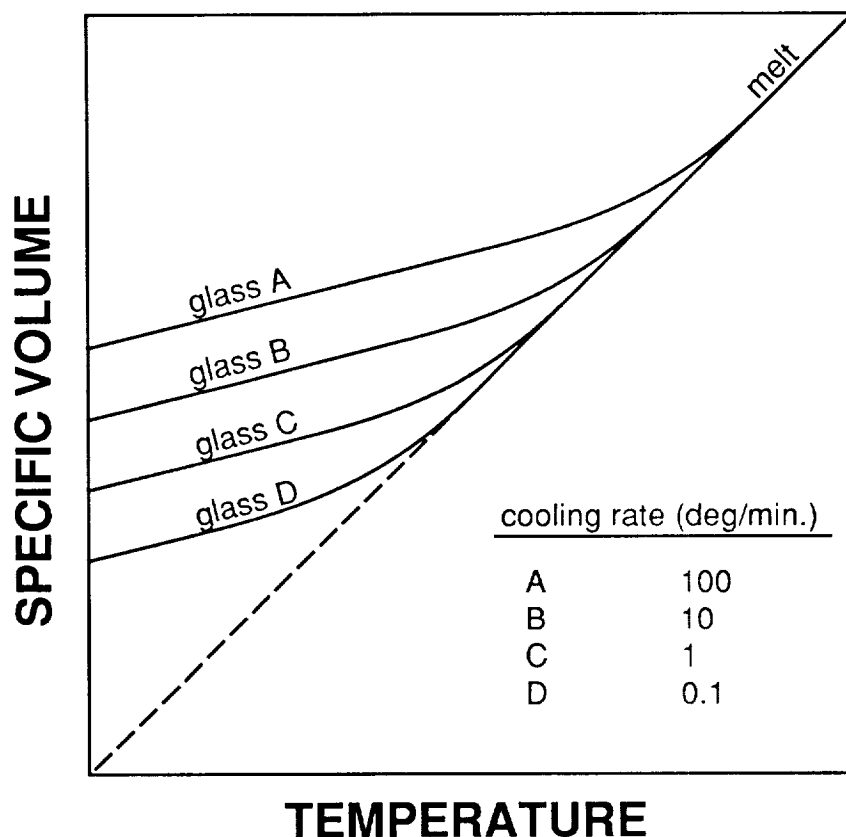


Figure 2. Volume-temperature relationship for a glassy polymer.

The nature of polymer crystals or crystalline domains is quite complex.⁴ Several different crystalline forms are known including spherulites and lamellae. The type, size and distribution of the crystalline domains are known to be functions of the crystallization conditions. Again, as in the case of the polymer glasses, little is known about the effects of gravity on the formation of crystallinity in polymers. It is possible that highly oriented, highly crystalline materials could be produced in the microgravity environment which would show interesting and useful properties.

The study of phase transformations in polymeric materials in the microgravity environment would require a wider temperature range and better thermal control than in the polymer chemistry studies. Temperatures as high as 700 °C could be needed to melt or soften some of the materials. Heating and cooling rates in the range of 0.1-100 deg/min could be required with temperature stability of +/- 0.1 °C. Hold times in the range of minutes to hours would be anticipated.

4. POLYMER COMPOSITE PROCESSING STUDIES

Many useful applications of polymers involve the fabrication of composite materials. In the context of this paper, a composite should be understood to be any mixture or blend of different materials. The advantages of composites are of course that the desirable properties of widely different materials may be incorporated into a single element. A well known example of this would be the high strength, lightweight graphite/epoxy composites. The availability of a particular composite material clearly depends on its processability. In general, composites are made by "mixing" two or more components and then allowing the system to "set" in some manner. In some cases, the "mixing" has to be carried out in a highly controlled fashion. An example of this would be the production of fiber reinforced polymer resin composite prepreg which is used to fabricate multi-ply laminate structures. In the case of particle reinforced composites, however, the key to good performance involves true mixing of the components to achieve a homogeneous blend and maintaining the good mixture during cure. This can become a problem if the densities of the components are significantly different. Consider the hypothetical example of a polymer filled with macroscopic metallic spheres. If the uncured resin had a suitably low viscosity to allow for good mixing, then it would be difficult to keep the metal spheres from settling out during the initial stages of cure. Such mixing problems could be overcome in the microgravity environment and could allow for the fabrication of some highly unusual composite materials.

The conditions of cure for polymer-based composites are similar to those required for the phase transition studies. The temperatures would be in the range of 50-400 °C. Heating and cooling rates would be in the range of 1-50 deg/min. A typical temperature sequence for the cure of composite is shown schematically in figure 3. Cure times would range up to many hours. One additional complication would be that in some cases, it would be desirable to cure under high pressure (up to 1000 kPa), as in an autoclave. It is not clear what sort of problems, if any, this requirement would raise.

5. SUMMARY

The microgravity environment presents some interesting possibilities for the study of polymer science. Properties of polymeric

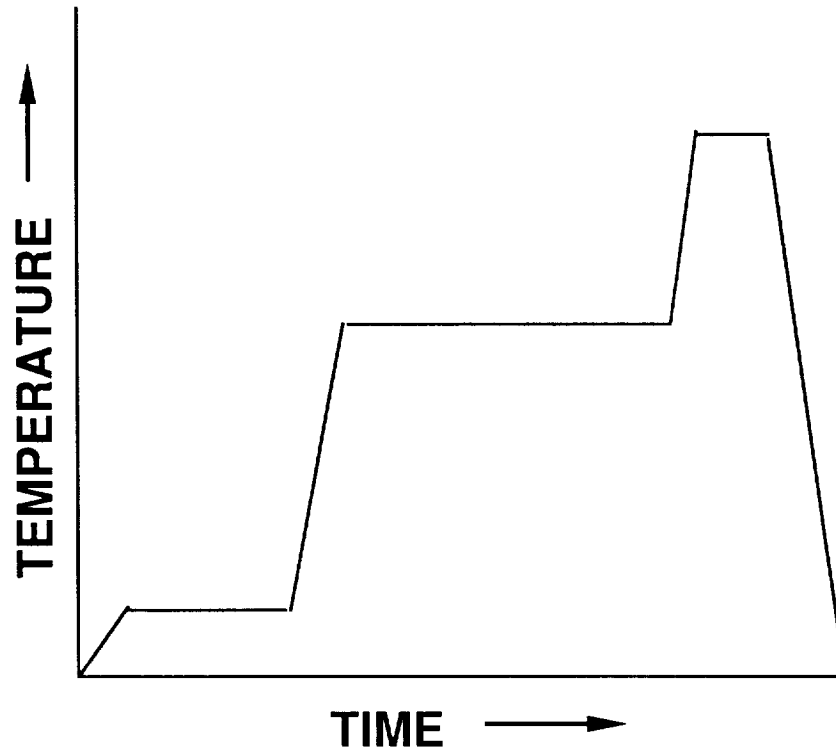


Figure 3. Typical heating curve for cure of composites.

materials depend heavily on their processing history and environment. Thus, there seem to be some potentially interesting and useful new materials that could be developed. The requirements for studying polymeric materials are in general much less rigorous than those for studying metals, for example. Many of the techniques developed for working with other materials, including heat sources, thermal control hardware and noncontact temperature measuring schemes should meet the needs of the polymer scientist.

6. REFERENCES

1. See "Materials For Space - The Gathering Momentum", ed. by J.T. Hoggatt, S.G. Hill and J.C. Johnson, Proceedings of the 18th International SAMPE Technical Conference, Seattle, Washington, October, 1986, 1117p.
2. Stephen L. Rosen, Fundamental Principles of Polymeric Materials, John Wiley & Sons, New York, 1982, 346p.
3. A. Ravve, Organic Chemistry of Macromolecules, Marcel Dekker, New York 1967, 495p.

4. R.S. Stein and A.V. Tobolsky, "Crystallinity in Polymers", in Polymer Science and Materials, ed. by A.V. Tobolsky and H.F. Mark, Wiley-Interscience, New York, 1971, p.161-188.

Temperature Control and Calibration Issues in the Growth, Processing and Characterization of Electronic Materials

B.A. Wilson,
Jet Propulsion Laboratory, California Institute of Technology

This paper summarizes the temperature control and calibration issues encountered in the growth, processing and characterization of electronic materials in the Microdevices Laboratory of JPL's Center for Space Microelectronics Technology. The primary problem area is identified as temperature control during epitaxial materials growth. While qualitative thermal measurements are feasible and reproducibility is often achievable within a given system, absolute calibration is essentially impossible in many cases, precluding the possibility of portability from one system to another. The procedures utilized in the MDL for thermal measurements during epitaxial growth are described, and their limitations discussed.

INTRODUCTION

The charter of JPL's Microdevices Laboratory (MDL) is the development of electronic materials and devices for space applications. The MDL, a 38,000 square foot facility opened in late 1988, contains class 100,000 area for materials growth and characterization, class 100 and 1,000 areas for deposition and device processing, and class 10 areas for e-beam and photolithography. The facilities also include a variety of deposition, processing and characterization capabilities, as detailed in Table I. In the area of semiconductor materials and device development, the main program thrusts include strained-layer superlattices, silicides and amorphous silicon, medium to far infrared silicon-compatible detectors, photonic devices, and neural network systems. There are also strong programs in conventional and high-temperature superconducting materials, SIS mixers, superconducting electronics, and miniature electron-tunneling based sensors. Low-temperature STM capabilities, and a new technique developed in the MDL, ballistic electron emission microscopy, which enables microscopic imaging of the electronic properties of subsurface interfaces, enhance these programs.

Among the wide variety of deposition, processing and characterization methods utilized in the MDL, the primary area where temperature control remains an unsolved problem is in the epitaxial growth of electronic materials. Three important epitaxial growth techniques, molecular beam epitaxy (MBE), metal-organic chemical vapor deposition (MOCVD), and laser-assisted chemical vapor deposition (LACVD) have been selected for the focus of this paper. While thermal control is

critical for the reproducible fabrication of high-quality films by any of these techniques, in each case the growth environments interfere with accurate temperature measurements of the growth surface. For each deposition technique, I discuss the thermal control requirements, the growth environment, the methods currently utilized for temperature measurement and control, and the limitations of these methods.

MOLECULAR BEAM EPITAXY (MBE)

MBE places the most demanding requirements on thermal control of any of the epitaxial growth techniques. Reproducible growth of high-quality films requires reproducible sample temperatures controlled to within 1 K. Sample homogeneity requires even better uniformity across the growth surface, which is typically 1 to 3 inches in diameter. This is because the mobility of the deposited atoms is thermally activated, and thus depends exponentially on the local ambient temperature. Thus small variations in temperature across the growth surface can result in large changes in surface atom kinetics, causing significant sample inhomogeneity. MBE growth is carried out in ultra-high vacuum, typically $\sim 10^{-11}$ Torr, and temperatures of 400 - 600 °C for the growth of III-V materials, and room temperature and up for group IV samples. Growth occurs when a beam of the desired atoms or molecules impinges on a substrate. For growth homogeneity the sample mount is often rotated during deposition, making good thermal contact difficult or impossible. In addition, the thermal capacity, and surface emissivity evolve as deposition occurs, so that the sample temperature can vary greatly even when a fixed heater current is provided. In addition, the deposition of material within the chamber is not totally limited to the substrate surface, and any surfaces in the vicinity of the growth surface will eventually become coated with sample material.

An approximate measurement of the temperature in the growth chamber is normally obtained using a thermocouple. In order to escape contamination during sample growth, the thermocouple must be placed under the sample mount where it is shielded from the beams of atoms/molecules which are impinging on the growth surface. If the sample mount is stationary during growth, the thermocouple can be inserted in a well carved out at the back of the mount for better thermal contact. However, if the sample mount is being rotated, which is frequently done for better deposition uniformity, then the thermocouple must be placed below the mount, and cannot be effectively heat sunk to provide an accurate measure of the sample mount temperature. Even when an accurate measure of the sample mount is obtained, there can also be large thermal gradients between the back of the sample mount and the sample surface, so an estimate of the temperature at the back surface may

not provide a realistic measurement of the growth surface temperature. Since the discrepancy depends on the instantaneous sample emissivity, it can be strongly dependent on the evolving (and usually unknown) sample characteristics during growth, and consequently cannot be effectively calibrated.

Another method of calibrating the growth temperature takes advantage of an easily observable eutectic critical point. For example, the sharp transition at ~ 570 °C for the interdiffusion of aluminum on silicon, which can be identified by a large change in reflectivity, is often used to determine the control settings required to achieve this temperature in a given growth chamber. Such calibration measurements are normally carried out in separate runs with no gas flow, rather than during an actual sample deposition, and are especially useful in establishing consistent growth temperatures within a given system over long periods of time. This method offers the advantage of measuring the temperature at the *front* surface of the substrate where growth actually occurs, rather than at the back of the substrate holder, and thus avoids problems associated with thermal gradients in the sample mount and substrate. Inherently, it also provides a solid thermal contact with the substrate. However, since the surface temperature of a growing sample depends on the instantaneous surface emissivity, this calibration cannot provide an absolute measure of the growth surface temperature for an arbitrary sample, and as mentioned earlier, fixed heater current may not be equivalent to a fixed sample temperature if the surface emissivity changes during growth.

Standard IR pyrometry, in which one measures the difference in brightness of the sample emission at two IR wavelengths in order to determine the equivalent black-body temperature, offers an alternative approach. Since it is inherently a contactless measurement, it bypasses the problems associated with poor heat sinking. In principle it can also be used during the deposition process, offering the possibility of active feedback for temperature control during growth. However, this method suffers from its own set of problems. First, the emission flux from the sample is often rather low, because the deposition is carried out at relatively low temperatures. Coupled with the small solid angle for optical access available in typical MBE systems, this weak emission can be difficult to observe with enough sensitivity for an accurate determination of the temperature. In addition, since the samples are usually rather imperfect black-body emitters, a two-point determination may not provide enough information for an accurate determination of the temperature. However, the measurement of the entire spectrum is not usually practical given the low flux and the changing emissivity of the sample surface. Finally, in most cases the sample and substrate materials are transparent to the IR emission, so that the desired signal from the sample surface may be

completely overwhelmed by the emission from the sample mount and heater elements.

Finally, an additional contactless optical method, photoreflectance, offers many advantages. In this technique, the optical gap of the deposited material is determined from the photoreflectivity spectrum, which in turn is used to determine the temperature from previously determined data on the band gap of the material as a function of temperature. This technique samples only the material within the optical absorption length of the sample surface, and for heteroepitaxy can even be used to determine the temperature of the growing layer without interfering signals from the substrate. The measurement can be made using light of relatively high intensity travelling in an optical fiber within the deposition chamber, offering more readily observable optical signals than available with IR emission pyrometry. However, a wide enough range of frequencies must be scanned to permit a fit to the complex derivative spectra. Since the temperature dependence of semiconductors is typically on the order of 0.1 to 1.0 meV per degree Kelvin, this method will not provide accurate temperature readings if the spectrum is greatly broadened by crystal imperfections or by thermal effects at high growth temperatures. In addition, this method is not useful for the deposition of alloys, because the band gap depends not only on the temperature, but also on the precise alloy composition, which cannot be determined independently. The effects of confinement on the electron states will also tend to cause calibration difficulties for thin-layer structures. Of course this method also fails for the deposition of gapless materials such as metal overlayers. Nevertheless, it offers distinct advantages over the other methods described, and is likely to become more widespread in the future.

METAL-ORGANIC CHEMICAL VAPOR DEPOSITION (MOCVD)

As with MBE deposition, temperature control is critical for the growth of high-quality films by MOCVD. The most stringent requirements are actually for the source temperatures (± 0.1 K), but fortunately these demands are relatively easily met, since the sources can be immersed in constant-temperature baths. In reality, control of the substrate temperature to a desired uncertainty of ± 2 K is considerably harder to achieve. The vacuum used for MOCVD deposition is not as extreme as for MBE, typically only in the range 0.1 to 1 atmosphere, and the growth temperatures range from 600 - 750 °C for III-V materials, and 350 - 450 °C for II-VI growth. The primary additional constraint on techniques for thermal control in MOCVD growth is the presence of toxic, corrosive and almost opaque vapors in the growth chamber during deposition. Their presence requires that any in situ sensor be encapsulated for protection

from the environment, and precludes any optical measurement during growth. In addition, the relatively high density of these gases in the vicinity of the sample surface results in significant convective cooling of the growing surface, as well as continuous deposition on all nearby exposed surfaces.

The two primary techniques used in the MDL for temperature measurements in MOCVD growth are the thermocouple and IR pyrometry approaches described in the previous section on MBE growth. The corrosive gas environment requires that the thermocouple be encapsulated, normally in a glass tube, which further degrades the thermal link between the sensor and sample. The thermocouple must also be placed behind or inside the sample mount to keep the device away from the area of heavy materials deposition. IR pyrometry capabilities are also limited by the MOCVD growth environment. The relatively opaque gases present in the chamber during growth preclude the use of this technique during actual growth cycles. IR pyrometry can only be used to precalibrate the control settings before growth is commenced, and the additional convective cooling which occurs under growth conditions limits the accuracy of such pregrowth calibrations.

LASER-ASSISTED CHEMICAL VAPOR DEPOSITION (LACVD)

Since LACVD growth is not a heater-driven process, temperature control of the sample environment is less critical than for the previously-described growth techniques, and ± 25 K is considered acceptable. The growth environment is basically the same as for MOCVD, with the exception of the ambient vacuum, which is typically held at $\sim 10^{-6}$ Torr for LACVD growth, intermediate to that of MOCVD and MBE. LACVD is an ultra-low temperature growth technique, typically utilizing temperatures close to room temperature. Growth is stimulated at these low ambient temperatures by pulsed laser excitation of the surface.

The only technique currently employed for monitoring the temperature during LACVD growth within the MDL is thermocouple based. The IR emission signals are too small for the IR pyrometry approach due to the low growth temperatures. As with MBE growth, the thermocouple is placed inside the sample mount, rather than at the growth surface where material deposition is occurring. Unfortunately, this does not provide a good measure of the temperature at the laser-stimulated growth surface. The discrepancy has been measured directly using a second thermocouple at the surface with all conditions identical to those during growth, but without initiating the gas flow, and temperature gradients as large as 100 K have been observed between the back of the sample mount and the substrate surface. In addition this discrepancy depends on the ambient temperature and sample parameters, and thus cannot easily be calibrated

and corrected for. Finally, the laser pulses may cause transient local excursions in the temperature which are not reflected by the thermocouple measurement which has a rather slow response. The ability to measure these transient surface effects would not only allow growth temperature specifications which would be portable from one system to another, but would also be useful in elucidating the underlying mechanisms responsible for growth by this technique. Unfortunately, there is currently no method capable of obtaining such measurements.

SUMMARY

This manuscript has summarized the temperature measurement and control issues important in the growth, processing and characterization of electronic materials in JPL's MDL. Although accurate thermal control is required for a variety of processes, the major obstacles remain in the area of materials growth. In this paper these issues have been examined in detail for MBE, MOCVD and LACVD growth. In all three cases, the existing temperature measurement technologies are marginally adequate. In general it is possible to reproduce consistent growth conditions for the growth of a particular type of sample in a given growth chamber. However, sample-to-sample differences due to effects such as surface emissivity (MBE), convective cooling (MOCVD) and laser heating effects (LACVD) cause unknown variations in the temperature at the growth surface during the deposition of an arbitrary new material or structure. The inability to measure the temperature of the growth surface itself precludes the ability to compare the actual growth temperature among different growth chambers. As a result, portability of precise growth conditions is unfortunately still beyond existing capabilities, and the optimal growth parameters must be determined empirically for each growth chamber and for each new material or structure.

The author acknowledges helpful discussions with F. Grunthaner, C. Lewis, P. Grunthaner, G. Radhakrishnan, P. Maker and B. Lewis. The work described in this paper was carried out by the Jet Propulsion Laboratory (JPL), California Institute of Technology, and was sponsored by the Strategic Defense Initiative Organization, Innovative Science and Technology Office, the National Aeronautics and Space Administration, and the Defense Advanced Research Projects Agency. The work was performed as part of JPL's Center for Space Microelectronics Technology.

TABLE I. CAPABILITIES OF THE MICRODEVICES LABORATORY

<p>MATERIAL DEPOSITION</p> <ul style="list-style-type: none"> • evaporation • molecular beam epitaxy (Si and III-V) • liquid phase epitaxy (LPE) • metal organic chemical vapor deposition (MOCVD) • laser assisted chemical vapor deposition (LACVD) 	<p>SURFACE / INTERFACE CHARACTERIZATION</p> <ul style="list-style-type: none"> • STM / BEEM • ESCA / SAM • TEM • SEM
<p>LITHOGRAPHY / DEVICE FABRICATION</p> <ul style="list-style-type: none"> • electron-beam and optical lithographies • diffusion and oxidation furnaces • wet and dry etching • reactive ion etching 	<p>BULK MATERIALS AND DEVICE CHARACTERIZATION</p> <ul style="list-style-type: none"> • transport • optoelectronic

FLUX LATTICE MELTING IN THE HIGH T_c SUPERCONDUCTORS

D.J.BISHOP, P.L.GAMMEL, L.F.SCHNEEMEYER
ATT-BELL LABORATORIES
MURRAY HILL, NEW JERSEY 07974

ONE OF THE IMPORTANT ISSUES FOR TECHNOLOGICAL APPLICATION OF THE HIGH T_c SUPERCONDUCTORS IS THEIR BEHAVIOR IN A MAGNETIC FIELD. A VARIETY OF EXPERIMENTS INCLUDING ELECTRICAL TRANSPORT¹, MECHANICAL OSCILLATORS² AND MAGNETIC DECORATION³ HAVE SUGGESTED THAT THESE MAGNETIC PROPERTIES WILL MAKE APPLICATIONS MORE DIFFICULT THAN ORIGINALLY ANTICIPATED.

IN A TYPE II SUPERCONDUCTOR, WHICH INCLUDES ALL KNOWN OXIDE SUPERCONDUCTORS, WHEN A MAGNETIC FIELD IS APPLIED IT BREAKS UP INTO DISCRETE BUNDLES EACH CONTAINING ONE QUANTUM UNIT OF FLUX. THESE FLUX LINES ORGANIZE THEMSELVES INTO A FLUX LATTICE WHICH IS HEXAGONAL IN SHAPE. THE FORMATION OF THIS HEXAGONAL LATTICE IS IMPORTANT FOR A VARIETY OF REASONS. THIS LATTICE WITH LONG RANGE POSITIONAL ORDER WILL HAVE A FINITE SHEAR MODULUS WHICH WILL ALLOW FOR HIGH CRITICAL CURRENTS IN THESE MATERIALS. THIS CAN BE SEEN BY THE FOLLOWING ARGUMENT. WITH A CURRENT FLOWING IN THE SAMPLE EVERY FLUX LINE WILL BE SUBJECT TO A LORENTZ FORCE WHOSE MAGNITUDE IS GIVEN BY THE CURRENT TIMES THE FIELD. IF THE FLUX LINES MOVE IN RESPONSE TO THIS FORCE THEN ENERGY WILL BE DISSIPATED AND THE SUPERCONDUCTING STATE WILL BE DESTROYED. THIS CAN BE AVOIDED BY HAVING THE FLUX LINES PINNED TO DEFECTS IN THE SAMPLE. HOWEVER IT IS NOT POSSIBLE TO PIN ALL OF THE LINES AS TO DO SO WOULD INTRODUCE SO MUCH DISORDER THAT THE TRANSITION TEMPERATURE WOULD BE LOWERED FOR ELECTRONIC REASONS. THE SOLUTION WHICH WORKS IN CONVENTIONAL MATERIALS IS TO PIN JUST A FEW OF THE FLUX LINES WITH DISORDER AND HAVE THE REST OF THEM HELD IN PLACE BY THE FINITE SHEAR MODULUS OF THE LATTICE. IT IS THE EQUIVALENT OF HOLDING A CARPET IN PLACE BY NAILING IT IN JUST A FEW PLACES. THEREFORE IT CAN BE SEEN THAT THE FORMATION OF A FLUX LATTICE MAY BE CRUCIAL TO OBTAINING HIGH CRITICAL CURRENTS IN THESE MATERIALS.

THE PROBLEM WHICH HAS COME TO LIGHT IS THAT IN THESE MATERIALS THE FLUX LATTICE MELTS WELL BELOW THE SUPERCONDUCTING TRANSITION TEMPERATURE. THIS CAN BE SEEN IN A VERY DRAMATIC FASHION BY USING VARIABLE TEMPERATURE FLUX LATTICE DECORATION EXPERIMENTS AS SHOWN IN THE FIGURE.

IN A DECORATION EXPERIMENT MAGNETIC PARTICLES ARE EVAPORATED ONTO THE CRYSTAL SURFACE AT LOW TEMPERATURES WHEN THE FLUX LATTICE IS PRESENT. THESE PARTICLES ARE MAGNETICALLY ATTRACTED TO AND DECORATE THE FLUX LINES. ONE CAN THEN WARM UP THE SAMPLE AND OBSERVE THE POSITIONS OF THE FLUX LINES BY LOOKING FOR THE PILES OF MAGNETIC PARTICLES WHICH HAVE BEEN LEFT BEHIND. THE VARIABLE TEMPERATURE FLUX LATTICE DECORATIONS SHOWN IN THE FIGURE SHOW THAT AT TEMPERATURES WELL BELOW THE SUPERCONDUCTING TEMPERATURE THE FLUX LATTICE IS A LIQUID. THUS THIS LOWER FLUX LATTICE MELTING POINT NOT THE MUCH HIGHER TRANSITION TEMPERATURE WILL BE THE UPPER LIMITING TEMPERATURE FOR MOST APPLICATIONS OF THE OXIDE SUPERCONDUCTORS. THIS MAKES POTENTIAL APPLICATIONS FOR THESE MATERIALS HARDER TO ACCOMPLISH. IT MAY BE POSSIBLE THAT WITH PROPER PROCESSING OF THESE MATERIALS PINNING CAN BE INTRODUCED WHICH WILL REPLACE THE NEED FOR A FLUX LATTICE. THIS IS A DIRECTION IN WHICH MUCH WORK IS BEING DONE BY WORKERS AROUND THE WORLD. OUR RESULTS DO NOT UNAMBIGUOUSLY IMPLY THAT THE OXIDE SUPERCONDUCTORS WILL BE IMPOSSIBLE TO USE IN APPLICATIONS BUT MERELY POINT OUT THE NECESSITY FOR FURTHER RESEARCH IN TRYING TO UNDERSTAND THE STATICS AND DYNAMICS OF THE FLUX LATTICES IN THESE MATERIALS⁴.

REFERENCES

1. T.T.M.PALSTRA, B.BATLOGG, L.F.SCHNEEMEYER AND J.V.WASZCZAK, PHYS. REV. LETT. 61, 1662 (1988).
2. P.L.GAMMEL, L.F. SCHNEEMEYER, J.V. WASZCZAK AND D.J.BISHOP, PHYS. REV. LETT. 61, 1666 (1988).
3. P.L.GAMMEL, D.J.BISHOP, G.J.DOLAN, J.R.KWO, C.A.MURRAY, L.F.SCHNEEMEYER AND J.V.WASZCZAK, PHYS. REV. LETT. 59, 2592 (1987).
4. FOR A REVIEW OF MANY OF THE ISSUES RELEVANT TO FLUX LATTICES IN THE HIGH T_c SUPERCONDUCTORS ONE CAN SEE THE ARTICLE IN *PHYSICS TODAY*, MARCH 1989, PAGE 17.

IMAGE SOLID AND LIQUID LATTICE

T=15K



YBCO
(SOLID)



BSCCO
(LIQUID)

FOR $\tau=1\text{sec}$ $D = \langle x \rangle^2 / \tau$

VORTEX DIFFUSIVITY:

$$D_L \gg D_S$$

This electron microscope photograph shows simultaneous flux lattice "decorations" of yttrium barium copper oxide (left) and bismuth strontium calcium copper oxide (right) at 15K in a field of 20 gauss. In contradistinction to the yttrium barium copper oxide, the flux lines in the bismuth strontium calcium copper oxide move significantly during the decoration time of about one second. This measurement provides convincing visual evidence that the flux lattice in bismuth strontium calcium copper oxide melts into a liquid significantly below the critical temperature for a superconductor.

COMBUSTION PROCESS SCIENCE AND TECHNOLOGY

Robert R. Hale
Jet Propulsion Laboratory
California Institute of Technology

An important and substantial area of technical work in which noncontact temperature measurement (NCTM) is desired is that involving combustion process research. In the planning for this workshop, it was hoped that W. Serignano would provide a briefing regarding the experimental requirements for thermal measurements, to support such research. The particular features of thermal measurement requirements included those describing the timeline for combustion experiments, the requirements for thermal control and diagnostics of temperature and other related thermal measurements and the criticality to the involved science to parametric features of measurement capability including precision, repeatability, stability, and resolution. In addition, it was hoped that definitions could be provided which characterize the needs for concurrent imaging as it relates to science observations during the conduct of experimentation.

A general discussion of the present plans for research in this area was given by G. Santoro in Section 1 of these proceedings. Several flight projects and related research are under the cognizance and direction of the NASA Lewis Research Center.

During the week following this NCTM workshop (held in Pasadena, California) an International Workshop on Microgravity Combustion was held at the NASA Lewis Research Center in Cleveland, Ohio. A substantial number of technical poster sessions were presented and the principal technical discussion groups were organized into two sessions, each of which had three parallel meetings. The technical topics were: Pre-Mixed Gases; Droplets, Particles, Sprays and Clouds; Fire Safety; Non Pre-Mixed Gases; Pools and Bulk Solids; and Diagnostics.

Of these technical discussion groups, two seemed particularly well suited to the interests of investigators desiring to develop noncontact temperature measurements. These were: the second session, Droplets, Particles, Sprays, and Clouds, which was chaired by William A. Serignano, and the last group, Diagnostics, which was chaired by Alan Eckbreth. Readers having particular interest in additional details in this science and technology area are referred to the proceedings from this workshop, which will be available from NASA Lewis Research Center.

On the Temperature of Surfaces

J. Adin Mann, Jr.
 Robert V. Edwards
 Department of Chemical Engineering*
 Case Western Reserve University
 Cleveland, Ohio 44106

Abstract

The concept of the temperature of a surface is introduced from the viewpoint of the physical chemistry of surfaces. The surface, near surface and microlayer regions of the interface are defined. Most methods measure the temperature of the microlayer or at best the near surface region and may err in representing the surface temperature. Methods based on capillary ripples actually measure the surface temperature since surface tension (or surface tension tensor when a monolayer has been spread or adsorbed at the interface) is the main restoring force that controls their propagation. Light scattering methods are described for determining the elevation of very small amplitude capillary waves through the computation of various correlation functions from which the surface tension can be estimated. Procedures for estimating the surface temperature are described.

The Surface Temperature

In order to speak of the "temperature of a surface" a length scale for the surface must be specified: the interface spans a length over which the normal derivative of the density is non-zero, Figure 1. It is well understood theoretically and experimentally that away from critical temperatures, the width of the interface is at most a fraction of a nanometer and corresponds to a few atomic or molecular dimensions. (See ref. (1,2).)

It is useful to define two additional length scales. The *near-surface* extends to about 10 nm. The near surface properties are some superposition of surface and volume properties which may, with careful analysis, be separated to some extent. The *microlayer* can be thought of as extending to roughly 1 micrometer from the surface. The properties determined in the microlayer *cannot* be separated into distinct surface and volume effects.

A property such as the *surface temperature* refers only to the first few molecular (atom) diameters of the interface; rigorously, it is not either the near-surface temperature or the microlayer temperature. Most methods in fact report the near surface or microlayer temperature. When the system (e.g. two-phase with one component) is at equilibrium, the temperature is uniform so that $T' = T_{\text{surf}} = T''$; even the microlayer temperature represents the temperature of the entire system. When the system is not in equilibrium, the near surface or microlayer temperatures may differ significantly from the surface temperature. The hypothesis that the near surface and surface temperatures are the same must be established experimentally or supported by careful analysis.

* BITNET: MANN@CWRU; INTERNET: MANN@CWCHME.ECHEM.CWRU.EDU

Ellipsometry, reflectometry (especially in the x-ray wave lengths) as well as theory and computer simulation provide the basis for asserting that the liquid/vapor interface is at most a few tenths of nanometers in thickness. One representation of the density profile through the interface is that of the mean field, Figure (1):

$$n(z) = \frac{1}{2} [n^{(+)} + n^{(-)}] + \frac{1}{2} [n^{(+)} - n^{(-)}] \tanh \frac{z}{\xi} \quad (1)$$

where n is the volume density, $n^{(+)}$, $n^{(-)}$ the densities on either side of the interface, and z is taken along the normal. When $T < T_c$ and $\left| \frac{T - T_c}{T_c} \right| \gg 10^{-2}$, $\xi \sim .3$ nm. The actual value of ξ depends on T . In addition the interface fluctuates. Define the Gibbs surface associated with the interface by the integral

$$0 = \int_{-a}^{\zeta} [n(z) - n^{(-)}] dz + \int_{\zeta}^a [n(z) - n^{(+)}] dz \quad (2)$$

where $-a$ and a are taken so that $(n(\pm a) - n^{\pm}) \sim 0$.

The fluctuating interface can be represented by the differential manifold^{2,3}

$$\Sigma: = \begin{cases} x = x \\ y = y \\ z = \zeta(x, y, t) \end{cases} \quad (3)$$

One must think of ζ as a random variable, for the plane interface, or as a small fluctuation away from the average trace of a curved interface. The representation² for a plane interface

$$\zeta = \sum_{\vec{q}} \zeta_{\vec{q}}(t) e^{i\vec{q} \cdot \vec{x}} \quad (4)$$

for unit area leads to

$$\langle \zeta_{\vec{q}}^* \zeta_{\vec{q}} \rangle = \frac{kT}{\gamma q^2 + g \Delta n} \quad (5)$$

(for unit area of surface) where k is the Boltzmann factor, T the temperature, γ the surface tension, \vec{q} the wave number, $\Delta n = n^{(+)} - n^{(-)}$ the density difference and g the gravity constant. This formula has been studied experimentally and is considered accurate although a molecular level theory is incomplete.

Clearly, the measurement of $\langle \zeta_{\vec{q}}^* \zeta_{\vec{q}} \rangle$ will provide an estimate of the true surface temperature. However, the surface tension, γ , depends on temperature. So that the temperature dependence of the surface tension should be known.

In addition, the spectrum of the fluctuations can be calculated (Ref (2) and references therein)

$$G(\omega, q) = F(\langle \zeta_{\vec{q}}^*(0) \zeta_{\vec{q}}(t) \rangle) \quad (6)$$

where $\langle \zeta_{\vec{q}}^*(0) \zeta_{\vec{q}}(t) \rangle$ is the autocorrelation function of the \vec{q} component of the elevation function and $F(\cdot)$ is the Fourier transform.

Even though $\sqrt{\langle \zeta_{\vec{q}}^2 \rangle} \ll .1$ nm, continuum mechanics provides a formula for $\zeta_{\vec{q}}$ which is known to be accurate for small $|\vec{q}|$ (the "long" wave length limit). There is a substantial body of experimental work that supports this conclusion so long as $|\vec{q}|$ is sufficiently small that macroscopic formulas are valid. A fairly delicate argument leads to the following result (Ref (2) and references therein)

$$G_{\vec{q}}(\omega) = \frac{kT}{\gamma q^2 + g \Delta n} (M^{-1})_{11} [q, \omega, n, \mu, \gamma, \dots] \quad (7)$$

where \dots , represents surface visco-elastic coefficients appropriate for systems for which a monomolecular film can form; a one component, two phase system admits only γ .

Note that the determination of $G_{\vec{q}}(\omega)$ provides the surface temperature as well as the surface tension. However, there are conditions that must hold when the system is dynamic, and $\nabla T \neq 0$. The distribution function for $\{\zeta_{\vec{q}}\}$ must not change form from that of equilibrium when the system is dynamic; local equilibrium is assumed. Furthermore a sufficient area must be sampled so that area averaging is satisfactory; for an ℓ by ℓ surface patch, $\ell \gg \frac{1}{q}$ where $q \sim 1000 \text{ cm}^{-1}$.

In fact, the functions $\langle \zeta_{\vec{q}}^* \zeta_{\vec{q}} \rangle$ and $G_{\vec{q}}(\omega)$ can be determined by light scattering which will be described briefly.

Light Scattering Spectroscopy

Early in the century, the Maxwell equations for the scattering of light from thermally excited capillary waves^{2,3} was worked out with the result that in the far field for $\zeta_{\vec{q}} \ll \lambda_0$, with λ_0 the wave length of the incident light, the scalar electric field follows $E_{\vec{q}} = \zeta_{\vec{q}} \times f$ where f depends on the geometry of the scattering experiment (angles of incidence and scattering) and the refractive indices of the phases that join at the surface. Obviously, at least one of the phases must be transparent. Indeed $\langle E_{\vec{q}}^* E_{\vec{q}} \rangle = f^2 \langle \zeta_{\vec{q}}^* \zeta_{\vec{q}} \rangle$. However, the electric field is detected by a square-law device (photodiode or PMT detectors) so that the autocorrelation function actually generated is that of the current, $i = E_{\vec{q}}^* E_{\vec{q}}$. Thus a heterodyne system is required so that $\langle i(0) i(t) \rangle$ can be related directly to $\langle \zeta_{\vec{q}}^*(0) \zeta_{\vec{q}}(t) \rangle$ without loss of phase information^{2,4,5}.

A general schematic of the methodology^{2,4,5} is shown in figure 2. The essential feature is that a spatially filtered image of a grating of known wave number is projected onto the interface. The quality of the optical processing in projecting the grating onto the surface is crucial. The liquid surface is usually the highest quality optical component in the system and can be thought of as a very high quality but very inefficient phase grating following the rule^{4,5}

$$R = R_0(1 + \eta)e^{-i\varphi} \quad (8)$$

where R is the reflection coefficient of the surface, R_0 is the reflection coefficient of the ideally smooth surface, $\eta(x,y) \ll 1$ is the amplitude variation over the illuminated spot and $\varphi(x,y)$ is the phase variation. The phase function is $\varphi_q(x,y) = 2k_0\zeta_q$ wherein a real function representation of ζ_q is appropriate^{4,5}.

The product $RS^{(-)}$ provides the modulation of the reflected beam, $S^{(+)}$ by the capillary ripples; a particular component $\zeta_q(t)$ modulates $S^{(+)}$ ($= RS^{(-)}$) depending on the structure of $S^{(-)}$ as determined by the grating, F_1 , L_1 and L_2 . However, since the incident laser beam is of finite extent, the reflected beam $S^{(+)}$ carries a distorted representation of $\zeta_q(t)$. Fortunately, the "instrument function" can be computed accurately⁴. The one most characteristic dimensionless group for the instrument function is $k_g\sigma$ where k_g is the wave number of the grating as projected on the surface and σ the cross section of the Gaussian incident beam (4σ is the "beam diameter"). While not absolutely essential, the incident beam should be cleaned up so as to be accurately Gaussian since this makes the computation of the instrument function relatively simple.

It is practical to use optical components to manipulate the optical field $S^{(+)}$ so as to eliminate the zero-order beam and pass only the reference beam that is modulated by φ . The optical quality required for this step is modest, the entire reference beam must be collected excluding all other beams (higher order or lower order beams). The beam need not be of accurate Gaussian cross section and some distortion of the phase by the collection optics can be tolerated.

The computation of the correlation function $\langle i(0) i(t) \rangle = R_i(t)$ from the time series generated by the detector yields $\langle E_q^*(0) E_q(t) \rangle$ and therefore^{4,5}

$$R_i(t) = \int_{-\infty}^{+\infty} dq_x \int_{-\infty}^{+\infty} dq_y \langle \zeta_q^*(0) \zeta_q(t) \rangle F(q_x - k_g^s, q_y) \quad (10)$$

where k_g^s is the wave number of the grating as projected on to the surface (if the magnification is 1 then $k_g = k_g^s$). The instrument function F depends on $k_g^s\sigma$ so that

$k_g^S \sigma \rightarrow \infty$, $F \rightarrow \delta(q_x - k_g^S) \delta(q_y)$ and $R_i \rightarrow \langle \zeta_q^*(0) \zeta_q(t) \rangle$, see references (4,5).

A second dimensionless group useful for designing an experiment^{2,4,5} is $Y = (\omega_0 \tau_0)^2$ where $\frac{1}{\tau_0} = 2 \frac{(\mu' + \mu'')}{(n' + n'')} q^2$ where μ', μ'' are the shear viscosities in the volume of the phases surrounding the interface and n', n'' the densities. The frequency, ω_0 is defined by $1 = (n' + n'') \omega_0^2 / \gamma q^3$ which obtains for the ideal, clean surface, between fluids of vanishing viscosity.

When $Y \gg 1$ the capillary ripples are propagating and

$$\langle \zeta_q^*(0) \zeta_q(t) \rangle = \frac{kT}{\gamma q^2 + g \Delta n} e^{-\Gamma_q t} \cos \omega_q t \quad (11)$$

is a good representation of the autocorrelation function. The correlogram determined experimentally allows the estimation of Γ_q and ω_q (and their uncertainties and correlation) by fitting equation (11) through a maximum likelihood algorithm. In general ω_q is determined to $\sim .2\%$ and Γ_q to $\sim 1\%$. It then is easy to compute any two parameters n, μ, γ, \dots by using the dispersion equation, $\text{Det } \underline{M} = 0$, from equation (7).

The construction of equation (7) and in particular the response function matrix \underline{M} , has been done several times and is too lengthy to produce here; see references (2,3) for a guide to the literature. The analysis requires a careful construction of the mass and momentum balance at the surface including coupling to the substrate through the jump of the three dimensional pressure tensor across the interface projected along the normal to the interface as well as in the plane of the interface^{2,3}. The boundary conditions include:

$$\frac{d\zeta}{dt} = \hat{n} \cdot \vec{v}|_0$$

and

$$\frac{d\xi}{dt} = \vec{v}|_0 \cdot \underline{U} \hat{n}$$

where $\vec{v}|_0$ is the volume velocity field evaluated at the surface and projected either along the normal, \hat{n} , or into the plane by the tensor $\underline{U} \hat{n}$. The conditions for linearization obtain since $\zeta \ll \frac{1}{q}$ in the spectrometer specifications. \underline{M} is constructed from the set of linear equations that result from a Fourier transform in space and a Laplace transform in time. The M_{11}^{-1} component representing ζ is used in equation (7) while $\text{Det } \underline{M} = 0$ is the dispersion equation mentioned above.

Remarks on Implementation of the Fourier Transform Spectrometer

A research instrument, as figure (2) suggests, has required substantial room on an optical bench. Optics of focal lengths of ~ 1 meter are often used. We have built a much more compact system for various applications. Our latest instrument uses a ~ 40 mw diode laser, $\lambda_0 \sim 830$ nm, which is only a few centimeters long, wide and high. The power supply is built into this package. With care, a lens system of $f \sim 200$ mm works well to provide the necessary Fourier transforms and further, the optical path can be folded. The detector is a photodiode and is small. This system delivers correlograms of research quality without special manipulation of the output of the laser; the beam is elliptical but of Gaussian cross section in each direction. We are now working to reduce the size to that of a package measuring centimeters instead of meters.

A second problem with the light scattering methodology has been sensitivity to vibration. When the surface tilts slightly at low frequency ($\lesssim 10$ Hz) due to building vibration the correlograms become so badly distorted that Γ_q, ω_q cannot be determined. This has been overcome by a beam directing device in a feed-back circuit that locks the reference beam onto the detector accurately. The correlogram is then clean of the flicker effect; the slight distortion of the correlogram due to fluctuations of the angle of incidence of the laser beam about the normal is ignorable.

We have designed and are implementing a "single board" correlator that is driven by a PC (80286 processor + 80287 coprocessor) which provides a compact, clean system for data analysis.

We expect to have the first integrated prototype ready for a ship-board experiment in October, 1989 involving the measurement of the calm ocean surface tension in situ.

Discussion

The light scattering procedures for measuring the "true" surface temperature rather than the near-surface or microlayer temperature are two

- Measure the averaged, surface light scattering irradiance which is proportional to $\langle \zeta_q^* \zeta_q \rangle$ and thereby determine T through equation (5).
- Measure the correlation function of the scattered light, compute estimates of Γ_q and ω_q and determine T through their variation with T.

The determination of the averaged, surface light scattering irradiance is difficult because the signal is small and subject to distortion by flare. Moreover, even with the careful application of an interference filter with a narrow band-pass at the wavelength of the laser, the radiance of the heated, liquid metal pool may swamp the detector. However, since the laser can be modulated easily, lock-in detection is possible and should be effective in separating out the signal due to scattered light. The strong q dependence of the scattered irradiance also provides a way of separating out the part of the signal to be analyzed. These methods require some information about the equilibrium surface tension dependence with temperature but a limited data set should be sufficient because of the relatively small changes involved.

The measurement of the correlation function is quick and accurate. The radiance coming from the heated, liquid metal pool is uncorrelated but does contribute to the "dark" noise. An interference filter should make this effect tractable. Note that the reference beam is much more intense than the scattered light and so the signal-to-noise ratio will be substantially better than in the first procedure.

However, the relationship between Γ_q , ω_q and T is complex in that the surface tension dependence on temperature is involved as well as that of the density and viscosity. Even so, the methodology has the potential of being relatively easy to calibrate (ω_q , Γ_q with T for each material) under equilibrium conditions which provide working curves for determining T and γ for non-equilibrium systems.

While the theory of light scattering spectroscopy can be generalized to include temperature gradients, at this time we depend on the local equilibrium assumption. If light scattering can be observed from a small enough spot then local equilibrium can be asserted and an estimate of the surface tension or temperature, averaged over the illuminated spot, can be computed. However, as the spot is made smaller, q becomes less well determined by the optical system and thereby the estimate of the surface tension and temperature is less certain.

With the technology we have in place now, the minimum spot size that is practical is about 2 mm. It is likely that we can work with .2 mm spot sizes by using gratings with $k_g > 1000 \text{ cm}^{-1}$ but how well this works in practice must be determined. Note: The spot can be moved over the surface so that a profile can be developed.

It is entirely possible to do surface spectroscopy from curved surfaces. Indeed little needs to be changed for cylinder systems of 1 cm or so in length and a few mm in diameter or for spheres of 1 cm or so in diameter. It is an interesting question whether by careful application of Fourier transform optics it is possible to design an optical system that will separate out the higher frequency normal modes of a spherical drop for spectral analysis. Based on unpublished calculations done for spherical drops irradiated by an ultra-sound field we feel it is possible.

The question is whether an optical field can be produced in practice so that normal mode oscillation driven by thermal fluctuations in a small drop can be detected as a time series and analyzed. Indeed, it is not necessary to consider thermal fluctuations alone, external fields (e.g. sound or ultra-sound) can be used to drive the surface oscillations of the drop. The spectroscopy of such driven waves is also possible using the laser methods developed by the CWRU group.

It has been our experience that the light scattering methodology is the method of choice in determining the surface tension and interfacial tension of a system. It is fast, accurate and does not require manipulation of the sample. It is my opinion that this is the method of choice for determining the equilibrium surface tension of melts at high temperature. Whether the technology can be adapted for small samples with curvature can be determined by Fourier optical computations and a set of careful measurements.

Acknowledgments

Support by the Office of Naval Research, The Microlayer program, Dr. F. Herr program manager is acknowledged with gratitude. The initial work on the measurement of

thermal gradients over surfaces was sponsored by NASA.

References

1. Adamson, A.W., "Physical Chemistry of Surfaces"; 4th ed.; Wiley-Interscience; New York, 1982.
2. Mann, J.A., Jr., "Dynamics, Structure and Function of Interfacial Regions," *Langmuir* 1, 10, 1985.
3. Mann, J.A., Jr.; Porzio, K.C. *Int. Rev. Sci.; Phys. Chem., Ser. Two. 1975-1976*, 7, 47 (1975).
4. Edwards, R.V.; Sirohi, R.S.; Mann, J.A., Jr.; Shih, L.B.; Lading, L.; *Appl. Opt.* 21, 3555 (1982).
5. Lading, L; Mann, J.A., Jr.; Edwards, R.V.; *J. Opt. Soc. Am.*, in press 1989.

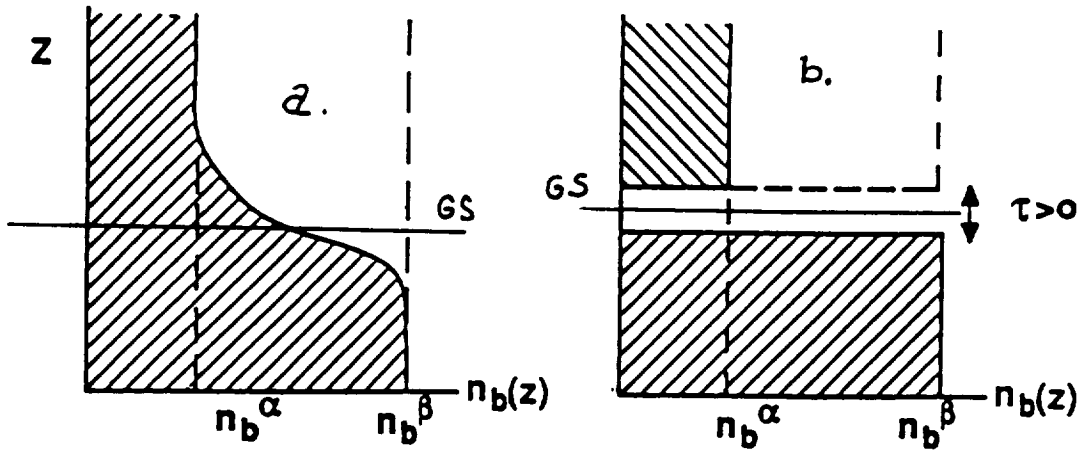


Figure 1 The density variation through the interfacial region between a liquid and its vapor. a) The variation of density as determined by theory and simulation. b) A model that can be defined to be consistent with the macroscopic continuum thermodynamics of interfacial behavior. In either case, the interfacial thickness, ξ , is < 1.0 nm for liquids at temperatures at least a few degrees below the critical temperature. $\xi \rightarrow \infty$ as $T \rightarrow T_c$, the critical temperature. The two lines, GS, represent the Gibbs surface.

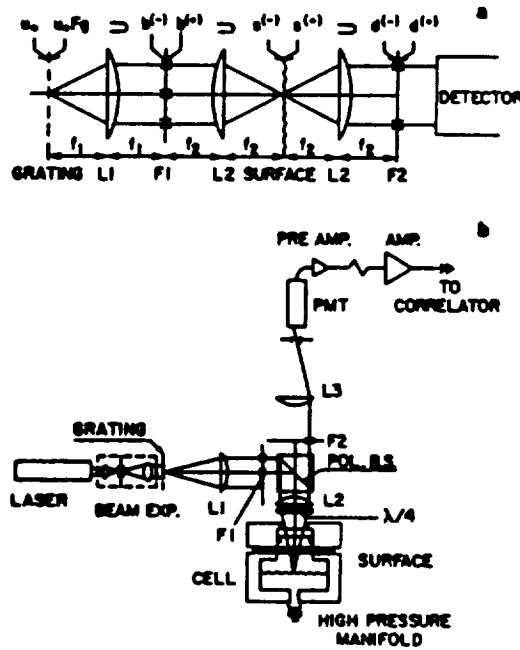


Figure 2 (a) Fourier optics method of design for a surface-light-scattering spectrometer. The symbol \supset implies a Fourier transform. Transmission (or reflection) functions relate $b^{(-)}$ to $b^{(+)}$, $s^{(-)}$ to $s^{(+)}$, and $d^{(-)}$ to $d^{(+)}$. In particular, for the surface $s^{(+)} \approx R_0(1 + \eta + i\phi)s^{(-)}$ where η depends on the monolayer density and is ignorable. The phase function ϕ depends on the ripple profile and is modeled easily. The grating transmits a zero-order beam of relatively high intensity which is passed along with higher order diffracted beams which can be filtered spatially by F1. (b) Schematic of an implementation for high-pressure work. Note that the grating along with filters F2 and F1 provide a heterodyne configuration. It is easy to block all beams at F1 except the zero-order beam so as to obtain a homodyne configuration. Note that the grating is imaged onto the surface. The polarizing beam splitter (POL.B.S.) and $\lambda/4$ plate isolate the laser from the reflected beams.

NON-CONTACT TEMPERATURE REQUIREMENTS (NCTM) FOR DROP AND BUBBLE PHYSICS

Anthony B. Hmelo and Taylor G. Wang

**VANDERBILT UNIVERSITY
Center for Microgravity Research and Applications
Nashville, Tennessee 37235**

February 1989

Many of the materials research experiments to be conducted in the Space Processing program require a non-contaminating method of manipulating and controlling weightless molten materials. In these experiments, the melt is positioned and formed within a container without physically contacting the container's wall. An acoustic method, which was developed by Professor Taylor G. Wang before coming to Vanderbilt University from the Jet Propulsion Laboratory, has demonstrated the capability of positioning and manipulating room temperature samples. This was accomplished in an earth-based laboratory with a zero-gravity environment of short duration. However, many important facets of high temperature containerless processing technology have not been established yet, nor can they be established from the room temperature studies, because the details of the interaction between an acoustic field and a molten sample are largely unknown.

Vanderbilt University's Center for Microgravity Research and Applications (MRA) was founded in 1988 to investigate the basic physics of drops and bubbles, and the influence of gravity on their properties. Containerless science experiments are conducted to study:

- drop dynamics;
- bubble dynamics;
- collision and coalescence;
- containerless science and technology;
- applications research.

The observation of these phenomena will lead to a better understanding of the contributions of fluid dynamics in the formation of raindrops, dispersal of aerosols in the atmosphere, manipulation of molten materials in a microgravity environment, etc.¹

Drop dynamics involve the observation of acoustically levitated silicone oil drops at temperatures near room temperature. We are interested in:

- the resonant frequencies of free and statically formed drops;
- non-linear large amplitude oscillations;
- oscillation-induced rotation and fission;
- ratio of decay of oscillating drops.

In bubble dynamics², we are interested in the centering characteristics of the internal void, in addition to:

- rotational and vibrational behavior of free liquid shells;
- mode splitting and coupling;
- core centering mechanisms.

Concerning the collision and coalescence behavior of drops and bubbles, we consider:

- drop deformation upon collision;
- energy dissipation upon coalescence;
- drop separation and rupture.

In these experiments, we seek to set up stable low temperature environments, where the drop or bubble is in thermal equilibrium with its surroundings. Temperature measurement requirements under these circumstances are relatively straightforward and non-demanding, as shown in the Table.

At MRA, we are also interested in Containerless Science and Technology, which mandates a different set of NCTM requirements. These experiments study the properties of levitated molten metals. Of interest are:

- the stability of the containerless system;
- the shaping of liquid drops in an acoustic field;
- thermal acoustic interactions (thermal streaming phenomena);
- effects of acoustics on nucleation and undercooling.

We are applying both electromagnetic levitation and acoustic levitation methods to the processing of molten metals. These require NCTM in a higher temperature range, as indicated in the Table.

In the case of thermal streaming phenomena, we are interested in making a set of closely spaced temperature measurements across a two-dimensional pattern of several centimeters. We want to distinguish the temperature of the suspended sample from the temperature distribution in the field surrounding the sample. Studies of this kind help to distinguish the regimes of gravity-dominated and acoustically-dominated fluid flow interactions with the specimen. We feel that a thermal imaging system with a spatial resolution quoted in the Table may be most appropriate.

At MRA, we are employing novel material characterization technologies, which may also be utilized as NCTM techniques.

Synchrotron x-ray microtomography has been developed since its suggestion in 1983 for the nondestructive evaluation of small samples.³ X-ray tomography is a method of reconstructing the three-dimensional distribution of x-ray attenuating material within a volume. The technique is described elsewhere.⁴

Essentially, the technique utilizes a monochromatic x-ray beam from an electron storage ring to electronically collect a set of x-ray radiographs on a high resolution solid state television system. The radiographs are collected at a number of discrete rotational displacements of the specimen in the x-ray beam, and reconstructed with the aid of a computer to form a 3-D representation of attenuating material within the specimen. X-ray microtomography has been successfully demonstrated on both solid and liquid

media. The state of the art is able to achieve a 1 μ m spatial resolution for a 1% variation in the local x-ray attenuation coefficient, under the best experimental conditions.⁵

For an x-ray beam of intensity I_0 , the intensity transmitted through a slab of material of thickness L is given by

$$I = I_0 e^{-\mu L}$$

where μ is the linear absorption coefficient. It is a function of the atomic number of the attenuating material and the x-ray photon energy. For the 25 KeV photons employed at storage rings for microtomography, the dominant attenuation process is the photoelectric effect.

In general, in a specimen which is a mixture of materials of varying atomic number, the total linear absorption coefficient is given by a mixture rule

$$\mu_{\text{mix}} = \left[\sum_i W_i (\mu/\rho)_i \right] \rho_{\text{mix}}$$

where W_i = weight fraction of the i th component and (μ / ρ) = the mass absorption coefficient for the i th element.

Here we see that a measurement of attenuation coefficient is sensitive to the atomic composition, and also to the density (ρ). Thus, in chemically homogeneous material, measurement of μ can yield information on ρ .

Such a situation can be envisioned at the solid/liquid interface. Often, in metal systems, the difference in density between solid and liquid phases can be a few percent, well within the detectability of x-ray microtomography. By assuming equilibrium conditions, the melting temperature at the solid/liquid phase boundary can be sensed in such a two-phase system.

In addition, in material systems such as Pb-Sn⁶, which have well-defined density versus temperature relationships, the measurement of density variation with position within a sample can be equated with temperature measurement.

At MRA, we are currently applying this technique to the characterization of metal shells, and also solid/liquid phase boundaries in low-melting temperature metals.

REFERENCES

- 1) Proceedings of the Second International Colloquium on Drops and Bubbles, Monterey, CA 1981, JPL Publication 82-7.
- 2) T. G. Wang, D. D. Elleman, and M. M. Saffron, Prog. Astr. and Aeronautics 52, 1977.
- 3) Grodzins, L., Nucl. Inst. and Methods 206, 541-552, 1983.
- 4) Johnson, Q. C., J.H. Kinney, V. Bonse, M.C. Nichols, R. Nussart and J.M. Bras, Mat. Res. Soc. Symposium Proc. 69, 203-208, 1986.
- 5) Flannery, B.P. , H.W. Deckman, W.G. Roberge and K.L. D'Amico, Science, 237, 1439-1444, 1987.
- 6) D.R. Poirier, Met. Trans 19A, 2349-2354, 1988.

REQUIREMENTS FOR NON-CONTACT TEMPERATURE MEASUREMENT

	Temperature Range	Spatial Resolution	Temporal Resolution	Temperature Gradient
Drops, Bubbles Collision and Coalescence	$10^{\circ} < T < 40^{\circ} \text{C}$ $\pm 1\%$	1 measurement/cm	1 measurement/min	1°C/cm
Containerless Science and Technology	$20^{\circ} < T < 2000^{\circ} \text{C}$ $\pm 1\%$	50 measurement/cm	60 measurement/min	10^{-4}C/cm

MATERIALS PROPERTIES NUMERICAL DATABASE SYSTEM

ESTABLISHED AND OPERATIONAL AT CINDAS/PURDUE UNIVERSITY

C. Y. Ho and H. H. Li

Center for Information and Numerical Data Analysis and Synthesis
Purdue University
West Lafayette, Indiana

Abstract

A computerized comprehensive numerical database system on the mechanical, thermophysical, electronic, electrical, magnetic, optical, and other properties of various types of technologically important materials such as metals, alloys, composites, dielectrics, polymers, and ceramics has been established and operational at the Center for Information and Numerical Data Analysis and Synthesis (CINDAS) of Purdue University. This is an on-line, interactive, menu-driven, user-friendly database system. Users can easily search, retrieve, and manipulate the data from the database system without learning special query language, special commands, standardized names of materials, properties, variables, etc. It enables both the direct mode of search/retrieval of data for specified materials, properties, independent variables, etc. and the inverted mode of search/retrieval of candidate materials that meet a set of specified requirements (which is the computer-aided materials selection). It enables also tabular and graphical displays and on-line data manipulations such as units conversion, variables transformation, statistical analysis, etc. of the retrieved data. The development, content, accessibility, etc. of the database system are presented and discussed.

Introduction

The Center for Information and Numerical Data Analysis and Synthesis (CINDAS) was founded at Purdue University on 1 January 1957, originally as the Thermophysical Properties Research Center (TPRC). It is dedicated to the advancement of science, engineering, and technology through better knowledge of the properties of materials.

For 30 years since its inception CINDAS has been extracting and compiling material property data from worldwide scientific and technical literature and has been evaluating, analyzing, correlating, and synthesizing the compiled experimental data to generate reliable reference data (the so-called recommended values). As a result, CINDAS has developed a number of comprehensive and authoritative numerical databases. The existing databases established at CINDAS contain a total of over 125,000 sets of data* on the properties of all types of technologically important materials, which will be detailed later.

Since 1972 CINDAS has been developing a computerized "Materials Properties Numerical Database System." The data already available at CINDAS are gradually and selectively being computerized. The new data for databases developed in recent years are, however, all fully computerized.

One of the salient features of the databases developed by CINDAS is that each database contains both the experimental data compiled from the worldwide literature and the evaluated reliable reference data (recommended values) for selected more important materials (as resources permit) resulting from critical evaluation, analysis, correlation, and synthesis of the compiled data, as CINDAS has always considered the quality and credibility of the data in a database to be of utmost importance.

The major databases in the materials properties numerical database system at CINDAS as well as their development, accessibility, etc. are presented and discussed in the following sections.

Development, Accessibility, and Characteristics of the Database System

The computerized numerical database system on materials properties established at CINDAS is an on-line, interactive, menu-driven, user-friendly system. A user can easily search, retrieve, and manipulate the data from the database system without learning special query language, special commands, standardized names of materials, properties, variables, etc. This on-line database system is managed by a data base management system (DBMS) developed by CINDAS over the years particularly for the management and operation of numerical databases. This unique DBMS is well known for its user-friendliness and instant responsiveness and in the ease and versatility of operation in dealing with numerical databases.

*One set of data consists of numerical data points (as a function of temperature and/or other independent variable) and pertinent information on the specification and characterization of the test materials and on the method and conditions of the property measurement, plus the data source reference.

This database system enables the on-line interactive search/retrieval of at least the following:

- (1) Numerical property data in tabular and graphical forms and pertinent information on the test material and property measurement for specified materials, properties, independent variables, etc. (direct mode).
- (2) Candidate materials that meet a set of specified requirements (inverted mode), which is the so-called computer-aided materials selection (CAMS).
- (3) General descriptions of individual materials including composition, crystalline structures, synonyms, trade names, manufacturing processes, unusual properties and behavior, recommended applications, etc. (these general descriptions of materials are in addition to the specific descriptions and characterizations of individual test materials which are recorded together with the numerical data as part of the individual data sets).
- (4) Definitions of material properties and other relevant technical terms.
- (5) Summaries of ASTM test methods for material property measurements and their significance.
- (6) Bibliographic citations of references to specified materials/properties combinations or authors.

It enables also the on-line data manipulations such as units conversion, variables transformation, statistical analysis, etc. of the retrieved data.

The database system contains a number of databases and each database is on a large group of materials. The development of each database involves:

- (1) The in-depth cognizance and acquisition of the relevant worldwide scientific and technical literature.
- (2) The exhaustive extraction and compilation of data and information from the acquired pertinent research documents.
- (3) The critical evaluation, analysis, correlation, and synthesis of the compiled experimental data to generate reliable reference data.
- (4) The computerization of both the experimental data and the CINDAS-generated reliable reference data to create various data files.
- (5) The development of various ancillary files necessary for the database.
- (6) The integration of the various data files to establish an operational computerized database.

As the material property data recorded in the scientific and technical literature are often conflicting, widely diverging, and subject to large uncertainty, the literature data are critically evaluated and analyzed to generate reliable reference data. The availability of both the critically evaluated reference data and the experimental data in the database is one of the salient features of CINDAS' comprehensive materials properties database system. The methodology of critical evaluation, analysis, correlation, and synthesis of material property data used at CINDAS has been discussed in detail elsewhere [1]. Basically, it involves critical evaluation of the validity of the available data and related information, judgment on the reliability and accuracy of the data, resolution and reconciliation of disagreements in conflicting data (distinguishing first the real difference in data due to sample difference from the disagreement in data due to

experimental error), correlation of data in terms of various affecting parameters (sometimes in reduced forms using the principle of corresponding states), curve fitting with theoretical or empirical equations, synthesis of the often fragmentary data (sometimes by combining the available data with the values derived from the data on related properties or related materials) to generate a fuller range of coverage of internally consistent values, comparison of the resulting values with theoretical predictions or with results calculated from theoretical relationships, etc.

As an example to illustrate our work on the critical evaluation and analysis of experimental data, Figure 1 shows part of the available experimental data as well as CINDAS' recommended values for the thermal conductivity of tungsten. It can be observed from Figure 1 that a large portion of the experimental data are conflicting, widely diverging, and subject to large uncertainty, and the spread of data is over three hundred percent. The true values of the thermal conductivity of tungsten had not been known even with the availability of over 400 publications on this subject published beginning in 1914 until CINDAS critically evaluated and analyzed the discordant experimental data and generated the recommended reference values in 1964 as shown in the figure. These CINDAS' recommended values have been recognized as national standard reference data. Similarly, Figure 2 shows the available experimental data and CINDAS' recommended values for the thermal diffusivity of tungsten and that the lower portion of the experimental data are utterly erroneous, being about five times too low.

Our work on the correlation and synthesis of experimental data is illustrated by Figures 3 to 8. Figure 3 shows the available experimental data on the thermal conductivity of aluminum + copper alloys, which are very limited, fragmentary, and conflicting. Based on the results of evaluation and analysis of these thermal conductivity data and on CINDAS' recommended values for the electrical resistivity and the thermoelectric power of these alloys, the full-range recommended values for the thermal conductivity of these alloys were generated as shown in Figure 4.

Figure 5 presents the recommended values for the electrical resistivity of iron + nickel alloys as the final results of correlation and synthesis of the available experimental data which are not shown. Similarly, Figure 6 presents the recommended values for nickel + iron alloys. The pronounced effect of the ferromagnetic-paramagnetic transition on the electrical resistivity of the alloys at the Curie temperature is strikingly shown in the two figures. These two sets of recommended values together cover the thermal conductivity of the entire iron-nickel alloy system for all alloy compositions and all temperatures.

Figure 7 shows the recommended values for the absolute thermoelectric power of copper-nickel alloy system covering all alloy compositions and all temperatures up to 1,300 K. The effect of the ferromagnetic-paramagnetic transition on the thermoelectric power of the alloys is also clearly shown.

As an example to show the results of our work on mechanical properties, Figure 8 shows a stress-fracture map for 316 stainless steel such that we have extended the tensile stress versus failure time curves into the short-time domain, in which data from constant-load rapid-heating testing as well as from constant strain-rate testing after rapid heating are shown also. Such a stress-fracture map presents a considerable body of mechanical property information in a single figure wherein the regions for all the material fracture mechanisms under load are indicated, including ductile transgranular fracture, transgranular creep fracture, intergranular creep fracture, rupture, and mixed mode of fracture.

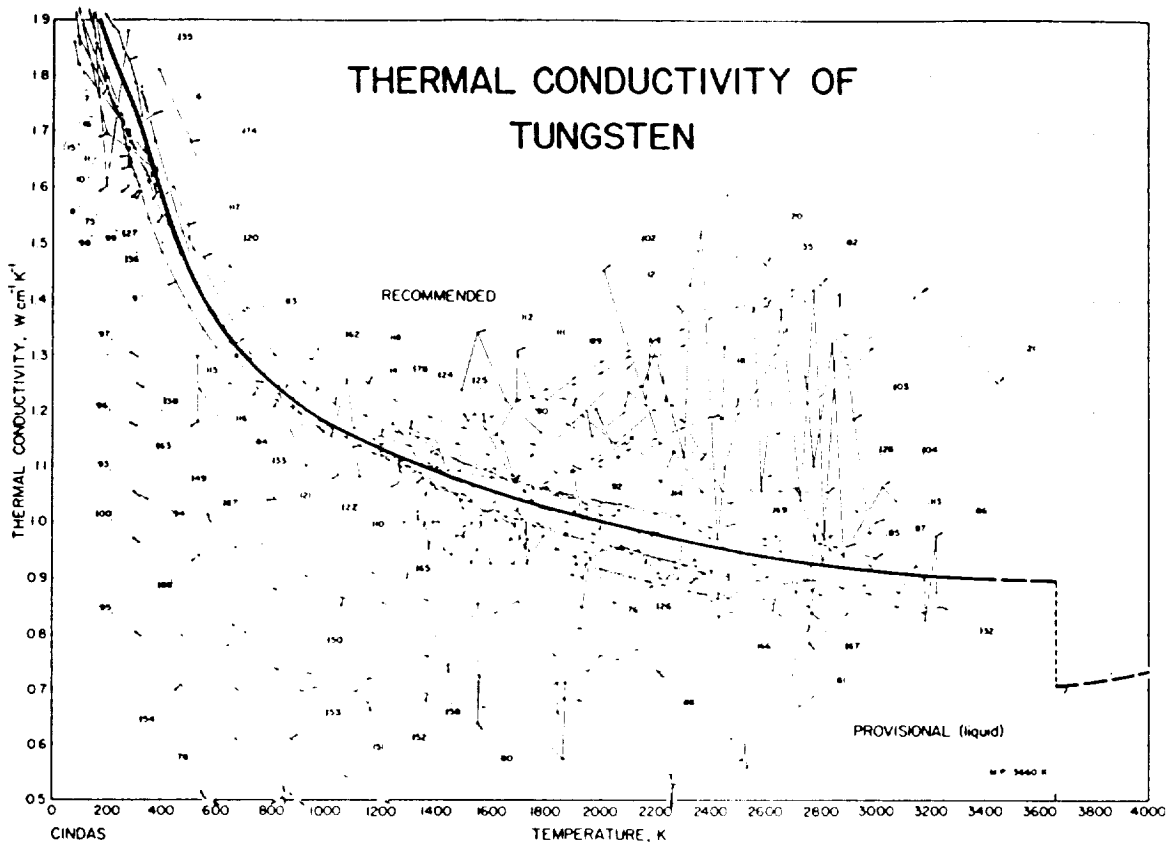


Figure 1. Experimental data and recommended values for the thermal conductivity of tungsten.

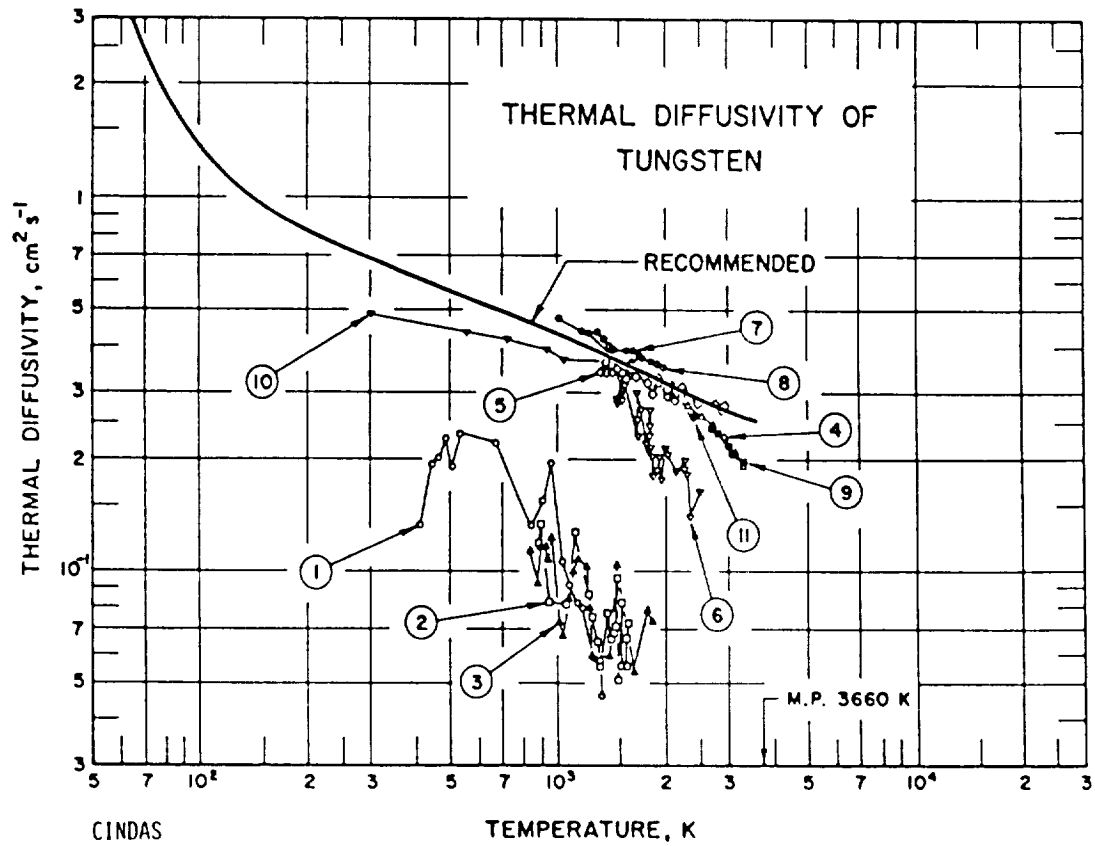


Figure 2. Experimental data and recommended values for the thermal diffusivity of tungsten.

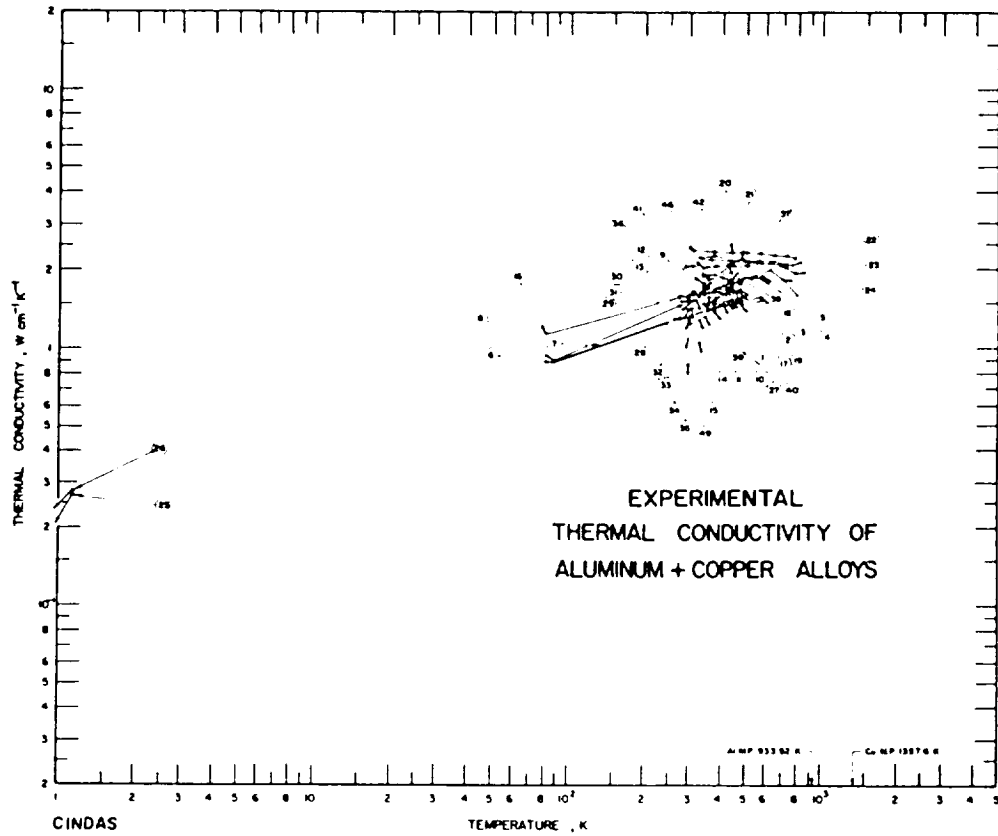


Figure 3. Experimental data on the thermal conductivity of aluminum + copper alloys.

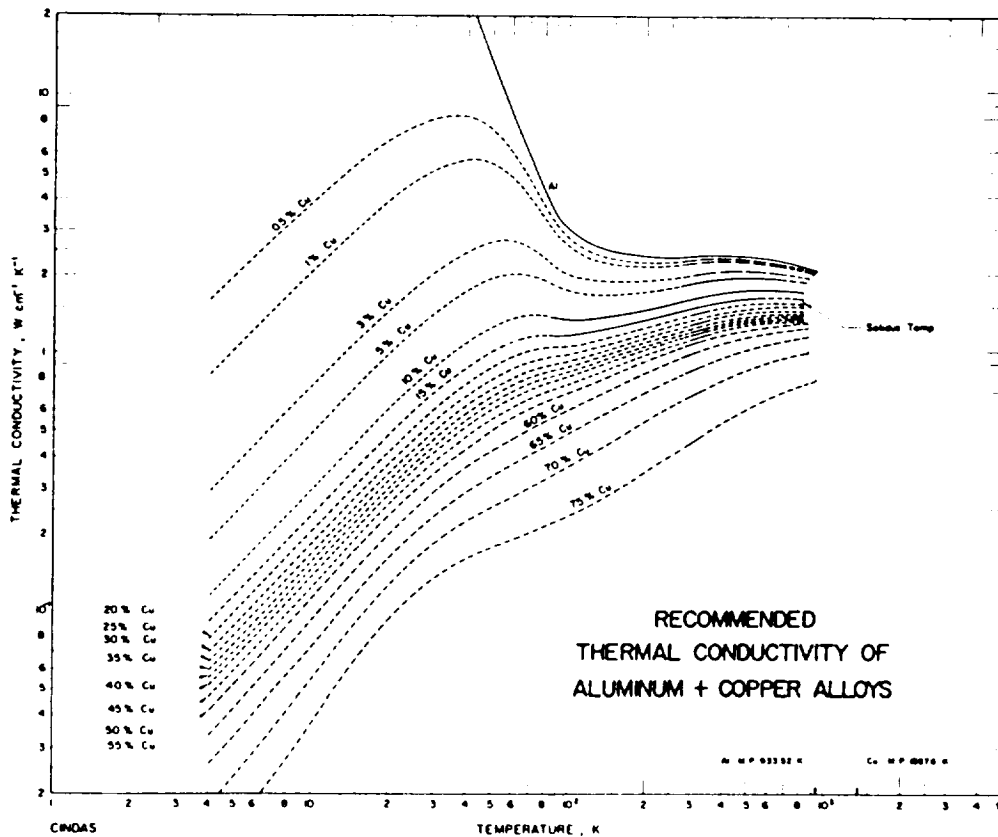


Figure 4. Recommended values for the thermal conductivity of aluminum + copper alloys.

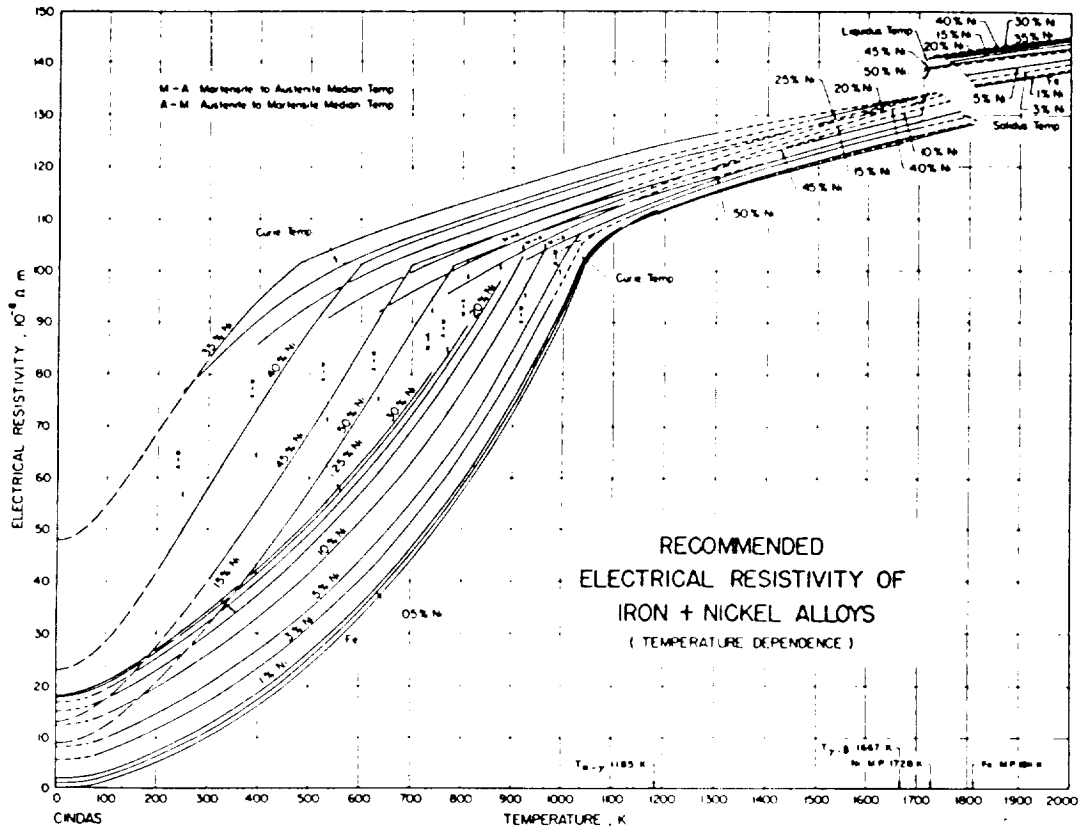


Figure 5. Recommended values for the electrical resistivity of iron + nickel alloys.

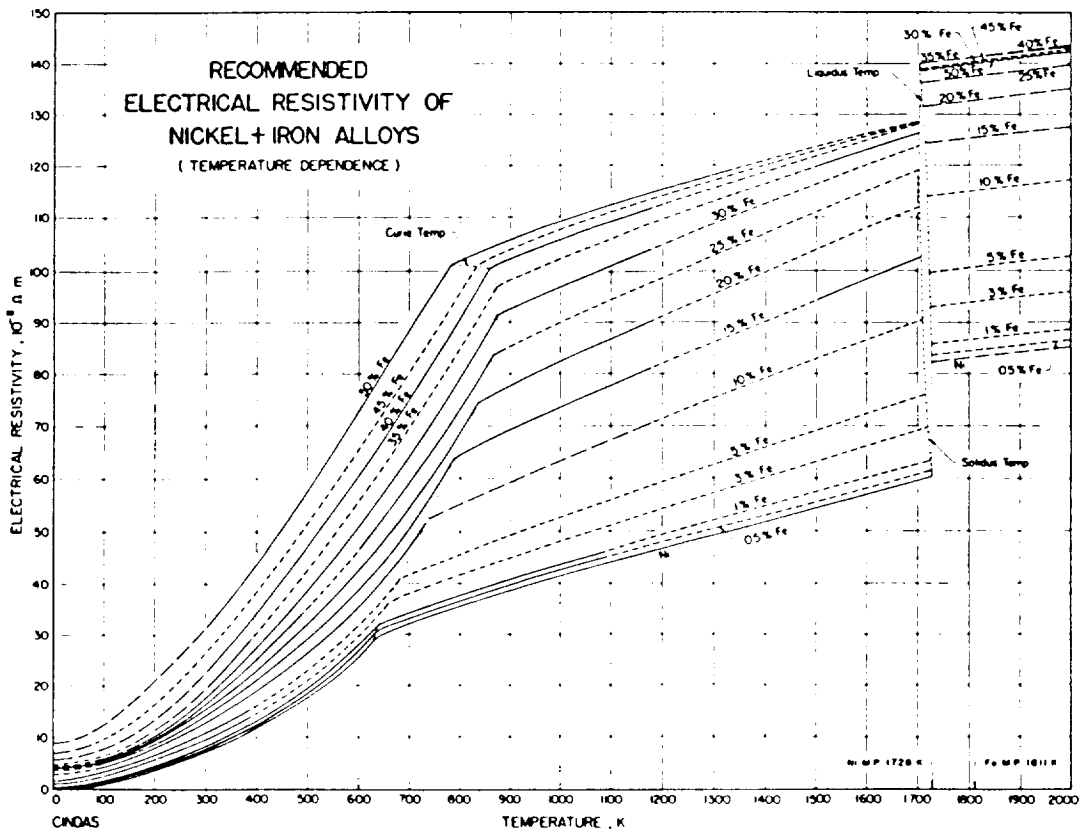


Figure 6. Recommended values for the electrical resistivity of nickel + iron alloys.

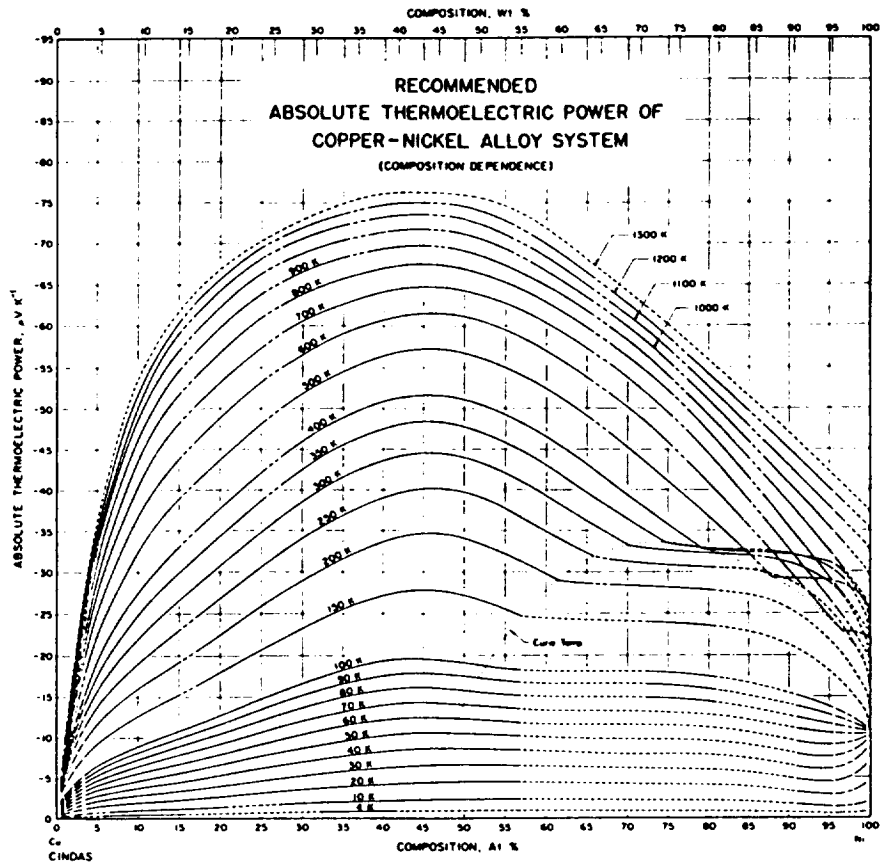


Figure 7. Recommended values for the absolute thermoelectric power of copper-nickel alloy system.

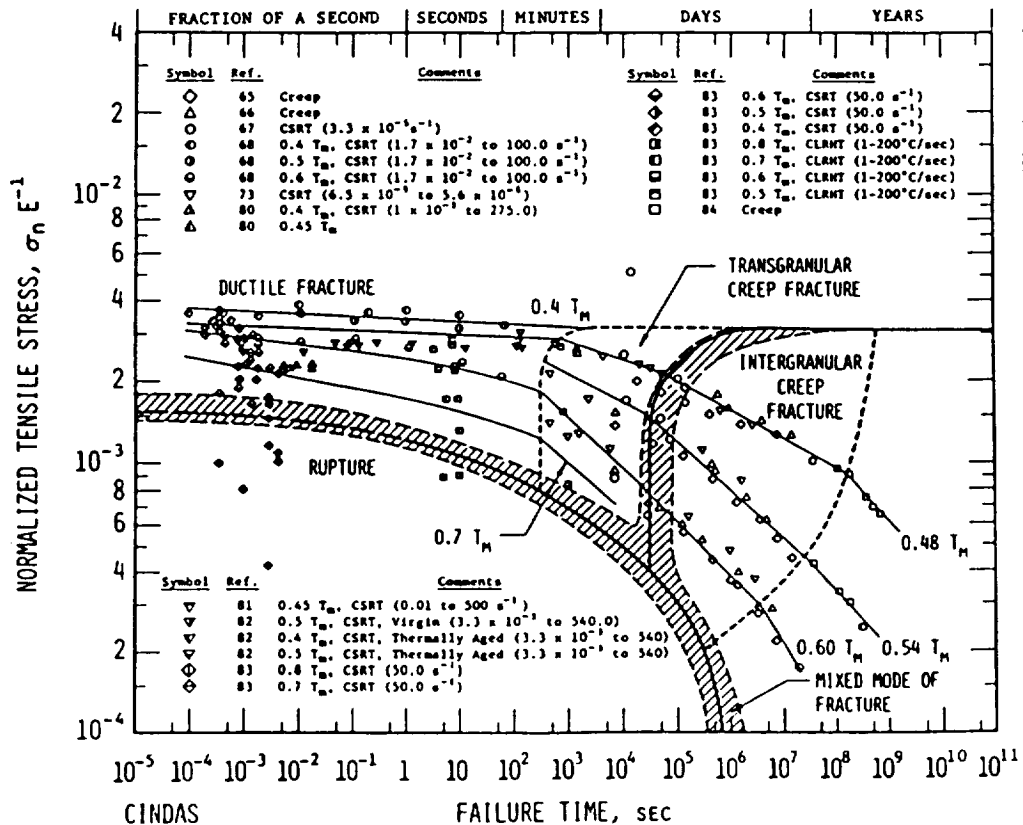


Figure 8. Stress-fracture map for 316 stainless steel extended to short-time domain.

As mentioned before, our critically evaluated reference data (recommended values) as well as the experimental data compiled from worldwide literature are all stored in the various databases.

Contents of the Materials Properties Numerical Database System

This database system contains a number of numerical databases. Major databases that have been developed at CINDAS are briefly discussed below.

1. High Temperature Materials Properties Database

This database is developed by the DoD High Temperature Materials - Mechanical, Electronic and Thermophysical Properties Information Analysis Center (HTMIAC), which is operated by CINDAS for the U.S. Department of Defense (DoD) under the sponsorship of the Office of the Undersecretary of Defense Research and Engineering. So far this database contains about 12,000 sets of data on the thermophysical, thermoradiative, optical, electronic, and mechanical properties of aerospace structural composites and metals and infrared detector/sensor materials (about 82% of the data are extracted from worldwide open literature and unclassified, unlimited-distribution U.S. Government reports). All the data in this database have been computerized.

These 12,000 sets of data cover 280 varieties of aerospace structural composites (including 32 varieties of carbon/carbon composites, 63 varieties of carbon/phenolic composites, 16 varieties of fiberglass/epoxy composites, 9 varieties of graphite/bismaleimide composites, 118 varieties of graphite/epoxy composites, 23 varieties of graphite/polyimide composites, 7 varieties of Kevlar/epoxy composites, and 12 varieties of silica/phenolic composites), 102 varieties of composite constituents, 120 varieties of aerospace structural alloys, and 53 varieties of infrared detector/sensor materials [2]. Additional aerospace structural materials and infrared detector/sensor materials will be covered in the future.

Since material property data are meaningful only if adequate information on the test material and on the property measurement is also provided, each set of data in our database consists of numerical data points (as a function of temperature and/or other independent variable) and pertinent information on the specification and characterization of the test material and on the method and conditions of the property measurement, such as composition, purity, density, porosity, microstructure, material construction configuration, material processing, sample preparation, specimen geometry and dimensions, material history, heat treatment, cold working, surface condition, producer, supplier, method of measurement, test environment, heat flow direction, heating rate, heat-up time, heat-up temperature, holding time at temperature, type of heat source, and loading rate, insofar as these are contained in the original document.

As an example to show the data and information stored in this computerized database, one set of data on the thermal linear expansion along a specific direction of a particular sample of Hercules AS/3501-6 graphite/epoxy composite is shown in Table I.

The compiled experimental data for selected priority materials and properties have been and are being critically evaluated and analyzed to generate recommended values, which are also included in the database. Furthermore, in order to support the DoD high energy laser community for their studies of the effects of lasers on materials, structures, and detectors as well as for the vulnerability, survivability, and hardening assessments, we have been generating high temperature, high heating rate,

Table I. Example of One Set of Data on the Thermal Linear Expansion of a Particular Sample of Hercules AS/3501-6 Graphite/Epoxy Composite along a Specific Direction in the High Temperature Materials Properties Database

MATERIAL: HERCULES AS/HERCULES 3501-6 HTMIAC/CINDAS
PROPERTY: THERMAL LINEAR EXPANSION DATA SET 1

COMPOSITION :

65.0	WEIGHT PERCENT	HERCULES MAGNAMITE AS GRAPHITE FIBER
35.0	WEIGHT PERCENT	HERCULES 3501-6 EPOXY

SUPPLIER/PRODUCER/FABRICATOR :
PREPREG TAPES FROM HERCULES, INC.

COMPOSITE MATERIAL ARCHITECTURE, FIBER DESCRIPTION :
REINFORCEMENT ARCHITECTURE : 2D (0)
NUMBER OF PLYS : 5

PROCESSING HISTORY, MATRIX DESCRIPTION :
CURING/DENSIFICATION SEQUENCE :
PREPEG TAPE CUT TO SIZE AND 5 PLYS LAID UP BY HAND TO PROPER DIMENSIONS OF 12 INCH X 24 INCH X 0.025 INCH ON RELEASE-AGENT COATED STAINLESS STEEL PLATE; ON THE TOP WERE PLACED IN ORDER, A LAYER OF RELEASE CLOTH, A LAYER OF OPEN CELL FOAM/RANDOM FIBER BLEEDER CLOTH, AND A LAYER OF POLYETHYLENE FILM; ENTIRE UNIT WAS PLACED IN BLANKET PRESS AND CURED.
CURED AT 100 C FOR ONE HOUR, AND AT 177 C FOR THREE HOURS.

ADDITIONAL PREPARATION/CONDITIONING :
ADDITIONAL CONDITIONING/PREPARATION : MOISTURE
DESCRIPTORS-TEXTUAL :
MOISTURE CONDITIONED AT 98 PERCENT RELATIVE HUMIDITY FOR 30 DAYS AT 65.5 C (1.69 PERCENT AVERAGE MOISTURE CONTENT).

SPECIMEN IDENTIFICATION :
DIMENSIONS (GEOMETRY) :

LENGTH	57.2	MM
WIDTH	6.35	MM

ORIENTATION WITH RESPECT TO MATERIAL : INTERLAMINAR, THROUGH THICKNESS

MEASUREMENT/EVALUATION METHOD :
NAME/DESCRIPTION :
QUARTZ DILATOMETER EMPLOYING DAYTRONIC MODEL DS200 LVDT.
MEASUREMENT ACCURACY WAS 0.0001 INCH WITH 0.1 PERCENT ERROR.
THE QUARTZ PUSH-ROD EXERTED A FORCE OF 9 GRAMS.

MEASURED/EVALUATED PROPERTIES :

X	: TEMPERATURE	K
Y	: THERMAL LINEAR EXPANSION	PERCENT

Table I (Continued)

DATA POINTS :

X	Y	REMARKS:
2.081E+02	-1.810E-01	SPECIMEN G4
2.306E+02	-1.350E-01	
2.673E+02	-6.990E-02	
2.868E+02	-3.110E-02	
3.135E+02	3.040E-02	
3.378E+02	7.380E-02	
3.638E+02	1.420E-01	
2.086E+02	-1.900E-01	SPECIMEN G5
2.306E+02	-1.420E-01	
2.673E+02	-8.960E-02	
2.861E+02	-3.490E-02	
3.140E+02	3.650E-02	
3.376E+02	1.000E-01	
3.644E+02	1.590E-01	
2.081E+02	-1.740E-01	SPECIMEN G6
2.299E+02	-1.320E-01	
2.673E+02	-8.050E-02	
2.868E+02	-2.960E-02	
2.980E+02	-7.000E-04	
3.140E+02	4.260E-02	
3.378E+02	8.900E-02	
3.644E+02	1.510E-01	
2.031E+02	-1.880E-01	SMOOTH VALUES (1.87 PERCENT MOISTURE)
2.231E+02	-1.580E-01	
2.431E+02	-1.250E-01	
2.631E+02	-8.700E-02	
2.731E+02	-6.700E-02	
2.831E+02	-4.700E-02	
3.031E+02	-2.000E-03	
3.231E+02	4.600E-02	
3.431E+02	9.800E-02	
3.631E+02	1.540E-01	

DATA -- COMMENTS :

AVERAGE MOISTURE CONTENT WAS 1.69 PERCENT FOR THE MEASURED DATA, AND WAS 1.87 PERCENT FOR VALUES OBTAINED FROM A POLYNOMIAL FIT. THERMAL LINEAR EXPANSION (TLE) = $-6.745E-02 + 2.047E-03T + 4.546E-08T^2$ FOR TLE IN PERCENT AND T IN CELSIUS.

REFERENCE:

MOISTURE AND THERMAL EXPANSION OF COMPOSITE MATERIALS.
 CAIRNS, D. S. AND ADAMS, D. F.
 UNIV. WYOMING, MECH. ENG. DEPT. REPT. UWME-DR-101-104-1
 204 PP., 1981.
 (AD-A109 131, ARO-16370.5-MS)

and/or high strain rate data through analysis, correlation, synthesis, and extrapolation of the available experimental data for moderate temperatures, low heating rates, and/or low strain rates, and through theoretical estimation based on our knowledge gained by intensive studies of the effects of high heating rates and high strain rates on material properties. All these efforts add much value to the existing data and greatly enhance this database.

The properties covered by this database are listed below:

(A) Thermophysical, thermoradiative, optical, and electronic properties:

- (1) Ablation energy
- (2) Ablation temperature
- (3) Absorptance
- (4) Absorption coefficient
- (5) Boiling point
- (6) Density
- (7) Electrical resistivity
- (8) Emittance
- (9) Heat capacity
- (10) Heat of fusion
- (11) Heat of vaporization
- (12) Melting point
- (13) Reflectance
- (14) Refractive index
- (15) Thermal conductivity
- (16) Thermal diffusivity
- (17) Thermal linear expansion
- (18) Transmittance

(B) Mechanical properties:

- (1) Compressive modulus
- (2) Compressive strain at fracture
- (3) Compressive strength, ultimate
- (4) Compressive strength, yield
- (5) Elastic constants
- (6) Elongation
- (7) Energy release rate
- (8) Flexural modulus
- (9) Flexural strength
- (10) Fracture toughness
- (11) Hardness
- (12) Impact energy
- (13) Poisson's ratio
- (14) Reduction in area
- (15) Shear modulus
- (16) Shear modulus, in-plane
- (17) Shear strain at fracture
- (18) Shear strength, in-plane
- (19) Shear strength, interlaminar
- (20) Shear strength, ultimate
- (21) Shear strength, yield
- (22) Stress-strain curves, compression
- (23) Stress-strain curves, shear
- (24) Stress-strain curves, tension
- (25) Tensile modulus
- (26) Tensile strain at fracture

- (27) Tensile strength, ultimate
- (28) Tensile strength, yield

This database is continually being updated and expanded by HTMIAC/CINDAS.

2. Engineering Materials Properties Database

This database has been developed by CINDAS since 1957 through multiple supports of DoD, other Government Agencies, numerous industrial organizations, research institutes and foundations, professional societies, and Purdue University. It contains approximately 100,000 sets of data on the following properties of more than 7,000 materials*:

(A) Thermophysical and thermoradiative properties:

- (1) Accommodation coefficient
- (2) Prandtl number
- (3) Solar absorptance to hemispherical total emittance ratio
- (4) Specific heat
- (5) Thermal absorptance
- (6) Thermal conductivity
- (7) Thermal diffusivity
- (8) Thermal emittance
- (9) Thermal linear expansion
- (10) Thermal reflectance
- (11) Thermal transmittance
- (12) Thermal volumetric expansion
- (13) Viscosity

(B) Electronic, electrical, magnetic, and optical properties:

- (1) Absorption coefficient
- (2) Dielectric constant
- (3) Dielectric strength
- (4) Electrical resistivity
- (5) Hall coefficient
- (6) Magnetic susceptibility
- (7) Refractive index
- (8) Thermoelectric properties
- (9) Work function

The mechanical properties of selected alloys are also covered.

The over 7,000 selected materials covered in this database are from the following groups of materials:

- (1) Metallic elements
- (2) Graphites and nonmetallic elements
- (3) Ferrous alloys (15 groups)
- (4) Nonferrous alloys (41 groups)
- (5) Intermetallic compounds
- (6) Inorganic compounds
- (7) Organic compounds
- (8) Ceramics
- (9) Cermets

*It should be understood that the number of properties covered by the available data for each of the materials varies greatly, ranging from almost all to only few of the properties listed.

- (10) Glasses
- (11) Polymers
- (12) Composites
- (13) Applied coatings
- (14) Systems
- (15) Insulations
- (16) Fabrics
- (17) Natural substances
- (18) Biological materials

However, only a small portion of the data in this database have been computerized and the remaining major portion of the data are yet to be computerized.

In addition to experimental data extracted and compiled from worldwide scientific and technical literature, this database contains also many thousands of evaluated data sets (sets of recommended values).

3. EPRI Database on Dielectric Materials

This database is developed by CINDAS under the sponsorship of the Electric Power Research Institute (EPRI) [3]. It is to serve as a centralized source of technical, commercial, and applications data on dielectric materials, and to disseminate such data directly to the fingertips of engineers, scientists, designers, researchers, etc. through computer terminals across the nation.

The database contains data and information on the following properties (or information items) of electrical insulating liquids, solids, gases, and combinations thereof:

- (1) Electrical properties
- (2) Physical properties
- (3) Chemical properties
- (4) Thermal properties
- (5) Optical and thermoradiative properties
- (6) Mechanical properties
- (7) Flammability properties
- (8) Aging and degradation information
- (9) Health hazard and environmental effects
- (10) Processability and manufacturing information
- (11) Recommended applications
- (12) Producer, supplier, and availability information
- (13) Price range and other commercial information

This database is fully computerized and on-line operational. It covers so far 371 dielectric liquids, 1,120 dielectric solids, 12 dielectric gases, 271 properties, and 76 independent variables.

Although the establishment of this database is for the benefit of the electric power industry, its manufacturers and suppliers, and the dielectric research and development community, data on dielectric materials are very much needed in many other areas of applications, such as in the field of nuclear fusion and in high voltage dc and pulsed power applications in advanced weapons systems and electronic military hardware (such as high power laser weapons).

4. Thermophysical Properties Database on Fluids

This database is fully computerized and contains data and information on 13 properties of some 300 fluids.

Thermophysical properties of fluids are important for all applications involving heat, mass, and/or momentum transfer using fluid as a medium, including also military applications such as the design of engine cooling systems, lubricating systems, fuel systems, and combustion and exhaust systems of military vehicles, tanks, airplanes, warships, etc.

5. Thermophysical and Mechanical Properties Database on Rocks and Minerals

This database contains data and information on the mechanical, thermophysical, electrical, magnetic, and optical properties of 155 types of rocks and 293 minerals.

The data and information on the properties of rocks and minerals are important for various applications such as in the site selection, design, and construction of underground nuclear waste disposal facilities, hardened missile silos, nuclear test sites, underground power plants, and deep underground defense facilities. In the geosciences, such data are important for the calculation of accurate values for heat flow in the earth's crust, which are needed to obtain a better understanding of the earth's history and its current makeup. Rock property data are also needed for the evaluation of the theories on sea floor spreading and plate tectonics in addition to supplying details for the substantial deep sea rock coring program. Geothermal power generation techniques and earthquake prediction analysis both depend to some degree on thermophysical properties and heat flow of rock masses.

6. SRC Packaging Materials Database

This database is being developed by CINDAS under the sponsorship of the Semiconductor Research Corporation (SRC). It covers the thermal, electrical, physical, mechanical, and other properties of selected semiconductors, metals, alloys, nonmetallic elements, ceramics, inorganic compounds, epoxies, plastics, composites, and fluids.

This database is intended to serve the microelectronic packaging needs of the semiconductor/electronics industry for comprehensive, reliable data on packaging materials.

References

1. C. Y. Ho and Y. S. Touloukian, "Critical Evaluation, Correlation, Analysis, and Synthesis of Thermophysical, Electrical, Thermoelectric, and Optical Properties Data," in Proceedings of the Eighth Symposium on Thermophysical Properties (J. V. Sengers, ed.), Vol. 2 (New York, NY: American Society of Mechanical Engineers, 1982), 419-430.
2. C. Y. Ho and R. H. Bogaard, "Materials, Properties, Parameters, and Independent Variables Covered in HTMIAC's Computerized High Temperature Materials Properties Data Base," (HTMIAC Report 4, DOD High Temperature Materials Information Analysis Center, Purdue University, 1986).
3. C. Y. Ho, H. H. Li, and Nirmal Singh, "Establishment of a Computerized Comprehensive On-Line Intelligent Data Base on Dielectric Materials," in Proceedings of the 17th Electrical/Electronics Insulation Conference (New York, NY: The Institute of Electrical and Electronics Engineers, Inc., 1985), 230-236.

SECTION 4

SPLINTER SESSION TECHNICAL PAPERS

An Update of Commercial Infrared Sensing and
Imaging Instruments

Herbert Kaplan

Honeyhill Technical Company
193 East Avenue, Norwalk, Connecticut, 06855

Abstract

This paper will begin with a classification of infrared sensing instruments by type and application, listing commercially available instruments, from single point thermal probes, to on-line control sensors, to high speed, high resolution imaging systems.

A review of performance specifications will follow, along with a discussion of typical thermographic display approaches utilized by various imager manufacturers.

The paper will conclude with an update report on new instruments, new display techniques and newly introduced features of existing instruments.

Classification of Instruments

Infrared sensing instruments are traditionally classified into three categories:

- A. Spot Measuring
- B. Line Scanning
- C. Thermographic (Two Dimensional Scanning)

Spot measuring devices collect radiant energy from a spot or area on a target surface and provide an indication of radiance, or infer a temperature based on the energy from that spot which produces an electrical response from the instrument's detector. Line scanning instruments provide an output, generally an analog trace, of the radiant energy (or, in ideal cases, temperature) distribution along a single straight line projection from the target surface. Thermographic instruments provide an image of the energy distribution over a scanned area on the target surface. This is presented in the form of an intensity-modulated black and white picture or a synthesized color display.

Categories A. and C. can be further divided into three groups each and this paper will review commercially available instruments along the line of this further breakdown:

- A. Spot Measuring
 - 1. Probes
 - 2. Portable Hand-held
 - 3. On-line (Monitoring and Control)
- B. Line Scanning
- C. Thermographic
 - 1. Thermal Viewers
 - 2. Pyrovidicon Imagers
 - 3. Thermal Raster Scanners (Imaging Radiometers)

Instrument Manufacturers

Particularly in Category A. there are many companies offering the same instrument under different private label arrangements. In order to avoid duplication, only the original manufacturer or prime distributor will be listed wherever possible.

The charts of Table 1. provide a tabulation of all instruments known to the author on which descriptive literature was available at the time of preparation of this paper. Table 2. is a listing of current addresses and phone numbers of equipment manufacturers listed in Table 1. Table 3. is reprinted from paper 371-01 (H. Kaplan, Thermosense V) and summarizes proven industrial applications for thermal sensing and imaging instruments. The following discussions will highlight the applications for which each instrument category and group is particularly suited based on configuration or performance characteristics.

Discussion of Instruments

A. Spot Measuring

1. Probes

Temperature probes are the most recent addition to the spot measuring category. They are characterized by low price (from \$350 to \$1,000), pocket-portability and wide collecting angle. They are battery powered and are generally optically pre-adjusted for minimum spot size at short working distance; a 1/4" spot at a 3/4" working distance is typical. Some models are designed to operate into a conventional multimeter and some incorporate their own readout box with an LCD display. They usually feature disposable batteries and some models have AC adapters. Temperature ranges are from about zero F., or slightly below, to +600°F. and a sensitivity of 1°F is easily achieved. Emissivity adjustments are available on some models.

Probes are ideal for close-up measurements and find applications in circuit board analysis, trouble shooting of electrical connections, inspection of plumbing systems and, most recently, application to biological and medical studies.

2. Portable Hand-held

With few exceptions these instruments are pistol-shaped and designed for middle distance measurements. They are usually optically preadjusted for infinity focus. A typical 2 degree field of view resolves a 3" spot at a 60" working distance and a 1' spot at a 30' working distance. Prices range from about \$500 to more than \$3,500. Sighting and aiming methods vary from simple aiming notches to enclosed illuminated reticles. There are instruments with extremely narrow fields of view (0.5°) that include a rifle stock and telescopic sight. Most instruments in this group incorporate emissivity adjustments and some include microcomputers with limited memory. Most are available with a recorder output, although this feature is seldom used. A meter is always provided and, with one exception that reads in BTU/Sq.Ft./Hr., the readout is always in temperature units. Analog displays are still available, although decreasing in popularity. Digital readouts featuring LED's were first introduced about 12 years ago, but the LCD display, introduced more recently, is more in demand, mainly because its tiny power drain extends battery life. For this reason the more recent instruments offer replaceable rather than rechargeable batteries and battery life approaches one year. Some

instruments in this group have zeroing adjustments, but all of the newer instruments include auto-zeroing features. Temperature ranges are, typically, from -20 to 2000°F. Temperature sensitivity and readability are usually 1° (F or C) or 1% of scale, although sensitivities on the order of 0.1°F are achievable.

This instrument group is particularly suited to applications where spot checking of target temperatures is sufficient and continuous monitoring is not required. A typical use would be for periodic maintenance checks of rotating machinery to detect whether or not bearings are beginning to overheat. These instruments, over the past few years, have become an important part of many plant energy conservation programs, but are equally useful in checking mix temperatures of food products, cosmetics and industrial solvents. Although many of these instruments provide extremely accurate readings, this feature, like the recorder output, is less important to the user than repeatability, ruggedness, portability, reliability and ease of use.

3. On-line (Monitoring and Control)

The one feature that distinguishes this instrument group from the others is dedicated use. The instrument is generally mounted where it can measure the temperature of one specific target, and remains there for the life of the instrument or the process. With few exceptions, these instruments operate on line power. The output signal of the instrument can be observed on a meter, used to operate a switch or relay, feed a simple or sophisticated process control loop, or be used in any combination of these functions.

Early on-line instruments consisted of an optical sensing head and an electronics/control readout unit at the other end of an interconnecting cable. This configuration still exists to some extent, but most of the newer units feature sensing heads that are more stable electronically, and hence more independent of the remote control units. The trend is for these new sensors to mate with universal indicator/control units that accept inputs from various types of industrial sensors.

Because this instrument group is selected to perform a specific task, a "Shopping List" format is provided the customer by the manufacturer in order that all required features can be purchased.

Manufacturers offer sensing head features such as variable or fixed focus, sighting tubes, "light pipes", water-coolable housings, air purge fittings, air curtain devices and see-thru aiming with target-defining reticles. The "Shopping List" for the indicator/controller unit might include digital readout, BCD output, analog output, single, double, or proportional set point, rate signals, sample and hold, peak or valley sensor and datalogger interface. Emissivity controls, located in a prominent place on a general purpose instrument, are more likely to be located behind a bezel on the sensor on these dedicated units, where they are set one time and locked.

Spectral characteristics are worth mentioning separately, although, technically, they are part of the sensing head "Shopping List". The spectral interval over which the sensing head operates is selected to optimize the signal from the target, to reduce or eliminate the effect of an interfering energy source, or to enable the instrument to measure the surface temperature of thin films of material that are largely transparent to infrared energy. This last application has made these instruments important factors in the manufacture of thin film plastics and also of glass.

Two-color or "ratio" pyrometers are one special case of the on-line instrument. These are particularly useful in high temperature applications, in measuring small targets. The emittance of the target need not be known providing it is constant and reflections are controlled. The target need not fill the field of view providing the background is cool, constant and uniform. Also, impurities in the optical path resulting in broad band absorption do not effect the measurement, since the measurement is based on the ratio of energy in two spectral bands.

Another special case is the fiber optic-coupled thermometer, where inaccessible targets can be measured by replacing the optic with a flexible or rigid fiber optic bundle. This, of course, limits the spectral performance, and hence the temperature range to the higher values, but it has allowed temperature measurements to be made when, previously, none were possible.

The infrared microscope is a third special case. This instrument is configured like a conventional microscope and, through the use of reflective microscope objectives and beam splitters, it enables the operator to simultaneously view and measure targets down to 0.0003" in diameter with an accuracy of about 0.5-F.

Most recently another special case known as the "laser pyrometer" has been introduced. This instrument uses the reflected energy of an active laser to measure target reflectance. A built-in microcomputer calculates target emittance and uses this to provide a corrected "true temperature" reading. The laser pyrometer is useful for high temperature diffuse target surfaces.

Prices of instruments in the on-line control instrument group vary from about \$1,000 for an "infrared switch", to more than \$13,000 for infrared microscopes and on-line instruments equipped with many control features. Generally speaking, the price goes up when sensitivity, small spot size and speed of response are all required, and, of course, when many "Shopping List" items are added.

B. Line Scanners

The purpose of spatial scanning is to derive information concerning the distribution of radiant energy over a target scene. Quite often a single straight line scanned on the target is all that is necessary to locate a critical thermal anomaly. The instantaneous position of the scanning element is usually controlled or sensed by an encoder or potentiometer so that the radiometric output signal can be accompanied by a position signal output and be displayed on a chart recorder, an oscilloscope or some other recording device. All commercially available single line scanners scan in object space so that wide angle scanning can be accomplished. Probably the first approach to line scanning adopted commercially was in an aerial-type thermal mapper in which the line scanner was mounted on a moving vehicle and scanned lines normal to the direction of motion. The outputs representing these individual scan lines were intensity-modulated and serially displayed in shades of gray on a strip map, representing the thermal map of the surface being overflown by the vehicle.

A portable line scanner, widely used commercially, scans a single line on target, develops a visible "temperature trace" using light emitting diodes and, by means of optical beam splitting techniques, superimposes this trace over the visible scene viewed by the operator. The operator selects the line to be scanned by aiming the instrument's horizontal center line. Photorecording of the composite scene is accomplished by aiming a conventional instant color camera through the eyepiece of the scanner. This instrument has no recorder output and is, therefore, not suitable for process control applications. Unlike most thermal viewers, however, (see next section) absolute temperatures are obtainable with this device. Good applications for this line scanner include electrical switchgear and transmission lines, plumbing systems troubleshooting and web process profiling.

A more modern, high speed commercial scanner develops a high resolution thermal map by scanning normal to the motion of a moving target such as paper web or a strip steel process. The output signal information is in real-time computer compatible format and can be used to monitor, control or predict the behavior of the target. The best applications for this scanner are in on-line real-time process monitoring and control.

C. Thermographic

An important advantage of radiation thermometers over contact thermometers is their speed of response. The measured energy travels from the target to the sensor at the speed of light. The response of the instrument can then be in milliseconds or even microseconds. This important feature has allowed the field of infrared radiation thermometry to expand into real time thermal scanning and thermal mapping. When problems in temperature monitoring and control cannot be solved by the measurement of one or several discrete points on a target surface it becomes necessary to spatially scan, that is to move the collecting beam (instantaneous field of view) of the instrument relative to the target. This can be done by moving the target with the instrument fixed or by moving (translating or panning) the instrument, but is more practically accomplished by inserting movable optical elements into the collected beam.

The purpose of spatial scanning is to derive information concerning the distribution of infrared radiant energy over a target scene. The detector output is intensity-modulated in proportion to the total exitant radiant energy at each point so scanned on the target surface, and the image produced is presented in monochrome or color where the gray shades or color hue are intended to represent a thermal level at the target surface. These thermal images are called *thermograms*.

Although an almost infinite variety of scanning patterns can be generated using two moving elements, the most common pattern is rectilinear, and this is most often accomplished by two elements each scanning a line normal to the other. A typical rectilinear scanner employs two rotating prisms behind the primary lens system (refractive scanning). An alternate approach to scanning uses two oscillating mirrors behind the primary lens (reflective scanning). This is also commonly used in commercially available scanners, as are combinations of reflective and refractive scanning elements. Another approach to thermal imaging is the pyrovidicon, or thermal video system, where scanning is accomplished electronically. Both rectilinear and electronic scanners will be discussed.

Classification of thermographic (thermal imaging) instruments

Commercial thermal imaging systems fall into three categories as follows:

1. Thermal viewers
2. Pyrovidicon imagers
3. Thermographic raster scanners (imaging radiometers)

The charts of Table 1. provide a listing of all instruments known to the author on which descriptive literature was available at the time of preparation of this paper. Table 2. is a listing of current addresses and phone numbers of equipment manufacturers listed in Table 1. Table 3. summarizes proven industrial applications for thermal imaging instruments. The following discussions will highlight the applications for which each instrument category and group is particularly suited based on configuration or performance characteristics.

Discussion of instruments

1. Thermal viewers

Thermal viewers are inexpensive (\$10,000 to \$14,000) battery powered scanning instruments producing a qualitative image of the (thermally associated) radiant exitance distribution over the surface of a target. The battery packs are rechargeable and usually provide 2-3 hours of continuous operation. These are one piece, lightweight instruments designed to be simple to operate. The first thermal viewers required cryogenic cooling of the detector elements accomplished by means of a small tank of compressed argon. Newer units feature thermoelectric detector cooling provided by a battery powered cooler.

Thermal viewers were not designed for absolute temperature measurements, but they can demonstrably sense temperature differences of tenths of degrees. Some manufacturers have modified thermal viewers and introduced absolute temperature references so that absolute measurements are possible in certain applications. This generally requires an additional box, however, and diminishes the portability that defines the instrument group. (It also increases the price). Thermal viewers operate most effectively with cooler targets (0-200°F.) but, through the use of optical attenuators, they can be used for targets up to 2000°F. Typically, the area scanned (field of view) of thermal imagers is from 6 to 8 degrees high and from 12 to 18 degrees wide, with spatial resolution (instantaneous spot size) of 2 milliradians (0.1" at 5 feet). A hard copy of the thermal image is acquired by through-the-eyepiece recording using either conventional or Polaroid film.

Applications for thermal viewers fall into virtually all the areas listed in Table 3. but are limited to those in which the temperature measurements are not critical and recording quality need not be optimum. The combination of a thermal viewer (to locate thermal anomalies) and a hand-held thermometer (to quantify them) is a powerful and cost-effective one. Thermal viewers are particularly useful industrially in tight spaces or, conversely, when a sizable area must be traversed and user fatigue becomes a factor.

2. Pyrovidicon imagers

Pyrovidicon imaging systems are not unlike home videorecording systems except that the camera tube is a pyroelectric vidicon (pyrovidicon) rather than a conventional vidicon, and records target radiation in the infrared rather than the visible spectrum. The significant difference is that the pyrovidicon has no dc response; that is, if the camera is not continuously panned over the target, or the collecting beam optically "chopped", the image fades from the screen. This behavior is caused by the fundamental photoelectric response characteristics of the detector material. Aside from the tube, which is rather costly, and the lens, which is generally germanium and also costly, these systems utilize commercially available television equipment and recording accessories. The price of a complete pyrovidicon recording system is as low as \$13,000.

By comparison with other infrared imaging systems, the picture quality and resolution are good, approaching conventional TV format. The thermal image can be viewed or videotaped with equal convenience, and no cooling is required. The requirement for continuous target panning can be made less objectionable by the ability to play back an image and freeze the frame for detailed image inspection. Mechanical "chopper" options are offered by most instrument manufacturers, but, except for the very costly "synchronous choppers", they degrade image quality and thermal resolution. Pyrovidicon systems do not offer absolute measurement capability, but a thermal profile feature, available on some units, provides an analog of the center scan line displayed to the side of the image. Also, one manufacturer offers a model in which a spot measuring sensor is boresighted with the scanner and its measurement is superimposed on the video display along with a defining reticle in the center of the display. Thermal resolution of these instruments is between 0.2 and 0.4 F. in panned mode and double that (half as good) in "chopped" mode.

Pyrovidicon systems are particularly suited to moving targets, airborne scanning and distant measurements. They operate well in the 8-14 micron atmospheric transmission window. They are susceptible to momentary loss of sensitivity from saturation phenomena known as "depoling" when suddenly aimed at very hot targets with the aperture improperly open, and the automatic repoling circuits require about a 30 second restoration time, resulting in some operator inconvenience. Operating costs are very low since no coolant is required and common, erasable videocassettes are used for recording purposes. Videotapes can be monitored on conventional television receivers.

3. Thermographic raster scanners (imaging radiometers)

Thermographic scanners (also called imaging radiometers) constitute the "top-of-the-line" of commercial thermographic instruments. They provide potentially quantitative temperature measuring capability and high resolution image quality. Cryogenic detector cooling is often required and this is usually done with liquid nitrogen. Most commercially available thermographic scanners use a single detector but some manufacturers offer dual-detector or multidetector instruments. Some multielement systems are offered at a premium price, for special applications such as high resolution aerial mapping and search. These are commercial versions of military FLIR (forward-looking infrared) systems used in night vision and surveillance applications.

Thermographic scanners use refractive, reflective or hybrid scanning systems and operate in either the 3-5 or the 8-14 μ atmospheric window. In addition to quantitative temperature measuring capability in idealized circumstances, these instruments feature excellent capabilities for both spatial resolution (about 1 milliradian) and minimum resolvable temperature (0.05 to 0.1°C). Most manufacturers offer isotherm graphics features, spectral filtering, interchangeable optics for different total fields of view, color or black and white displays, flexible videorecording capabilities and computer compatibility. Most general purpose systems in use today feature compact, field-portable, battery-operable sensing heads and control/display units. A complete system, including battery and videorecorder can usually be handled by one person, by either mounting the components on a cart or assembling them on a personal harness arrangement. Some special purpose systems are not so configured. The Barnes CompuTherm, intended for the thermal examination of microcircuit chips and other small devices, is arranged in a bench type configuration. The Inframetrics IRAMS, the Hughes ThermaScan and the UTI 9000, designed for testing of printed circuit boards and similar targets, are also made to be integrated into a test bench with automatic test equipment.

Base prices range from \$20,000 to \$40,000 for basic field portable scanners and up to \$70,000 for special high resolution FLIR-type scanners (Commercial FLIR systems). The addition of computer based diagnostic software packages can increase the price to well in excess of \$100,000.

Recent trends

Several new features and new options have been touched upon in previous sections. The most recent of these will be highlighted in this section.

In the point sensing category, the probe sensor suitable for mating with a conventional multimeter was introduced by Linear Laboratories. Dickson and Testatemp offer similar units.

Telatemp and Everest offer laser and light beam aiming accessories similar to the feature offered by Mikron on some of its hand-held models. Several manufacturers added linearized outputs to their on-line units and more high quality modular sensors have become available. Several manufacturers offer reticle sighting with temperature display projected into the viewer. Microprocessors have been added to hand-held units, such as the Raytek PM series; these provide limited memory for on-site datalogging and "max, min, mean" storage.

Within the last few years many imports, specifically from Japan, have been introduced in the United States. Hand held thermometers by, Chico, Horiba and Optex are being distributed by various US manufacturers. Introduction of on-line control sensors from these manufacturers will probably follow.

In the thermographic category, pyrovidicon systems have come down slightly in price, reflecting the somewhat reduced costs of lenses and tubes. ISI has introduced models incorporating a built-in boresighted radiation thermometer and limited microprocessor-based diagnostics. Inframetrics recently offered their model 522L scanning radiometer at a new base price under \$20,000, which may compete effectively with the pyrovidicons. Early in 1986 the AGEMA 870, the first commercially-available non-cryogenically cooled thermographic scanner was introduced. This system uses a "SPRITE" type thermoelectrically-cooled detector operating at 195°K., and offers performance generally equivalent to other "top-of-the-line" scanners at about the same price. This is an important development in that it eliminates the most commonly encountered objection among users of thermographic scanners; that is, the need to frequently refill or recharge cryogenic devices and to have the necessary supplies on hand. Hughes Aircraft Company introduced the series 7000, a competitive thermoelectrically-cooled multidetector scanner, in 1987. It is reasonable to expect that, in the not-too-distant future, all thermographic scanners intended for field use will not require cryogenic cooling. The most recent entry, as of this writing, is the AGEMA 450, which is a "camcorder" type scanner with the sensing head (including thermoelectrically-cooled detector), control electronics and eyepiece video display integrated into a single shoulder-mounted unit.

Clearly the most dramatic recent development in the use of thermographic raster scanners has been the introduction of computer-assisted thermal image storage and processing, causing thermographic scanning to become a far more exact science and greatly expanding its usefulness. Innovative software has been tailored specifically for detailed image and thermal data analysis, and has been rapidly updated and expanded. This capability is generally offered separately from the basic scanning instrument, although some limited diagnostic software is usually included in the basic package for on-site analysis. Most software packages for thermographic image analysis and diagnostics offer features that include spot temperature readout, multiple X and Y analog traces, image shift, rotation and magnification, area analysis with histogram display, image averaging and filtering and permanent disk storage.

Perhaps the single most powerful feature of these new routines is the capability for archiving thermal images of acceptable components, assemblies and mechanisms, and using these stored images as models for comparison to subsequently produced items. Subtractive routines produce differential images illustrating the deviation of each pixel (picture element) from its corresponding model. Another powerful routine recently introduced by Barnes Engineering Division, EDO Corporation, is a spatial emittance determination and correction program which produces true surface temperature thermograms of microelectronics devices and other very small targets. To perform this function, the unpowered device is heated sequentially to two known, low level temperatures and the stored thermal images are used to allow the computer to calculate the emittance of the object space area viewed by each pixel. The device is then powered and the image produced is corrected, point-by-point, for the emittances previously computed.

There is great interest in applying this spatial emittance correction to larger targets such as printed circuit boards, where several military programs are concerned with infrared mass screening of printed circuit boards for gross faults at the depot level. The approach used is to archive a standard thermal profile of a known acceptable board, and use this as a model against which to compare the profile of a powered unit under test. Variations in component surface characteristics within acceptably small ranges of variation, and conformal coatings introduce some degree of uncertainty to the comparison and the resulting differential image. The difficulty in developing a reliable emittance matrix lies in achieving tight control over the temperature and temperature uniformity while heating a target of this size and in controlling component surface and coating.

Table 1. Instrument Characteristics

	Manufacturer Model (s)	Characteristics
A. Spot Measuring		
1. Probes		
Dickson	IB500	32-500°F., LCD display
Exergen	Microscanner	10-550°F., one piece with bar graph, no numerical display
Horiba	IT330	32-500°F., LCD display, emissivity control (e set)
Linear	C500, C600 series	0-600°F., C500 connects to a multimeter, C600 has LCD Box, e set, multiple models with various ranges
Testoterm	Pyroterm	50-700°F., LCD display, e set
2. Hand-held (use 9V disposable batteries unless indicated)		
Capintec	Thermohunter HB	-50 to 900°F., e set
Everest	Industratherm	Various models from -30 to +1000°F., LCD display, analog output, aiming light, peak Sampler, differential available. rechargeable battery
Ircon	Ultimax series	Various models, -58 to 5432°F., thru-lens sighting, variable focus, reticle display
Land	Cyclops series	High and low temperature (to 5500°F.), small targets, variable focus, reticle display
	Compac 3	Low temperature, -50 to 950°F., thru-lens sighting, fix-focus reticle display
Linear	TherMonitor	TherMonitor- -20 to +2000°F., F.-C. switch, LCD display, e set, peak-hold.
	ThermoFlow	ThermoFlow reads in BTU/sq.ft./hr., differential scale
Mikron	Model 90 series	Various Models from -50 to +5432°F., thru-lens sighting, reticle display, variable focus
	Model 80 series	Various models from -20 to 3180°F., analog & LCD displays, Options: aiming light, telescope, e set, various FOV's.
Pyrometer	InstaTherm	Various models from -30 to +1145°F, analog & LCD Displays, differential scale, audible seeker, analog output
Raytek	Raynger PM series	Various models from 0-1600°F., dual LCD display, hi-lo alarms BS-232/analog output, datalogger, max-min-mean, differential,
	Raynger II Plus	Various models from -20 to +5400°F. LCD displays, max-min-mean differential, thru-lens sighting; scope, 120:1 optics available

(continued)

Table 1. Instrument Characteristics (continued)

	Manufacturer Model (s)	Characteristics
A. <u>Spot Measuring</u> (continued)		
2. <u>Hand-held</u> (continued)		
Telatemp	Models 43&44	Various Models from 0 to 1000°F., Rechargeable Battery, e set, LED Display. laser aiming & scope available
Wahl	Heat Spy Series DHS	Various Models from -40 to +3100°F., analog, LED, LCD display e set, peak-hold, various FOV's including telescopic.
Williamson	600, Viewtemp, Truetemp	Viewtemp is 75-3000°F.,LED inside reticle, e set, rechargeable battery; Truetemp is 2-color, 1500-4000°F., Model 600 has analog display, various Ranges from 75-3000°F.
3. <u>On-line</u>		
Barnes	RM2	Infrared microscope - spot size down to 0.0003".
Capintec	Hotshot, Bedeye Ratioscope 1400,1500,1700	3 Models of 2-color from 300-6500°F., various other models from -60 to +4500°F.,spectral selection
E ³ Technology	Heat Switch 100 &300, Pulsar II Nova	Infrared Pulse Switches, 2 Models of on-line units, ranges from 32 to 3000°F.
Everest	2000,3000 series 4000 series	Ranges from -30 to +3000°F., spot size available down to 0.010" Multiplex up to 8 heads thru electronics
Ircon	Modline 4 series Modline Plus and Mirage series Maxline series Temprox switch and Series 1100	Various models and accessories, 0-2500°F.,integrated, fix-focus, 2 wire transmitters, spectral selection Various models, 2 piece, 0-6500°F.,thru-lens sighting, LCD display, spectral selection Various models, 2 piece, 0-6500°F.,thru-lens sighting, LCD display, spectral selection, plus control and output options IR Pulse switches, fiber optic-coupled head available
Irtronics	Argosy, Citation Spartan, others	Various ranges from 30-4100°F., spectral selection, telephoto fiber optic-coupled heads available.
Land	Systems 1,2,& 3	120-4000°F., 2 color, spectral selection, telephoto lens option., modular, many accessories
Linear	TN1000 series M series	Modular sensors, ranges from 0-2732°F.,thru-lens sighting, spectral selection,linearized outputs,control options available. Low cost modular sensors, many control options available

Table 1. Instrument Characteristics (continued)

	Manufacturer Model (s)	Characteristics
A. <u>Spot Measuring</u> (continued)		
3. <u>On-line</u> (continued)		
Mikron	M67/68S series M210/210S series M500 M77/78	Modular, Ranges from 0-3000°F., spectral selection, fixed and variable focus, thru-lens sighting, many accessories 2 piece, 0-5400°F., spectral selection, fixed and variable focus, thru-lens sighting, many accessories Small, low cost, 2 piece, various models 0-500°F. M77 is 2 color, M78 is fiber-optic coupled
Pyrometer	Optitherm II Optitherm 87 Pyrolaser Laser Pyrometer	Integrated head, various ranges, spectral selection (s.s.). 2-piece, thru-lens sighting, telephoto lenses, s.s. var.rnges. 1100-2730°F., uses laser to measure reflectance, thru-lens sighting, rechargeable battery
Quantum Logic	Model 1300 Laser Pyrometer	1475-5500°F., uses laser to measure reflectance, thru-lens sighting, reticle display, disposable AA batteries(6), 0.9μ
Raytek	Thermalert IT series Thermalert BT series Thermalert III series Thermalert IV series	Various models, 0-1000°F., 2 piece, small sensing head, e set Various models, 0-3000°F., integrated sensing head, e set, processing options, s.s. Various models, 0-5400°F., 2 piece, LED display, e set, processing options, s.s. Various models, 0-5400°F., 2 piece, dual LED display and set points, e set, processing options, s.s.
Vanzetti	Series TM1&TM2	Fiber optic coupled systems, 104-5000°F., s.s. to 4.5um, many accessories; models without fiber optics available.
Watlow	Thermoducer	Various models, 32-932°F, small sensor, electronics
Williamson	Series 3000,4000 6000,7000,8000,9000 Transtemp 1000 series Transtemp 590	Various models including 2 color, fiber optic coupled, 75-4000°F., s.s., many accessories. Various models, 0-4500°F, 2 wire fix focus transmitters 0-100°F 2 wire fix focus transmitter
B. <u>Line scanners</u>		
Agema	Thermoprofile 5 series	Modular, thermoelectrically cooled, high resolution analog and digital outputs; operates with control system host computer
Pyrometer	ThermaTrace	Uncooled, provides composite visual image and IR linescan of temperature; portable, rechargeable battery, SX70 photorecording

continued

Table 1. Instrument Characteristics (continued)

Manufacturer Model (s)		Characteristics
C. Thermographic		
1. Thermal Viewers		
AGEMA	110	Thermoelectrically cooled, CRT display, thru-eyepiece recording, Polaroid or conventional film, rechargeable battery., 6"x12" FOV, -23 to 1100°F range.
Hughes	Probeye	Argon-cooled, LED Display, thru-eyepiece recording, Polaroid or conventional film, rechargeable battery, 2.5"x18" FOV, range to 1337°F.
2. Pyrovidicon Imagers		(Uncooled- operate at ambient temperatures)
I.S.I.	86, 91, 93, 94	Portable & 2 piece systems, FOV (lenses) from 9° to 60°, iris attenuators, profile & chopper options, 93 has environmental enclosure, 94 has built-in thermometer and diagnostics.
I.T.M.	202 & 203	Custom portable & 2 piece systems; many optional features
Xedar	XS410, XS412	Portable & 2 piece systems, 18° & 30° FOV, profile, chopping, synchronous chopper option, & image processing options available
3. Raster Scanners		(Liquid nitrogen cooled unless indicated)
AGEMA	870, 880, 450	Reflective Scanner based on SPRITE technology, 870 and 450 are TE-cooled. Rechargeable battery or line power, FOV (lenses) from 7° to 40°, 3-5 or 8-12-, filter wheel, TV scan rates isotherms, color, VCR, image processing, expandable software
Barnes	CompuTherm	Microimager, spot down to 0.0003", bench top unit, IBM AT/based features spatial computation & integral image diagnostics, (storage, subtract, manipulate, etc.) interchangeable FOV's Scan speed 1, 1/2 second, 3-5x reflective scanner.
FLIR Systems	100	2 element high resolution usually airborne; refractive/reflective optics, 8-14°, TV scan rates
Hughes IPD	7100, 7300	TE-cooled, 30 element HgCdTe reflective scanner, 20°Vx28°H FOV Image storage & comparison capability; computer interface, videorecording and expandable software; TV scan rates, rech. or line power.
	5000, 3000 series	Argon-cooled 10 element InSb reflective scanner, rech. battery or line power, field or lab, expandable software
Hughes SS	ThermaScan	System for printed circuit card screening and diagnostics; includes high resolution 8-12° scanner, power supplies, computer, holding and positioning fixtures, extensive diagnostic software.

continued

Table 1. Instrument Characteristics (continued)

Manufacturer Model (s)		Characteristics
C. <u>Thermographic</u> (continued)		
3. <u>Baster Scanners</u> (continued)		
Inframetrics	522,522L,600 600L,610,	1 element reflective scanners, rechargeable battery or line power, FOV 14°Vx18°H with 4:1 zoom available, TV Scan Rate, 3-5 & 8-12μ, Features: Isotherms, color, VCR, image processing, expandable software
	IRAMS	System for printed circuit card screening, similar to Hughes ThermaScan
JEOL	(marketed by UTI)	High resolution reflective scanner, cart-portable, line powered FOV 20°Vx25°H, frame rate-1, 2 & 4/ second, X & Y profile, color, VCR, video processor, printer
	JTG 3110	InSb detector; 0.6, 1.3, 5.2 second/scan; 300 elements/line, 230 lines; line power; IBBB bus
	JTG 3210	HgCdTe detector; otherwise same as 3110
Mikron	6T62,63	High resolution, 3-5, 8-13μ, reflective scanner, line-powered with battery option, FOV 25°Vx30°H, Frame rate-1, 2, & 4/second, color monitor, VCR, image processing and expandable software
UTI CCT 9000		Bench top unit aimed at production circuit board analysis, reflective scanner, FOV 30°x30°, 2-12μ, fully computerized with extensive analysis & storage capacity. RGB Color, Scan rate 1/second.

Table 2. Instrument Manufacturers

<u>Company Name</u>	<u>Mailing Address</u>	<u>Telephone Number</u>
AGEMA Corporation	550 Country Ave., Secaucus, NJ 07094	(201) 867-5390
Barnes Division, EDO Corp.	88 Long Hill Cross Rds., Shelton, CT 06484	(203) 926-1777
Capintec Instruments Inc.	6 Arrow Rd., Ramsey, NJ 07466	(201) 825-9500
The Dickson Company	930 S. Westwood Drive, Addison, IL 60101	(312) 543-3747
E ² Technology Corp.	1545 Morse Ave., Ventura CA 93003	(805) 644-9544
Everest Interscience Corp.	PO Box 345, Tustin, CA 92680	(714) 992-1461
Exergen Corporation	307 W. Central St., Natick, MA 01760	(508) 875-2387
FLIR Systems	11830 SW Kerr Pkwy, Lake Oswego, OR	(503) 245-0771
Hughes Industr. Products Div.	6155 El Camino Real, Carlsbad, CA 92008	(619) 438-9191
Hughes Support Systems	P.O. Box 9399, Long Beach, CA 90810	(213) 513-4786
Horiba	1021 Duryea Avenue, Irvine, CA 92714	(714) 250-4811
Image Technology Methods	103 Moody St., Waltham, MA 02154	(617) 894-1720
Inframetrics	16 Esquire Road, N. Billerica, MA 01862	(508) 670-5555
Ircon, Inc.	755 N. Linder Ave., Skokie, IL 60077	(312) 967-5151
Irtronics	59 Commerce Rd., Stamford, CT 06902	(203) 348-2671
I.S.I. Group, Inc.	9617 Acoma St. SE, Albuquerque, NM 87123	(505) 295-7646
JEOL Ltd. (USA) (see UTI)	235 Birchwood Ave., Cranford, NJ 07016	(201) 272-8820
Land Instruments, Inc.	Box 1623 Fox & Main, Tulleytown, PA 19007	(215) 943-7882
Linear Laboratories	2490 Charleston Rd, Mountain View, CA 94043	(415) 969-4999
Mikron Instrument Co., Inc.	PO Box 211, Ridgewood, NJ 07451	(201) 891-7330
Pyrometer Instrument Co.	234 Industrial Pkwy., Northvale, NJ 07647	(201) 768-2000
Quantum Logic Corp.	99 E. Kansas St., Hackensack, NJ 07601	(201) 342-0303
Raytek, Inc.	1201 Shaffer Rd., Santa Cruz, CA 95060	(408) 458-1110
Teletemp Corp.	PO Box 5160, Fullerton, CA 92635	(714) 879-2901
Testoterm, Inc.	PO Box 111509, Nashville, TN 37211	(615) 834-5082
UTI Instruments Co.	497 S. Hillview, Milpitas, CA 95053	(408) 738-3301

continued

Table 2. Instrument Manufacturers (continued)

<u>Company Name</u>	<u>Mailing Address</u>	<u>Telephone Number</u>
Vanzetti IR Systems, Inc.	111 Island St., Stoughton, MA 02072	(617) 828-4650
Wahl Instruments, Inc.	5750 Hannum Ave., Culver City, CA 90203	(213) 641-6931
Watlow Manufacturing	1 Richmond Square, Providence, RI	(401) 521-7410
Williamson Corp.	1152 Main St., Concord, MA 01742	(617) 369-9607
Xedar Corp.	2500 Central Ave., Boulder, CO 80301	(303) 447-1822

Table 3. Compilation of Typical Industrial Applications of Thermal Imaging Instruments

Typical Applications by Industry

<u>Industry</u>	<u>Applications</u>
Metals	Continuous casting, strip annealing, extrusion presses, rolling mills, induction heating, resistance heating, heat treating, electrolytic refining
Glass	Tank refractories, glass body temperatures, mold temperatures, bottle machines, float glass, tempering and annealing, fiberglass manufacturing
Cement	Kiln shell, refractory insulation, bridge delamination inspection
Textiles	Permanent press heat setting, dye setting, foam lamination, carpet backing
Plastics	Vacuum forming, extrusion, film process monitoring and control
Paper	Dryer drums, coating ink drying
Chemical and Petroleum	Furnace tube temperatures, pipe and vessel corrosion, mixing process monitoring and control
Food and Confectionery	Rotary Cooker temperatures, continuous infrared ovens, mixers, continuous baking ovens, freeze-dry processes
Asphalt Paving	Road stone dryer, mixing temperature, rolling temperature
Rubber	Hot rubber sheets-cooling and rolling, tire testing

Typical Applications by Discipline

<u>Discipline</u>	<u>Applications</u>
Design	Exhaust stacks, flue pipes, Heating units (ovens, boilers, furnaces) Buildings (offices, schools, hospitals, plants) Process pipes, vessels, lines: steam and water lines Kilns Cryogenic Storage Vessels Electrical and electronic circuits and microcircuits
Workmanship	Operational procedures Installation of refractory materials Installation of foam insulation materials Installation of fiberglass materials (roof insulation, etc.) Replacement of parts and other repairs Roof inspection for moisture saturation
Component Failure	Steam traps, underground steam lines Electrical lines and substations Electrical and electronic components and modules Insulation-foam, fiberglass and refractory Seals, low and high temperature Doors, ports, windows Cooling towers, heat exchangers Plumbing lines and systems Motors, pumps, ventilators, bearings

A SPACE QUALIFIED THERMAL IMAGING SYSTEM USING A Pt Si DETECTOR ARRAY

ROBERT W. ASTHEIMER
EDO CORPORATION
BARNES ENGINEERING DIVISION

1.0 INTRODUCTION

EDO Corporation, Barnes Engineering Division has designed and constructed a high resolution thermal imaging system on contract to Lockheed for use in the SDI Star Lab. This employs a Pt Si CCD array which is sensitive in the spectral range of 3 - 5 microns. Star Lab will be flown in the shuttle bay and consists basically of a large, reflecting, tracking telescope with associated sensors and electronics. The thermal imaging system is designed to operate in the focal plane of this telescope.

The configuration of the system is shown in Figures 1 and 2. The telescope provides a collimated beam output which is focussed onto the detector array by a silicon objective lens. The detector array subtends a field of view of $1.6^\circ \times 1.22^\circ$. A beam switching mirror permits bypassing the large telescope to give a field of $4^\circ \times 3^\circ$. Two 8 position filter wheels are provided, and background radiation is minimized by Narcissus mirrors. The detector is cooled with a Joule-Thompson cryostat fed from a high pressure supply tank. This was selected instead of a more convenient closed-cycle system because of concern with vibration; The latter may couple into the extremely critical Starlab tracking telescope.

The electronics produce a digitized video signal for recording. Offset and responsivity correction factors are stored for all pixels and these corrections are made to the digitized output in real time.

A Space Qualified Pt Si Thermal Imaging System

This system has been evaluated as a thermal imager using a simplified optical system consisting of a 2" diameter germanium lens of 3.5" focal length. This configuration is well adapted for thermal imaging and non contact temperature measurements in space experiments such as zero gravity processing. This is the type of application addressed in this paper.

2.0 DETECTOR ARRAY

Platinum silicide infrared detectors are Schottky-barrier type diodes formed by the deposition of Pt Si on a silicon substrate. The incident radiation is transmitted through the silicon and absorbed in the silicide layer. Such detectors are particularly adaptable to the formation of two-dimensional arrays since, having a silicon substrate, they can be combined monolithically with a charge-coupled device (CCD) structure for reading out the signal on each detector element.

Typical spectral response of a Pt Si detector element is shown in Figure 3. It has useful response out to 5 microns, although the quantum efficiency is only about 1% at this wavelength. The silicon substrate must be shared with the CCD read out, which requires considerable space between elements in the array. The ratio of the active detector area to the total pixel area is 39%. This fill factor loss and the low quantum efficiency at longer wavelengths makes the effective D^* of a single element considerably lower than other cooled detectors used for this spectral region such as InSb. However, this is compensated by the fact that each element views the scene during the entire frame time and builds up charge which is read out at the end. This makes its imaging performance competitive with a single element InSb scanning system.

A Space Qualified Pt Si Thermal Imaging System

The short wavelength response of the Pt Si array can be used advantageously to provide an optional near-infrared reflected image. The target would be illuminated with an incandescent lamp which will give ample radiation in the 1.2 - 2.5 micron region. The short wavelength response of the array is limited to 1.2 microns by the silicon substrate, while the glass envelope of the lamp will cut out wavelengths beyond 2.5 microns. The display could be rapidly changed from the near infrared reflected image to a thermal image by switching filters in front of the array from glass to a 2.5 micron long pass filter.

3.0 IMAGE COMPENSATION

In order to accurately measure radiance or temperature with a Pt Si array, three corrections must be made for variations in dark current, background radiance and responsivity between pixels. Dark current arises from thermally generated charge carriers and is dependent upon detector temperature. Back-ground is the radiance impinging on the detector elements from sources other than the desired image. This is primarily radiation from the optics and internal baffles, and is dependent upon ambient temperature. Both the dark current and background signal are unaffected by target signal strength and are, therefore, subtracted from the signal. Lastly, there are small variations in the responsivity of individual detector elements and this correction must multiply the target signal.

A Space Qualified Pt Si
Thermal Imaging System

These corrections are different for each pixel and are made in real time from three stored arrays of correction factors through the algorithm shown in Figure 4. The dark current array D is measured and stored when a liquid nitrogen cooled plate is placed in front of the detector array, while the background array B is stored when the cooled plate is placed in front of the telescope. The responsivity array is stored when viewing a uniform temperature field producing a signal about midway in the dynamic range of the detectors.

The dark current correction is adaptively adjusted for detector temperature through a single multiplier K_1 which is controlled by the detector temperature. The same multiplier (K_1) is applied to all correction terms in the array. Similarly, the background correction array is adaptively adjusted for the temperature of the optics through the single multiplier K_2 .

The Starlab system is designed to measure the radiation from small targets against a space background and, under these conditions, the dark current and background compensation is essential. A saturation signal on the detector produces 4095 counts from the A/D converter. On this scale, the dark current is about 200 counts and the background 300 counts. The responsivity variation is 1% - 2%, which could be up to 80 counts. Thus we see that, even when used with a room temperature back-ground, all three compensation factors are necessary to make accurate absolute radiance or temperature measurements.

A Space Qualified Pt Si Thermal Imaging System

The variation in dark current of a typical element with detector temperature is shown in Figure 5. If the detector temperature can be well controlled at LN₂ temperature (77°K), the adaptive temperature factor K₁ can be eliminated. Also if the ambient temperature does not change much, the factor K₂ need not be adaptive. In this case, the D and B arrays can be combined into a single non-adaptive OFFSET compensation array. This is probably adequate for shuttle experiments and would simplify the system.

4.0 IMAGER PERFORMANCE

The Starlab detector/electronics were preliminarily evaluated as a thermal imager by substituting a simple germanium lens for the Starlab optics. A photograph of this system is shown in Figure 6, and the major parameters are listed in Figure 7.

Figures 8 to 10 show typical false color images of near ambient objects. Unfortunately, the adaptive offset and responsivity compensation features, although operating electronically, were not yet incorporated in the system at the time these photos were made. Figure 8 shows warm water being poured from a beaker, while Figure 9 shows the same warm water being poured over a person's hand. Figure 10 shows a printed circuit board with several hot components.

A unique feature of these images, which is not evident in the photographs is that, when viewed on the TV screen, there is almost no discernable noise on any individual pixel. However in a temperature (or radiance) measuring imaging system, the performance is determined by how accurately the temperature of any

A Space Qualified Pt Si Thermal Imaging System

element in the picture can be determined. Responsivity and offset variations between pixels produce differences in the apparent temperature of objects which must be considered as "noise", which is why, in Figure 7, we list the NET as 0.5° at 110°C without compensation. However with compensation, this will be greatly reduced and, although tests have not been completed at this date, the NET with compensation is expected to be less than 0.02° at 100°C .

A complete engineering model using flight optics and fully compensated will be tested by February 15, 1989 and the flight system will be tested in April 1989.

The Pt Si spectral response makes this detector particularly attractive for the non-contact measurement of small variations in temperature of moderately hot targets in the range of $80+^\circ\text{C}$. The rising responsivity at shorter wavelengths greatly enhances temperature contrast and suppresses emissivity errors.

5.0 CONCLUSIONS

This Pt Si CCD camera system is well suited for microgravity experiments in space, requiring accurate radiance and temperature measurements in the 3 - 5 micron region. It is very compact and directly compatible with TV. Cooling can be accomplished with a J-T cryostat as in the Starlab system or preferably with a Stirling closed-cycle cooler. The increasing detector response at short wavelengths enhances thermal contrast and enables one system to act as both a thermal and reflectively illuminated TV. Arrays with higher resolution are being developed and units with 512×512 pixels are now available.

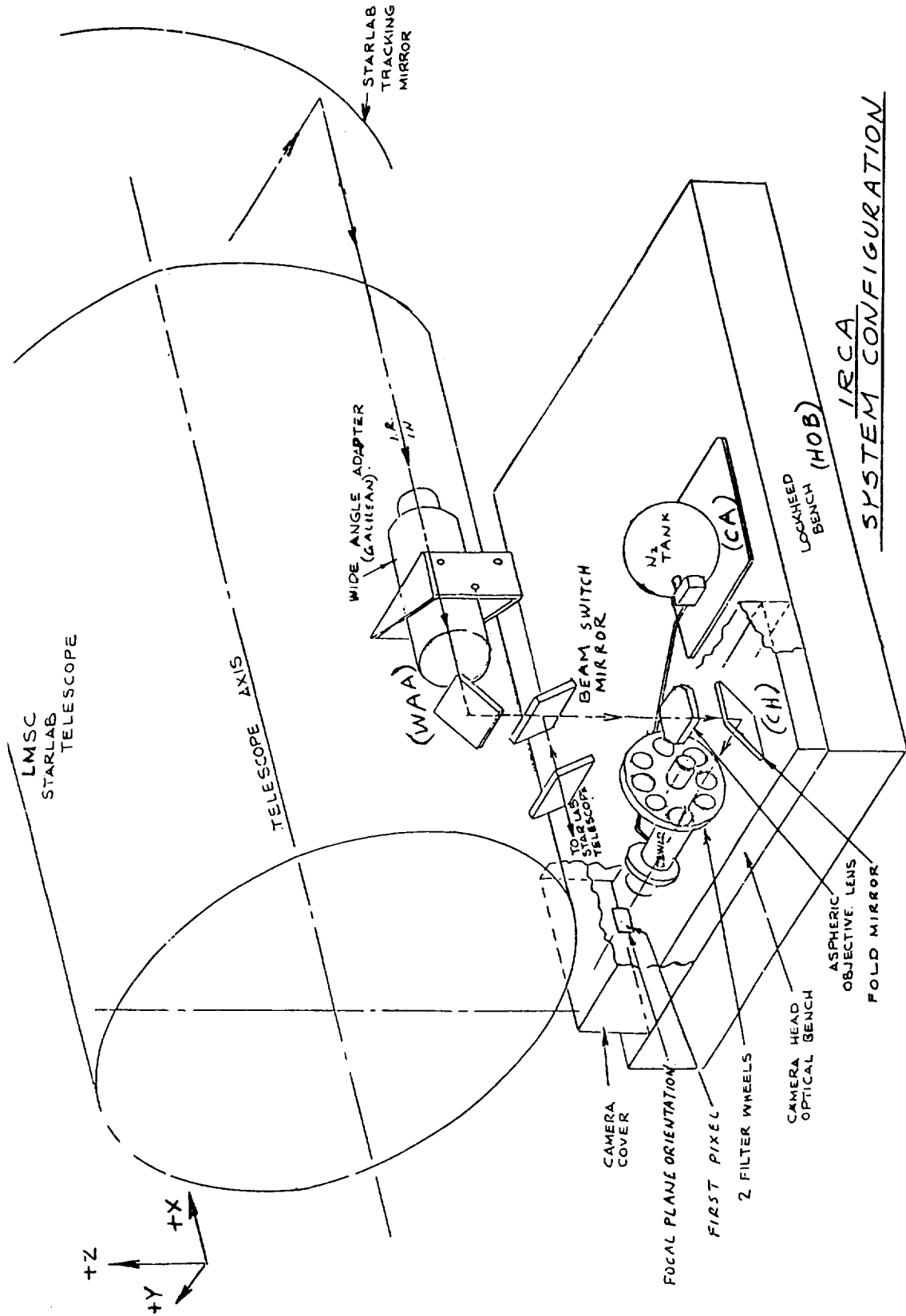
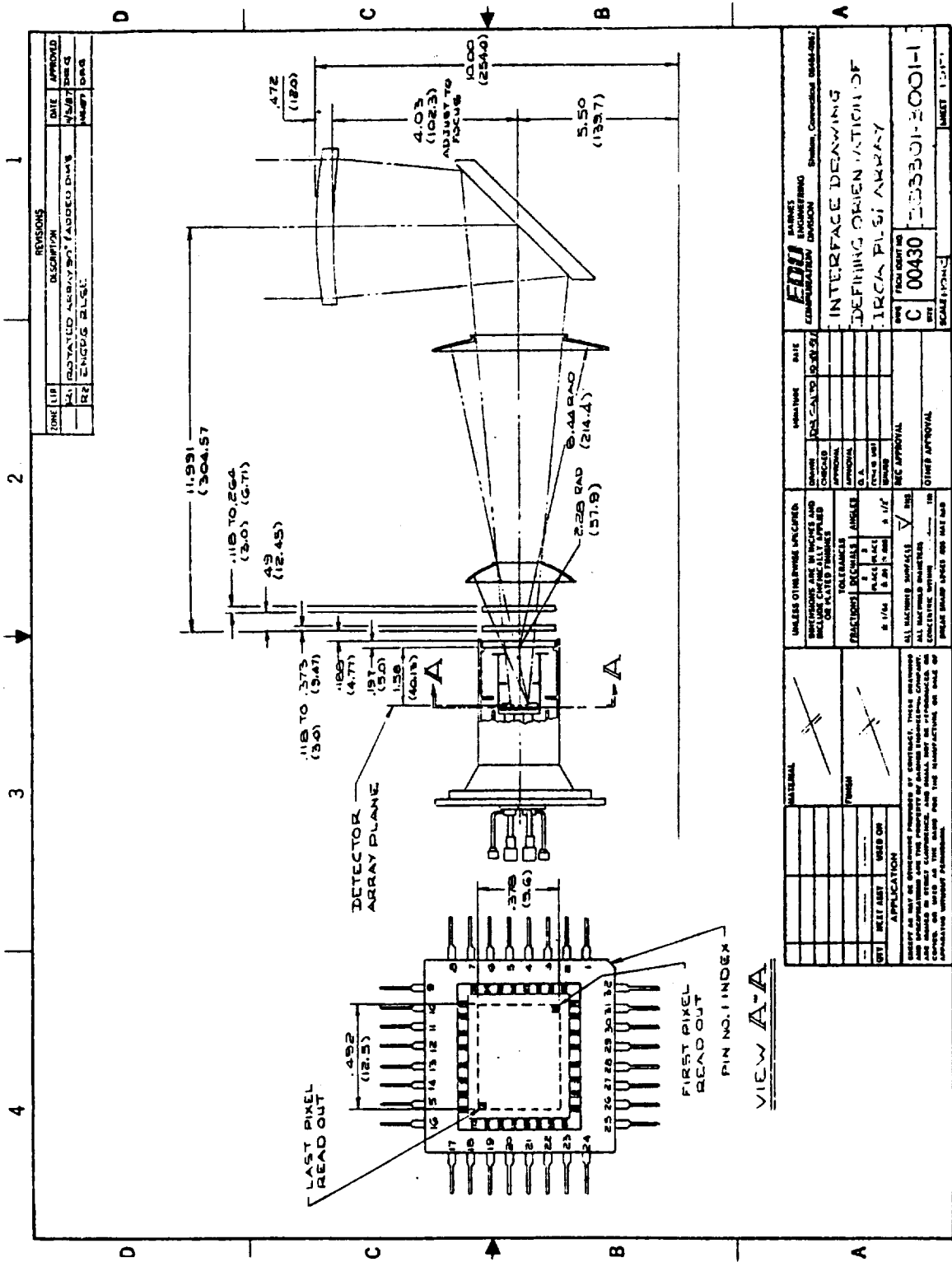


Figure 1.



REVISIONS		DATE	APPROVED
ZONE	DESCRIPTION		
1	CONSTANT ARRAY PIN ADDRESS DATA	11/27/68	DRG
2	ENGINEER'S LABEL	11/27/68	DRG

EEO CORPORATION		ENGINEERING DIVISION		Drawing Conventions	
INTERFACE DRAWING					
DEFINING ORIENTATION OF IRCA PIXEL ARRAY					
REV	REV. DATE	REV. DATE	REV. DATE	REV. DATE	REV. DATE
C	00430				
SCALE: 1"=1"					
UNLESS OTHERWISE SPECIFIED, DIMENSIONS ARE IN INCHES AND DECIMALS THEREOF ARE TO BE ROUNDED UP TO THE NEAREST THOUSTH PART OF AN INCH.		TOLERANCES UNLESS OTHERWISE SPECIFIED:		FRACTIONS: 1/16, 1/8, 1/4, 3/8, 1/2, 5/8, 3/4, 7/8	
ALL DIMENSIONS UNLESS OTHERWISE SPECIFIED ARE TO BE TAKEN FROM THE CENTERLINE OF THE PART.		ALL DIMENSIONS UNLESS OTHERWISE SPECIFIED ARE TO BE TAKEN FROM THE CENTERLINE OF THE PART.		ALL DIMENSIONS UNLESS OTHERWISE SPECIFIED ARE TO BE TAKEN FROM THE CENTERLINE OF THE PART.	
MATERIAL		FINISH		APPLICATION	
COPYING AND REPRODUCTION OF THIS DRAWING IS PROHIBITED WITHOUT THE WRITTEN PERMISSION OF EEO CORPORATION.					

EEO
CORPORATION
ENGINEERING DIVISION

Figure 2.

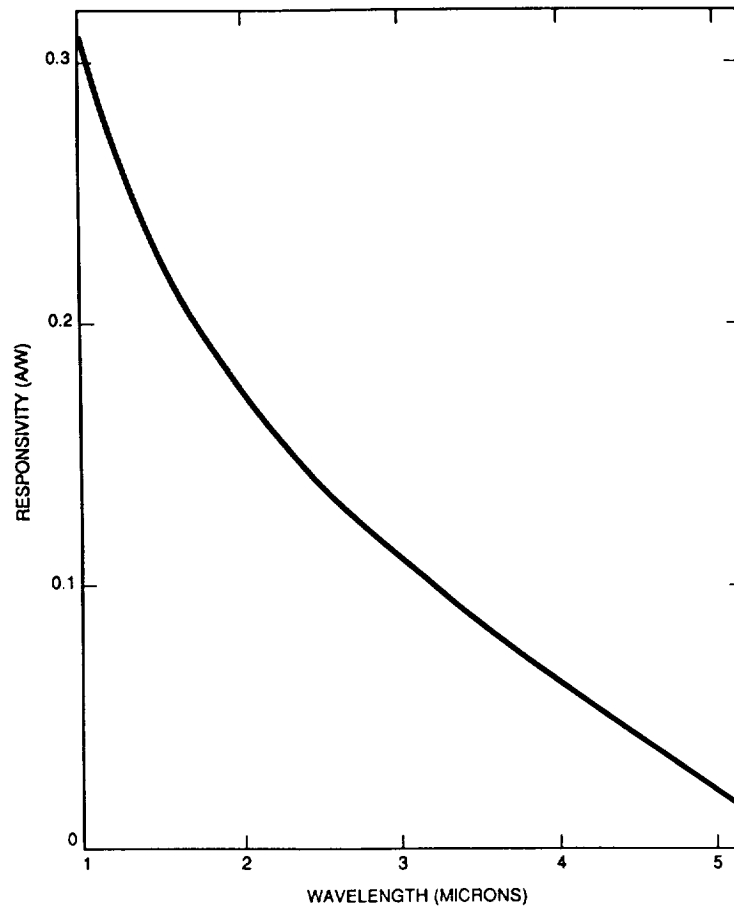


Figure 3.

$$O = (S - K_1 D - K_2 B) \times K_3 R$$

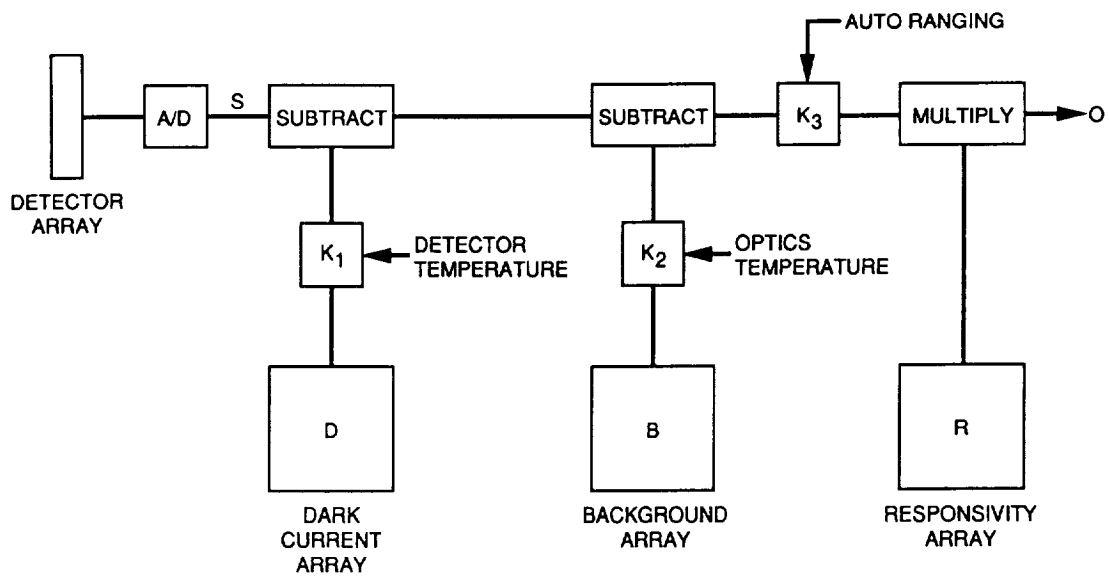


Figure 4.

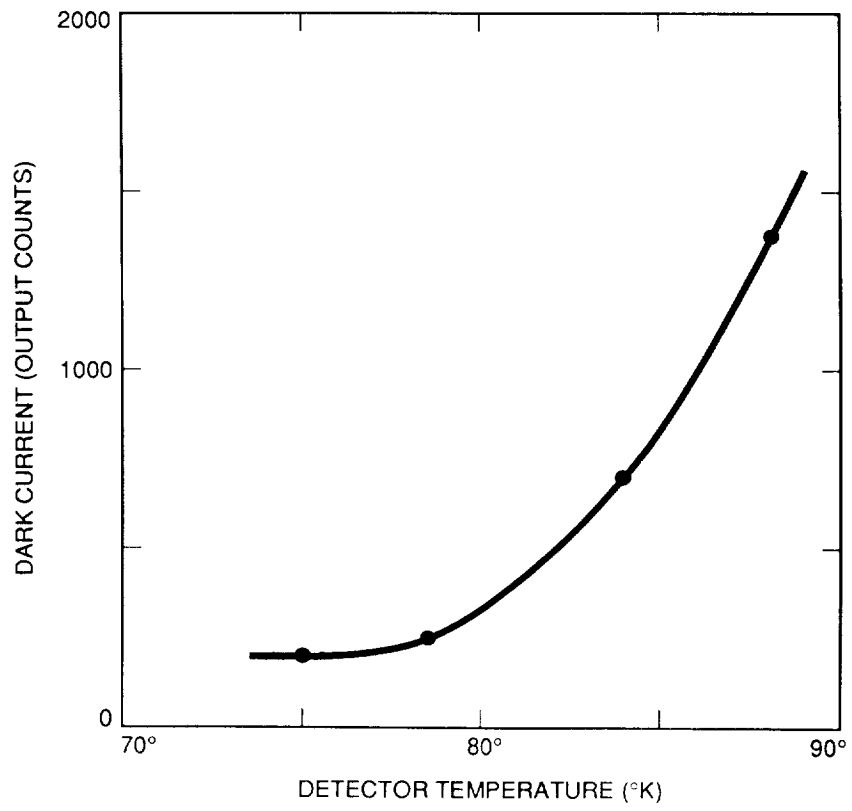


Figure 5.

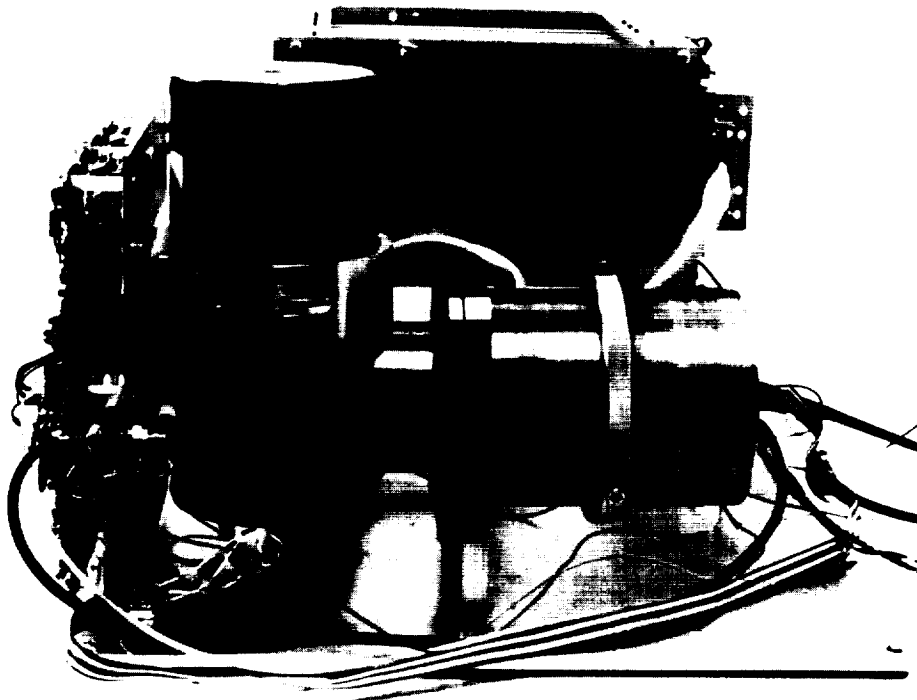


Figure 6.

THERMAL IMAGING SYSTEM

OBJECTIVE LENS	GERMANIUM 2" DIAMETER 3.5" FOCAL LENGTH
PT SI ARRAY	160 x 244 ELEMENTS PIXEL SIZE 0.080 x 0.040 FILL FACTOR 39% TOTAL AREA 12.8 x 9.8 MM
FIELD OF VIEW	8.2° x 6.3°
PIXEL FIELD	0.9 x 0.45 MRAD
NET	0.5°C AT 100°C PATTERN NOISE LIMITED <0.02°C AT 100°C WITH COMPENSATION

Figure 7.

ORIGINAL PAGE
BLACK AND WHITE PHOTOGRAPH

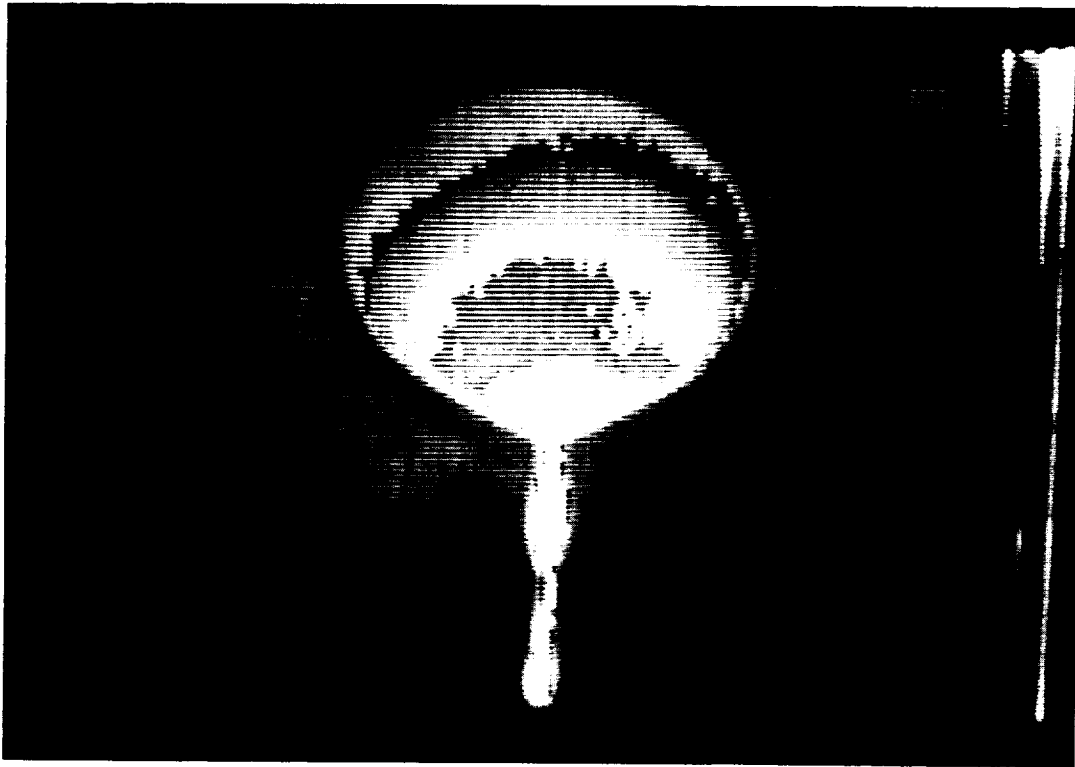


Figure 8.

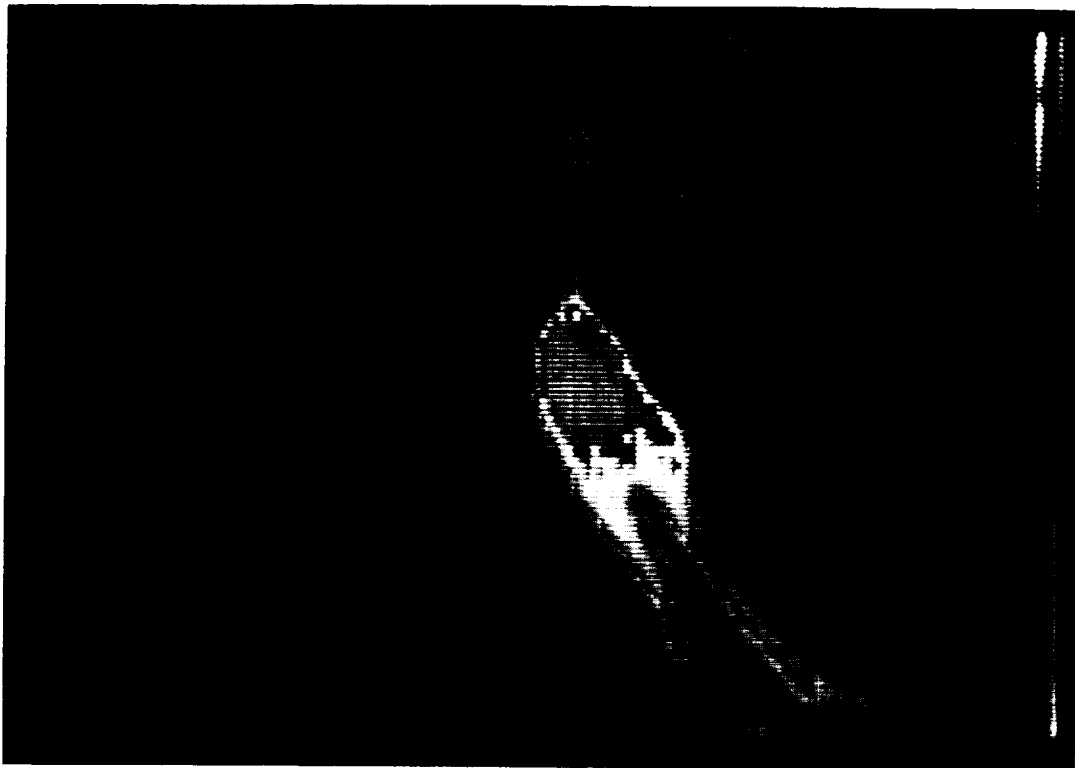


Figure 9.

ORIGINAL PAGE
BLACK AND WHITE PHOTOGRAPH

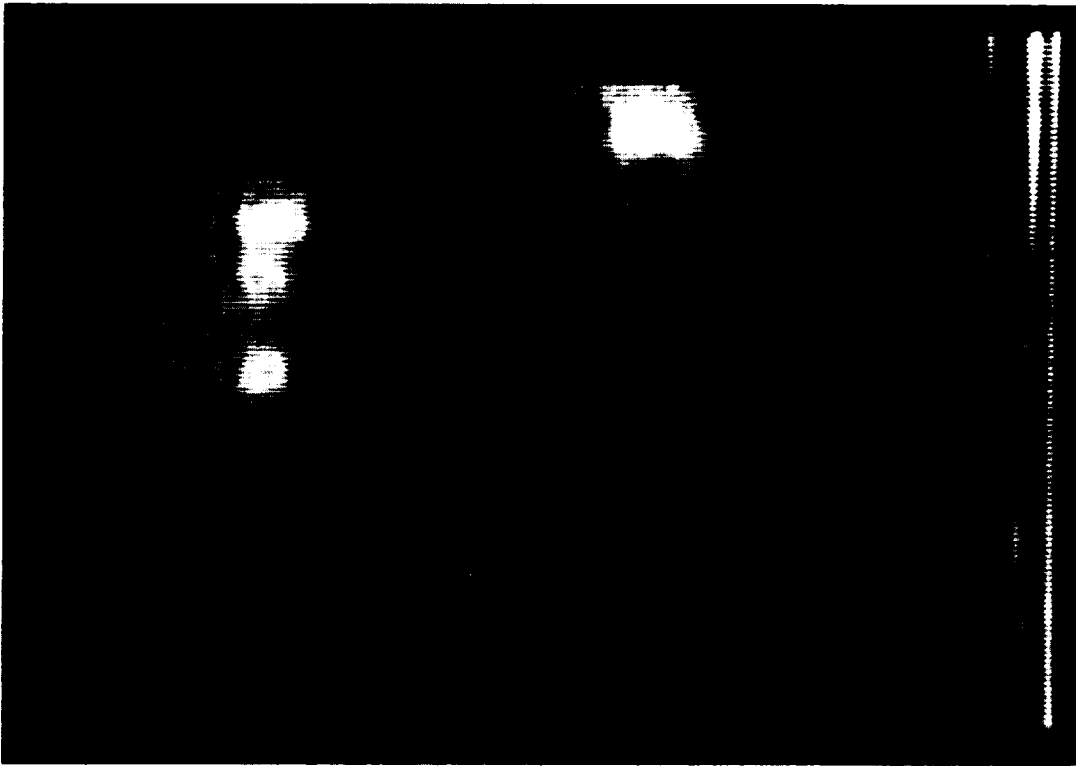


Figure 10.

DEVELOPMENT OF AN INFRARED IMAGING SYSTEM FOR
THE SURFACE TENSION DRIVEN CONVECTION EXPERIMENT

Alexander D. Pline

*NASA Lewis Research Center
Cleveland, Ohio 44135*ABSTRACT

An infrared imaging system is used to quantify the imposed surface temperature distribution along a liquid/gas free surface in support of the Surface Tension Driven Convection Experiment, a planned Space Transportation System flight experiment. For ground-based work a commercially available instrument was used to determine the feasibility of using this type of imaging system for this experiment. The ground-based work was used as a baseline for compiling specifications for a flight qualified imager to be designed, fabricated, tested and qualified for flight. The requirements and the specifications for the flight model are given along with the reasons for departures from the ground-based equipment. The flight qualification requirements discussed are a representative sample of the necessary procedures which must be followed to flight qualify diagnostic equipment for use aboard the STS. The potential problems and concerns associated with operating an imaging system on orbit are also discussed.

INTRODUCTION

A non-contact surface temperature measurement system is being developed in response to the need for quantitative, full field characterization of the resulting surface temperature distributions during the Surface Tension Driven Convection Experiment (STDCE). The STDCE is a space flight experiment to study thermocapillary flows, during the USML-1 Spacelab mission. The current STDCE schedule is to have flight hardware ready for shipment by April 1, 1991 for the USML-1 Spacelab mission planned for March 1992. Thermocapillary flows are generated by a thermally induced surface tension variation which acts as a surface tractive force along a liquid/gas free surface from regions of low surface tension (high temperature) to high surface tension (low temperature).

During the STDCE a 10 cm diameter by 5 cm deep cylindrical container of silicone oil is heated centrally either internally or externally while the resulting thermocapillary flows are visualized by illuminating a cross section with a sheet of light. The internal heating case (or CT experiment) uses a 1.1 cm diameter by 5 cm height resistance heater (heated wall) placed centrally in the test cell (cooled wall) to establish the temperature gradient along the free surface. For the externally heated case (CF experiment) the resistance heater is removed and the free surface heated using focused CO₂ laser radiation.

Because liquid/gas free surfaces are ubiquitous to containerless processes, the understanding

of surface tension driven flows in reduced gravity as well as terrestrial gravity is important in the commercialization of containerless materials processing techniques.¹ The surface temperature distribution is a critical parameter for these types of flows as it is the driving force.^{2,3} In reduced gravity, a liquid/gas free surface may not be stationary due to small accelerations, called g-jitter, aboard the vehicle. Consequently, when the thermal boundary layer along the free surface is thin contact surface temperature measurement methods are sensitive to these disturbances. Therefore, development of a non-contact temperature measurement system to quantitatively characterize the thermal signature is an essential part of the development of the STDCE.

The system development is divided into two phases: a testing phase, to study the feasibility of using a commercially available infrared imaging system to characterize the surface temperature distributions, and a flight hardware development phase. The testing phase was based on the science objectives put forth by the Principal Investigator, S. Ostrach and the Co-Investigator, Y. Kamotani, both of Case Western Reserve University, in the STDCE Science Requirements Document.⁴ An absorption study of silicone oil was conducted to determine the most appropriate operating wavelength for the imager and the surface layer thickness measured by the imager. Based on study results, the Model 600 Infrared Imaging System was purchased from Inframetrics Inc. Testing was conducted using this system to determine its accuracy compared to thermocouple measurements and numerical calculations as well as an effective emissivity for these experimental conditions (reference 5).

The flight hardware development phase consists of procuring a space flight qualified infrared imager. In addition to the technical specifications derived from the testing phase, the Statement of Work (SOW) in the Request for proposal (RFP) also contains a plethora of requirements which *the manufacturer* must meet in order to fly on the Spacelab. These requirements include related development work, design reviews, vibration levels, safety and qualification/acceptance testing which must be met within the constrained schedule associated with the USML-1 deadlines. This procurement will result in a fully tested and space flight qualified infrared imager delivered to NASA Lewis Research Center for integration with the balance of the STDCE hardware.

DEVELOPMENTAL TESTING

Science Requirements

The requirements for the surface temperature measurement system are for a full field non-intrusive measurement using a thermographic technique. The operational wavelength should be chosen so that the detected radiation comes from a region as close to the surface as possible. The spatial resolution should be less than or equal to 1 mm and the temporal resolution should be 0.1 second or less. The accuracy of the instrument should be within $\pm 5\%$ of the ΔT between

the center and side wall except near the center and wall regions where $\pm 10\%$ is acceptable. To satisfy these requirements, the technique should be calibrated by thermocouple measurement as well as be consistent with numerical analysis.

Absorption Study

The absorption characteristics of silicone oil must be known in order to select the operational wavelength of the imager and to determine how deep the imager "sees" into the oil. Using an infrared spectrophotometer, transmission of radiation as a function of wavelength through a variable thickness of silicone oil was measured. From this data an empirical relationship in the form of the most simplified version of Bouguer's Law was determined. The thickness of fluid which attenuates nearly 100 percent of the incident radiation in the imager operating wavelength region is called the "surface" thickness.

The transmission versus wavelength results show that silicone oil is quite transparent at wavelengths of less than 8 micrometers (μ). Therefore an imager which operates in the far infrared (8-12 μ) is needed. In order to find how silicone oil attenuates radiation in this region, transmission was averaged numerically and plotted against fluid thickness. In addition transmission at 10.6 μ was plotted against fluid thickness to determine the penetration of CO₂ laser radiation. From these relationships (Fig. 1), the fluid thickness which attenuates nearly 100% of the

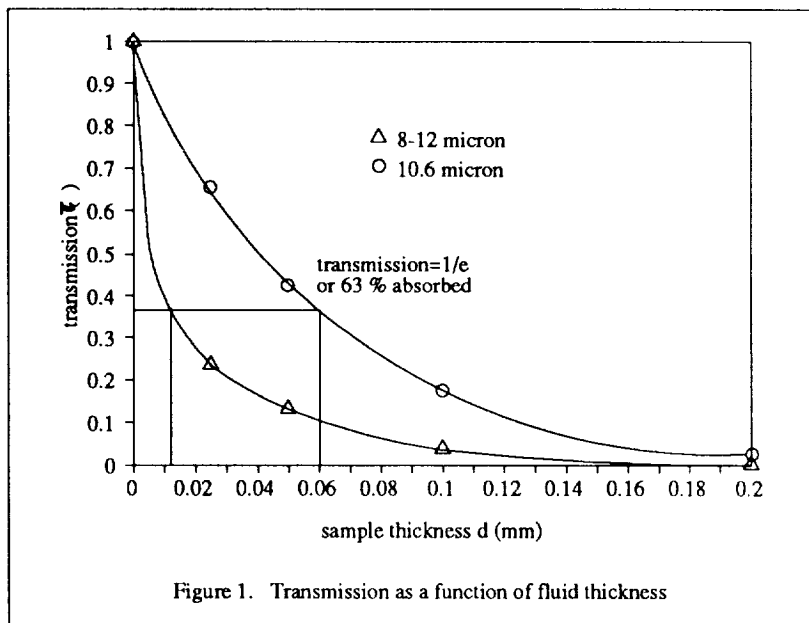


Figure 1. Transmission as a function of fluid thickness

incoming radiation is found to be 0.200 mm and 0.256 mm for the 8-12 μ region and 10.6 μ wavelength respectively. Therefore, it is concluded that the "surface" the imager "sees" is 0.200 mm thick. The fact that the CO₂ laser radiation penetrates deeper than this is advantageous. If the situation were reversed, the temperature indicated by the imager would be an average over a region where a much larger temp-

erature gradient would exist.

Imager Selection

The conclusions drawn above indicate the need for an imager which operates in the far infrared. Satisfying this requirement, as well as the other science requirements, based on manufacturers specifications, the Inframetrics Model 600 and Thermal Image Processing System were

purchased. The Model 600 has a spatial resolution of 2 milliradians (mr), or 0.8 mm at 40 cm working distance, and a temporal resolution of 0.033 seconds (RS-170 video frame rate). A more complete description of the Model 600 can be found in references 5 and 6.

Effective Emissivity

Because no surface is an ideal radiator, there is an emissivity (<1) associated with that surface. This emissivity value is needed as an input to the thermal image processing system to account for non-ideal radiation and reflected background radiation. Due to the lack of existing literature documenting the emissivity of silicone oil, an emissivity was determined empirically by comparison of the imager surface temperature data with other techniques. This emissivity value of 0.90 is called the "effective emissivity" because it accounts for all the non-ideal radiative properties of silicone oil only for *this imager under these experimental conditions*.

Accuracy

Data acquired using the infrared imaging system were analyzed and compared to thermocouple measurements and a calculated surface temperature distribution to establish the accuracy of the system for this experiment. Both heating modes used during the STDCE were analyzed.

Comparison of the three techniques is shown in Figure 2 for the maximum temperature gradient expected during the CT Experiment where the ΔT is near 50 °C. This is the most difficult (i.e. sharpest temperature gradient) CT measurement case with an input power to the

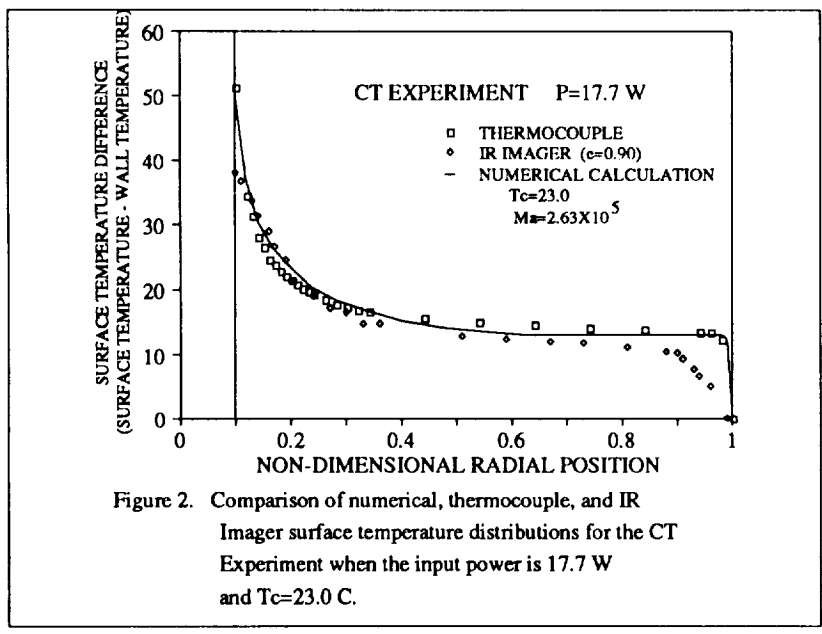


Figure 2. Comparison of numerical, thermocouple, and IR Imager surface temperature distributions for the CT Experiment when the input power is 17.7 W and Tc=23.0 C.

heater of 17.7 W. Plotted in the figure is the surface temperature difference between the oil surface the test chamber wall against nondimensional radial position, measured with the target emissivity set to 0.90. The agreement among the three techniques for this case is $\pm 5\%$ of the overall ΔT excluding the near wall regions. The errors in the wall regions are $\pm 10\%$ of the ΔT and are caused, predominantly, by the

imager spatial resolution, which is not small enough to resolve these gradients. Similar results were obtained for the CF experiment except measurement errors near the center were a result of the thinner thermal boundary layer and consequent averaging of cooler bulk fluid.

FLIGHT HARDWARE DEVELOPMENT

The development work described was used as a baseline from which specifications for the flight model were developed. In addition to the technical specifications, other design and qualification requirements were compiled to guide the manufacturer in the design, fabrication and testing so that the final instrument is a *fully space flight qualified* imager, which will meet all performance specifications for the STDCE and satisfy all STS requirements.

Technical Specifications

The major technical specifications of the desired imager are summarized in Table 1. Like the ground based imager it will produce an analog output in the form of an RS-170 video signal which can be recorded and analyzed after the fact. Care was given not to specify any operational characteristics particular to the commercial equipment such as the image acquisition scheme (i.e. scanners versus focal plane arrays). The intention was to procure a black box which would produce data per the specifications without regard to the operational details, because the design of a new imager or redesign of a commercial system to meet the space qualification requirements is the responsibility of *the contractor*. By writing the specifications in this manner a maximum number of manufacturers could be eligible.

The major deviations from the commercial equipment are the detector cooling, the spatial resolution and the minimum sensitivity (NETD). The liquid nitrogen detector cooling scheme used for the commercial equipment is not acceptable for space applications for obvious reasons. Both a Joule-Thompson (J-T) cryostat and a Stirling Cycle cryocooler were considered to replace the LN₂ dewar. The Stirling Cycle cryocooler was chosen because it is inherently safer than a J-T cooler while providing non-exhaustible cooling. This type of cooler is also routinely used for military applications (e.g. U.S. Army common module).

Due to errors caused by sharp temperature gradients near the side and heater walls, the spatial resolution (IFOV) specification was tightened from 2 mr for the commercial instrument to 1 mr. This increase in spatial resolution will allow the instrument to better resolve the sharp temperature gradients. The minimum sensitivity of the solicited instrument is also better than the commercial imager, improving the low temperature range sensitivity, in order to resolve small amplitude temporal thermal oscillations likely to be encountered during the STDCE.

Other specifications were changed to accommodate the STDCE packaging and STS restraints. The size specified was the maximum envelope allotted for the imager during the packaging/layout of the STDCE hardware. The 30 pound specified weight, an increase of approximately 5 times over the ground-based weight should accommodate the added weight of the cryocooler and space flight qualified structure.

The differences in electrical specifications include the input voltage, power consumption and computer interface. 28 VDC was specified as the input voltage for compatibility with the STDCE

main circuit, although 12 VDC could be used because there are other 12 VDC components in the

Table 1. Major Technical Specifications		
specification	flight	ground-based
spectral response	8-12 μ	8-14 μ
NETD	0.1 $^{\circ}$ C	0.2 $^{\circ}$ C
MRTD	0.1 $^{\circ}$ C	0.1 $^{\circ}$ C
detector cooling	closed cycle cryocooler	LN ₂
FOV	15 $^{\circ}$ V \times 20 $^{\circ}$ H	15 $^{\circ}$ V \times 20 $^{\circ}$ H
IFOV	1 mr (50% response)	2 mr (50% response)
dynamic range	minimum of 48 dB	42 dB
frame rate	30 Hz (2:1 interlace)	30 Hz (2:1 interlace)
output format	RS-170 video	RS-170 video
measurement ranges	5,10,20,50,100,200 $^{\circ}$ C movable between 0 and 500 $^{\circ}$ C both man/auto select	5,10,20,50,100,200 $^{\circ}$ C movable between -20 and 400 $^{\circ}$ C + x-rng center man/auto select
Post flight Image analysis	similar to Thermoteknix system	Thermoteknix system
size		
sensor head	8.0"D \times 9.0"W \times 9.0"H	8.1"D \times 4.8"W \times 4.9"H
electronics	9.3"D \times 10.3"W \times 3.8"H	9.3"D \times 10.3"W \times 5.4"H
weight		
sensor head	30 lbs	6.5 lbs
electronics	7.5 lbs	7.5 lbs
power consumption	maximum of 150 watts	10 watts
input voltage	28 VDC	11-17 VDC
non-operational shelf life	2 years	NA

STDCE package. Power consumption was increased to account mainly for the added draw by the cryocooler. It is not expected that 150 W will be needed but was the maximum available. The RS-232 computer interface specified will be used to control the imager during operation. Temperature range and center temperature will be selectable or, if desired, will be set to automatic via this interface. The ground-based equipment has automatic center temperature but not automatic range selection. Automatic operation of both the temperature range and center temperature is required because of the largely automated nature of the STDCE.

Contractor Development Phases

Three phases of development are specified in the SOW. The first is the design phase. The milestones associated with the design phase are at 50% completion and at final design review. In order to assure the design concept is sound and will meet NASA requirements for design of safety critical structures, materials usage, and safety, the pertinent NASA documentation was researched and incorporated into the design and test requirements (Table 2.). From the STS point

of view, safety is the most important aspect of the flight qualification procedure. This is reflected by the nature of most of these documents. If the safety guidelines for design are followed, the payload developer is assured that his equipment will not harm the STS or its crew.

In addition to the design, a safety verification plan must be presented to show the design meets these safety requirements. NHB 1700.7A outlines the requirements "intended to protect flight and ground personnel, the STS, other payloads, ground support equipment, the general public, public-private property, and the environment from payload related hazards." Not listed in Table 2 is JA-012D Payload Safety Implementation Approach, which is issued to implement NHB 1700.7A. It is not part of the contract because these requirements are the responsibility of the STDCE. The purpose of the document is to "delineate the activities leading to safety certification of instruments that constitute an STS payload for which the Spacelab Payload Project Office has management and integration responsibility."

The second phase of the development is the fabrication/inspection during which the hardware shall be built to the NASA approved design. During the third phase the space flight qualification testing will be performed in an environment similar, if not more rigorous, than that of the STS. The major tests which must be conducted for qualification are vibration, electromagnetic compatibility (EMC) and toxic offgassing. Toxic offgassing tests will insure that in the event the Spacelab module depressurizes no potentially harmful gases will be produced. EMC tests are conducted to insure that the equipment will not interfere electrically, either by radiation or conduction, with the Spacelab instruments or power bus.

Table 2. Documentation Requirements	
Document #	Document Name
NHB 1700.7A	Safety Policy and Requirements for Payloads using the STS
MSFC HB 527	Materials Selection List for Space Hardware Systems
SLP/2104	Spacelab Payload Accommodation Handbook
NHB 8060.1B	Flammability, Odor, and Offgassing Requirements and Test Procedures for Materials in Environments that Support Combustion
JA-418	Payload Flight Equipment Requirements for Safety-Critical Structures
JA-016B	Payload Mission Manager Interface and Safety Verification Requirements for Instruments, Facilities, MPE and ECE on STS Spacelab Payload Missions
JSC 11123	STS Payload Safety Guidelines Handbook

In conjunction with safety, survivability/reliability testing is a prime concern of the payload element developer. Both periodic and random vibration tests are conducted to insure survivability against low frequency transient responses due to engine ignition and cutoff, separation, and docking.

and random vibrations caused by the Spacelab response to acoustic noise in the cargo bay. The levels to which this imager will be subjected are found in the Spacelab Payload Accommodations Handbook (SLP/2104). Because the equipment is situated in a Spacelab rack the vibration levels at the rack/module interface are used. An example of these levels is given in Table 3. In addition to these levels, a magnification factor is added to account for amplification of the vibration levels by the rack and STDCE structure: five times above the levels shown. This magnification factor may be changed as data becomes available from the STDCE engineering model analyses using a dummy mass in lieu of the imager. Because two units will be built and tested, the first will be a protoflight-qualified unit and the second a flight qualified unit. The protoflight unit will be tested to 5 times the levels in SPAH/2104 (prototype testing), refurbished and retested to 1.5 times SPAH levels (qualification testing). This unit will be used as a spare. The second unit is tested only to qualification levels and will be the primary flight unit.

Table 3. Random Vibration Testing Levels			
Frequency (Hz)	Level (g ² /Hz)		
	X axis	Y axis	Z axis
20	0.005	0.002	0.002
20-80	+3 dB/oct	+6 dB/oct	+5 dB/oct
80-200	0.02	0.015	0.01
200-2000	-4 dB/oct	-4 dB/oct	-4 dB/oct
2000	0.00093	0.00047	0.00063
comp. g (rms)	3.1	2.4	2.4
comp. g×5	15.5	12.0	12.0
duration: 60 seconds per axis			

ON-ORBIT CONCERNS

Several problems are expected which are ubiquitous to operation of the STDCE aboard Spacelab. These include the effect of direct CO₂ laser beam reflections, automatic operation of the imager and angular emissivity variations due to the curved free surface.

Because silicone oil reflects specularly, reflections from the CO₂ laser beam, directed normal to the surface, are not incident on the imager detector when the imager is positioned approximately 15 degrees from axis of the test chamber. During operation on Spacelab, however, if the free surface deforms due to g-jitter, direct reflections may be incident on the detector. The reflected flux is low (≈ 0.4 W/cm²) and will result in saturation of the detector resulting in data loss during this time. But, no damage of the imager will occur and if the reflections are periodic there will be intervals in which data can be analyzed.

These reflections may affect the automatic operation of the imager. During automatic operation the imager selects the temperature range and center temperature based on the maximum intensities in the field of view. If reflections cause saturation of the detector, this may, depending on the duration, influence the automatic range and center temperature selection. The time constant should be sufficiently long in order to decrease the sensitivity to this type of transient.

Thirdly, target emissivity is angularly dependent. During the STDCE tests conducted using curved surfaces, the surface normal will be between 0 and 70 degrees from the axis of the test chamber. The directional spectral emissivity predicted from electromagnetic theory as a function of emitted ray angle measured from the unit normal⁷ shows that there is little variation until the angle is larger than 45 degrees. Therefore, only near the walls where the angle between the surface normal and the axis of the test chamber increases past 45 degrees will substantial measurement errors occur. Additional ground-based testing in this area is planned to fully evaluate these effects.

SUMMARY

While most of the development work is complete at this time, developmental testing is an ongoing activity. Concerns associated with operating the imaging system on orbit are being addressed as well as problems involving integration of the system with the STDCE hardware. Until a flight unit is delivered, the commercial unit will be used as an engineering model and will be integrated with the STDCE engineering model hardware.

Flight hardware development was begun in August, 1988 with the compilation of technical specifications, schedule, design and qualification requirements in parallel with the advertised announcement of procurement. The RFP was released on September 19, 1988 and responses received November 1. The contract, expected to be awarded on February 1, 1989, provides 15 months for development, design, manufacture, and qualification testing.

ACKNOWLEDGEMENTS

The author would like to acknowledge the efforts of the members of the STDCE design team for their research into the STS qualification requirements and the organization of the procurement process. David Petrarca wrote the Statement of Work for the Request for proposal for the Flight qualified Infrared Imaging System and William Coho was responsible for coordinating the entire procurement process. Also, NASA Lewis Research Center's Procurement Division was instrumental in expediting the release of the Request for Proposals.

REFERENCES

1. Ostrach, S., "Low Gravity Fluid Flows," Annual Review of Fluid Mechanics, vol. 14, 1982, pp. 314-375
2. Ostrach, S, "Convection Due to Surface Tension Gradients", COSPAR Space Research, Vol. 19, M.J. Rycroft, ed., 1979, pp. 563-570
3. Kamotani, Y. and Ostrach, S., Design of a Thermocapillary Flow Experiment in Reduced Gravity, *J. Thermophys. Heat Trans.*, vol. 1, no. 1, Jan. 1987, pp. 83-89
4. Ostrach, S. and Kamotani, Y., "Science Requirements Document for the Surface Tension Driven Convection Experiment in Reduced Gravity", Department of Mechanical and Aerospace Engineering, Case Western Reserve University., 1987
5. Pline, A., "Surface Temperature Measurements for the Surface Tension Driven Convection Experiment", NASA TM 101353, 1988
6. Lee, M., ed., Non-Contact Temperature Measurement, NASA CP-2503, 1987
7. Siegel, R and Howell, J., Thermal Radiation Heat Transfer, Mc-Graw Hill, 1972, p. 103

SECTION 5

WORKSHOP SUMMARIES

NCTM Workshop Splinter Session,
IR Thermal Measurement Instruments

Herbert Kaplan,
Session Chairman

The splinter session dealing with commercial industrial thermal measurement state-of-the-hardware had a total attendance of 15; a copy of the sign-in sheet is attached.

Two papers were presented in the splinter session as follows:

- 1 "Development of an Infrared Imaging System for the Surface Tension Driven Convection Experiment", Alexander D. Pline, NASA LeRC
- 2 "A Space-qualified PtSi Thermal Imaging System", Robert W. Astheimer, Barnes Engineering Div., EDO Corp.

In addition a brief description of SPRITE detector technology was presented by Richard F. Leftwich of Magnavox.

As anticipated, the discussions were concerned mainly with thermal imaging figures of merit rather than those for point measurement instruments. The need for uniform guidelines whereby infrared thermal imaging instruments could be specified and evaluated was identified as most important, particularly where temperature measurements are required. Presently there are differences in the way different manufacturers present significant performance parameters in their instrument data sheets. Furthermore, the prospective user has difficulty relating these parameters to actual measurement needs, and procedures by which performance can be verified are poorly defined.

The current availability of powerful thermal imaging diagnostic software was discussed. It was suggested that approaches similar to those described in Astheimer's paper could be used to make in-situ measurements for measuring emittance and isolating artifacts due to background and narcissus. It was also agreed that there is a need to extend emissivity characterization programs to longer wavelengths (lower temperatures) than those currently reported at the workshop. One anticipated advantage in this area is that fluids and other

relatively inert surfaces do not normally undergo the changes-in-state that metals experience at higher temperatures. Consequently, emissivity is not expected to vary as widely on these surfaces, and emissivity characterization should be simpler.

A discussion of present technology barriers (other than the need for performance guidelines) was initiated and the list appearing in page 2 of the summary viewgraphs resulted.

The emissivity uncertainty and related background artifacts in point temperature measurements, identified by most of the workshop presenters, was considered an important barrier to quantitative thermal imaging as well. Line of sight restrictions and some of the unexpected complications that result when "IR transmitting" windows are used were also listed as barriers. This led to discussions of fiber optics approaches to bypass line-of-sight problems, and another barrier recognized was the limited performance of available infrared (2-12 μ) fiber optics. Some concern was expressed that there is uncertainty regarding the actual spatial resolution obtained with thermal imagers. (This relates back to the need for performance guidelines) It was also agreed that there is only limited appreciation of the potential of currently available IR thermal imaging instrumentation among current and prospective experimenters.

Some ideas for possible solutions of some of the problems introduced in the workshop were discussed as follows:

- 1 For flame shape and temperature characterization an approach whereby a modulated blackbody reference surface was placed behind the flame was introduced. Thermal images could be obtained of both the composite (background + flame) image and the background image alone. This should yield information regarding the flame shape, temperature and, possibly, the composition of the combusting material. Additional imaging using a 10.6 "flame suppression" filter and a 4.3 "flame emission" filter was also suggested.
- 2 Multispectral thermal imaging was suggested as a means to characterize emissivity distribution across a target.
- 3 Platinum silicide (PtSi) mosaic imaging was suggested for fast moving targets. Since every pixel is always active, the location and size of the moving target is always known. The use of PtSi was also suggested for simultaneous visible and IR imaging since the spectral response is from 1-5 μ . This could be accomplished using simple beam splitters to separate the visible and IR information.
- 4 The possible use of coherent long wavelength fiber bundles was suggested for imaging of otherwise inaccessible targets. The combination of such a bundle with a low cost imager such as a pyroelectric vidicon camera might provide useful qualitative thermal distribution information at modest cost.

NASA NCTM WORKSHOP

January 17-19, 1989
Pasadena, California

Summary of Subsession II
(Dynamic Response for Thermal Control and
Measurement and Fast Radiation Thermometry)

R. L. Shepard (ORNL) and A. Cezairliyan (NIST)

Two-Color Ratio Pyrometer Temperature Sensing for Dynamic Control of MEL

A preliminary evaluation was made by ORNL of a two-color ratio pyrometer (TCRP) for temperature control in the Modular Electromagnetic Levitation (MEL) experiment. A discussion was presented by Eric Spjut at the 1987 NASA Non-Contact Temperature Measurement Workshop (NASA Conf. Publ. 2503, pp. 182-213) in which he described the non-linear characteristic of the time response of TCPs. We replicated his model and results and note that the non-linear response behavior is minimized for small temperature steps at high temperatures. We then used the predicted response in a model for a proportional or integral feedback controller and predicted the control characteristics for heating and cooling a 5-mm diameter sphere of niobium at high (1500-2750 K) temperatures. The analysis shows that for a slow (25-ms) time response for a commercial TCRP, overshoots of several hundred kelvins will result from a 100-K decrease in the setpoint, and temperature tracking errors of 14 to 45 K will occur for control temperature ramps of 1000K/s. For a fast (<0.1 ms) time response, the overshoot and ramp response errors are largely eliminated.

Additional analysis should be performed and provisions for decreasing the TCRP response time should be employed before considering the TCRP as a sensing element for feedback heating control in the MEL experiment. Such a control system would also require the incorporation of an algorithm which describes the non-linear response characteristics of the TCRP, and probably the present and intended temperatures as well. In spite of many concerns about the universality of the TCRPs independence of the samples emissivity, the TCRP should be considered as a control sensor, but its unusual dynamic response must be recognized. An alternative approach might use only one channel as the control signal, normalized to the correct temperature at steady state by two-channel ratio.

Fast Radiation Thermometry

A review of the development and operation of millisecond and microsecond resolution radiation thermometers (pyrometers) at NIST - the National Institute of Standards and Technology (formerly National Bureau of Standards) was given at the First Non Contact Temperature Measurement Workshop in 1987.

In this session, progress made at NIST in fast pyrometry since the last Workshop was summarized. Special emphasis was placed in the development of the fast spatial scanning pyrometer. This pyrometer is capable of measuring

the spectral radiance temperature at 1024 points along a straight line in the target field about every one millisecond. The pyrometer utilizes a self-scanning linear array of silicon photodiodes as a detector. The electrical signals are recorded with a digital oscilloscope every one microsecond (12 bits) and processed with a computer.

The preliminary tests indicate satisfactory stability and reproducibility. At 2000K, imprecision is about 1 K and estimated total uncertainty is 4 K. Work is in progress to further assess the operational characteristics of the pyrometer. It is expected that the spatial scanning pyrometer will become completely operational by the end of 1989.

The spatial scanning pyrometer will permit performance of experiments which have not previously been possible: (1) accurate determination of the temperature uniformity or nonuniformity in pulse-heated specimens in transient experiments. This pyrometer is likely to be very useful also in measurements of temperature distribution in specimens under steady-state conditions. The short scanning times will minimize the effect of some of the changing conditions and improve the diagnostic procedures.

NASA NCTM WORKSHOP

January 17-19, 1989

Summary Comments

R. L. Shepard (ORNL)

Noncontact temperature measurement science as applied to NASA materials research and space applications is a multi-dimensional problem. Such applications include (a) various materials: metals, semiconductors, insulators, and organics, (b) a spectrum of temperatures ranging from 300 to 3000 K, (c) properties such as solidification and crystallinity, and (d) spatial requirements including very fine detail, imaging, and mapping.

It is clear that there is no universally applicable temperature measurement technique that can cover all the applications. Development of a wide choice of diverse techniques is essential in meeting the varied requirements. While research studies reported at this meeting provide many phenomena related to and useful in thermometry, each technique is strongly application dependent. Many of these applications require a specialized knowledge of the technique and of the application requirements to be successfully used in thermometry. Workshops such as this provide an essential vehicle for transporting such knowledge between the developer and the user, and in identifying applications for which no successful thermometry technique has been developed.

NASA is to be commended for supporting the workshop and the studies which were reported. These studies have produced several new and potentially useful thermometry techniques that were developed since the last workshop held in Washington in 1987. These new studies include surface modulation reflectance in semiconductors, UV laser fluorescence, Raman scattering, ellipsometry, and Johnson noise. A recurring theme was the application of multicolor radiation thermometry and its pros and cons, with some encouraging reports of success in some applications. Additional emphasis appears in the use of laser and fiber optic technology.

Problem areas reported at the meeting or inferred from the presentations include (a) accurate noncontact measurements at temperatures below about 1000 K, (b) inference of bulk temperatures from surface temperature measurements, (c) competing requirements for high temperature accuracy and fast response time, (d) application of discrete or large-area temperature determinations to thermal imaging, and (e) development of related techniques for calorimetry, phase identification, and crystallinity.

One specific application problem still remains unsolved. There does not appear to be any one radiometric method that can provide an accurate non-contact measurement of the surface temperature of a molten metal sphere without some knowledge or assumption about the metal's emissivity, the shape of the sphere, and its surface texture. The problem is compounded by two additional practical considerations: (a) the effects of the speed of response of the measurement system on the temperature control and (b) the occlusion of the radiation by window fogging. Four general methods have been proposed: (1) multicolor pyrometry, (2) brightness pyrometry supported by reflectance measurement, (3) brightness pyrometry supported by ellipsometry, and (4) very short wavelength ("high power of T") pyrometry. Each have been used successfully in some applications, but each has some limitations or implicit assumptions

that limit its application to the temperature measurement of a molten metal drop. Multicolor pyrometry (1) is reported to be susceptible to large temperature errors if the functional relationship of emissivity to temperature or to wavelength is not simple, well-behaved, and continuous. It has however been used at Purdue, MIT, Georgia Institute of Technology, Vanderbilt, and Physical Sciences Inc. to provide good temperature accuracy in some applications. Laser reflectance (2) has been used by workers at Rice and JPL to obtain normal incidence emissivity for correcting brightness measurements, but its application to spherical, irregular, or rough surfaces presents some problems. Ellipsometry (3) has been used at Rice and Intersonics to correct brightness measurements with notable success, but it requires off-normal incidence and very smooth surfaces. Very short UV radiometry (4) minimizes the error in temperature due to an uncertainty in the emissivity, but is apparently difficult to implement in practice. Additional progress could be made in developing each of these techniques. Several (2 and 3) would profit from a variable wavelength laser that would encompass the effective wavelength of the brightness pyrometer. Each will be difficult to employ for measurement of a moving, pulsating, or dancing metal sphere. The laser reflectance technique now seems most likely to be used in near-term applications, but it might be coupled with one of the other methods (e.g., two-color ratio pyrometry) to reduce the temperature uncertainty and provide temperature control system signals.

A general problem in the NCTM program is the validation of data produced by various investigators, which highlights needs for test method, calibration, and material property standards. Calibration capabilities of the NIST were addressed by Barry Hillard, and materials properties were addressed by C. Y. Ho of Purdue. Test method standards do not appear to be well supported.

Particular problems for transfer of terrestrial laboratory techniques to space applications include (a) miniaturization and remote operation of equipment, (b) interfacing of temperature sensors with control systems, and (c) management, storage, and transmission of copious amounts of data.

The workshop produced a sense of optimism about our abilities to measure temperatures in many exacting and difficult applications. It appears that the imminent problems to be faced in the NASA program are the engineering application of these techniques to the control and data production in specific space missions.

Summary of Splinter Workshop on**MATERIALS THERMAL & THERMORADIATIVE
PROPERTIES/CHARACTERIZATION TECHNOLOGY**

**D.P. DeWitt, Professor
School of Mechanical Engineering
Purdue University
West Lafayette, IN 47907**

**and
C.Y. Ho, Director
CINDAS/Purdue University
2595 Yeager Road
West Lafayette, IN 47908**

ABSTRACT

Reliable properties data on well characterized materials are necessary for design of experiments and interpretation of experimental results. The activities of CINDAS to provide data bases and predict properties are discussed. An understanding of emissivity behavior is important in order to select appropriate methods for non-contact temperature determination. Related technical issues are identified and recommendations are offered.

INTRODUCTION

The intent of this splinter workshop session was to define technical issues and offer recommendations on the thermophysical and thermoradiative properties that are important for materials science characterization in microgravity of thermally important events and behavior. Two presentations were given by the authors and are summarized below. While many of the topics were given discussion by other participants, the remarks are personal rather than consensus opinions.

THERMOPHYSICAL PROPERTIES

The need for reliable thermophysical properties in the design of microgravity experiments, applications related work and the interpretation of experimental results was clearly made in the proceedings of the last workshop [1, see for example, pp. 72, 76, 81 and 214]. While the goal of the program is to develop new materials, much of the present activity focuses on materials for which there exists literature information which may be quite fragmented, but could be useful for prediction and estimation analyses. We refer to this activity as *data physics*, the methodology for synthesizing existing information and knowledge to property values.

The *Center for Information and Numerical Data Analysis and Synthesis* (CINDAS) founded in 1957 has been recognized as the largest single source of reliable materials property data. Its major functions are:

- literature searches
- data compilation
- data evaluation and analysis
- data synthesis and prediction
- numerical data base development
- on-line operation of data bases
- property research and measurements
- material property publications
- inquiry service

While CINDAS provides these services to a variety of industrial and governmental organizations, its major commitment is to the Department of Defense (DoD) as the *High Temperature Materials - Mechanical, Electronic and Thermophysical Properties Information Analysis Center* (HTMIAC). Further details on HTMIAC and CINDAS services and how they can be accessed are provided in Appendix A.

The *technical issue* is the availability of thermophysical and thermoradiative properties. The resources of HTMIAC-CINDAS, developed over a period of more than 30 years through extensive governmental and industrial support, can be utilized in a cost-effective manner to meet many of the present and future needs of the Microgravity Program. Toward developing a relationship between program investigators and CINDAS, the following *recommendations* are offered:

- the investigators should use the inquiry service to determine the extent *and* value of literature holdings and compiled data on the properties/materials of interest to them,
- program management should develop a priority list of materials and properties of interest so that the coverage and quality of data can be assessed, and
- some special cases where data is not available but is urgently needed should be identified and a demonstration synthesis (data physics) effort initiated to make predictions/estimations.

To effectively support the Microgravity Program, a relationship between NASA and CINDAS should be established which will permit CINDAS to serve as the central source for all properties-related requirements.

EMISSIVITY AND ITS EFFECT ON TEMPERATURE DETERMINATION

A reoccurring theme voiced during the paper presentations and their discussions was the need to understand material emissivity behavior in order to make reliable non-contact (radiometric) measurements. Specific situations within the Microgravity Program where emissivity data or behavior knowledge is lacking have been identified in the proceedings of the last workshop [1, see for example, pp.58, 59, 72, 75, 76, 149, 180 and 183]. These needs are not specific to only microgravity studies; similar challenges to the radiation thermometrist have been addressed for several decades [2,3]. While the literature on spectral emissivity and radiation thermometry is extensive, it is widely spread and not easily accessed. Recent re-newed interests by the metals processing [4] and petrochemical [5] industries, seeking improved temperature measurement accuracy to achieve increased productivity, have stimulated efforts to address the *central problem*

of noncontact temperature determination: how to account for emissivity effects [3].

There are two major *issues* related to understanding material emissivity behavior. First, it is essential to obtain reliable measurements of the spectral emissivity as a function of wavelength and temperature on well-characterized materials under controlled environmental conditions. This information can be generated in apparatus designed specifically for that purpose as has been the case for the large majority of the data reported in the literature. Alternately, this information will come as a consequence of special efforts made during experiments devoted to wider purposes such as are being conducted in the Microgravity Program now.

The second major issue is that of understanding the effect of emissivity on different non-contact or radiometric methods for inferring surface temperatures. In subsequent subsections, five methods are briefly discussed with a view to establishing the role of emissivity behavior or uncertainty in inferring temperature with confidence.

Narrow-Band or Spectral Methods

From the temperature equation for the spectral method using the Wein's approximation to the Planck spectral distribution law [2] (see also Eq. 2 in Appendix B), the relative uncertainty in inferred temperature due to the uncertainty in the emissivity is

$$\frac{\Delta T}{T} = -\frac{\lambda T}{c_2} \cdot \frac{\Delta \epsilon}{\epsilon} . \quad (1)$$

Since most practical radiometric systems are operated at $\lambda T \ll 2898 \mu\text{m}\cdot\text{K}$ (that is, to the short wavelength side of the spectral radiance maximum of the blackbody curve) and with $c_2 = 14,389 \mu\text{m}\cdot\text{K}$, it follows that the $\lambda T/c_2$ term can range from 1/5 to typically as low as 1/15. Hence, for relative uncertainties in the spectral emissivities as high as $\pm 10\%$, there are situations where the resulting error in the inferred temperature may be acceptable. For high emissivity materials, such as many ceramics and oxidized metals, it is reasonable to estimate emissivity values within $\pm 10\%$. For well polished metallics, particularly in the emissivity range of 0.1 to 0.2, it may not be possible to make estimates with suitable accuracy to infer temperature with decent confidence.

There are two special features of the spectral method that should be noted. First, the method offers the greatest sensitivity between spectral radiance and temperature changes, implying that instrumentation noise will have the least effect on the temperature determination. Second, experimentally observed spectral radiance temperatures that are not corrected for emissivity are still of value since, when such knowledge is available, the data can be manipulated easily to infer true temperatures.

There are other pitfalls in applying the spectral method, the most difficult of which is avoiding or making corrections for irradiance from the surroundings reflected off the target into the radiometer. This situation occurs frequently when viewing targets being heated in furnaces. If the surroundings are large and isothermal, the correction procedure is straight forward [2]. Such is not the case in many practical situations and the correction procedure is tedious if not very approximate.

The Ratio Method

The ratio method has two special features: (1) the target need not fill the radiometer field-of-view and (2) effects of absorption on observed spectral radiances along the line-of-sight due to windows or atmospheric gases may be minimal, especially if the two spectral bandpasses are close together. Further, if the emissivity spectra in the region of the bandpasses is gray (spectrally flat), then the ratio temperature determined from the spectral radiance ratio is equal to the true temperature. There are limited situations, such as high emissivity, heavily oxidized surfaces, where the target emissivity behavior is sufficiently gray that true temperature can be inferred with high accuracy by ratio thermometers.

Ratio thermometry was first introduced in steel making applications. As requirements for greater accuracy developed, other methods have been sought, the most successful of which at present are hybrid methods requiring the use of ancillary furnaces, mirrors and multiple detectors [2].

Ratio thermometry has been proposed or is being used in several experiments within the Microgravity Program. Some of these applications take advantage of the aforementioned special features. But non-grayness of sample targets, particularly metallics, will likely cause disappointing temperature determination results. Further, observed ratio temperatures cannot be corrected easily for nongrayness and irradiance effects if, at a later time, knowledge of the spectral emissivity becomes available. Ratio thermometers with adjustable off-sets are commercially available and find good utility in many industrial processes. Such instrumentation and practice for use on materials science experimentation is to be discouraged.

Recommendations. (1) The applicability and limits of error for ratio thermometer methods to determine true temperature should be thoughtfully examined before reporting temperature determination results. (2) Dual wavelength methodology should be investigated for applications seeking higher accuracy which do not require the two special features of ratio thermometry. A brief overview of recent developments is provided in Appendix B.

The Multispectral Method

Considerable attention was given to the multispectral (typically 6 to 100 spectral bands) method during the workshop. In separate contributions of this proceedings, Kahn and Spjut conclude that *a priori* emissivity information, such as the form of the emissivity function, is not required and that the method can yield a statistical estimate of the uncertainty in the inferred true temperature. Using six spectral bands in the visible, Oshe and co-workers at the European Transuranium Institute have successfully used the indirect multispectral method with a linear emissivity function on alloys and ceramics [6,7]. The particular application is to determine the rapid change of material temperature during pulse heating experiments to observe thermodynamic and transport properties. A version of the six-wavelength pyrometer based upon this technology has been offered commercially [8].

Recommendations: (1) Continued inquiry should be directed toward understanding the features and limitations of multispectral methods. Particularly useful would be in-depth archival literature on recent developments that could be carefully studied by a wide community of workers in the field. (2) While most of the experiences to date with multispectral methodology have been based upon silicon photodetector technology ($\lambda < 1.1 \mu\text{m}$), its implementation to the moderate temperature range below 1000 K needs to be considered. Candidate detector arrays for the mid-IR region multispectral radiometers need to be evaluated.

Laser Pyrometry

Laser pyrometry [9,10] provides the means to infer the target temperature from observations of the spectral radiance temperature and the directional (near-normal) reflectance. For a specular or diffuse surface, the bidirectional reflectance is directly related to the normal emissivity required of the spectral temperature equation.

If the target material is neither specular nor diffuse, or its degree of diffuseness changes during the course of time as is the case in many materials processes, the bidirectional reflectance is no longer directly related to the normal emissivity. For example, the bidirectional reflectance of a slightly non-specular (due to microstructure changes, for example) surface can be remarkably different than that of the specular surface, yet their normal emissivities may be only slightly different.

Nutter [11] proposed a technique to overcome this difficulty which measures the bidirectional reflectance ratio between two or three wavelengths depending upon whether the surface is either diffuse or specular or has an unknown degree of diffuseness, respectively. Appendix C provides a brief overview of the critical feature of the method, namely, whether R_{ij} , the ratio of the normal-hemispherical reflectance ρ_{ih} to the bidirectional reflectance ρ_{ij} , is a linear function with wavelength. Because there is a dearth of bidirectional reflectance distribution function (BRDF) data in the literature, this issue cannot be addressed without conducting specially planned experiments.

Recommendations: There is growing national interest and capability in making BRDF measurements on materials with different surface characteristics. Through the design of critical experiments utilizing BRDF data on selected materials, the feasibility of the two- or three-wavelength pyrometry as proposed by Stein and Nutter should be evaluated.

OTHER TECHNICAL ISSUES

Methods for measuring the spectral emissivity and optical properties of small samples, especially if they are spherically shaped, are limited to ideal smooth surfaces. Krishnan, et al., in a separate contribution to these proceedings, have effectively demonstrated a rotating analyzer-ellipsometry method on ripple free liquid metals. This study has created a significant knowledge base for understanding the changes in emissivity as a function of wavelength and temperature for metals in the liquid state.

Other reliable methods for metallics or ceramics in the solid state have yet to be demonstrated. *Recommendation:* Attention should be given to developing and thoroughly evaluating methods for obtaining thermoradiative and/or optical properties of materials in their processing environment.

Contributions to the archival literature should not be overlooked. It is important that results of experimental studies, especially high quality properties data and temperature measurement methodology, should be disseminated and undergo the peer review process. *Recommendation:* Investigators should be encouraged to publish the results of studies. Special attention should be given to characterization of the materials for which properties data are reported. Further, the investigators should participate in the traditional and specialty conferences organized by technical societies.

During the course of the workshop, the need for radiation thermometer calibration and standardized procedures was discussed. The possibility of requiring improved calibration accuracies at elevated temperatures nearly twice that of present NIST capability was suggested. At present, calibration requirements for ratio thermometers and standard test methods are undefined. *Recommendation:* Because of the long lead time to established improved metrological practices, NIST should remain involved in this program. Their contributions will be welcomed also in the traditional industrial areas.

SUMMARY AND CONCLUSIONS

The purpose of the splinter workshop session was to identify technical issues and offer recommendations. The first major technical issue discussed was the status of thermophysical and thermoradiative properties. Using CINDAS as a resource, we are recommending that

- investigators utilize CINDAS data bases to determine extent and value of current literature, compiled data, etc., to this problem,
- program management develop a property list of property/materials and an assessment of coverage to be performed, and
- to meet urgent needs, a demonstration synthesis effort be initiated.

Through these steps, the role of CINDAS to serve as a central source for all property related requirements can be demonstrated.

The central problem of radiation thermometry or non-contact temperature determination, how to account for emissivity effects, requires an understanding of the target material emissivity behavior. Two technical issues can be identified: (1) the need for reliable spectral emissivity data on well characterized materials under controlled environmental conditions and (2) understanding the effect of emissivity on different radiometric methods for inferring surface temperature. The first of these issues can be best addressed by individual materials investigators as an integral part of experiments designed for a broader purpose. In regards to methodologies, five recommendations were offered:

- applicability and limits of error for ratio thermometry need to be assessed for each application,
- dual wavelength methodology should be investigated for applications seeking higher accuracies,
- continued inquiry should be directed toward understanding the features and limitations of multispectral (≥ 3 wavelengths) methods especially as related to not requiring any *a priori* information and providing estimates for accuracy of inferred temperature,
- evaluation of candidate detector arrays for mid-IR region multispectral radiometers, and
- performing critical experiments to establish the feasibility of two- and three-wavelength laser pyrometry to account for non-gray, non-diffuse material behavior.

The importance of contributions by the program investigators to the archival literature should be stressed. Publication of well-characterized, high quality data will be a stimulus to a wide technical community. Finally, it is recommended that the NIST should remain closely involved in the program in order that improved standards and metrological practices will be available as required.

REFERENCES

1. Lee, M.C., Editor, Noncontact Temperature Measurement, NASA Conference Publication 2503, NASA, pp. 429, 1988.
2. DeWitt, D.P., "Inferring Temperature from Optical Radiation Measurements," *Optical Engineering*, 25(4), 596-601, 1986.
3. DeWitt, D.P. and G.D. Nutter (Eds.), *Theory and Practice of Radiation Thermometry*, John Wiley and Sons, pp. 1138, 1988.
4. Richmond, J.C., and D.P. DeWitt (Eds.), *Applications of Radiation Thermometry*, Amer. Soc. for Testing and Materials, Monograph 895, pp. 171, 1986.
5. DeWitt, D.P., and L.F. Albright, (Eds.), *Measurement of High Temperatures in Furnaces and Processes*, AIChE Symposium Series 82, No. 249, pp. 100, 1986.
6. Babelot, J.F., Magill, J., Ohse, R.W. and M. Hoch, "Microsecond and Submicrosecond Multi-Wavelength Pyrometry for Pulsed Heating Technique Diagnostics," *Temperature, Its Measurement and Control in Science and Industry*, J.F. Schooley, Ed., American Institute of Physics, pp. 439-446, (1982).
7. Hiernaut, J.P., Beukers, R., Heinz, W., Selfslag, R., Hoch, M. and Ohse, R.W., "Submillisecond Six-Wavelength Pyrometer for High-Temperature Measurements in the Range 2000 to 5000 K," *High Temperatures - High Pressures*, 18, pp. 617-625, (1986).

8. Neuer, G., (IKE, University of Stuttgart, West Germany), Private Communication, November 18, 1988.
9. Stein, A., "Laser Pyrometry," Reference 1, Op. Cit., pp. 279-290.
10. Stein, Alex, (Quantum Logic Corp., Hackensack, NJ), Private Communication, April 6, 1989.
11. Nutter, G.D., "Reflectance-Ratio Radiation Thermometry Applied to Aluminum Samples: Status Report," Proceedings of the Aluminum Association, May 1988, pp. 271-279.
12. Tsai, B.K., Shoemaker, R.L., DeWitt, D.P., Cowans, B.A., Dardas, Z., and Delgass, W.N., "Dual-Wavelength Radiation Thermometry: Emissivity Compensation Algorithms," *Int. J. of Thermophysics*, (accepted for publication, January 1989).
13. G.M. Foley, "Modification of Emissivity Response of Two-color Pyrometers" *High Temp.-High Pressures* 10, p. 391 (1978).
14. M. Watari, et al., "A New Two-color Radiation Pyrometer" *Yokogawa Tech. Rep.* 29, p. 25 (1985).
15. M. Watari, et al., "Optical Fiber Radiation Pyrometer" *Yokogawa Tech. Rep.* 31, p. 8 (1987).
16. A.S. Anderson, "Accurate Noncontact Measurement of the Aluminum Surface" *Workshop Sens. Volume 91*, Aluminum Association, Washington, DC (1986).
17. A.S. Anderson, "An Improved Radiometer for Temperature Measuring of the Aluminum Surface" *Instrum. Soc. Am.* (1985).
18. G.J. Dail, M.G. Fuhman and D.P. DeWitt, "Evaluation and Extension of the Spectral-Ratio Radiation Thermometry Method" *Proc. Fourth Int. Alum. Extrusion Technol. Semin.* Volume 2, pp. 281-286 (1988).
19. Tanaka, F., and DeWitt, D.P., "Theory of a New Radiation Thermometry Method and an Experimental Study Using Galvannealed Steel Specimens," accepted for publication by Society of Instrumentation and Control Engineers (SICE-Japan), November 1988.
20. Tanaka, F., and DeWitt, D.P., "Experimental Study of a New Radiation Thermometry Method on Oxidizing Steel," 1989 National Heat Transfer Conference, (August 1989), Paper No. 89-xxxx.

Appendix A

A CENTRAL SOURCE FOR THERMOPHYSICAL PROPERTIES OF MATERIALS:

HTMIAC-CINDAS

The Center for Information and Numerical Data Analysis and Synthesis (CINDAS) was founded at Purdue University on 1 January 1957, originally as the Thermophysical Properties Research Center (TPRC). For over 30 years, CINDAS has devoted its efforts solely to the properties of materials. Since 1960 CINDAS has been operating for the Department of Defense (DoD) an information analysis center on materials properties, which evolved to become the Thermophysical and Electronic Properties Information Analysis Center (TEPIAC) in 1973 and to become the High Temperature Materials - Mechanical, Electronic, and Thermophysical Properties Analysis Center (HTMIAC) in 1986. CINDAS has developed for various sponsors the following numerical data bases on materials properties:

- High Temperature Materials Properties Data Base.
- Data Base on Dielectric Materials.
- PC-Version Data Base on Microelectronic Packaging Materials.
- Engineering Materials Properties Data Base.
- Thermophysical Properties of Fluids Data Base.
- Thermophysical and Mechanical Properties of Rocks and Minerals Data Base.

Furthermore, CINDAS' bibliographic data bases on materials properties contain bibliographic information on over 270,000 pertinent worldwide scientific and technical documents.

The properties coverages for different types of materials in different data bases are more or less different. As a typical example, the properties covered in the High Temperature Materials Properties Data Base, which is developed through the operation of HTMIAC for the DoD, are given below:

(A) Thermophysical, Thermoradiative, Optical, and Electronic Properties:

- | | |
|--------------------------|------------------------|
| • Ablation energy | • Heat of fusion |
| • Ablation temperature | • Heat of vaporization |
| • Absorptance | • Melting point |
| • Absorption coefficient | • Reflectance |
| • Boiling point | • Refractive index |
| • Density | • Thermal conductivity |
| • Electrical resistivity | • Thermal diffusivity |
| • Emittance | • Thermal expansion |
| • Heat capacity | • Transmittance |

(B) Mechanical Properties:

- Compressive modulus
- Compressive strain at fracture
- Compressive strength, ultimate
- Compressive strength, yield
- Elastic constants
- Elongation
- Energy release rate
- Flexural modulus
- Flexural strength
- Fracture toughness
- Hardness
- Impact energy
- Poisson's ratio
- Reduction in area
- Shear modulus
- Shear modulus, in-plane
- Shear strain at fracture
- Shear strength, in-plane
- Shear strength, interlaminar
- Shear strength, ultimate
- Shear strength, yield
- Stress-strain curves, compression
- Stress-strain curves, shear
- Stress-strain curves, tension
- Tensile modulus
- Tensile strain at fracture
- Tensile strength, ultimate
- Tensile strength, yield

HTMIAC/CINDAS has been disseminating data and information on materials properties through publications, inquiry services, and through on-line operation of the data bases. Over the years CINDAS has published the resulting data and information on materials properties so far in 36 volumes of data books and 26 volumes of properties research literature retrieval guides with a total of over 50,000 pages, and in more than 150 technical reports and numerous research articles. CINDAS has responded to more than 12,000 inquires for data and information on materials properties and for technical consulting, advisory, analysis, and other user support services.

In the on-line operation, the data base is interactive, menu-driven, and user-friendly. Since it is menu-driven, no special query language or commands need to be learned and any user can easily search and retrieve the needed data from the Data Base.

The procedures to use HTMIAC/CINDAS services are as follows:

- (1) Write HTMIAC/CINDAS or call (317) 494-9393 for its inquiry services or technical products.
- (2) Subscribe to HTMIAC/CINDAS on-line numerical database service.
- (3) Contact HTMIAC/CINDAS for major technical work through a purchase order, military interdepartmental purchase request (MIPR), contract, etc.

Appendix B

OVERVIEW ON DUAL-WAVELENGTH RADIATION THERMOMETRY METHODS

Introduction

Dual-wavelength methods are extensions of the ratio method wherein two spectral radiance temperatures, T_{λ_1} and T_{λ_2} , are directly measured, usually with a single detector, rather than the ratio of the spectral radiances for two closely spaced spectral bands [12]. Different algorithms, frequently referred to as emissivity compensation algorithms, have been evaluated by various investigators to infer true temperature from the observed spectral radiance temperatures. An overview of six methods follows.

Principles of the Methods

The *spectral* temperature equation for the spectral method using the Wein's approximation to the Planck spectral distribution law is

$$\frac{1}{T} = \frac{1}{T_\lambda} + \frac{\lambda}{c_2} \ln \epsilon_\lambda. \quad (2)$$

For the ratio method, using the same relation but written for two spectral conditions, the *ratio* temperature equation is

$$\frac{1}{T} = \frac{1}{T_r} + \frac{\Lambda_r}{c_2} \ln \left(\frac{\epsilon_1}{\epsilon_2} \right) \quad (3)$$

where the ratio temperature, T_r , and the equivalent wavelength, Λ_r , are defined such that

$$\frac{1}{T_r} = \Lambda_r \left[\frac{1}{\lambda_1 T_{\lambda_1}} - \frac{1}{\lambda_2 T_{\lambda_2}} \right] \quad \Lambda_r = \frac{\lambda_1 \lambda_2}{\lambda_2 - \lambda_1}. \quad (4,5)$$

To achieve emissivity compensation, the second term on the right-hand side of Eq.(3) needs to be zero or a known constant independent of temperature and surface conditions; that is, the ratio method requires that $\epsilon_1/\epsilon_2 = \text{constant}$.

The temperature equation and compensation algorithms for the dual-wavelength methods are provided in Table B-1. The Foley method, Eqs. (6-8), is a variation of the ratio method where K_f is the parameter which is adjusted to account for non-gray behavior [13]. Note that when $K_f = 0$, T_{mr} , the modified-ratio temperature, becomes the ratio temperature. The Watari method, Eqs. (9,10), is yet another variation of the ratio method and is based upon an exponential spectral emissivity function, Eq. (10) [14,15]. The next three methods shown in the Table B-1 have temperature equations which are empirical in nature. The *ratio-with-offset* (RWO) relationship is commonly used in commercial ratio instruments where emissivity compensation is achieved by

adjusting the parameter B. Anderson [16,17] recognized that for metallic surfaces the spectral radiance and ratio temperatures are systematically low and high, respectively, compared to the true temperature. Referred to as the *linear spectral-ratio* (LSR) method, the temperature equation, Eq. (12), is a linear combination of the ratio and spectral radiance temperatures. A variation of this approach, that is slightly improved in some situations, is the *inverse spectral-ratio* (ISR) method, Eq. (14) [12,18]. The forms of the emissivity compensation algorithms for these two methods, Eqs. (13) and (15), are quite complicated but similarly require that the ratio $\ln\epsilon_2/\ln\epsilon_1$ remain constant. The advantage of the ISR method is apparent from the algorithms by noting that y_o is independent of temperature while x_o for the LSR method is not. The Tanaka-DeWitt method [19,20], requires *a priori* information in the form of an emissivity function, Eq. (17), which must be determined by separate experiments over a range of surface conditions the target material might have.

Discussion and Summary

The Watari, LSR, and Tanaka-DeWitt methods have been reduced to practice. The Watari method has been demonstrated with steels that undergo heat treatment with subsequent oxidation. A commercial instrument based upon the LSR method is being used in the aluminum industry. The Tanaka-DeWitt method has been successfully demonstrated on the galvaneal (zinc dip on steel) process and hot strip mill in the steel industry.

While dual-wavelength methods have been successfully applied to specific applications, as yet there is no general approach to be recommended for new situations. Determining the appropriate form for the emissivity compensation algorithm is the challenge, which of course, depends upon understanding the behavior of the spectral emissivity of the target material in its process environment. There are strong incentives to continue investigations on dual-wavelength methodologies: accuracies of $\pm 3K$ (in the 800-1000K) have been demonstrated and environment-hardened instrumentation can be built for reasonable costs. Clearly, the obstacle to an improved technology is an improved understanding of the behavior of material.

TABLE B-1 Dual-Wavelength Temperature Equations and Algorithms

Method/Author	Temperature Equation	Compensation Algorithm	Adjustable Parameter(s)
Foley [13]	$\frac{1}{T} = \frac{1}{T_{mr}} + \frac{\Lambda_r}{c_2} \left[(1 - K_r \lambda_1) \ln \epsilon_1 - (1 - K_r \lambda_2) \ln \epsilon_2 \right]$ $\frac{1}{T_{mr}} = \Lambda_r \left[\frac{1 - K_r \lambda_1}{\lambda_1 T_{\lambda 1}} - \frac{1 - K_r \lambda_2}{\lambda_2 T_{\lambda 2}} \right]$	$\frac{\ln \epsilon_1}{\ln \epsilon_2} = \frac{1 - K_r \lambda_2}{1 - K_r \lambda_1}$	K_r
Watari [14,15]	$\frac{1}{T} = \frac{1}{T_r} + \frac{\Lambda_r}{c_2} \alpha (\lambda_1^2 - \lambda_2^2)$	$\epsilon_\lambda = \exp(\alpha \lambda^2)$	α
Ratio with Offset (RWO) [18]	$T = T_r + B$	---	B
Linear Spectral-Ratio (LSR) [16,17]	$T = (1 - x_0) T_r + x_0 T_{\lambda 2}$	$x_0 = \frac{\frac{\lambda_1 T}{c_2} \ln \epsilon_1 - 1}{\Lambda_r \left[\frac{\ln \epsilon_2}{1 - \ln \epsilon_1} \right] - 1}$	x_0
Inverse Spectral-Ratio (ISR) [12,18]	$\frac{1}{T} = \frac{(1 - y_0)}{T_r} + \frac{y_0}{T_{\lambda 2}}$	$y_0 = \frac{-1}{\Lambda_r \left[\frac{\ln \epsilon_2}{1 - \ln \epsilon_1} \right] - 1}$	y_0
Tanaka-DeWitt [19,20]	$T = f(L_{\lambda 1}, L_{\lambda 2}, \epsilon_1, \epsilon_2)$	$\epsilon_2 = f(\epsilon_1)$	---

Appendix C

OVERVIEW ON LASER PYROMETRY

Laser pyrometry technology has been demonstrated to provide marked improvement in the accuracy of temperature determination as compared to passive techniques [1, p.304]. However, the technique as presently practiced is limited to diffuse (lambertian) targets [10]. Effects due to reflected irradiation, from a hotter furnace wall, for example, can be accounted for in the same manner as treated for passive spectral methods. There are many situations where the target material is diffuse and laser pyrometry can be applied with high confidence. Further, if the degree of diffuseness of the target material is unchanging during the observation periods, the technique can then account for changes in the emissivity of the material due to process variables, temperature or other parameters.

Stein [10] and Nutter [11] have addressed extending the single-wavelength or spectral laser pyrometry method to two and three wavelengths, respectively, in order to account for non-diffuse effects. The technical issue underlying their efforts centers about relationships between three thermal radiative properties: the directional spectral emissivity, $\epsilon_{\lambda,i}$; the directional-hemispherical reflectance, $\rho_{\lambda,ih}$; and the bidirectional reflectance distribution function (BRDF), ρ_{ij} . For the temperature equation, such as Eq. (2) for a spectral condition, knowledge of $\epsilon_{\lambda,i}$, where the direction is nearly normal, is required. From a radiation balance,

$$\epsilon_{\lambda,i} = 1 - \rho_{\lambda,ih} \quad (18)$$

where $\rho_{\lambda,ih}$ is the reflectance corresponding to directional irradiation (i) and hemispherical (h) collection. In the laser pyrometry technique, the property that is measured using laser irradiation is the bidirectional reflectance $\rho_{\lambda,ij}$ where the directions (i,j) are slightly off the normal. For a perfect, diffuse reflector, $\rho_{ij} = 1/\pi \text{ sr}^{-1}$; for a perfect, specular reflector, ρ_{ij} can be zero, unity or any intermediate value depending upon the magnitudes of the solid angles of viewing/collection and the choice of directions (i,j). Of special interest is the behavior of

$$R_{ij} = \frac{\rho_{ih}}{\rho_{ij}} \quad (19)$$

the ratio of the directional-hemispherical to the bidirectional reflectance. According to Stein [10], if this ratio is independent of wavelength, then a *two-wavelength* laser technique will provide emissivity compensation. If this ratio is a linear function of wavelength, Nutter [11] postulates that a *three-wavelength* laser technique will be required to provide compensation. To date there have been no demonstrations of either technique.

Report on the multicolor pyrometry session at the second NASA non-contact temperature-measurement workshop.

R. Erik Spjut – Chairman

The session met jointly with the other special sessions. Due to time constraints, the concerns of multicolor pyrometry were not addressed in depth. Hence, the views expressed represent the author's bias more than a consensus of those present.

Multicolor pyrometry attempts to determine an object's temperature and emittance as a function of wavelength from simultaneous measurement of the spectral radiance of the object at multiple wavelengths. The main issues are those of the most appropriate model for the wavelength dependence of the emittance, the number of undetermined parameters, and the error in the measured temperature. It has long been known that it is inappropriate to attempt to model the emittance with a functional form that contains as many unknowns as wavelengths (*e.g.*, it is inappropriate to use the second order polynomial,

$$\varepsilon = \varepsilon_0 + \varepsilon_1\lambda + \varepsilon_2\lambda^2 ,$$

with undetermined parameters ε_0 , ε_1 , ε_2 , and temperature, T , to fit data from a four-color pyrometer). Such attempts will lead to gross errors in the measured temperature. However, more recent work by Hunter and Khan has indicated that emittance can be modeled by a function with many fewer degrees of freedom than sampled wavelengths (*e.g.*, it may be appropriate to use a second order polynomial to fit data from a forty-color pyrometer). In a platform lecture, Khan described algorithms for determination of the parameters by minimization of the errors between the model and the data in a least-squares sense. The first was a linear method which required that the emittance was of the form

$$\varepsilon = \exp (\varepsilon_0 + \varepsilon_1\lambda + \varepsilon_2\lambda^2 + \varepsilon_3\lambda^3 + \dots),$$

and the second was a non-linear method where the emittance could assume any functional form. Both methods were shown to be very sensitive to random noise and non-linearity in the measurement system. However, when the noise level was kept low (at experimentally attainable levels), the error in temperature for a multicolor pyrometer ($n > 30$) was typically less than five percent and very often less than one percent. Hence, multicolor techniques can prove valuable when minimal information is

available about the emittance. A multicolor pyrometer eliminates the need for knowledge of the absolute value of the emittance and replaces it with the need for knowledge of the functional form of the emittance.

Time response of multicolor pyrometers as compared to single-color and ratio pyrometers was not discussed. However, several assumptions can be made. In terms of real-time response, multiwavelength pyrometers will be much slower for two reasons: the required data manipulation or regression fit would be very difficult to accomplish with high-speed analog circuitry, and while straightforward in digital circuitry, any sort of minimization routine on thirty to forty data items per time step would be an order of magnitude slower than the simple look-up routines that suffice for single-color pyrometers. For post-processed data, the factor that limits sampling speed is the need to store thirty to forty samples per time step, which is much faster than storing a complete video frame, but still much slower than storing one or two data items per time step.

The main theoretical questions that remain in multicolor pyrometry are: What is the optimal functional form for the emittance: polynomial, exponential, Fourier series, or others, such as Bessel functions? Does the optimal functional form vary from material to material? Which form is best for an unknown material? What is the optimal number of undetermined parameters for a given pyrometer, and, conversely, what is the optimal number and spacing of sampling wavelengths?

Once these questions are answered, engineering concerns remain in consistently obtaining the required linearity and low noise in the detection system, and in faster algorithms for determining the minima in the non-linear method.

In conclusion, multicolor pyrometry based on least-squares fitting shows great promise for giving reasonably accurate measurements in systems where the emittance is unknown, but there are no commercial systems presently available.

References:

P.B. Coates, *Metrologia*, 17 (3), 1981, pp. 103-109

G.B. Hunter, *et al.*, *Opt. Eng.*, 25 (11), Nov 1986, pp. 1222-1231

M.A. Khan, Ph.D. Thesis, M.I.T., May 1988

APPENDIX A
LIST OF ATTENDEES

Harvey Mudd College
Attn: Prof. R. Erik Spjut
301 East 12th St.
Claremont, CA 91711

University of Alabama
Attn: Thomas Rathz
Dept. JRC, M/S R1-A11
Huntsville, AL 35899

Purdue University
Attn: C.Y. Ho
2595 Yeager Rd.
W. Lafayette, IN 47906

Wyman Gordon Co., R&D Div.
Attn: Mansoor Ali Khan
244 Worcester St.
North Grafton, MA 01536

Physical Sciences, Inc.
Attn: Jonathan Frank
P.O. Box 3100
Andover, MA 01810

EDO Corporation
Attn: Robert Barnes
P.O. Box 867
88 Long Hill Cross Rd.
Shelton, CT 06484-0867

NASA Marshall Space Flight Center
Attn: William Powers
M/S EB22
Marshall Space Center, AL 35812

Houston Area Res. Center
Attn: Robert Hauge
4802 Research Forest Dr.
The Woodlands, TX 77381

Honeyhill Technical Company
Attn: Herbert Kaplan
195 East Ave.
Norwalk, CT 06855

Purdue University
Mechanical Engineering
Prof. David P. DeWitt
W. Lafayette, IN 47907

Houston Area Res. Ctr.
Attn: Leif Fredin
4802 Research Forest Dr.
The Woodlands, TX 77381

Intersonics Inc.
Attn: Shankar Krishnan
3453 Commercial Ave.
Northbrook, IL 60062

NASA Marshall Space Flight Center
Attn: Dinah Higgins
M/S JA56
Huntsville, AL 35812

NASA Lewis Research Ctr.
Attn: John Prince
M/S 500-205
21000 Brookpark Rd.
Cleveland, OH 44135

Case Western Reserve Univ.
Dept. of Chemical Engrg.
Attn: J. A. Mann
Cleveland, OH 44106

NASA Headquarters
Attn: Larry Spencer
Code EN
Washington, DC 20546

NASA Lewis Research Center
Attn: Paul S. Greenberg
M/S 500-217
21000 Brookpark Rd.
Cleveland, OH 44135

NASA Marshall Space Flight Center
Attn: William Witherow
M/S ES74 SSL, Bldg. 4481
Huntsville, AL 35812

NASA Headquarters
Attn: Mark C. Lee
Code EN
Washington, DC 20546

Everest Interscience Corp.
Attn: Gene Everest
P.O. Box 3640
Tustin, CA 92634-3640

NASA Headquarters
Attn: R. Schmitz
Code EN
Washington, DC 20546

Hughes Aircraft Co.
Attn: Chris Sexton
6155 El Camino Real
Carlsbad, CA 92008

Bionetics Corp.
Attn: Richard Bradfield
600 Maryland Ave. NW
Washington, DC 20024

NASA Langley Res. Ctr.
Attn: A.M. Buoncristiani
M/S 468
Hampton, VA 23665-5225

NASA Lewis Research Ctr.
Attn: Alexander D. Pline
M/S 77-3
21000 Brookpark Rd.
Cleveland, OH 44135

NIST
Attn: G. Barry Hillard
Bldg. 221/A221
Gaithersburg, MD 20899

NASA Langley Res. Ctr.
Attn: David Bowker
M/S 473
Hampton, VA 23665-5225

NASA Marshall Space Flight Center
Attn: Michael Robinson
M/S ES74
Huntsville, AL 35812

Intersonics, Inc.
Attn: R. Charles Rey
3453 Commercial Ave.
Northbrook, IL 60062

Lawrence Livermore National Lab.
Attn: Oscar H. Krikorian
P.O. Box 808
M/S L-369
Livermore, CA 94550

NIST
Attn: Ared Cezairliyan
Bldg. 236
Gaithersburg, MD 20899

NASA Marshall Space Flight Center
Attn: Robert Naumann
M/S ES71
Huntsville, MD 35812

NASA Lewis Research Center
Attn: Gilbert Santoro
Code 500-205
Cleveland, OH 44135

Intersonics, Inc.
Attn: R. Schiffman
3453 Commercial Ave.
Northbrook, IL 60062

Massachusetts Inst. of Tech.
Attn: Michael Wargo
Rm. 13-4057
Cambridge, MA 02139

Oak Ridge National Lab.
Attn: R.L. Shepard
Bldg. 3500, M/S 6003
P.O. Box 2008
Oak Ridge, TN 37831-6008

Case Western Reserve Univ.
Attn: Rafat Ansari
Dept. of Chemical Engrg.
Cleveland, OH 44106

University of New York
Attn: Prof. Michael Anbar
Dept. of Biophysical Sci.
School of Medicine
Buffalo, NY 14214

Vanderbilt University
Attn: A.B. Hmelo
Box 6079, Station B
Nashville, TN 37235

Physical Sciences, Inc.
Attn: Michael E. Frish
Dascomb Res. Park
P.O. Box 3100
Andover, MA 01810-7100

Vanderbilt University
Attn: William Hofmeister
Dept. of Mech. & Materials Engrg.
Nashville, TN 37235

Virginia Tech., F and EO
Research Center
Attn: Russell May
648 Whittemore Hall
Blacksburg, VA 24061

EDO Corp.
Barnes Engrg. Div.
Attn: Robert Astheimer
88 Long Hill Cross Rd.
P.O. Box 867
Shelton, CT 06484-0867

Sverdrup Technology Inc.
AEDC Group
Attn: Andrew Jackson
M/S 960
Arnold Air Force Base,
TN 37389

Charly Allemand
22 Oakwood Rd.
Newtonville, MA 02160

Physical Sciences Inc.
Attn: B. David Green
P.O. Box 3100
Andover, MA 01810

Eastman Kodak Co.
Attn: George T. Keene
970 W. 190th St.
Torrance, CA 90502

Virginia Tech.
EE Dept.
Attn: Richard O. Claus
Blacksburg, VA 24061

TRW
Attn: C.K. Chan
One Space Park
Redondo Beach, CA 90278

N.C. State University
NCSU
Attn: Klaus Bachmann
Dept. of Materials Sci. & Engrg.
Raleigh, NC 27695-7907

Magnovox OES
Attn: Richard F. Leftwich
46 Industrial Ave.
Mahwah, NJ 07430

AT&T Bell Labs.
Attn: David Bishop
Rm. 10-231
600 Mountain Ave.
Murray Hill, NJ 07974

Land Instruments, Inc.
Attn: Peter Kirby
2525 Pearl Buck Rd.
Bristol, PA 19007

JPL

Barmatz, M.
183-401

Coulter, D.
67-201

Croonquist, A.
183-401

Dolgin, B.
157-507

Elleman, D.
183-401

Frazer, R.
125-177

Glazer, R.
157-102

Grumm, R.
183-801

Hale, R.
183-401

Houseman, J.
169-314

Ladner, G.
125-112

Leung, E.
183-401

Lewis, D.W.
183-801

Macenka, S.
169-314

Manatt, S.
183-901

Morrison, A.
183-801

Ohsaka, K.
183-401

Rajan, S.
183-501

Rhim, W.
183-401

Rooney, J.
183-901

Schutz, F.
183-801

Seaman, C.
125-18

Sobel, H.
11-116

Trinh, E.
183-401

Wiker, G.
125-177

Wilson, B.
302-205

CALTECH

Robert Housley
114-36

APPENDIX B

NCTM REQUIREMENTS LIST

NCTM REQUIREMENTS

(DERIVED FROM THE NCTM WORKSHOP (1987) PROCEEDINGS)

Lehosky - Electronic Materials

+ - 1.5C for 200-700 deg

+ - 2.5 for 700-1100

+ - 3.5C for 1100-1350

+ - 5C for >1350

5 samples per sec. sampling rate

Probably cannot be met due to errors resulting from the lack of precise information on thermophysical properties

Temp resolution from approx 0.2 - 4C

For imaging purposes, sampling rates in the range of 30 samples/sec

Spatial resolution of 0.1 to 1mm

Perepezko- Metals and Alloys

High temperature

500 to 4000 K with +-1 K resolution

Fast Response

Cooling rates: 10^4 - 10^6 K/sec

Recalescence: 10^5 K/sec

Fine Spatial Resolution

Temperature gradients: 0.1 K/cm - 10^5 K/cm

Thermal profiles < 1 micron, $dT < 1$ degC, $1-5\text{cm}^2$

Thermal maps for morphological development and thermosolutal flows

Monitor crystal growth rates: 10^{-2} cm/s to 100 cm/s

Doremus - Glass/ Transparent Materials

Non-quantitative response.

Desires temperature gradient measurement capability.

Warns of variable emittance of glasses as a function of temperature and the possible problems associated with observing transparent samples.

Salzman - Fluids and Transport Phenomena

Temperatures ranging from -271 C (lambda point of helium) to 1000 C (liquid metals and eutectics) with control measurement accuracies in some cases of microdegrees. "In some cases, spatially defined true surface ... temperature measurements are required across the extent of the surface and in other cases accurately defined point measurements within the bulk fluid are required." The most common fluid temperatures encountered are from 0 - 100 C with required accuracies in the 0.001 to 1 deg range.

Sacksteder - Combustion

Knowledge of the temperature field in a combustion system.

	Temperature Range (deg K)	Resolution		Measurement Accuracy (deg K)
		Spatial (1mm)	Temporal (msec)	
Solid Phase Surface	270-800	1	20	5
Liquid Surface	270-350	0.5	40	0.2
Vapor	300-3000	1	20	5

Ronney - Combustion

Spatial resolution: 0.1 cm

Temporal resolution: 0.1 sec

Time aperture (to "freeze" the system) 0.001 sec

Test section size for 100x100 points: 10cmx10cm

Snyder - Biotechnology

No present need for NCTM, but some interest in temperature distribution over very small dimensions - eg a 10 micron diameter biological cell.

APPENDIX C

INVITATION LETTER WORKSHOP FINAL PROGRAM SELECTED ABSTRACTS

November 30, 1988

Dear Colleague:

This letter invites your participation in a NASA technical workshop on Non-Contact Temperature Measurement (NCTM) in Pasadena, CA. The two and one-half day meeting is from January 17 to 19, 1989 at the Pasadena Hilton Hotel, and it is being hosted by JPL. The enclosed materials describe the technical program and the logistics arrangement in further detail.

The purpose of the workshop is to establish and update an integrated set of technical recommendations for NCTM Advanced Technology Development (ATD) work, which is needed for a balanced science-support program to enable future microgravity and containerless processing experiments. Recent work by several NASA centers and investigators will also be presented through work-in-process poster sessions and as technical papers to be published in the conference proceedings. In particular, this meeting will update the preliminary requirements which had been identified in the initial workshop chaired by Mark Lee in April-May 1987, documented in 1988 as NASA Conference Publication 2503. The added feature of this workshop is the use of several technical splinter sessions to address challenges of and approaches to the thermal measurement issue in working groups with materials scientists.

The meeting is sponsored by NASA Headquarters, Code EN, the Microgravity Science and Applications Division (MSAD), and the ATD Program Manager for this work is Larry Spencer.

We are looking forward to your interaction with us in Pasadena in January and wish you a very enjoyable Holiday Season!

Very truly yours,



Robert R. Hale
Jet Propulsion Laboratory

RRH:sh
encl.

January 17, 1989

Dear Colleague:

Happy New Year and welcome to the second NASA technical workshop on Non-Contact Temperature Measurement (NCTM). During the next two and one-half days we plan to establish and update an integrated set of technical recommendations for NCTM Advanced Technology Development (ATD) work, which is needed for a balanced science-support program to enable future microgravity and containerless processing experiments. Recent work by several NASA centers and investigators will also be presented through work-in-process posters and as technical papers to be published in the conference proceedings. In particular, this meeting will update the preliminary requirements which had been identified in the initial workshop chaired by Mark Lee in April-May 1987, documented in 1988 as NASA Conference Publication 2503. The added feature of this workshop is the use of several technical splinter sessions to address challenges of and approaches to the thermal measurement issue in working groups with materials scientists.

Please note the attached Final Program, which closely parallels the preliminary agenda that I had sent with my letter of November 30, 1988. Also enclosed are selected abstracts for the technical papers and poster Session presentations. Thank you for your enthusiasm and interest in this workshop, and special thanks also to the presenters and session chairs for their planning and work.

This meeting is sponsored by NASA Headquarters, Code EN, the Microgravity Science and Applications Division (MSAD), and the ATD Program Manager for this work is Larry Spencer.

Very truly yours,



Robert R. Hale
Jet Propulsion Laboratory

RRH:bg

NASA NCTM WORKSHOP
JANUARY 17-19, 1989
THE PASADENA HILTON HOTEL
150 SOUTH LOS ROBLES
PASADENA, CA

WORKSHOP FINAL AGENDA

January 16,

7:00 – 9:30 pm Registration, Reception, Pasadena Hilton, Sliks, Top Floor

January 17,

8:15 – 9:00 am Registration, Check-in, Pasadena Hilton, Poster Session Set-up

9:00 – 9:05 Morning Session – Welcome, F. Schutz

NASA NCTM NEEDS BY CENTER

9:05 – 9:15 Opening remarks – Larry Spencer, Mark Lee. Code EN-HQ NASA MSAD
9:15 – 9:30 Bob Hale – JPL - Materials and Thermal Science Overview
9:30 – 10:00 Archie Fripp – LaRC
10:00 – 10:30 Gil Santoro – LeRC
10:30 – 10:45 BREAK
10:45 – 11:15 Bob Naumann – MSFC
11:15 – 11:45 Eugene Trinh – JPL
11:45 – 12:15 Discussion
12:15 – 1:15 LUNCH, Pasadena Hilton

TUESDAY, JANUARY 17 – AFTERNOON SESSION

NCTM Capabilities Technical Papers

1:15 – 1:30 Bob Hale – Introduction and Non-contact Science and Technology, JPL
1:30 – 1:50 Bob Shepard – "Optical Johnson-Noise Thermometry", ORNL
1:50 – 2:10 Paul Greenberg – "Laser Fluids Diagnostics and Thermal Measurements", LeRC
2:10 – 2:30 Marty Buoncristiani – "Non-contact Optical Fiber Pyrometry", LaRC
2:30 – 2:50 Jim Rooney – "Acoustic and Thermal Wave Material Characterization", JPL
2:50 – 3:00 BREAK
3:00 – 3:20 Barry Hillard – "Thermometry, Pyrometry, and IPTS Technology", NBS/NIST
3:20 – 3:40 Herb Kaplan – "Thermal Imaging Figures of Merit and R&D Prospects",
Honeyhill Technical Company
3:40 – 4:00 Mickey Frisch – "Multi-color Imaging Pyrometry", PSI
4:00 – 4:20 M.A. Khan – "Ratio and Multi-Wavelength Pyrometry", MIT/Wyman Gordon
4:20 – 4:40 S. Krishnan – "Spectral Emissivities and Optical Properties . . .", Rice University/
Intersonics

POSTER SESSION TOPICS NASA ATD WORK-IN-PROGRESS FOR NCTM

5:00 - 6:00 p.m., Tuesday, January 17, 1989
Chardonnay Room

JPL	-	James Rooney:	Time-resolved Non-Contact Methodology
		Don Lewis:	DPM Conceptual Design
		Stan Manatt:	MRI Research
LaRC	-	A. Martin Buoncristiani:	Fiber Optics Link R & D
VPI	-	R.O. Claus	
LaRC	-	D. Bowker:	Image Enhancement Technology
LeRC	-	P. Greenburg:	Combustion Optical Thermal Diagnostics

TOPICAL OUTLINE FOR MICROGRAVITY MATERIALS SCIENCE THERMAL REQUIREMENTS PRESENTATIONS (MORNING SESSION—DAY 2)

- Typical experiment timeline vs. thermal control and measurement (C&M) required
- Science impact and criticality of thermal C & M performance
 - Precision, repeatability, stability, resolution
 - Auxiliary thermal measurements (calorimetry, P,V, enthalpy, entropy)
- Concurrent imaging needs for science observations
- Sample translation, velocity, acceleration
- Spatial resolution – coupled temporal resolution requirements, their criticality, and trade-off issues
- Other critical thermal science factors (phase transformation, state-change thermodynamics)
- Functional definition of "non-perturbing" measurement system parameters (for active measurement approaches)

**NASA NCTM WORKSHOP
FINAL AGENDA
JANUARY 18, 1989, WEDNESDAY
DAY (2) MORNING SESSION**

**TECHNICAL RECORDERS – (TBA)
Microgravity Materials Science Thermal Requirements
(See Attachment for topical outline)**

Discipline Working Group Update: Eugene Trinh, Chairman (20 minutes/presenter)

8:30 – 8:50	K. Bachmann – Epitaxial and Bulk Crystals
8:50 – 9:10	W. Hofmeister – Metals & Alloys
9:10 – 9:30	D. Coulter – Polymeric Materials
9:30 – 9:50	B. Wilson – Electronic Materials
9:50 – 10:10	D. Bishop – High Tc Materials
10:10 – 10:30	BREAK
10:30 – 10:50	W. Serignano – Combustion Processes
10:50 – 11:10	A. Hmelo – Drop Physics and Fluid Dynamics
11:10 – 11:30	Discussion – Common Measurement issues
11:30 – 12:00	Discussion – Material Class-specific issues
12:00	Ad hoc LUNCHEON

**SPLINTER WORK-SESSIONS
JANUARY 18, 1989, AFTERNOON
(CONCURRENT SESSIONS)**

Session I	H. Kaplan – Honeyhill Technical Co.	Industrial Commercial Thermal Measurement: State-of-the Hardware
Session II	R. Shepard – ORNL and A. Cezairliyan – NBS/NIST	Dynamic Response for Thermal Control and Measurement: Spatial and Spectral Time Constants
Session III	D. De Witt and C. Y. Ho – Purdue	Materials Thermal and Thermoradiative Properties/Characterization Technology
Session IV	R. E. Spjut	Multiple-Color Pyrometry Problems and Solutions

*Summary Technical Recorder interpretive statements to be provided by Session Chairs.

- Output from these work sessions is to include Tutorial and Bibliographic outlines for Materials Science characterization in Microgravity of Thermally-important events, characteristics, and behavior. Technical approaches, resources, and organizational issues shall be emphasized in the recommendation summaries.

NASA NCTM WORKSHOP

JANUARY 19, 1989, FINAL 1/2 DAY

Presentations by Working Groups – (~15 minutes each)

9:00	Session I	H. Kaplan	FOM & SOTH
9:15	Session II	R. Shepard	DRTCM
9:30	Session III	D. DeWitt	MTP/C
9:45	Session IV	R. E. Spjut	MCPPS

BREAK

10:00	Panel Discussion – R. Hale, Chairman
	<ul style="list-style-type: none">● Technology Gaps Identified● Methods to Close the Gaps● Technical Resource Identification, Scope & Schedule
11:30	<ul style="list-style-type: none">● Summary
12:00	<ul style="list-style-type: none">● Adjourn

**SECOND NASA NCTM WORKSHOP, JANUARY 17-19, 1989
PASADENA, CA**

Issues/Questions

Please write down any issues or questions that you would like to have addressed which were not adequately covered during the workshop. Please leave this form with a JPL host or mail it by February 14, 1989 to:

**Jet Propulsion Laboratory
4800 Oak Grove Drive
Pasadena, CA 91109
R. R. Hale, 183-401**

Who is your question for?

State your Issue or Question:

Name and Address for written reply:

NASA NCTM WORKSHOP

JANUARY 17-19, 1989

**THE PASADENA HILTON HOTEL
150 SOUTH LOS ROBLES
PASADENA, CA**

SELECTED PRE-PUBLICATION ABSTRACTS

Non-Contact Temperature Measurement (NCTM)

Advanced Technology Development (ATD)

R. R. Hale
Jet Propulsion Laboratory

In April-May 1987, Mark C. Lee chaired NASA's initial workshop on NCTM in Washington, D.C. The proceedings of that workshop are documented as NASA Conference Publication 2503 from NASA's Scientific and Technical Information Division, 1988. An excerpt from the foreword of that document identifies NCTM and the several other ATD areas and gives a rather general definition of their purpose:

"Non-contact Temperature Measurement Instrument has been identified as one of the eight Advanced Technology Development (ATD) areas to support the Microgravity Science and Applications Division's effort in developing the six Space Station Flight Experiment Facilities. The other seven ATD's are High Resolution/High Rate Video Technology, Microgravity Fluid Diagnostics, Laser Light Scattering Instrument, Vibration Isolation Technology, High Temperature Furnace Technology, High Temperature Material [SIC] Technology and Interface measurement. Those ATD areas are defined as generic areas of technology advancement that will enhance the scientific integrity and quality of flight experiments. These technologies shall not be in the critical path of on-going programs or near-term facility development programs."

This workshop is a follow-up to the initial one, and it is intended to report on progress to date by the NASA centers involved in this broad technical NCTM task. Clarification of particular scientific needs is also sought in order to effectively manage the technology advancement activities oriented toward "enhancement," "enablement," and "barrier removal" for flight experiments. The scope includes condensed and uncondensed matter and processes for present and contemplated future containerless science and microgravity science investigations of phenomenological materials behavior.

TEMPERATURE MEASUREMENT REQUIREMENTS OF THE JPL FLIGHT AND
GROUND-BASED RESEARCH PROGRAMS

E.H. TRINH
JET PROPULSION LABORATORY

The Microgravity program at the Jet Propulsion Laboratory is responsible for the development of flight equipment and of the accompanying scientific and technological research necessary to carry out containerless investigations in the low gravity of Earth orbit. The requirement for sample temperature measurement is just one of the many physical properties determination needs that must be satisfied before the useful exploitation of low gravity and containerless experimentation techniques can be achieved. The specific implementation of temperature measurement for the ground-based containerless processing research program is different from that of the flight apparatuses development project. The needs of the latter must also be differentiated according to the chronological order of the relevant space flight missions. Immediate demands of Spacelab instruments must be addressed by the adaptation of existing and reliable technology to the special and restrictive on-orbit environment, while more advanced and yet unperfected techniques will be assigned to enterprises further in the future. The wide range of application of the containerless methods to the study of phenomena involving different states of matter and environmental conditions requires the satisfaction of a variety of boundary conditions through different approaches. An important issue to be resolved will be whether an integrated program dedicated to solve the problems of all of the Microgravity experimental effort will allow the solution of specific demands of existing as well as future flight equipment.

A POTENTIAL NUCLEAR MAGNETIC IMAGING APPROACH
FOR NONCONTACT TEMPERATURE MEASUREMENT

Stanley L. Manatt
Applied Sciences and Microgravity
Experiments Section
Jet Propulsion Laboratory

Nuclear Magnetic Resonance (NMR) is a form of radio frequency spectroscopy of atomic nuclei possessing spin. To observe NMR signals from a sample requires a magnet, R.F. transmitter receiver system and data acquisition system. Currently NMR is very important in research and diagnosis of problems in biology, chemistry, physics and biomedicine.

NMR experiments can be done many different ways and measure a number of different parameters that are directly related to molecular structure, physical state, molecular dynamics and temperature. NMR imaging (MRI-magnetic resonance imaging) has become an extremely important medical diagnostic tool recently.

It is proposed that in an MRI experiment it should be possible to measure temperature throughout an extended volume. The basis for such a measurement would depend upon sensing a temperature dependent NMR parameter in an inert, volatile molecule filling the extended volume of interest.

Inert molecules containing the nuclei ^1H , ^2H (enriched), ^{10}B , ^{11}B , ^{13}C , ^{14}N , ^{15}N (enriched), ^{17}O (enriched), ^{19}F , ^{21}Ne (enriched) ^{29}Si , ^{31}P , ^{35}Cl , ^{37}Cl , ^{83}Kr (enriched), ^{127}I , ^{129}Xe and ^{131}Xe are candidates. Exploratory work on ^{35}Cl and ^{37}Cl in CCl_4 , CCl_3H and CCl_2H_2 has shown that these possess NMR lines that are too broad but CH_3Cl might be a suitable candidate to study the line width temperature dependence. What parameters, other inert gases, and measurement schemes might provide such temperature measurement will be discussed.

SIGNAL PROCESSING APPLIED TO PHOTOTHERMAL
TECHNIQUES FOR MATERIALS CHARACTERIZATION

JAMES A. ROONEY
JET PROPULSION LABORATORY
CALIFORNIA INSTITUTE OF TECHNOLOGY
PASADENA, CALIFORNIA 91109

There is a need to make noncontact measurements of material characteristics in the microgravity environment. Photothermal and photoacoustic techniques offer one approach for attaining this capability since lasers can be used to generate the required thermal or acoustic signals. The perturbations in the materials that can be used for characterization can be detected by optical reflectance, infrared detection or laser detection of photoacoustics. However, some of these laser techniques have disadvantages of either high energy pulsed excitation or low signal-to-noise ratio. Alternative signal processing techniques that have been developed at JPL can be applied to photothermal or photoacoustic instrumentation. One fully coherent spread spectrum signal processing technique is called time delay spectrometry (TDS)¹. With TDS the system is excited using a combined frequency-time domain by employing a linear frequency sweep excitation function. The processed received signal can provide either frequency, phase or improved time resolution. This signal processing technique has been shown to outperform other time selective techniques with respect to noise rejection and has been recently applied to photothermal instrumentation. The technique yields the mathematical equivalent of pulses yet the input irradiances are orders of magnitude less than pulses with the concomitant reduction in perturbation of the sample and can increase the capability of photothermal methods for materials characterization. ¹ R.C. Heyser, J. Audio Eng. Soc. 15 370 (1967).

CONTACT TEMPERATURE MEASUREMENTS
IN
BRIDGMAN CRYSTAL GROWTH

A.L. Fripp, W.J. Debnam and G.A. Woodell
Langley Research Center
Hampton, Virginia

and
S.K. Sorokach
P.R.C. Corporation
Hampton, Virginia

Control of the crystal growth process when using the Bridgman directional solidification technique requires knowledge of both the temperature and solutal fields within the ampoule. The temperature field must be controlled not only for the very obvious reasons of providing a solidification temperature and maintaining sufficient gradient to prevent interfacial breakdown but also to control interface shape and otherwise influence the convection flow patterns.

This paper will discuss recent efforts to measure the thermal field anticipated in a Bridgman crystal growth. Instrumented calibration samples have been constructed. These samples have similar thermal properties to the desired crystal melt. Instrumentation is via thermocouples. Calibration, placement, movement due to thermal expansion and degradation are all serious problems to obtaining good furnace characterization. Techniques to address these problems will be discussed.

NASA Non-Contact Temperature Measurement Workshop

**"Non-Contact Optical Fiber-Based Non-Contact Pyrometer For Drop Tube
Instrumentation**

**R.G. May, S. Moneyhun, W. Saleh, S. Sudeora and R.O. Claus
Fiber and Electro-Optics Research Center
Virginia Tech
Blacksburg, VA 24061**

**A.M. Buoncristiani
Mail Code 468
NASA-Langley Research Center
Hampton, VA 23665**

Abstract

A non-contact multiwavelength pyrometer which uses a network of infrared optical fibers to measure the temperature of a heated particle as it falls in an evacuated drop tube has been designed and tested in the laboratory. The design uses an array of bundles of IR-transmitting fibers. Each bundle is connected between a single access port in the tube and a pair of broadband optical detectors. Because the particle is small and because it moves quickly through the field of view of each port, the optical power budget of the detection system is severely limited. To increase the total coupled power we have modified the effective numerical aperture of the viewing ends of the fibers, utilized antireflection fiber endface coatings, and implemented wideband differential spectral passband measurements to determine the temperature of the particle as it passes each port. The design, operation and limitations of the optical fiber pyrometer are presented.

This work has been supported in part by NASA Grant NAG-831.

Submitted for Presentation at the
NASA Noncontact Temperature Measurement
Workshop hosted by the Jet Propulsion Laboratory,
Pasadena, California, January 17 - 19, 1989

MICROGRAVITY NONCONTACT TEMPERATURE REQUIREMENTS
AT THE LEWIS RESEARCH CENTER

by

Gilbert J. Santoro
NASA Lewis Research Center
21000 Brookpark Road
Cleveland, Ohio 44107

ABSTRACT

The Lewis Research Center (LeRC) is currently supporting sixty-six microgravity science and application projects. The projects consist of in-house, grant and contract activities, or some combination of these activities, and involve the participation by personnel in the Space Experiments Division of the Space Flight Systems Directorate, and the Materials Division and the Structures Division of the Aerospace Technology Directorate. The LeRC microgravity science and application program is divided into flight projects and ground-based projects. For the flight projects, ground-based work is required to better define the experiment, develop and check out the flight hardware, and to provide a 1-g data base for comparison.

Several purposes exist for ground-based experimenting. Preliminary information is necessary before a decision can be made for flight status. The short low-gravity durations available in ground facilities are adequate for a particular study, or extensive ground-based research must be conducted to define and support the microgravity science endeavors contemplated for space. Knowledge of gravity-related effects in the ground-based projects (i.e., in a suborbital setting) is obtained by conducting experiments in drop tower facilities or aircraft. Low-gravity durations of up to 20 seconds are available using these facilities.

Not all of the sixty-six microgravity science and application projects at LeRC have temperature requirements, but most do. Since space allocation does not permit a review of all the pertinent projects, a decision was made to restrict the coverage to the science flight projects. Very little is lost by this decision as the types of temperature requirements for science flight projects can be considered representative of those for the ground-based projects. This paper then will discuss the noncontact temperature needs at LeRC, as represented by the science flight projects, by describing briefly the experiments themselves, by displaying an illustration of each experimental setup, and by specifying their temperature requisites.

NASA Non-Contact Temperature Measurement Workshop

Abstract

Temperature Measurements in support of Microgravity Combustion Diagnostics

Paul S. Greenberg
NASA Lewis
Research Center

Advances in the understanding of microgravity combustion processes have been accompanied by a demand for diagnostic systems of greater sophistication. Influenced predominantly by the harsh operational constraints imposed upon space flight hardware, diagnostic apparatus to date has been relatively primitive, and primarily qualitative in nature. In the absence of the relatively strong force of buoyant convection, microgravity combustion phenomena are generally more fragile and easily perturbed than their normal gravity counterparts. Hence, the primary emphasis has been placed on nonperturbing optical diagnostic techniques. Various considerations, such as limited supplies of expendable reactants, or periods of reduced gravity time of limited duration, coupled with more fundamental questions regarding inherent length and time scales, stability, and repeatability, have favored multi-point or multidimensional diagnostic techniques. It is the unfortunate reality, however, that many techniques frequently utilized in terrestrial laboratories are intractable in the present context. The additional requirements for operational reliability and autonomy have tended to promote somewhat less commonly emphasized and configurationally simpler techniques such as refractive index mapping and molecular Rayleigh scattering.

Marshall Space Flight Center
Non Contact Temperature Measurement Requirements
Abstract

January 17, 1989
Dinah B. Higgins

The Marshall Space Flight Center is involved with levitation experiments for Spacelab and Space Station operation. These levitation experiments have temperature determination requirements, that of course must be non contact in nature. The experiment modules involved are the Acoustic Levitator Furnace(ALF), and the Modular Electromagnetic Levitator(MEL).

Since the experimenter's requirements for the MEL will be covered in a separate presentation, they will not be covered in detail here. This presentation will focus on NCTM options for MEL, and associated problems of interfacing the NCTM with the sample heating mechanism. Experimental requirements for the ALF will be addressed, including a brief overview of the experimental setup and operation.

NON-CONTACT TEMPERATURE MEASUREMENT OF A FALLING DROP

William Hofmeister and R.J. Bayuzick
Center for the Space Processing of Engineering Materials
Vanderbilt University
Nashville, TN 37235

M.B. Robinson
NASA Marshall Space Flight Center
Huntsville, AL 35812

ABSTRACT

The 105-meter drop tube at the Marshall Space Flight Center has been used in a number of experiments to determine the effects of containerless, microgravity processing on the undercooling and solidification behavior of metals and alloys. These experiments have been limited, however, because direct temperature measurement of the falling drops has not been available. Undercooling and nucleation temperatures are calculated from thermophysical properties based on droplet cooling models. In most cases these properties are not well known, particularly in the undercooled state. This results in a large amount of uncertainty in the determination of nucleation temperatures. If temperature measurement can be accomplished then the thermal history of the drops could be well documented. This would lead to a better understanding of the thermophysical and thermal radiative properties of undercooled melts. An effort to measure the temperature of a falling drop is under way at Vanderbilt and Marshall Space Flight Center. The technique uses two-color pyrometry and high speed data acquisition. The approach will be presented along with some preliminary data from drop tube experiments. The results from droplet cooling models will be compared with non-contact temperature measurements.

Thermometry, Pyrometry, and IPTS Technology

G. Barry Hillard

Radiometric Physics Division

National Institute of Standards and Technology

An overview of activities at NIST in radiation thermometry and related IPTS technology will be presented. An expansion of calibration services for pyrometers will be described as well as efforts to develop calibration services for blackbody simulators. Research relevant to the realization of the new international temperature scale (ITS 90) will be discussed.

MULTICOLOR IMAGING PYROMETER

Michael B. Frish
Jonathan Frank
Henry Beerman

Physical Sciences Inc.
Research Park
PO Box 3100
Andover, MA 01810

Abstract

A passive imaging pyrometer has been assembled which is capable of accurately determining the temperature distribution across the surface of a moving heated object. The pyrometer employs an optical system which measures the object's radiance at a wavelength that is short compared to the peak of the blackbody spectrum for the temperature range of interest, thus minimizing errors associated with a lack of knowledge about the heated sample's emissivity. To enable measurement of temperatures ranging nominally from 800 to 2500 K, six wavelengths between 350 and 950 nm are available. The wavelength selected for the measurement decreases as the temperature increases. The available wavelengths have been chosen to make the temperature measurement at least ten times more accurate than the knowledge of the heated object's emissivity.

The heart of the pyrometer is a Sierra Scientific Model 4032 Variable-Integration-Time CCD camera, coupled to a Data Translation Model 2851 frame-grabber and a Compaq 286 computer. The frame grabber digitizes the output of the camera into an array of 512 x 512 pixels with 8-bit precision, thereby providing better than 0.5 percent temperature measurement precision. The pyrometer's optical system projects all six different-wavelength images of the moving object onto the camera's CCD array simultaneously. Based on the measured radiance, the computer automatically selects the appropriate image to use for the temperature calculation. There are no moving parts. The system was designed to study samples of acoustically-levitated materials subjected to radiant heating in the microgravity of space, and therefore observes a field of view one centimeter in diameter from a distance of 36 cm with a spatial resolution of about 40 μm .

The pyrometer collects and displays false color temperature maps at video rates, 30 frames per second. The images can be analyzed to provide data to a temperature control feedback loop at a rate of about ten times per second. In addition, a unique interface enables computer control of the exposure time, which is continuously variable from 1 to 1000 ms. This provides a capability to accurately resolve rapidly moving objects, or to increase the measurement sensitivity when observing stationary objects.

SPECTRAL EMISSIVITIES AND OPTICAL PROPERTIES OF
ELECTROMAGNETICALLY LEVITATED LIQUID METALS AS FUNCTIONS OF
TEMPERATURE AND WAVELENGTH*

S. Krishnan

Intersonics, Inc., 3453 Commercial Ave., Northbrook, IL 60062
R. H. Hauge and J. L. Margrave
Rice University, Houston, TX 77005

The development of a unique, non-contact temperature measurement device using rotating analyser ellipsometry is described. The technique circumvents the necessity of spectral emissivity estimation by direct measurement concomitant with radiance brightness. Initial studies involved the measurement of the optical properties and spectral emissivities at 633 nm for several resistively heated metals. These metals included Hf, Ir, Mo, Nb, Pd, Pt, V and Ta, and were studied in the temperature range 1000 - 2500K.

Using this approach, the optical properties of electromagnetically levitated liquid metals Cu, Ag, Au, Ni, Pd, Pt and Zr were measured in situ as functions of temperature and wavelength. These measurements were performed at 1064, 632.8, 514.5 and 488 nm. Temperature dependences were examined up to 600K superheat in the liquid. Additionally, measurements on the levitated undercooled liquid and solid were performed.

The data suggest an increase in the emissivity of the liquids compared with the incandescent solids. Moderate temperature dependences of the spectral emissivities and dielectric constants were observed for the liquid metals studied. The spectral emissivities of the undercooled liquids were virtually the same as those of the liquids but slightly lower for moderate undercoolings (< 50K). Excellent agreement with available data for the dielectric constants and refractive indices was seen.

The design and theory of a new polarimetric pyrometer will be described. The polarimeter can reject depolarization due to sample surface roughness, in addition to making precise brightness measurements in the presence of a hot background. The applications and properties of such a device will also be discussed.

* Supported by NASA Microgravity Sciences Program and U.S. Department of Energy

NON-CONTACT TEMPERATURE REQUIREMENTS FOR DROP AND BUBBLE PHYSICS

Taylor G. Wang
Center for Microgravity Research and Applications
Vanderbilt University
Nashville, Tennessee 37235

Many of the materials research experiments to be conducted in the Space Processing Shuttle program require manipulation and control of weightless molten materials in a non-contaminating method. In these experiments, the melt is positioned and formed within a container without physically contacting the container's wall. An acoustic method which was developed at the Jet Propulsion Laboratory has demonstrated the capabilities of positioning and manipulating a room temperature sample. This has been accomplished in an earth-based laboratory and in a zero gravity environment of short duration. However, many important facets of high temperature containerless processing technology have not been established yet, nor can they be established from the room temperature studies, because the details of the interaction between an acoustic field and a molten sample are largely unknown.

Containerless processing experiments are underway at Vanderbilt to study drop dynamics, bubble dynamics, collision and coalescence, stability of containerless systems, thermal acoustic interaction, and the effects of acoustics on nucleation and undercooling. Drop and bubble dynamics experiments will pose no special NCTM requirements. Our maximum future requirements for the containerless experiments are for a system capable of $20^{\circ}\text{C} < T < 2000^{\circ}\text{C} \pm 1\%$. The system should be capable of at least one measurement per second, with a spatial resolution of fifty measurements per centimeter across the specimen.

DEVELOPMENT OF AN INFRARED IMAGING SYSTEM FOR
THE SURFACE TENSION DRIVEN CONVECTION EXPERIMENT
ABOARD THE USML-1 SPACELAB MISSION

by

Alexander D. Pline

NASA Lewis Research Center
Cleveland, Ohio 44135

ABSTRACT

In support of the Surface Tension Driven Convection Experiment (STDCE), a planned Space Transportation System (STS) flight experiment, a thermal infrared imaging system was used to quantify the imposed thermal signature along a liquid/gas free surface. For ground-based work a commercially available instrument was used to determine the feasibility of using this type of imaging system for the STDCE. The system was tested and calibrated for the STDCE with ground-based equivalents of the STDCE hardware. Before using the system, consideration was given to the radiation characteristics of the target (silicone oil). Absorption coefficients were calculated to understand the "surface" depth as seen by the imager and the penetration depth of the surface heater (CO₂ laser). Measurements made with the system were compared to thermocouple measurements and a calculated surface temperature distribution to determine the accuracy of the system under the actual experimental conditions. This ground-based work was used as a baseline for compiling specifications for a flight qualified imager to be designed, fabricated, tested, and qualified for flight aboard the USML-1 Spacelab Mission under contract. The specifications are given along with the reasons for differences between the ground-based and flight equipment. The potential problems and concerns associated with operating an imaging system on orbit are also discussed.

NASA Non-Contact Temperature Measurement Workshop

Abstract

"A Space-Qualified PtSi Thermal Imaging System

Robert W. Astheimer
EDO Corporation
Barnes Engineering Division

High resolution PtSi CCD vidicons are now available which enable thermal imaging in the 3-5 micron spectral region with a system similar to those used with visual CCD vidicons. A space-qualified system of this type has been designed and fabricated for the Air Force STARLAB mission. This employs a silicon objective lens and Joule-Thomson cryogenics with a 4600 PSI nitrogen gas reservoir which provides 6-7 hours of continuous operation. In order to improve radiometric accuracy, real time corrections are made to each pixel for offset and responsivity, from stored arrays of correction factors. While developed for an SDI mission, the system is well suited for spaceborne microgravity experiments where thermal imaging may be needed. This system will be described and examples of the thermal imagery of near ambient objects shown.

NASA Non-Contact Temperature Measurement Workshop

Abstract

"Solid State Lasers for the Noncontact Measurement of Temperature"

A. Martin Buoncristiani
NASA Langley Research Center
Hampton, VA 23665

Recent advances in solid state laser technology have important implications for thermal metrology. Detailed understanding of the optical properties of ions doped into solids, coupled with the ability to control growth of crystalline and amorphous materials now allows the design of solid state lasers to prescribed specifications including wavelength, bandwidth and pulse length. The parallel development of high power semiconductor diode lasers will provide efficient pump sources for solids and will allow an all-solid state laser technology as it pertains to non-contact temperature measurements. Special emphasis will be placed on recent developments in crystal fiber spectroscopy and its applicability to remote thermal sensors, especially to its potential for integrated active optical sensors.

